# MOSFIRE: MULTI-OBJECT SPECTROMETER FOR INFRA-RED EXPLORATION

Preliminary Design Report

March 31, 2006
Version 4.0

MOSFIRE: Multi-Object Spectrograph For Infra-Red Exploration
Preliminary Design Report
March 31, 2006

Table of Contents

Table of Contents

Table of Contents

Table of Contents

Figures and Tables

Figures and Tables

Figures and Tables

Figures and Tables

MOSFIRE: Multi-Object Spectrograph For Infra-Red Exploration
Preliminary Design Report
March 31, 2006

1 EXECUTIVE SUMMARY

The MOSFIRE Preliminary Design Report is presented. MOSFIRE is a new instrument intended for the Keck I Cassegrain focus. The optical design provides near-IR (~0.97-2.45 μm) multi-object spectroscopy over a 6.1′ x 3′ field of view with a resolving power of R~3,270 for a 0.7″ slit width (2.9 pixels in the dispersion direction), or imaging over a field of view (FOV) of 6.14′ with 0.18″ per pixel sampling. A special feature of MOSFIRE is that its multiplex advantage of up to 45 slits is achieved using a cryogenic Configurable Slit Unit or CSU (being developed in collaboration with the Swiss Centre for Electronics and Micro Technology, CSEM) that is reconfigurable under remote control in less than 5 minutes without any thermal cycling of the instrument. Slits are formed by moving opposable bars from both sides of the focal plane. An individual slit has a length of 7.3″ but bar positions can be aligned to make longer slits. When the bars are removed to their full extent and the grating is changed to a mirror, MOSFIRE becomes a wide-field imager. Using a single 2K x 2K H2-RG HgCdTe array with exceptionally low dark current and low noise, MOSFIRE will be extremely sensitive and ideal for a wide range of science applications.

During the preliminary design phase all of the major, perceived risks have been mitigated or retired. An all-spherical refractive optical design has been developed to the detailed design, pre-construction level sufficient to order glass blanks. An independent CCD-based Guider design has also been developed. CSEM has modified an existing zero-gravity CSU design and constructed a prototype (2-bar) cryogenic reconfigurable slit unit that meets our specifications and which is now being tested under cryogenic conditions. All aspects of the MOSFIRE mechanical design have been analyzed. A preliminary flexure analysis of the large cylindrical dewar shows that the instrument design is intrinsically stiff, and a thermal analysis shows that the temperature distribution is adequately isothermal. Using two large CCR heads, the instrument can achieve operational conditions in 7-8 days. Cryogenic mechanisms have been kept to a minimum. Apart from the CSU, there is a dual filter wheel, a rotating pupil mechanism and a turret carrying a plane mirror and a diffraction grating mounted back-to-back. Only one diffraction grating is employed. The grating remains at a fixed angle and order-sorting filters provide spectra that cover the K, H, J or Y bands by selecting 3rd, 4th, 5th or 6th order respectively. A folding flat following the field lens is equipped with piezo transducers to provide tip/tilt for flexure compensation at the 0.1 pixel level. Another piezo actuator is installed in the detector head to provide a small amount of focus motion to aid in setting up the instrument. Lenses will be mounted in individual cells using bonded flexures. Finite element analysis (FEA) using Algor v18 shows that the lenses will experience acceptable stress levels (< 500 psi). Although slightly over budget on weight, the overall design of the vacuum dewar and handling system is consistent with operation within the Keck I Cassegrain enclosure. Using heritage from other Keck instruments, the preliminary electronics and software design is also complete, including the adoption of the Application Specific Integrated Circuit (ASIC) technology for detector control.

MOSFIRE is a large and challenging instrument. Nevertheless, analysis of the preliminary design is very encouraging. Although considerable work still remains to be done in the detailed design phase, we believe that the preliminary design meets or exceeds all requirements.

2   INTRODUCTION

One year ago, at the completion of a conceptual study, the W. M. Keck Observatory made a proposal to the Telescope System Instrumentation Program (TSIP) to fund the preliminary design of MOSFIRE, a cryogenic multi-object near-infrared spectrometer for the Keck I telescope. The successful feasibility study had convinced the Observatory that an instrument of this type with important scientific capabilities could be achieved at a realistic cost (<$12M) and on a competitive timescale. TSIP funding of ~$2.4M was received during the summer of 2005 and work began on the project. MOSFIRE is now at the completion of its preliminary design phase, and many of the outstanding issues related to instrument performance and technical risk have been resolved. Following completion of the preliminary design review (PDR), MOSFIRE will be ready to continue through the detailed design and construction phases with installation at the Keck Observatory planned for mid-2009.

A significant event in the funding of MOSFIRE occurred in December of 2005 when the Observatory received a gift of $4.9M from Gordon and Betty Moore towards the design and construction of MOSFIRE. This gift has been offered in annual amounts to complement the anticipated funding from TSIP for years 2 through 5 of the project. With the pending TSIP proposal for phases C and D (detailed design and full scale development) at a level of $4.9M over 4 years, MOSFIRE will be fully funded.

MOSFIRE will provide multi-object spectroscopy in the near-IR (from 0.97-2.45 μm) over a 6.1′ x 3′ field of view with a resolving power of R~3,270 for a 0.7″ slit width (2.9 pixels), or imaging over a field of view (FOV) of 6.14′ with 0.18″ per pixel sampling. With this resolution, MOSFIRE meets one of the driving scientific requirements which is to achieve sufficient spectral resolution to reduce contamination by OH emission lines. Using a single state-of-the-art Rockwell Hawaii-2RG HgCdTe detector with 2K x 2K pixels, MOSFIRE will capture most or all of an atmospheric window in a single exposure for any slit placed within a 6.1′ x 3′ field, and the instrument will employ a single, fixed diffraction grating used in multiple orders (3, 4, 5, and 6) for dispersion in the K, H, J and Y (a.k.a. Z) bands, respectively. A special feature of MOSFIRE is that its multiplex advantage of up to 45 slits is achieved using a cryogenic Configurable Slit Unit (CSU) being developed in collaboration with the Swiss Centre for Microelectronics (CSEM). The CSU is completely reconfigurable under remote control in less than 5 minutes without any thermal cycling of the instrument. MOSFIRE is intended for the Cassegrain focus of Keck I where it can be interchanged readily with LRIS.

MOSFIRE is being developed for the W. M. Keck Observatory (WMKO) by the University of California, Los Angeles (UCLA), the California Institute of Technology (CIT) and the University of California, Santa Cruz, (UCSC). The MOSFIRE Co-Principal Investigators are Ian McLean of UCLA and Charles Steidel (CIT), with other leading roles in optics, instrumentation and software being played by Harland Epps (UCSC), Keith Matthews (CIT) and James Larkin (UCLA). Engineering resources at CIT, UCLA, UCSC and CARA are being combined to build MOSFIRE. The project is managed by WMKO Instrument Program Manager, Sean Adkins.

3   SPECIFICATIONS AND REQUIREMENTS

3.1   Science Requirements

Multi-object spectrographs (MOSs) are required to understand object populations. The Keck community has already used the single object near-IR spectrograph NIRSPEC to study many young stars, galactic center objects, high redshift galaxies, and star formation in obscured galaxies. These observations have revealed much about the properties of small numbers of these objects, including numerous important and unique discoveries. However, detailed knowledge about object populations will elude us until we have hundreds or thousands of near-IR spectra of these objects, spanning a variety of environments and physical conditions. Many of the most exciting applications of near-IR spectroscopy are the most difficult, and will require extremely long integration times even with a 10 m aperture; the ability to observe many objects at once will make such challenging observations feasible for the first time. To pursue such studies the Keck Observatory needs a near-IR MOS.

A compelling science case for a powerful near-IR MOS capability on Keck includes the following broad research areas (details can be found in the Science Case assembled previously for KIRMOS and in the KONSAG report to the Keck Science Steering Committee):

- Young stars
- Galactic center objects
- Brown dwarfs and planetary mass objects in star forming regions
- Low mass end of the initial mass function (IMF)
- Stellar populations in nearby galaxies
- Surveys of star-forming galaxies and AGN at z~1.5-4
- Surveys of passively evolving galaxies beyond z~1
- Star formation and populations of dusty galaxies
- Searches for extremely high redshift objects ("first light" surveys)

The MOSFIRE team concurs that significant progress in these areas requires the capability to obtain hundreds or even thousands of near-IR spectra, and in some cases (e.g., searches for "first-light" objects at z > 7; continuum spectroscopy of distant passively evolving galaxies) little or no progress can be made until extremely deep exploratory spectroscopy in the near-IR is made cost-effective by the multiplex factor.

The importance of a near-IR MOS at WMKO is emphasized in the 2004 report from the second community workshop on the ground based O/IR system (Alcock et al. 2004) which states: "For example, many fields (e.g., young stars, initial mass function, high z galaxy studies, searches for first light objects, stellar populations, etc.) require near-IR spectra of hundreds or thousands of very faint objects to characterize their populations. Completing such surveys will require hundreds of nights, so it is very valuable to have visible and near-IR multi-object spectrographs (MOSs) on several large telescopes."

Many of the design decisions taken for MOSFIRE have been driven by experience in using NIRSPEC and other single slit instruments for pilot programs drawn from those listed above. In particular the need to be able to achieve spectral resolutions R>3,000 with slits sized for objects that are well resolved even in typical near-IR seeing conditions (relevant for all of the science involving distant galaxies) was considered to be of the highest priority. For example, extensive spectroscopy of faint galaxies (K~20-22.5) at redshifts 2 < z < 2.6 (placing the H-alpha line in the K-band window) by Erb et al. (2006) has shown that in typical seeing of 0.4-0.5″ the optimum slit width is ~0.8″ at which slit losses are still 40-50% (typically only ~20% of the H-alpha light would fall within a 0.4″ slit). Obtaining useful spectra in the J and H bands for the same objects has been extremely difficult, since the resolution of NIRSPEC with a 0.76″ slit is only R~1,300, at which only ~10% of the H-band window is free of strong OH emission features (e.g., Martini and DePoy 2000). The typical line widths of the same galaxies are σ~80 km s^{-1}, so that the emission lines are not well resolved at R~1,300 (FWHM~230 km s^{-1}) and dynamical inferences are therefore extremely uncertain. This example is illustrative of the need for a large Rθ product to achieve the maximum sensitivity for faint objects, *particularly resolved objects*, or for non-optimal seeing conditions. Of course, in achieving R=3,000 with a 0.75″ slit MOSFIRE is also capable of higher spectral resolution up to an implied maximum of R~4,800 with a 2-pixel projected slit (0.48″). This resolving power may not be obtained due to under-sampling, but spatial dithering can be used to improve sampling, making MOSFIRE a powerful instrument for point sources or brighter resolved objects for which the still-higher resolution is scientifically important.

Wide-field imaging is also very important for tackling the major problems in the above scientific areas, particularly when extremely deep near-IR imaging exposures are required to identify potential spectroscopic targets, or to achieve depths that are not practical using smaller telescopes or telescopes placed at warmer sites. While a number of 4 m-class telescopes are being outfitted with wide-field near-IR imaging capabilities, for many anticipated MOSFIRE programs the needed imaging depths would require heroic efforts on 4 m-class telescopes, whereas they would be routine using MOSFIRE's imaging mode. Such imaging capability is needed to identify candidates and deduce physical properties of objects in order to take maximum advantage of Keck time and ensure the highest scientific yield of MOS spectra. Furthermore, the Keck telescopes command uniquely high sensitivity in wide-field imaging surveys due to their large apertures, excellent seeing and cold environment.

3.2   Flow Down of Science Requirements to Technical Requirements

In order to establish a set of realistic requirements and goals consistent with the science goals and which reduce cost wherever doing so does not degrade the scientific utility of the instrument, the MOSFIRE team has simultaneously considered a large number of scientific and technical issues.

The key MOSFIRE design choices are summarized in Table 1, and the science-driven rationale for these choices is discussed briefly in the following sections.

Wavelength coverage	0.97–2.45 μm; fixed grating used in orders 6,5,4,3 (Y, J, H, K)
Spectral Resolution	$R\theta$=2290 $\Rightarrow$ R=3270 w/0.7″ slit, (2.9 pixels)
Simultaneous Wavelength Range	Coverage is 0.45 μm (21%) in K band; 1.97-2.42 μm for a slit at the center of the field; H band coverage 1.48-1.81 μm for the same slit
Pixel Scale	0.18″ in imaging mode
Field Size	6.1′ slit length, 3′ width, >18 arcmin^2; 6.1′ field for imaging
Multiplex	Cryogenic Configurable Slit Unit (CSU): ~45 remotely configurable slits each 7.3" long; configurable as a smaller number of longer slits. Each slit width can be adjusted arbitrarily.
Image Quality	Design delivers < 0.25″ rms diameter images over 0.97–2.45 μm with no re-focus.
Stability	<0.1 pixel residual image motion at detector over 2 hr observation. Open-loop flexure compensation using tip/tilt mirror, look-up table.
Guiding	Optical CCD guider, exterior to the cryostat. Must cover at least 7 arcmin^2. Any significant relative motion between guider and detector must be removed by the flexure compensation system.
Throughput: spectroscopy	>35% not including telescope, on order blaze
Mask configuration time	<5 minutes for full re-configuration; goal <2.5 minutes
Filters	Minimum complement is order sorting filters for K, H, J, Y; additional Ks photometric filter for imaging. Goal: up to 5 additional photometric broad or narrow-band filters.
Accessible Pupil	Optical design allows for an accessible pupil image so that a suitable cold mask can be used to minimize stray thermal radiation.
Detector	2048 x 2048 Rockwell Scientific Hawaii-2RG and ASIC; 18 μm pixels, long-wavelength cutoff @2.5 μm; low charge persistence; highest QE

Table 1: *Summary of the MOSFIRE design parameters*

3.2.1 Spectral Range

To complement faint object MOS capabilities at optical wavelengths, and to support the range of science envisioned for MOSFIRE in both imaging and spectroscopic mode, spectral coverage must extend from the silicon CCD cutoff at ~1 μm through the critically important K-band atmospheric window (~2.4 μm). Spectroscopic observations beyond wavelengths of ~1.5 μm require a cryogenic instrument in order not to be compromised by thermal background in the instrument.

3.2.2 Spectral Resolution

Spectral resolution serves a two-fold purpose: first, there is a minimum resolution required to allow measurement of spectral features or to resolve kinematic signatures for faint objects; second, a minimum resolution is required for maximum sensitivity because, over most of the 1-2.5 μm range, the background is dominated by discrete OH emission lines and not by sky continuum. There is no perfect resolution that optimizes sensitivity for all applications simultaneously. However, most studies have concluded that R~3,000 is required for effective OH suppression over substantial fractions of each atmospheric band, particularly in the J and H bands (e.g., Martini and

DePoy 2000). R~3,000 is also required for measuring radial velocities to ~10 km s^{-1}, velocity dispersions down to σ~30-40 km s^{-1} as required for intrinsically faint galaxies, and for providing access to unique spectral features in Galactic sources. Although seeing in the near-IR can be in the 0.3″-0.4″ range on Mauna Kea, many potential targets for multiplexed spectroscopy are resolved, and would suffer from significant slit losses (see discussion above) with very narrow entrance slits. Thus, R>3,000 must be achieved with a ~0.7″ slit that we believe will be the most commonly used aperture size for faint object work. The current design achieves R=3,270 using a 110.5 line/mm grating similar to the one made for the Gemini GNIRS spectrometer; for the commonly-quoted 2-pixel projected slit (0.48″ for MOSFIRE) the nominal resolution is R=4,770. For a given slit width, the resolution achieved is twice that of the Flamingos II instrument for Gemini South or the MMIRS instrument for MMT/Magellan.

3.2.3   Configurable Slit Unit

While the principal reason for adopting a configurable slit unit (CSU) instead of machined or laser-cut focal plane slit masks is to avoid design and operational issues that would be very costly in the long term, and would require frequent cryogenic cycling of a separate fore-dewar in order to install and remove focal plane masks, there are also scientific advantages to configuring the masks remotely. It will be possible for users to reconfigure masks in real-time to adjust to changing conditions (e.g. narrowing or widening of slits as seeing conditions change) or to allow for immediate reaction to discoveries or required changes in strategy in the course of executing an observing program. Flexibility is particularly important at WMKO, which is likely to remain classically scheduled into the foreseeable future. Optimal use of observing time and the pursuit of higher risk or experimental programs will benefit significantly from a CSU. The CSU allows for deployment of slits over the full imaging field of view of the instrument (6.8′ diameter field projected onto a 6.14′ square detector).

The disadvantages of a CSU compared to disposable focal plane masks, are that it will not be possible to use "tilted" slits (where the angle of each slit is different to follow the major axis of targets), or to place more than 1 slit on the same row (for higher multiplexing at the expense of spectral coverage). The former is unlikely to be used much for near-IR work because nodding along the slit is likely to be required for accurate sky subtraction. The proposed CSU will have a bar pitch of 5.8 mm and this allows an acceptable slit length of 7.3″ in the Keck f/15 focal plane and provides for up to 45 slits within the MOSFIRE field of view. In assigning slits to targets of very high surface density (>5 arcmin^{-2}), it should be possible to assign every slit to an object and still allow for small telescope nods along the slits for improving background subtraction. For significantly lower target surface density, a smaller number of objects will be accommodated, and adjacent slits can be combined to form a longer slit with no dead regions in between, so that multiple (continuous) slits of arbitrary length can be constructed in ~8″ intervals.

Figure 1 illustrates an example case in which bars have been configured to place slits on high redshift galaxies in the redshift range z=2-2.6 (with a surface density of 5 arcmin^{-2}). The field position was held fixed and targets were not allowed to be closer than 2.5″ to the end of a slitlet. When no suitable target was accessible to a particular bar within ±2′ of the center of the MOSFIRE field, a second search was done using 2 adjacent bars to form a slit of length 15.3″. In this

particular example, a total of 35 targets (of 144 total available targets in the 6.1′ by 4′ region) are observed with the mask configuration, including 10 objects observed with 15.3″ slits rather than single bar (7.3″) slits. In practice, more optimal solutions can be obtained using prioritized object lists, with PA and telescope pointing allowed to float as a free parameter. It should be noted that with the same telescope position and PA, only about 10% fewer objects are observed than in the (more conventional) case where slits could have arbitrary length with a minimum of 7.3″; in other words, the fixed format of the CSU bars makes only a small compromise in terms of the efficiency of observing targets. For targets with lower surface density on the sky, the "quantized" nature of the slit lengths will have a still less important effect on efficiency.
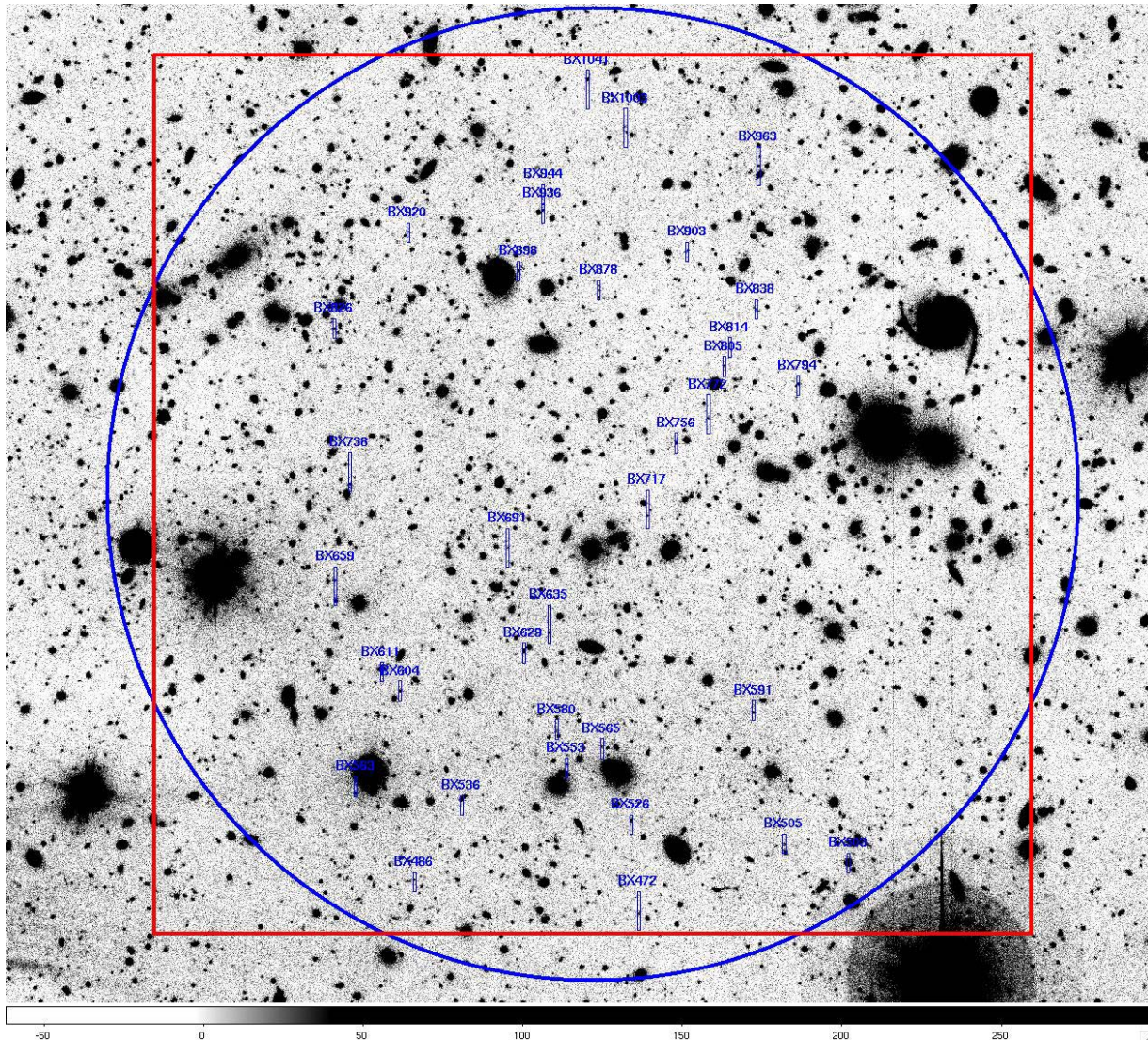
Figure 1: *The MOSFIRE layout on the plane of the sky.*

In Figure 1, the red square represents the field of view of the detector (6.14′ x 6.14′) while the blue circle is the field of view of the collimator (6.8′ diam.). In direct imaging mode, one obtains

images over the region of intersection of the two (i.e., only the corners are vignetted). Slits may be placed anywhere within the same region for spectroscopy. The labeled slits are distributed within ±2′ of the field center in the X-direction.

3.2.4   Field of View and Spectral Coverage

There is a strong desire to achieve wavelength coverage of at least a full atmospheric band while preserving the spectral resolution. This is difficult to achieve without a mosaic of detectors in the camera focal plane. For reasons of detector cost, increasing difficulty in the optical design, the cost of larger optics, and the optical performance impact, there was a strong impetus to map the spectral format onto a single 2K x 2K detector. Here there was some leeway to trade spatial sampling for spectral coverage (e.g. using more focal reduction), although this too is limited by the difficulty in designing extremely fast cameras with acceptable performance. A plate scale of 0.18″/pixel was the initial design goal, to provide reasonable sampling of the typical near-IR seeing of ~0.5″ for both imaging programs and for spatial resolution along slits. In the MOSFIRE case, the design choice of a reflection grating in the manner we are proposing, with an anamorphic magnification factor of 1.34, provides additional effective focal reduction in the dispersion direction, thus gaining spectral coverage without sacrificing spectral resolution. As a result, one can place a slit anywhere within a 6.1′ x 3′ field of view and still record essentially all of each atmospheric window on a single detector. The effective spatial sampling in the dispersion direction is 0.24″/pixel, so that the projected slit will be 2.9 and 2.1 pixels respectively for slits of 0.7″ and 0.5″. Thus, the proposed configuration meets the desired goals for spectral resolution and spectral coverage on a single detector, eliminating the complication of spectral and/or spatial "gaps" that occur in the case of a detector mosaic and which make data reduction considerably more complex.

The locations of spectra in each of the four MOSFIRE spectral bands are illustrated in Figure 2 for a set of 45 slits randomly placed within a 6.1′ x 3′ field. The black square outline represents the 2K x 2K detector. In the K and H bands, a fixed grating tilt centers the spectra on the detector, and only a small amount of wavelength coverage is lost for slits at the most extreme X-positions. The spectral format in the Y and J bands is less well-centered, and here we show in the lower panels of Figure 2 the spectra that result if the same slit positions are moved by 60″ (to the right) in the telescope focal plane; this is easily accomplished with the CSU and is accommodated by the spectrograph optics. Note that wavelengths at the short end of the 5th order (J) and 6th order (Y) are recorded in the 6th order and 7th order, respectively (in blue), so that missing wavelengths in the nth order are recorded in order (n+1).

Control over the grating tilt could re-center the spectral format for Y and J band spectra, but the stability gained by maintaining a fixed grating angle (in addition to saving the cost of another cryogenic mechanism) is seen as a compelling advantage. A decision has been made to fix the grating tilt so as to center K and H band spectra for slits placed at the center of the field, and to control the Y and J band spectra using shifts of the slits in the focal plane, as illustrated in the Figure 2.
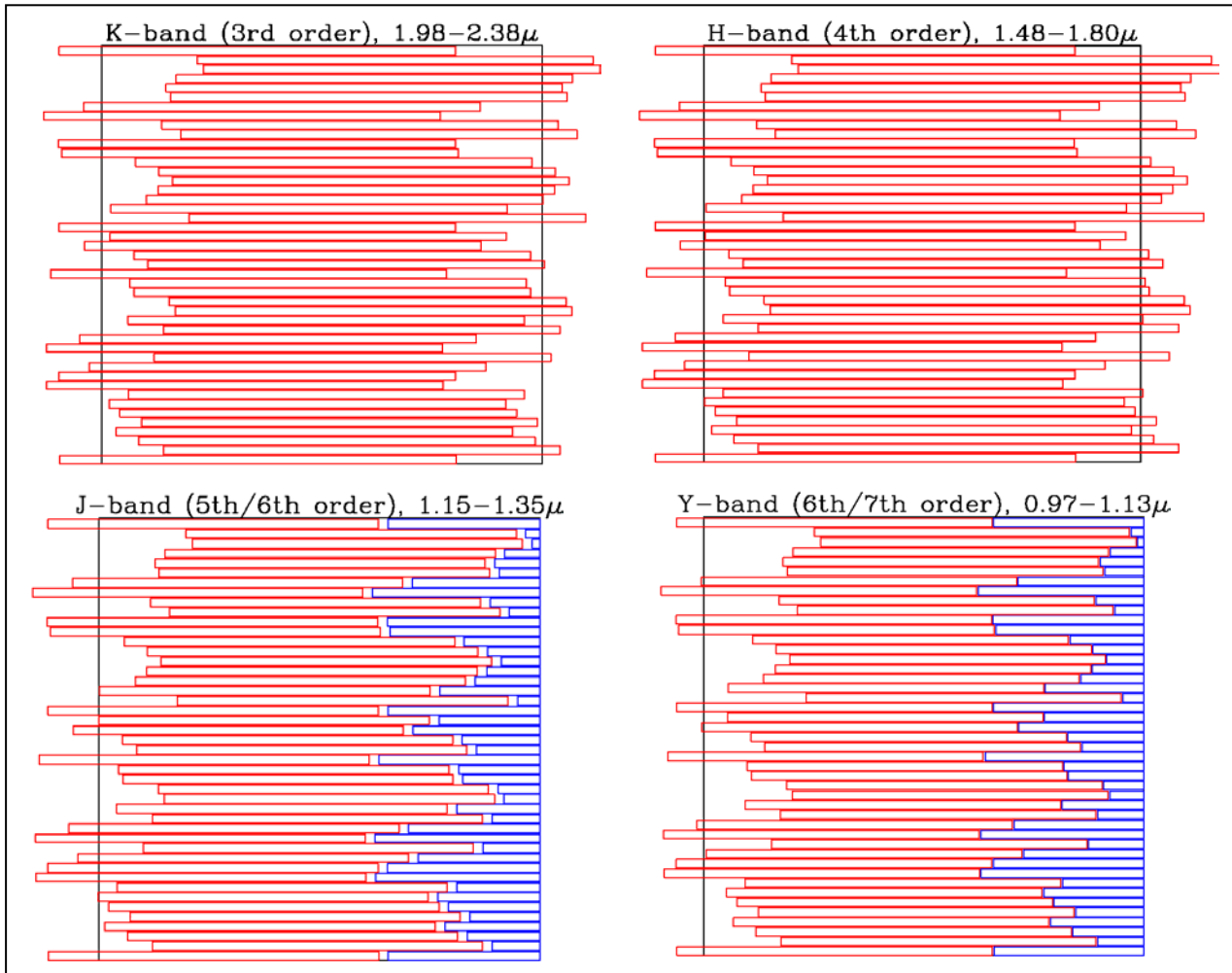
Figure 2: *Spectral format for 45 randomly generated slits deployed over a 6.1′ x 3′ field. The slit positions were shifted by 1′ in the focal plane for J and Y bands.*

Ray-tracing of the end-to-end telescope plus MOSFIRE optical design has shown that slits placed anywhere within the MOSFIRE imaging field maintain very good spectroscopic image quality. This flexibility also allows one to ensure that a particular wavelength is recorded for every slit, or to obtain spectra of objects distributed over a larger field at the expense of uniform spectral coverage. An example of a mask using objects distributed over a 6.1′ x 4.5′ field in the K-band is shown in Figure 3. More than 80% of the K-band spectrum is covered on an average slit.
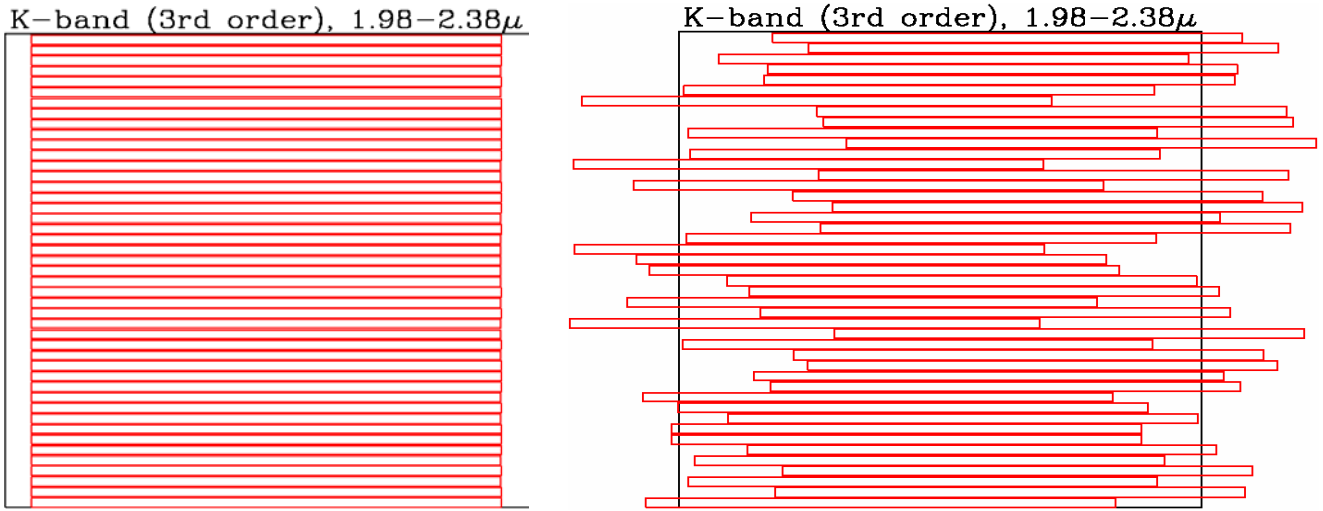
Figure 3: *Spectral format for 45 slits all at the central position (left) and 45 randomly generated slits deployed over a 6.1′ x 4.5′ field.*

3.2.5 Spectrograph Stability

MOSFIRE will be background-limited in all of its modes of operation, and thus the spectral sensitivity is ultimately limited by the intensity of the background and by the precision with which the background can be subtracted. With the exception of the long wavelength end of the K-band window, the background is dominated by atmospheric OH emission. Unless the spectrograph is very stable over time, spectral regions in the vicinity of bright OH lines will be rendered unusable by systematic errors in sky subtraction. Our goal for residual flexure *after* correction is 0.1 pixel (<3% of a spectral resolution element) with the maximum acceptable value <0.3 pixel. This requirement, together with the spectral resolution requirements above, is chosen to maximize the sensitivity and useful spectral regions by getting between OH lines and then insuring that sky subtraction residuals will be minimized in regions close to OH lines. The viability of controlling instrument flexure at this level using an open-loop scheme has been demonstrated already in ESI, another Keck instrument (Kibrick et al. 2000, 2003). This desired level of stability is also necessary to allow for efficient acquisition of multi-slit or long slit spectroscopic targets, and for the use of calibrations (e.g., flat fields) that may be obtained during the afternoon rather than during the night.

3.2.6 Acquisition and Guiding

External CCD-based guiders have been used successfully on most of the Keck instruments, including the near-IR instruments NIRC and NIRSPEC. Placing a fixed guider outside of the MOSFIRE cryostat, viewing a separate portion of the f/15 focal surface, was another up-front decision made to avoid the cost and complexity of internal guiders. Based on experience with NIRSPEC, suitable optical guide stars can be found even at the Galactic poles during full moon if

the guider field is ≥ 7 arcmin^2 (S.B. Larsen 1996). It is conceivable that guide stars will be scarce in the most heavily obscured regions of the Galaxy; here it is anticipated that the flexibility to rotate the position angle of the spectrograph (providing access to an annulus several times larger in sky area for potential guide stars) will allow optical (I band) guiding even in the most extreme regions. It is anticipated that field acquisition will be done using the guider for coarse alignment. The guider coordinate system and its relation to the near-IR focal plane should be known to better than a few tenths of an arc second. During mask design a guide star will be identified which, if placed at a pre-determined guider pixel, would place several fiducial objects (generally, brighter stars in the field) within apertures on the focal plane mask that are also pre-designed. A direct image of the field, through the focal plane mask, can be used to calculate the necessary offsets in rotator angle and RA/Dec for fine mask alignment. In principle, the CSU would allow one to deploy slits used for fine alignment onto science targets, so that no slit mask "real estate" would have to be used only for alignment objects. This scheme is very similar to methods used on LRIS and DEIMOS, and we anticipate adapting existing slit mask alignment software.

3.2.7   Detector & Sensitivity

On the basis of available information on performance, and the perceived low risk in procurement, the current MOSFIRE optical design is predicated on the 18 μm pitch of the Rockwell Scientific Hawaii-2RG detector. The advertised superior performance of the Hawaii-2RG in terms of charge persistence and dark current relative to the earlier generation of Hawaii-2 devices makes it a far superior choice in an instrument that depends on being background limited and as free as possible from sky subtraction artifacts. High quantum efficiency (QE >65%) will be required to achieve our instrument throughput goals. We have included the funds necessary to allow selection from among multiple devices.

The detection rate for sky in between OH lines in the darkest parts of the Y, J, and H bands (for even the most optimistic estimates) is 0.3 e$^-$/s/pixel for a 0.7″ slit assuming ~3 pixel sampling in the dispersion direction (R=3,270). A dark current of <0.05 e$^-$/s/pixel and an effective read noise below ~5e$^-$ would easily result in background-limited performance for most exposures; typical spectroscopic integrations are expected to be in the range 600 to 1800 s. Other researchers have recently demonstrated read noise performance in this range when using multiple sampling readout techniques, and have shown that charge persistence is no longer a significant issue. Persistence is very important for an instrument used as both an imager and a spectrometer.

The goals for total throughput of MOSFIRE from the slitmask to the detector have been set to match that of the best single-slit near-IR spectrometers (e.g., NIRSPEC). Table 2 summarizes the estimated throughput of MOSFIRE, showing that the goal is achievable as long as good AR coatings (<1.5% reflection losses per surface) can be obtained for the optics.

Component	Transmission/Reflectance		
	1.0µ	1.6µ	2.2µ
Dewar Window(double)	0.95	0.95	0.95
Collimator (6 x 2 surfaces)	0.84	0.84	0.84
Fold flat (Gold)	0.99	0.99	0.99
Camera (7 x 2 surfaces)	0.84	0.84	0.84
Internal transmission of all glasses	0.94	0.92	0.77
Filter	0.90	0.90	0.85
Detector (Hawaii2-RG)	0.80	0.80	0.80
Net Imaging Throughput	**0.45**	**0.44**	**0.35**
Grating (on blaze)	0.83	0.83	0.83
Net Spectroscopy Throughput	**0.37**	**0.37**	**0.29**

Notes to table: Average reflection loss is 2.4% per surface for ZnSe and 1.2% per surface for all others.

Table 2: *MOSFIRE Throughput Estimate*

Table 3 summarizes the estimated sensitivity of MOSFIRE using conservative estimates of the night sky background between OH emission lines (for spectroscopy) and broad band for imaging.

Passband	Spec. Sky Brightness, mag arcsec^{-2} Vega (AB)	Vega (AB) mag for S/N=10 in 1000 s, R=3270 with 0.7″ slit	Line flux for S/N=10 (unresolved line) in 1000s, R=3270 (erg s^{-1} cm^{-2})	Imaging sky brightness, mag arcsec^{-2} Vega (AB)	Vega (AB) mag for S/N=10 in 1000s , Broadband
Y (0.97-1.13µm)	17.3 (17.9)	20.9 (21.5)	0.9 x 10^{-17}	16.3 (16.9)	24.4 (25.0)
J (1.15-1.35µm)	16.8 (17.7)	20.4 (21.3)	0.8 x 10^{-17}	15.7 (16.6)	23.7 (24.6)
H (1.48-1.80µm)	16.6 (18.0)	20.1 (21.5)	0.5 x 10^{-17}	13.4 (14.7)	22.5 (23.9)
K (1.95-2.40µm)	14.4 (16.3)	18.6 (20.5)	0.9 x 10^{-17}	13.2 (15.0)	21.7 (23.6)

Notes to table: spectroscopic limits assume 0.05 e-/s dark current and effective read noise of 4e-/pixel, with background appropriate for spectral regions between OH emission lines, evaluated over a 3 pixel resolution element and assuming a 0.5 arcsec^2 extraction aperture. Imaging limits assume 3 x 3 pixel (0.54″) aperture for a point source under good seeing conditions.

Table 3: *Predicted MOSFIRE Spectroscopic and Imaging Performance*

3.2.8   Filter Complement

Given our design choice to use a fixed reflection grating in multiple orders, order sorting filters are essential to the MOSFIRE design. The minimum filter complement would be passbands designed for spectroscopy in 3rd, 4th, 5th, and 6th orders of the grating, corresponding closely to the photometric K, H, J, and Y passbands. The MOSFIRE filter wheels accommodate a total of 10 filters in two wheels (each carrying 5 filters and an "open"). It is anticipated that a K$_s$ filter for imaging will also be installed. More specialized intermediate-band filters will require funds.

3.2.9   Lyot Stop

Because MOSFIRE has been designed to achieve background-limited performance across its entire wavelength range, and as much of the science case for MOSFIRE depends on sensitivity, the design accommodates a two-position Lyot stop. The stop will circumscribe the pupil for shorter near-IR wavelengths to minimize vignetting and maximize throughput, but it will be stopped down to the shape of the pupil image, and then track the rotation of the pupil image, for longer wavelengths where stray thermal radiation would significantly increase the background (primarily for K-band observations).

3.2.10   Calibration Plans

Given the difficulty in producing internal illumination that adequately simulates the telescope illumination over MOSFIRE's large field-of-view a decision has been made to have no internal calibration lamps. Instead, we will rely on night sky lines for wavelength calibration (as is already done for other intermediate resolution NIR spectrometers) and dome illumination for spectroscopic flat fields. For flux and/or telluric absorption calibration using observations of stars there is clearly no practical way to place a standard star on every slit of every multi-slit combination made during the course of a night. For this reason, a long-slit mode of operation is planned in which it will be straightforward to acquire a calibration star onto one or several slits in user-selected portions of the focal plane. The optical quality of MOSFIRE in spectroscopic mode is expected to be sufficiently uniform throughout the useable portion of the telescope focal plane that telluric absorption stars obtained at any field position should provide good telluric feature calibration on any other slit provided that care is taken with flat-fielding.

One of the aims in requiring that MOSFIRE provide very good flexure correction is so that (dome) flat fields may be obtained during the afternoon or early morning hours so as not to require calibration exposures during the night. For those observers who would require flat fields temporally adjacent to their spectroscopic observations, it will be possible to rotate the dome in front of the telescope while the latter is at the same elevation and has the same instrument rotator angle as for the science observations.

More detailed calibration plans, and their integration with the mask design and data reduction software, will be developed during the detailed design phase.

3.3   Competing Instruments

To reinforce the case for the development of MOSFIRE, we have also reviewed the proposed capabilities of the instrument in the context of the near-IR MOS instruments under development at other observatories as shown in Table 4. The information in this table is taken from the most current information available on each instrument. All of the instruments except for KMOS-1 and EMIR use interchangeable slit masks. In the case of instruments with interchangeable slit masks the "object multiplex" column is somewhat arbitrary, but represents the typical number of slits that we expect will be used. The costs listed in Table 4 are approximate, and they may not all be directly comparable (e.g., MMIRS costs do not include observatory costs).

Telescope	Name	Spec. FOV Imag. FOV (arc min.)	Wavelength Range (μm)	R @ slit width	Object Multiplex	Pixel size, (arc sec.)	Number of 2K x 2K HgCdTe Detectors	Cost Est. $ M	Expected (Actual) Completion Year
Gemini-S	Flamingos-II	6 x 2 6 dia.	0.9 – 2.4	1540 @ 0.7"	>20	0.18	1	6.5	2006
GTC	EMIR	6 x 4 6 dia	0.9 – 2.5	3430 @ 0.7"	45**	0.2	1		2008
Subaru	MOIRCS	7 x 4 7 x 4	0.9 – 2.5	1030 @ 0.7"	~50	0.12	2		2004 (2005)
MMT/ Magellan	MMIRS	6.8x 2 6.8 x 6.8	1.0 – 2.5	1710 @0.7"	>20	0.2	1	3.8	2006
ESO VLT	KMOS-1	7 dia. 2"x 2"*	0.9 – 2.5	4000***	24	0.2	3	20	2010
Keck I	MOSFIRE	6.1x3 6.1x 6.1	0.97 – 2.45	3270 @ 0.7"	45**	0.18	1	12	2009

* = per IFU   ** = configurable "sliding slits"
*** = IFU, 2 pixel spectral sampling

Table 4: *Competitive Near-IR MOS Instruments*

FLAMINGOS, the predecessor of FLAMINGOS II, is one of only two near-IR MOS which has been completed, but is has been used overwhelmingly in imaging mode to date. Furthermore, very few of its data have been published. MOIRCS, the second near-IR MOS to be completed has so far only been commissioned in broadband imaging mode. Its spectroscopic capabilities will be very much reduced compared to MOSFIRE due to its low spectral resolution.

MOSFIRE offers a spectral resolution of R=3,270 with a slit width of 0.7″. Most of the competing instruments (with the exception of EMIR, which has capabilities similar to MOSFIRE) can only achieve this resolution with much smaller (0.3″ to 0.4″) slit widths. In the commonly quoted median seeing conditions (0.5″) these instruments will be at a considerable disadvantage in efficiency. The narrower slit widths also have important implications for guiding and astrometry that are also likely to reduce efficiency. When all of these factors are combined MOSFIRE is

readily understood to be the more capable instrument in terms of routinely useable spectral resolution and multiplex efficiency.

3.4   Preliminary Specifications

Table 1 above defined the basic, first level specifications for MOSFIRE. These parameters formed the input for the preliminary optical design and analysis. Several additional parameters can now be added and these are summarized in Table 5.

Parameter	Requirement (or Goal)
Optical focus	Achromatic
Collimated beam size	125 mm (derived from requirement on R)
Pupil image	Accessible for Lyot stop & mechanism
Filters	Diameter ~170 mm, min of 5, max of 10 filters.
Guider	1024 x 1024 CCD with 0.164″ pixels, externally mounted, warm optics
Window	No condensation, provide dust cover
CSU	Multiple requirements, see CSEM compliance Matrix
Vacuum enclosure (dewar)	Fits with Keck I Cassegrain volume & weight constraints
Flexure	~3.0 (1.5 goal) pixel shift (uncorrected) over 2 hours
Flexure compensation	10:1 reduction by look-up table & tip/tilt mechanism
Imaging/Spectroscopy mode change	Turret mechanism, fixed grating & mirror, reproducible to 0.1 pixel
Operating temperatures	70 – 150 K
Cool down time	7 – 10 days, closed-cycle refrigeration
Detector dark current	< 0.03 e$^-$/s/pixel
Detector read noise	~ 5 e$^-$ rms (with multiple reads)
Software	Support easy set up of CSU, support flexure correction look-up tables

Table 5: *A set of additional or derived MOSFIRE parameters used for the system design*

3.4.1   System Overview

The scientific and technical parameters for MOSFIRE result in the following basic system components:
1. An optical system to relay the required field of view onto the science detector and a dispersion system capable of achieving the required resolving power
2. A vacuum-cryogenic enclosure (referred to as "the dewar") to contain the opto-mechanical system
3. An opto-mechanical system consisting of:
    a. A support structure for the optical system
    b. A cryogenic cooling system capable of reaching operating temperatures of 120–130 K
    c. A CSU with up to 45 slits
    d. Mechanisms for selection of filters and imaging or spectroscopic mode

e. An internal flexure compensation system
f. A cable wrap
4. An instrument frame and rotator
5. An instrument handler system for installation in the Cassegrain focal station
6. Electronics consisting of:
   a. An IR detector system
   b. Dewar temperature and pressure monitoring
   c. Motion control systems for all mechanisms
   d. An external optical guider system
7. Instrument control software
8. A data reduction pipeline
9. Interfaces to the telescope and observatory systems

We have approached the organization of these components by defining a detailed product structure. The top level of this product structure is shown in Figure 4. A work breakdown structure (WBS) related to the product structure has been developed as well and serves to aid in a bottom up cost analysis.
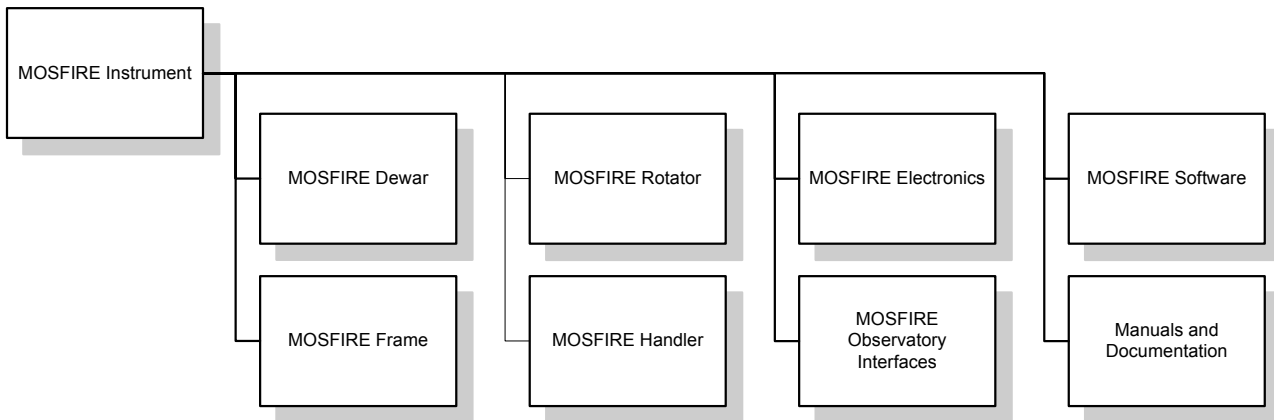
Figure 4: *Top Level MOSFIRE Product Structure*

3.5   Compliance Matrix for Requirements

The Compliance Matrix is available as Appendix document A.3 on the MOSFIRE web site. All other appendices, and documentation from CSEM, are posted on the web site rather than appended to this document.

4 PRELIMINARY DESIGN ACTIVITIES

4.1 Description of major work performed

The top-level objectives of the MOSFIRE project preliminary design phase were defined as follows:

1. Establish instrument technical requirements
2. Develop operational concepts for the instrument
3. Produce preliminary designs for the instrument hardware and software
4. Complete the optical design to the detailed design level
5. Establish the feasibility of the cryogenic configurable slit mask unit
6. Review and update the project plan to completion, including the schedule and budget

Technical requirements have been established through a flow down process from the science requirements, and these requirements, along with the operational concepts provide context for the preliminary designs. The preliminary designs are documented designs for each instrument system, sub-system and component, hardware or software, of sufficient detail to establish through inspection and analysis the feasibility of the proposed design, and the likelihood that the design will meet the requirements. Teams at Caltech, UCLA and UCSC have participated in the instrument design activities, while work on observatory interfaces has been handled by WMKO. Regular monthly project meetings are held and a summary report is provided to WMKO and TSIP each month. All written reports are maintained on the MOSFIRE Team web page, and design activities are documented in those reports and in formal Design Notes.

Areas of highest risk were identified and these were given the most attention. One of these areas was the cryogenic slit mask at the heart of the MOSFIRE design. The cryogenic configurable slit mask unit (CSU) is a fundamental component of the instrument design, and because of this a program to develop and test a prototype of the slit mask unit has been undertaken during the MOSFIRE preliminary design phase. Establishing the feasibility of this design and its ability to meet the requirements is crucial to the success of the MOSFIRE project. Following a study contract during the conceptual design phase, the Swiss Centre for Electronics and Micro Technology (CSEM) was awarded the contract for the development of the prototype CSU during the PDR phase.

The timeline for fabrication of the MOSFIRE optics requires the project to place orders for optical fabrication very early in the detailed design phase. Consequently, the optical design must be complete, or nearly so, at the detailed design level by PDR. This major activity has been led by Professor Harland Epps (UCSC) and has been successful in producing a feasible design.

In addition, using as much heritage as possible from other Keck instruments, especially LRIS and OSIRIS, preliminary designs for all other aspects of the instrument have been developed and analyzed. Due in large part to bureaucratic delays, the PDR phase began later than desired. However, sufficient progress has been made that delivery of the instrument by the summer of 2009 is still feasible and no evidence has emerged that would impact our budget.

5   PRELIMINARY DESIGN

5.1   Optical Design

5.1.1   Description

The underlying guideline for the MOSFIRE optical design is to keep it mechanically compact and as simple as possible to fabricate. A folded, all-spherical design was adopted as the basis of our original proposal for those reasons. During the past year, the preliminary collimator and camera designs shown in that proposal have been refined and brought to a "preconstruction" status. By this we mean that the individual lens forms in the design have been used in thermal and mechanical analyses, which establish that the lenses can be mounted, supported and cooled successfully. The preconstruction designs are also finalized with respect to the size and type of lens blanks that are required, and an initial order has been placed with Ohara Corp. to produce the optical glass required for the camera. Construction design updates will follow the arrival of melt-sheet (refractive index) data for the as-delivered lens blanks.

5.1.1.1   End-to-End Layout

Figure 5 is a depiction of the current overall MOSFIRE layout. All components in the optical path, including the CSU are shown. An optical design for the guider is described in §5.1.1.6.
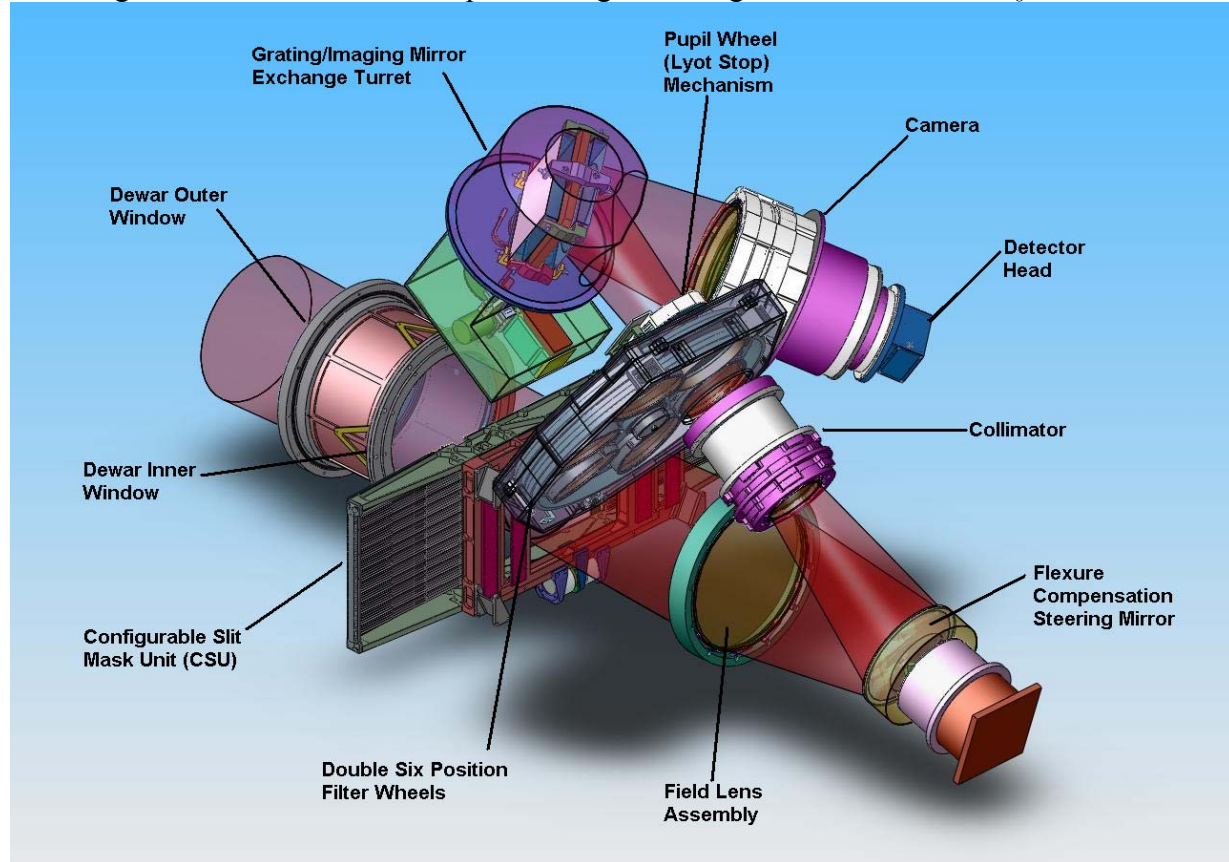
Figure 5: *MOSFIRE Optical Layout.*

5.1.1.2 Dewar Windows

A large (~370 mm full diameter) entrance window is required to accommodate the 6.8′ diameter field of view. This window is located in a tube or snout at the front of the dewar. To withstand the pressure differential under vacuum, while keeping the maximum stress within the "glass" below ~500 psi, an Infrasil window 35 mm thick is required. To prevent condensation forming as the center of this large window cools by radiation, a second thinner (12.7 mm) Infrasil window is located 229 mm away in the vacuum. An aluminum tube between the windows is resistively heated with ~8.4 W to provide radiation to maintain the outer window above the average Observatory dome temperature. Thermal analysis shows that this arrangement will not affect the optical performance and will have a negligible impact on the thermal background.

5.1.1.3 Collimator and Pupil

The collimator is a critical optical component. It must capture a large field of view and it must also produce a sharply focused, accessible pupil image so that a cold Lyot stop can be inserted to eliminate stray thermal radiation. We have refined the lens-element shapes for optimal optical performance and ease of construction, and moved the design from air at room temperature to vacuum at T = 76 K so as to demonstrate that the design will be viable when the actual operating temperature (~120 K to ~130 K) is selected later. Final thermal correction will be made to the design as part of the melt-sheet update for construction. The arrangement is shown in Figure 6.
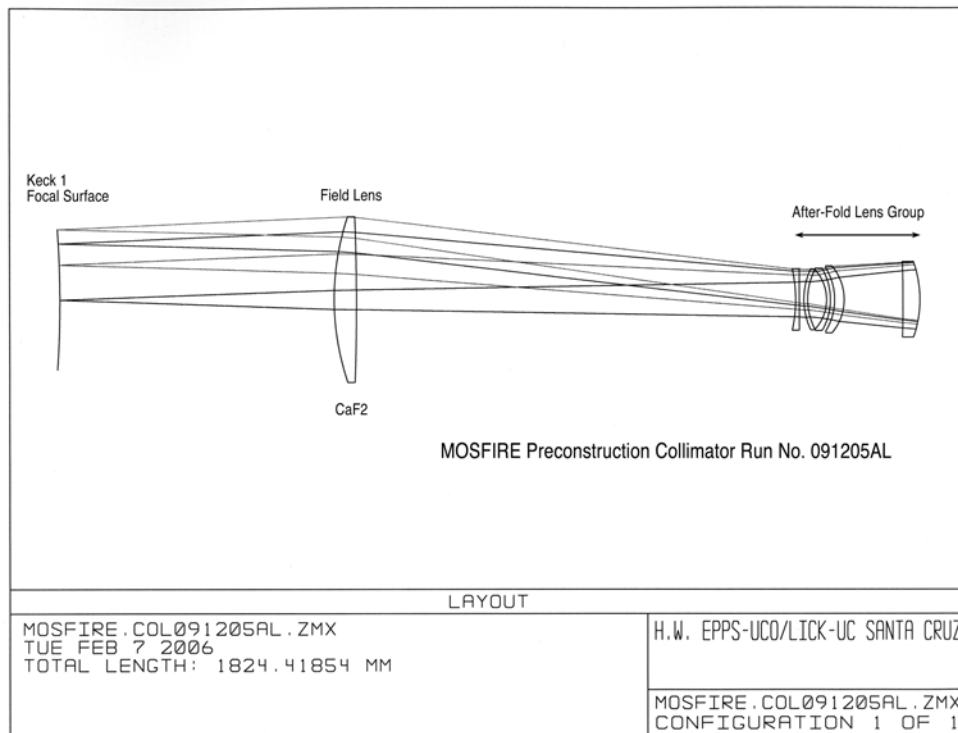
Figure 6: *The 6-element collimator*

The 6-element collimator contains a large field lens separated from a second lens group. A folding flat (not shown) can be placed between these groups. Note the curved Keck focal surface. This curvature (~2.124 m radius) is taken into account in the CSU design.

A close-up view of the collimator's five rear elements is shown in Figure 7, together with the pupil-image location. The pupil diameter is 125 mm as intended and it is stationary to ~2.4% over all field angles. This lens group has been shortened to provide more room for the filter carrier, for the Lyot stop mechanism and for additional compactness of the overall MOSFIRE package. A generic filter has been added as a placeholder.
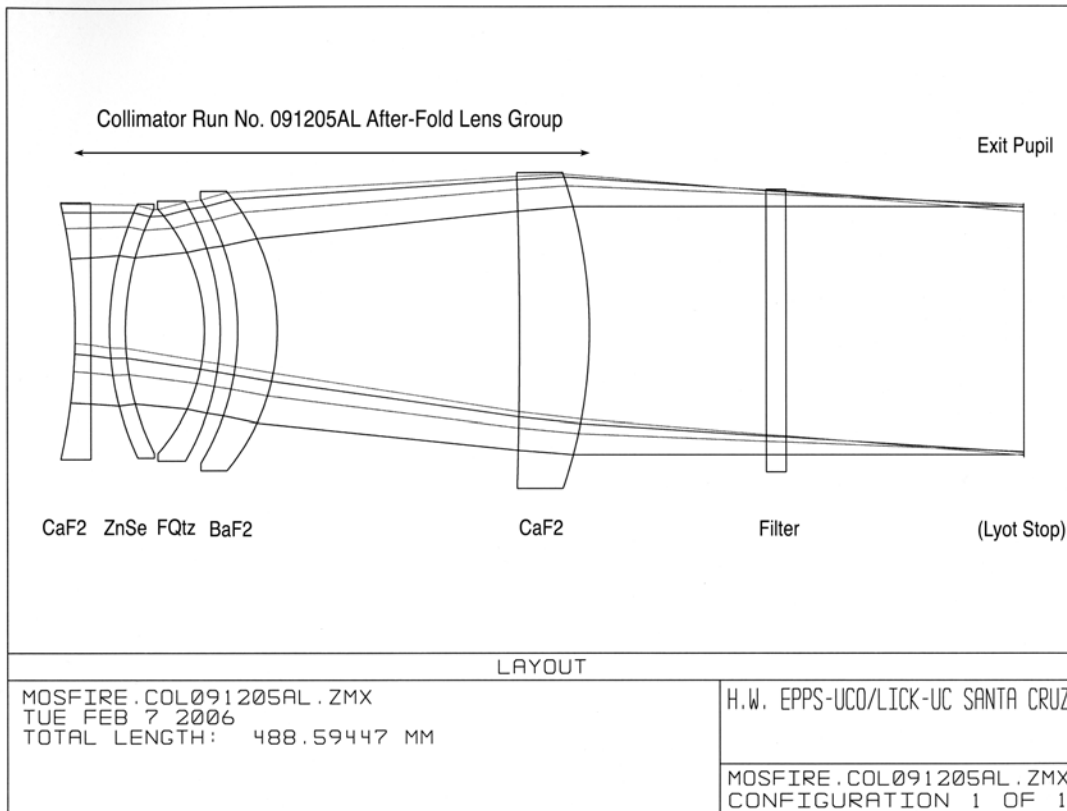
Figure 7: *A close up view of the 5 rear elements of the collimator and the location of the pupil image. The diameter of the pupil is 125 mm. FQtz refers to Heraeus Infrasil-301.*

When re-imaged by a "perfect" camera, the collimator shows rms image diameters of only 0.05″ +/- 0.01″, averaged over all field angles and all wavelengths in the 0.97 μm to 2.45 μm spectral region without refocus, with a maximum lateral color of 0.07″ rms. These residual aberrations are entirely negligible relative to those of the real preconstruction camera.

The collimator's pupil-imaging performance, neglecting diffraction, is illustrated in Figure 8, which shows negligible aberration in the pupil.
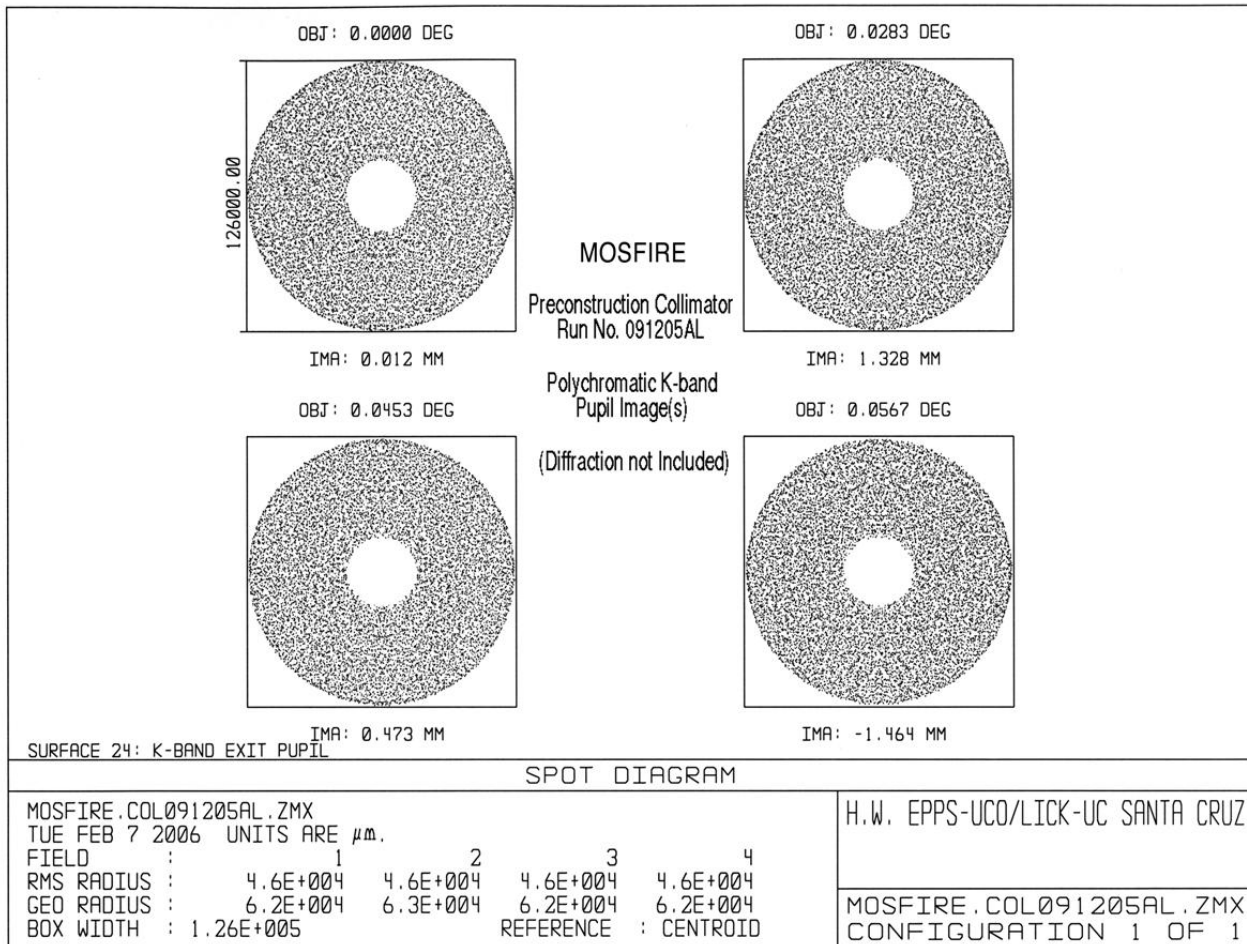
Figure 8*: Polychromatic K-band pupil images without diffraction.*

The images are shown for 0′, 1.7′, 2.72′ and 3.4′ field radii. Only 1.0 mm of pupil smear and ~ ± 1.5 mm of pupil-image walk occur. The box size is 126.0 mm. Diffraction effects from the narrowest (~0.7″) slits will cause larger but acceptable smear.

There is some passband dependent residual axial color (focus error) in the pupil. However that will be dealt with in the Lyot stop design and expected diffraction in the K-band and H-band pupil images will also be taken into account. The Lyot stop design will allow it to be retracted for J-band and Y-band observations where thermal background is not a problem.

We have obtained price quotations for all of the optical materials used in the collimator lens design. We have reviewed the literature and have established reliable cryogenic refractive indices for them also. Smaller lenses made with these materials are already in use in existing IR instruments so we are quite confident they will perform satisfactorily in MOSFIRE.

5.1.1.4 Camera

The camera system is always challenging in applications where the field of view is large and the scale reduction from the telescope image scale is significant. The large (328 mm) distance from the Lyot stop to the grating, combined with the (300 mm) distance from the grating to the camera causes a convoluted, anamorphic, wavelength and field-angle dependent compound-pupil presentation, which further complicates the design. The resulting camera requires a 250 mm focal length and a 270 mm entrance aperture such that it operates at f/0.93 (under-filled), which is unprecedented for a cryogenic 0.97 μm to 2.45 μm micron infrared camera of these dimensions. Its field radius is 6.0 degrees to cover the corners of the Hawaii 2RG array.

Nevertheless, we have produced a 7-element all-spherical preconstruction camera design shown in Figure 9. It satisfies all the goals for MOSFIRE, including the need to provide for direct imaging in the K, H, J, and Y passbands as well as spectral coverage in those passbands for any object located within a rectangle at the telescope focal surface whose dimensions are ±3.06′ along the slits and ±1.5′ perpendicular to them.
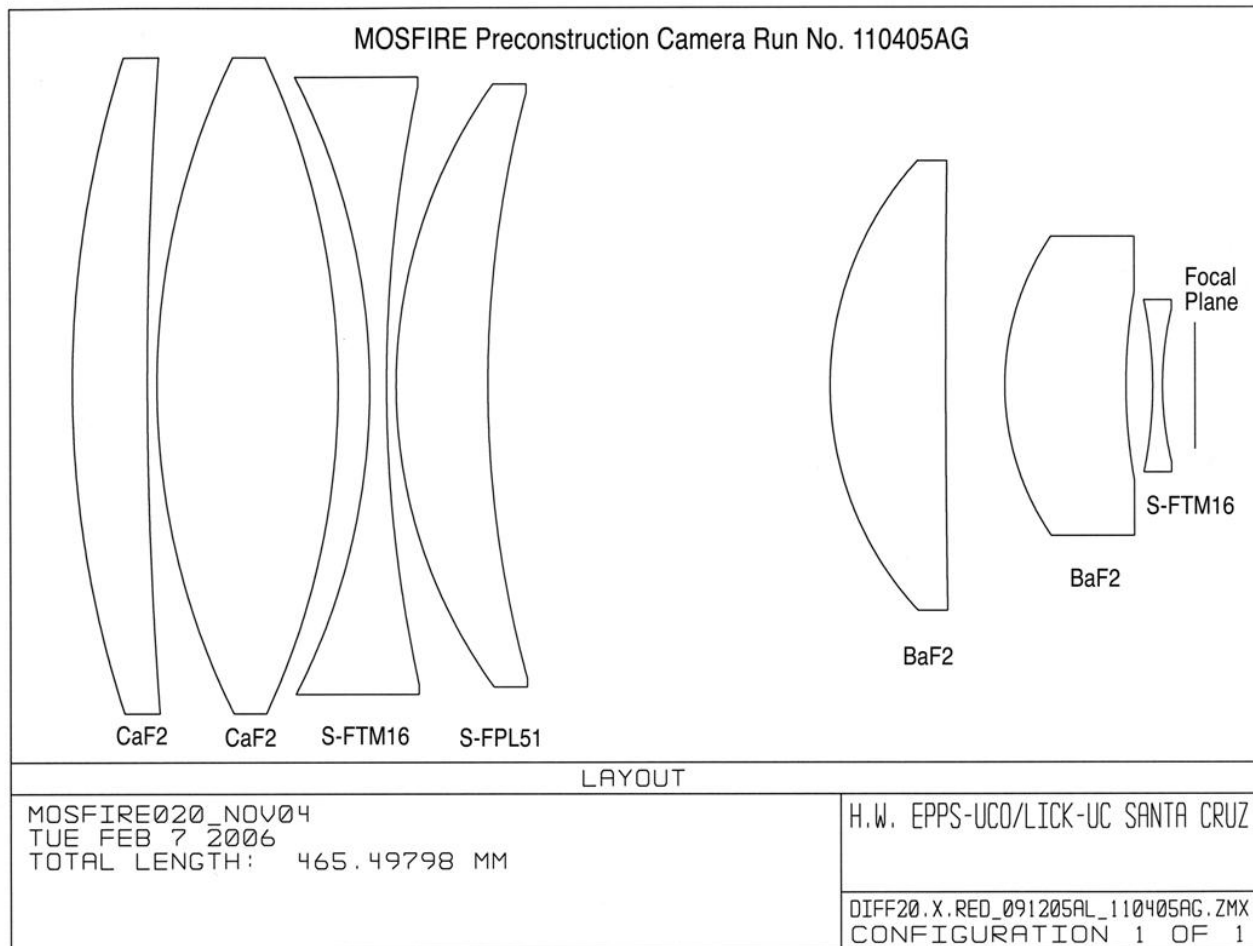
Figure 9: *The 7-element MOSFIRE camera, including field flattener and detector focal plane. For clarity, the rays have been suppressed to better show the lens forms.*
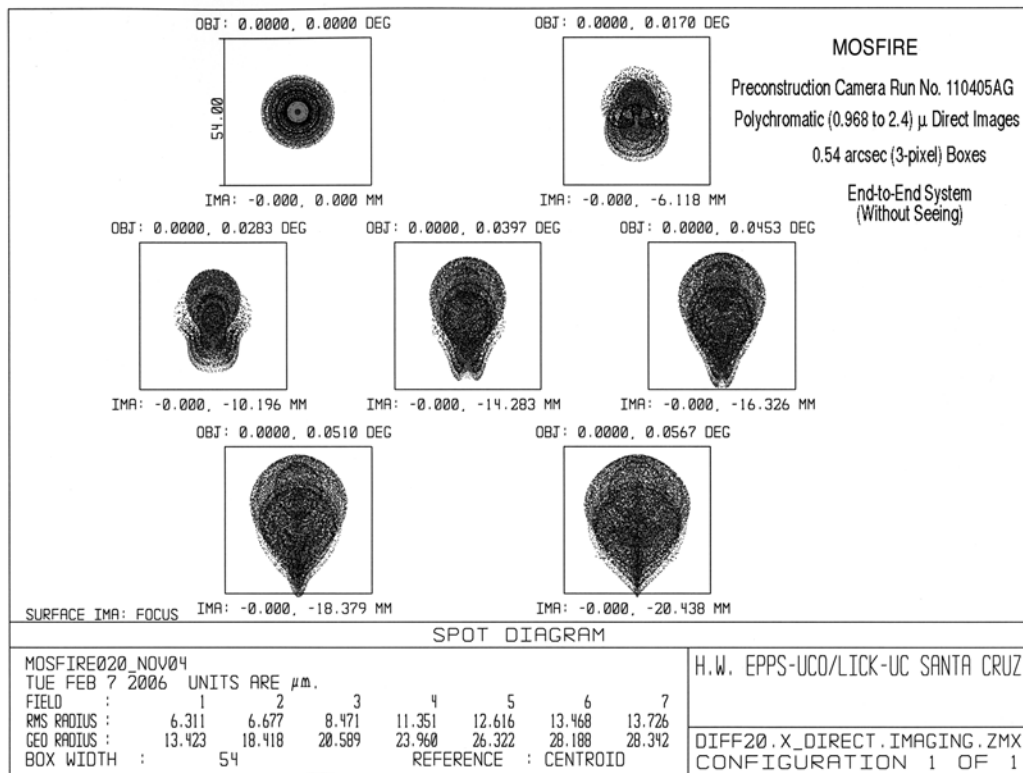
Figure 10: *End-to-end direct-imaging performance spot diagram.*

This spot diagram includes the telescope, collimator and camera in a broad (0.968 μm to 2.4 μm) passband and shows that even at the edge of the 6.8′ field diameter, all of the light falls within a 3-pixel (0.54″) box. Imaging will be even better in the K, H, J, and Y passbands, which can be focused independently with the telescope.

The end-to-end direct-imaging performance of the telescope, collimator and camera combination is excellent, as seen in Figure 10. These polychromatic spot diagrams show wavelengths from 0.968 μm to 2.4 μm plotted simultaneously without refocus, for field angles, which are 0.0, 30%, 50%, 70%, 80%, 90% and 100% of the full 6.8′ field diameter available for direct imaging. The area-weighted average rms image diameters are only 0.29″ ±0.07″.

Image quality in spectroscopic mode is harder to illustrate because of the many possible combinations of object locations and passbands. Furthermore, it is not well described by rms image diameters because the aforementioned anamorphism and compound-pupil presentation unavoidably result in some images whose geometries are asymmetric and irregular, including "tails" and other artifacts. We have adopted a spectroscopic image-quality goal for MOSFIRE, which seeks to put 80% or more of the light in any given image into a (2 x 2) pixel Nyquist sampling box centered on the image centroid. This criterion is appropriate, as it is well known that optics become pixel sampling limited under that condition.

A representative sample of worst-case spectroscopic images was calculated for three objects placed 3.06′ off-axis (at the top end of the slit), with offsets of -1.5′, 0.0′ and +1.5′. A 110.5 groove/mm grating was set to a 42.61 degree angle so as to put 2.18 μm light at field center in 3rd order. To determine whether or not a given image would be counted in the analysis, the criteria adopted were that it must fall on the detector and it must fall within the following wavelength ranges: 3rd-order K (1.95 to 2.45) microns; 4th-order H (1.45 to 1.83) microns; 5th-order J (1.15 to 1.35) microns; and 6th-order Y (0.97 to 1.13) microns. The resulting spectral image energy concentrations (ensquared energy) as percentages in the Nyquist box, averaged over all objects and wavelengths are given in Table 6.

The worst images were mostly at the extreme-wavelength ends of the spectrum and/or at the very corners of the detector. At nearby wavelengths or just a couple of mm away from the corner, those worst-case images got much better. We conclude from the worst-case evaluation that MOSFIRE's spectroscopic imaging performance will be strongly pixel sampling limited in almost all cases.

Passband	Average ensquared energy (2 x 2 pixels),%	Worst case ensquared energy (2 x 2 pixels), %
3rd-order K	90.0 ± 6.3	81
4th-order H	91.3 ± 2.9	88
5th-order J	89.5 ± 4.5	80
6th-order Y	88.0 ± 7.0	77

Table 6: *MOSFIRE spectral image energy concentrations*

5.1.1.5   Grating/Mirror and Filters

A diffraction grating master developed by the Newport/ Richardson Gratings Laboratory for the GNIRS project exists which meets our needs in terms of resolving power. This grating has 110.5 grooves/mm and a blaze angle of 22.0 degrees. The grating blaze allows it to be used in (3rd, 4th, 5th and 6th) orders with suitable blocking filters so as to cover the K, H, J, and Y passbands as with no requirement for a tilt adjustment of the grating. The GNIRS grating is undersized for MOSFIRE so we will purchase a new custom grating that will have 110.5 grooves/mm and a blaze angle of 22.6 degrees. This blaze angle will be optimal for MOSFIRE whose included angle between collimator and camera is 40.0 degrees.

Figure 11 shows the efficiency of the GNIRS grating across the 4th-order H-band as measured in a Littrow configuration. The efficiency is given relative to the reflectance of aluminum. Even when used in the off-Littrow mode at MOSFIRE's 40.0 degree included angle, the performance is excellent. We anticipate that our new custom grating will show comparable efficiency.

A flat mirror, mounted on a turret frame with the grating on the opposite side, can be rotated into the beam so as to switch between spectroscopic and imaging modes. A double filter wheel can

accommodate additional filters. For example, it is more efficient to use the Ks filter than the K filter for direct imaging.

1601-1, 110.5 g/mm, 22.0 deg. m=4
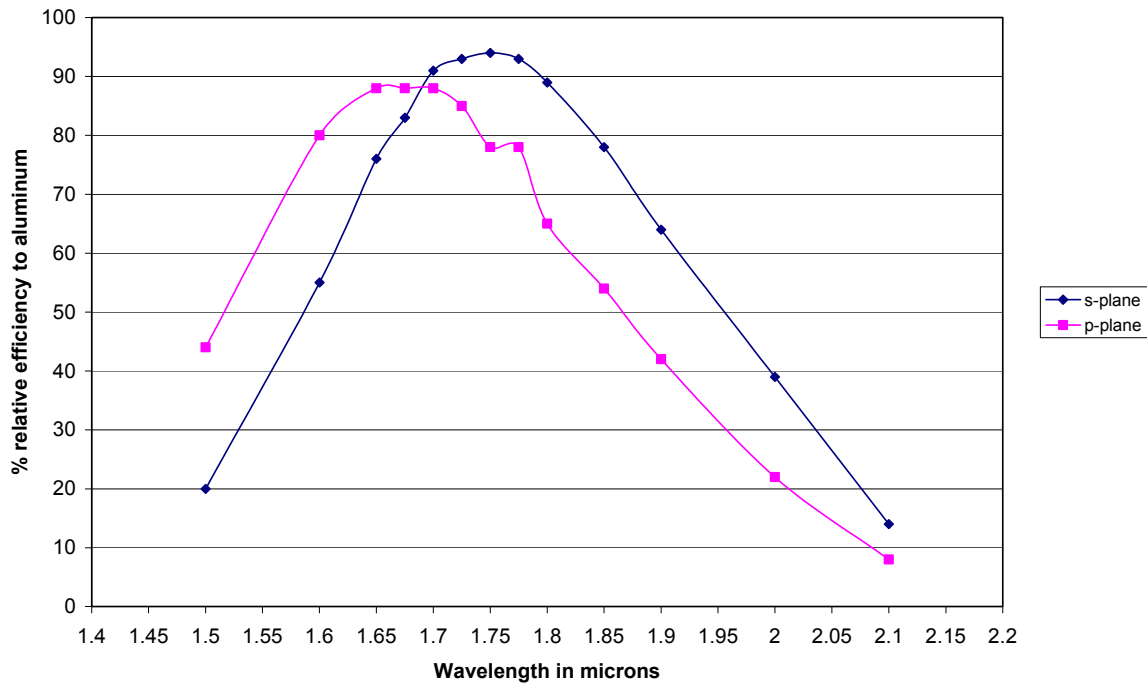
Figure 11: *Efficiency curve (H-band) for the existing GNIRS grating.*

5.1.1.6   Guider Optics

We have developed an all-spherical preconstruction design for a focal-reducing guider, which intercepts a 2.8′ by 2.8′ off-axis portion of the telescope field of view and images it on a (1024 x 1024 by 13 μm) frame-transfer CCD, the CCD47-20BT from E2V. The short-wavelength cutoff will be defined by an RG780 filter while the long-wavelength cutoff will be defined by the CCD's quantum efficiency. For an object whose spectral energy distribution is constant, the effective wavelength will be 0.85 μm. A passband of this style has been used successfully in the NIRSPEC guider. The guider contains a contact doublet, which focuses the light with about 21.1% of the needed scale reduction and also forms a pupil image at a second contact doublet; this is followed by a thick singlet and a dome-shaped field flattener. This field flattener also serves as the vacuum window for the small guide camera dewar. A 79.2 μm/″ final imaging scale is achieved. Pincushion distortion is only about 1.0 % at the detector corners. The thick singlet will be translated along the optical axis for focusing.

The guider's image quality is illustrated in Figure 12. The field of view is bilaterally symmetric about the X = 0.0 columns of images so only half of it is shown. The polychromatic rms image diameters are 0.39″ +/- 0.02″ averaged over the full field of view, which should be excellent for the intended purpose. All the optical glass needed for the guider has been ordered from Ohara Corp. The guider is folded with 2 flats into a compact "Z-shaped" geometry as shown in Figure 13.
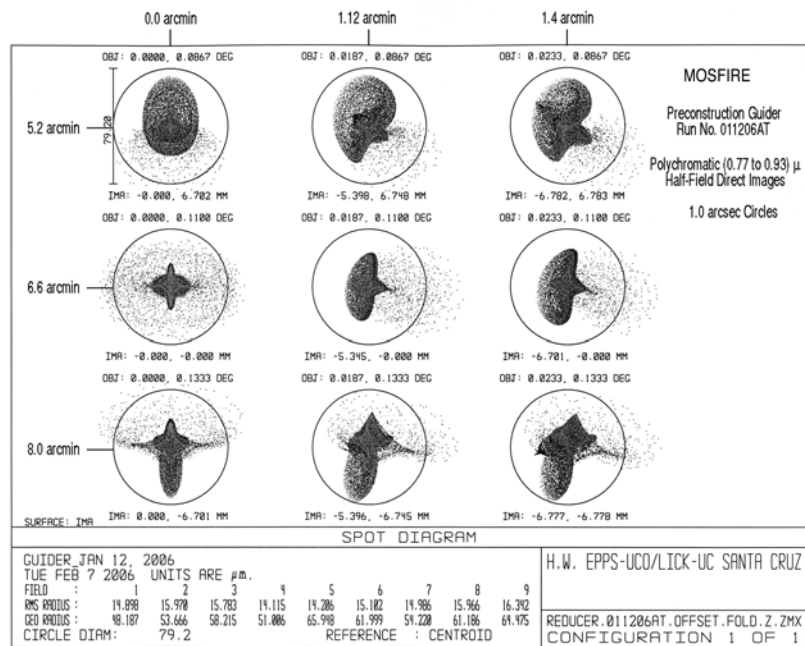
Figure 12: *Polychromatic guider images over half of the 2.8' by 2.8' bilaterally symmetric off-axis field of view. The circles are 1.0″ in diameter.*
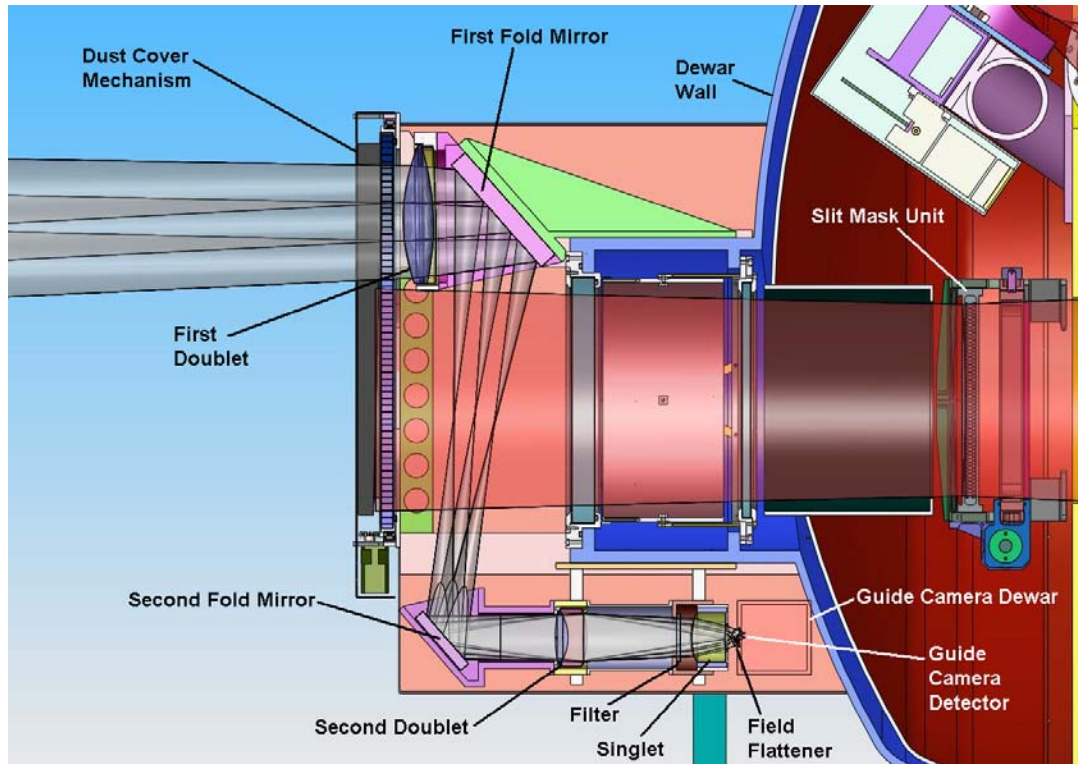
Figure 13: *The MOSFIRE guider layout.*

The guider's passive 2.8′ by 2.8′ off-axis field of view is large enough to provide suitably bright guide stars in any part of the sky. The folded geometry will enable its mechanical structure to be rigid relative to the CSU.

5.1.2   Optics Sensitivity Analysis

A study of the imaging performance characteristics of the MOSFIRE preconstruction optical design was carried out with regard to "de-center" and "tilt" of its individual optical elements.

5.1.2.1   Imaging Characteristics for the Collimated Preconstruction Design

The current prescription for the preconstruction optical design in direct-imaging mode is DIFF20.X_DIRECT.IMAGING.ZMX which contains our current collimator (Run No. 091205AL) and our current camera (Run No. 110405AG). For this study, attention was restricted to the K-band, represented by three wavelengths which were (2.0, 2.2, 2.4) microns. The design is so well corrected for chromatic effects that a more extensive sample of wavelengths was not needed. A focus run showed that best K-band focus occurred when the detector was moved 5.0 microns toward the optics. Although focus will be accomplished by refocusing the telescope in practice, this 5.0-micron change was adopted here for convenience.

Recall that MOSFIRE's final imaging scale is 100 microns/arcsec. Thus each micron of image diameter is equivalent to 0.01″, which is useful to remember. The full-field radius for imaging is 3.40′. K-band images were calculated for the collimated system. The rms image diameters are reported in Table 7.

Field Radius (%)	Rms Diam (microns)
0.0	22.9
30.0	19.7
50.0	17.3
70.0	19.5
80.0	21.9
90.0	24.0
100.0	25.0

Table 7: *Image diameters (rms) as a function of full field radius*

The images are round and well formed, with a slight hint of transverse coma pointing away from the optical axis. On nights of best seeing, when the atmosphere and the telescope might combine to deliver rms image diameters of about 0.33″ near 2.0 microns, we might expect that the worst-case K-band images would show rms diameters of about 0.41″ (2.3 pixels) if the system were perfectly collimated and perfect in every other regard.

5.1.2.2   Ray-Trace Sensitivities for the De-collimated Preconstruction Design

Apart from the two fold mirrors, MOSFIRE's optics components are axially symmetric in direct-imaging mode. Clearly, this symmetry is broken as soon as any of the lenses are de-centered and/or tilted. Combinations of de-centers and tilts are possible in enormous numbers. Such situations can be simulated by Monte Carlo statistical studies, which might be appropriate if many copies of MOSFIRE were being evaluated. However, such an approach is not applicable in our prototype situation where only one MOSFIRE will be constructed.

As a practical matter, we choose to perturb only one parameter at a time to determine what effect that particular perturbation has on the image quality and the image location in the focal plane. One might imagine that if such perturbations were random, their effects could be added in quadrature to estimate the global image quality and image location changes that would be produced by all of those perturbations taken simultaneously. There is a caveat however, because we must remember that "cross-talk" between perturbations, and possible systematic effects, are not assessed by this approach. Furthermore, it is a statistical fact that "one example" of a random process may well produce a result which differs greatly from the expected average. Thus quantitative predictions from this simplified approach must be regarded only as guidelines.

In the single-parameter mode, de-center in any one direction is equivalent to that in any other direction. It can therefore be thought of as a radial de-center. Similarly, a tilt about any axis that is perpendicular to the optical axis is equivalent to a tilt about any other. For the purposes of this study, de-centers were all calculated in the +x direction while tilts were always calculated about the +y axis.

Image quality and image location were determined by ray-tracing images located on-axis, and at three full-field position angles. We use the notation (X, Y) where X and Y are angles given in arcmin. Y is the "slit direction" and X is perpendicular to Y. In this notation, the ray-traced images were at (0.0, 0.0), (0.0, +3.4), (-3.4, 0.0) and (+3.4, 0.0). Note that since the tilt perturbations are symmetric with respect to +/-Y, no independent image at (0.0, -3.4) is needed. The primary purpose for including an on-axis image is to evaluate image motion, as de-center and tilt perturbations have little effect on the on-axis rms image diameters. The three full-field images provide worst-case evaluations of image motion relative to the on-axis image as well as worst-case changes in the rms image diameters that result from each perturbation.

Each lens element was de-centered, as a unit, in the calculations which follow. Each lens element was tilted about its front vertex, as a unit, in other calculations which follow. Front in this context means that surface which first interacts with the incoming photons. Lenses were de-centered by 100.0 microns and by 200.0 microns in two different spot diagram calculations (for all four images in the field). It was found that the image location displacements (dL) and the rms image diameter changes (drms) that occurred were approximately proportional to the de-center amount (dx). The on-axis image displacements and the worst-case rms image diameter changes for the 100.0-micron de-center of each lens are given below. Displacements of full-field images sometimes differed by small (~ few micron) amounts from that of the corresponding on-axis image. However, such 2nd-order differential image motion effects can be ignored for the present purpose.

In addition, each lens element was tilted by 1.0 mrad and by 2.0 mrad in two different spot diagram calculations (for all four images in the field). It was found that the image location displacements (dL) and the rms image diameter changes (drms) were approximately proportional to the tilt amount (dt). The on-axis image displacements and worst-case rms image diameter changes for the 1.0-milliradian tilt of each lens are given in (Table 8). Displacements of full-field images sometimes differed by small (~ few micron) amounts from that of the corresponding on-axis image. Again, those 2nd-order effects were ignored as they were above. These results can be thought of as the "sensitivities" of each lens to de-center and tilt (taken individually). Units for (dL) and (drms) are both μm.

Lens	Decen (dL)	Decen (drms)	Tilt (dL)	Tilt (drms)
Col #1	7	0.39	-1	1.85
Col #2	-21	0.32	1	2.05
Col #3	-11	1.28	8	1.89
Col #4	21	8.57	-3	6.84
Col #5	19	7.02	-7	4.49
Col #6	41	2.59	-10	4.74
Cam #1	19	1.36	1	4.84
Cam #2	65	16.59	29	27.62
Cam #3	-64	21.72	8	52.50
Cam #4	27	6.18	1	8.13
Cam #5	41	4.77	12	9.74
Cam #6	23	1.48	15	5.41
Cam #7	-11	6.44	2	6.33

Table 8: *The sensitivity to de-center and tilt for each lens individually*

While it is obvious that there is quite a bit of sensitivity variation from lens to lens, camera lenses #2 and #3 are clearly the worst offenders. Extra care will have to be exerted to be sure that they are manufactured with a vanishingly small amount of wedge (relative to their mechanical girdles) and that they are mounted with virtually no de-center and/or tilt. With the possible exception of collimator lens #4, which may require an extra bit of care with its centering, the rest of the sensitivities appear to be within the purview of what we think of as "machine-shop tolerances."

5.1.2.3   Initial-Alignment Error Parameters

In order to assess the precision with which each lens element must be centered and squared-on during the alignment process, we must estimate the combined global effect that the residual de-center and tilt of each lens will have on MOSFIRE's imaging performance. If one supposes that once aligned, the residual de-centers and tilts will remain fixed, then the initial image motion can be ignored as it only causes the image coordinate origin to have been displaced (by a fixed amount). Thus for initial alignment considerations, we only need to concern ourselves with the rms image diameter degradation which results from the combined residual de-centers and tilts.

Although cross-talk and systematic effects will surely be present in the actual system, we ignore those effects by assuming that the 13 residual de-centers and 13 residual tilts are 26 free parameters which are distributed randomly, and that their effects on the resulting rms image diameter(s) add in quadrature. Thus we can divine an "error budget," and we can calculate permitted values for each de-center and tilt such that the 26 contributions to the error budget are all equal to one another. Call that contribution C, such that for the worst-case images:

$$C = [(Single\text{-}parameter\_rms\_diam) - (Collimated\_rms\_diam)]$$

$$(Assembled\_rms\_diam)^2 = (Collimated\_rms\_diam)^2 + 26*(C)^2$$

The choice of (Assembled_rms_diam) for the worst-case images is somewhat arbitrary. Those images will occur at the very edge of the 6.8′ diameter field of view. Suppose we allow de-collimation effects to add an average of 20% to the worst-case rms image diameter for the collimated system, increasing it from 0.25″ to (Assembled_rms_diam) = 0.30″. With that selection, the individual allowed de-centers and tilts for the as-assembled system can be calculated (approximately) from the sensitivity information presented above. Results are as follows (Table 9):

Lens	Decen (microns)	Tilt (arcsec)
Col #1	736	363
Col #2	938	326
Col #3	217	325
Col #4	43	98
Col #5	46	149
Col #6	125	141
Cam #1	239	138
Cam #2	20	24
Cam #3	15	13
Cam #4	53	82
Cam #5	68	69
Cam #6	209	124
Cam #7	50	106

Table 9: *Allowed de-centers and tilts for the as-assembled system*

If the 26 individual perturbations were truly random, and they all had the amplitudes shown above, then a sampling of rms image diameters around the edge of the field would show an increase of 0.05″ on average. However there would also be some statistical variation, which might be of order [0.05/ √(26)] or +/-0.01″. If the distribution were Gaussian, a few percent of the diameters would have increased by 0.02″. The worst image in the field might have a 0.33″ rms diameter. Combined with the best-case 0.33″ atmosphere-plus-telescope performance mentioned above, we would expect the rms diameter of the average K-band image to have increased from 0.41″ to 0.45″ while

the worst image in the field would have increased to a 0.47″ (2.59-pixel) rms diameter. These results show that it is reasonable to adopt the arbitrary choice of (Assembled_rms_diam) = 0.30″.

5.1.2.4   Practical application

The previous section is *not* a "Tolerance Table" for MOSFIRE's alignment. Obviously, there will be a large number of other factors that will contribute to the so-called error budget, such as manufacturing errors, errors in axial lens-locations, "cross-talk" between the individual alignment errors, various systematic effects (such as a whole group of lenses being de-centered and/or tilted as a unit). Moreover, if some lenses can be aligned more precisely than the parameters given above would suggest, then others can be aligned a bit less precisely.

As in all prototype situations, we will engineer the lenses as carefully and precisely as possible. We will measure and machine each and every part precisely, while we have it in the lathe or on the mill. Our goal is to build the opto-mechanical units to meet spec without the need for adjustments.

5.1.2.5   Flexure Compensation

In practice, MOSFIRE will flex under variable gravity loading. The Sensitivity Table given above can be used to assess the amount of image motion and additional rms image diameter degradation that various flexure-induced de-centers and tilts will cause.

Image motion can be compensated by tilting the fold-mirror, which follows Col #1, by controlled amounts. However doing so will induce some rms image diameter degradation of its own. If we assume that we can tolerate half of a "C unit" (like the 26 of them mentioned in Section 3), then we will be able to tilt the fold-mirror by as much as +/- 0.60 mrad which will provide about +/- 7.39 pixels of image motion. That should be sufficient if the mechanical structure achieves the desired gross flexure of a few pixels. At that amplitude, the largest differential image motion is 0.07″ (0.39 pixels). It occurs at the edge of the 6.8′ field of view. The differential image motion effect is proportional to field radius for a given fold-mirror tilt amplitude. It is also proportional to tilt amplitude.

We note that although flexure-induced image motion can be corrected, flexure-induced rms image diameter degradation can *not* be corrected. Thus we must keep flexure to a minimum. Cam #2 and Cam #3 will be particularly critical in that regard.

In making the flexure and bonding agent parameter selections, it would be appropriate to try to constrain linear motions of various lenses to something like +/- 0.010 mm (0.0004 inches) and to restrict their angular motions to something like +/- 6.0″ (0.03 mrad). It would also be appropriate to try to restrict surface distortions to less than about 1/4 wave (0.25 micron). While the suggested linear-motion and angular-motion constraints appear to be somewhat too tight for some of the lenses, when compared to the Table 9, they are clearly about right for Cam #2 and for Cam #3 which are the most difficult lenses.

The fold mirror between Col #1 and the "group of 5" that forms the rest of the collimator has a sensitivity of 221 microns/mrad at the camera's focal plane. For the imaging mirror, mounted back-to-back with the grating, the sensitivity is 500 microns/mrad.

Analyzing the sensitivity of the grating is more complicated because diffraction effects can make the image move in unexpected directions if there is a rotation about any axis that is not parallel to the grooves. For now, we consider a rotation about an axis that is parallel to the grooves. Using the nominal set up angle for a 110.5 groove/mm grating of 42.614235 degrees, this puts 21,800 Angstrom light at field center in 3rd order and the resulting reciprocal dispersion is about 120.5 Angstroms/mm. If that angle is increased by 0.01mrad then the central wavelength becomes 21,800.5234 Angstroms so in effect, our original wavelength has "moved" some 4.3 microns on the detector (~ 0.24 pixels). As a first approximation, it would be okay to use the imaging mirror sensitivity for a grating rotation about an axis that is perpendicular to the grooves.

5.1.3   Modeling, simulations and prototyping

Zemax has been used to ray-trace all of the optical designs and .zmx files plus associated glass catalogs are available. As indicated by the previous section, the effect of de-centers and tilts on optical quality have been investigated, and the sensitivity of various elements has been fed into the mechanical finite element analysis. A prototype lens mount for the large field lens (Col #1) exists from a previous project.

5.1.4   Performance predictions

Spot diagrams have been produced for the most important instrument configurations. Image quality in both imaging and spectroscopic mode meets requirements. In fact, the design allows for additional imaging field and additional spectroscopic field, if desired.

5.1.5   Risk identification and risk mitigation

As already mentioned, the primary source of risk in the optical design lies in the long lead times required to obtain the blanks needed for lens fabrication. There is an associated risk if damage occurs during fabrication. To mitigate these risks we are ordering blanks of the materials that are hardest to obtain, and including spare blanks in these purchases. There has been a cost increase in the market price of these materials, but the additional costs, totaling $300k, have been included in the current.

5.2 Mechanical Design

All of the major mechanical elements of MOSFIRE now exist in preliminary designs that allow analysis of the mechanical performance (flexure and optical mounting tolerances), thermal behavior, and the weight and balance of the entire instrument.

5.2.1 Description

A sectional side view of MOSFIRE is shown in Figure 14. MOSFIRE is designed for mounting at the Cassegrain position of the Keck I telescope. This focal station imposes strict space envelope limitations as well as requirements to cope with varying gravity vectors during operation. The instrument design must meet specific weight and balance requirements and provide definition points compatible with the existing defining points used for the LRIS instrument on Keck I.
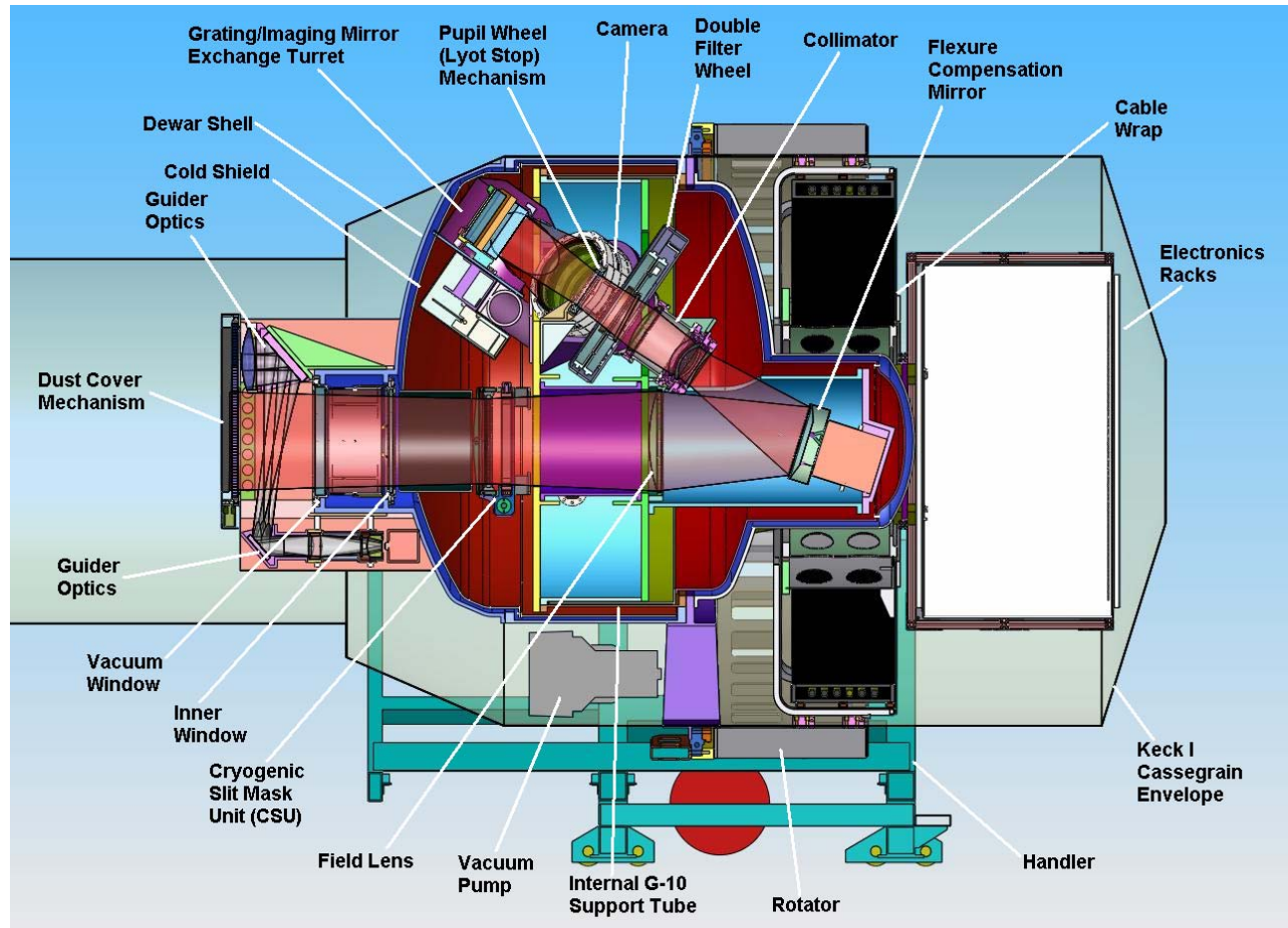
Figure 14: *Section view of MOSFIRE. The thin black outline indicates the Keck I Cassegrain envelope limits. Note that the handler shown in this figure is not attached to the instrument when it is mounted in the telescope.*

5.2.1.1 Overall Layout and Constraints

The basic approach is to attach a cylindrical vacuum enclosure (the dewar) to a Rotator Module that is a copy of the one used for LRIS. The dewar is sized to encapsulate the folded optical design and to fit within the Cassegrain space envelope. The instrument is divided into "cold" sub-systems which reside inside the dewar, and "warm" sub-systems that are located outside the dewar. Most of the cold sub-systems are mounted from a thermally-isolated Internal Structure or frame.

Following the photon path through the instrument begins with the dewar window. Photons then pass through a Cryogenic Slit Unit (CSU) which is located at the Keck I focal plane. The beam expands towards a collimator lens which is split into two parts: a field lens and a five-element collimator barrel assembly. The optical path is folded in the collimator with an articulated mirror which can be utilized for flexure compensation. Photons exit the collimator and pass through the filter wheel mechanism before reaching the pupil wheel. After the pupil, the optical path is folded a second time by the grating/mirror exchange turret. Finally, the photons enter the camera assembly and arrive at the detector head.

The warm sub-systems include a Dust Cover unit and Guider Unit at the front of the instrument. At the rear of the instrument, a large Cable Wrap assembly and a pair of Electronics Racks are attached behind the dewar. Vacuum fittings and closed-cycle refrigerator heads are positioned around the cylindrical body of the dewar. A standard Keck Handler, similar to that used for LRIS, is employed to transfer the instrument into the Cassegrain focus position.

Sub-System/Sub-Assembly	Conceptual Design Weight Estimate (lbs.)	Current Design Weight Estimate (lbs.)	Difference (lbs)	Difference (%)	Comments
Collimator Assembly	80	61.5	-18.5	-23.13	
Internal Structure Assembly	810	804	-7	-0.80	
Filter Wheel Assembly	95	85	-10	-10.53	
Camera Assembly	155	127	-28	-18.06	
Field Lens Assembly	35	32	-3	-8.57	
Pupil Mechanism Assembly	15	14	-2	-10.00	
Cryo-Slit Mask Assembly	77	77	0	0.00	
Thermal Strapping Assemblies	75	75	0	0.00	Thermal straps= 35 lbs
Guider System	100	95	-4.8	-4.84	Glass= 26.5 lbs
Optical Baffle Assemblies	30	30	0	0.00	CSU baffle =10 lbs.
Shield Assemblies	125	450	325	260.00	Initial shield wght under-estimated
Window Assembly	30	60	30	100.00	Glass= 24 lbs
Dust Cover Assembly	25	55	30	120.00	Includes Guider Assembly Cover
Cold Head Assemblies	80	148	68	85.00	Cold heads =75 lbs
Electronic Housings	400	469	69	17.25	Cabinet= 180 lbs; Supports= 89 lbs
Grating/Mirror Exchange Assembly	98	106	8	8.16	
Fold Mirror & Flexure Drive Assembly	32	37	5	14.69	Mirror= 5.6 lbs; stage= 25 lbs
Vacuum Chamber	1260	1295	35	2.78	
Cable Wrap	315	325	10	3.17	Includes extra pair of helium lines
Vacuum System	137	137	0	0.00	
Detector Mount Support Assembly	25	25	0	0.00	
Total Weight	3999	4506	507	12.69	
CG Location (relative to bearing CL):					
X Position (in)	-0.8				
Y Position (in)	2.8				
Z Position (in)	4.6				

Table 10: *MOSFIRE weight budget*

As can be seen from Table 10, the preliminary MOSFIRE design fits within the limits of the Keck I Cassegrain Envelope. A weight budget has been established. Table 10 gives the current status of

the design relative to the goals established during the conceptual design phase. Currently, the instrument weight is ~13% over the goal of 4000 lbs. This is due predominantly to an under-estimate of the shield weight during the conceptual design phase. The current balance of the instrument relative to the center of the rotator bearing is quite good. Further improvements in centering with respect to the bearing may be achieved during detailed design by selectively positioning electronics and other external components.

5.2.1.2   Dust Cover

Both the entrance window to the dewar and the guider optics must be protected from dust and damage when the instrument is not in use. The guider and the "snout tube" containing the window are enclosed in a light-weight sheet metal enclosure. The forward facing portion of this enclosure has a dust cover mechanism attached. A motorized sliding door closes off the instrument and guider optics. The door is fabricated from an aluminum honeycomb panel so that it is lightweight, yet strong and impact resistant. It is supported by a pair of roller slides and actuated by a stepper gear motor via a rack and pinion drive (Figure 15). Industrial switches will provide end of travel limits. To eliminate the chance of personnel injury the drive speed and drive force are adjustable. In addition, the leading edge of the door and the edge of the door opening will consist of broad surfaces to minimize pinching forces in case of a collision. The dust cover will be interlocked to prevent it from opening unless the instrument is mounted on the telescope.
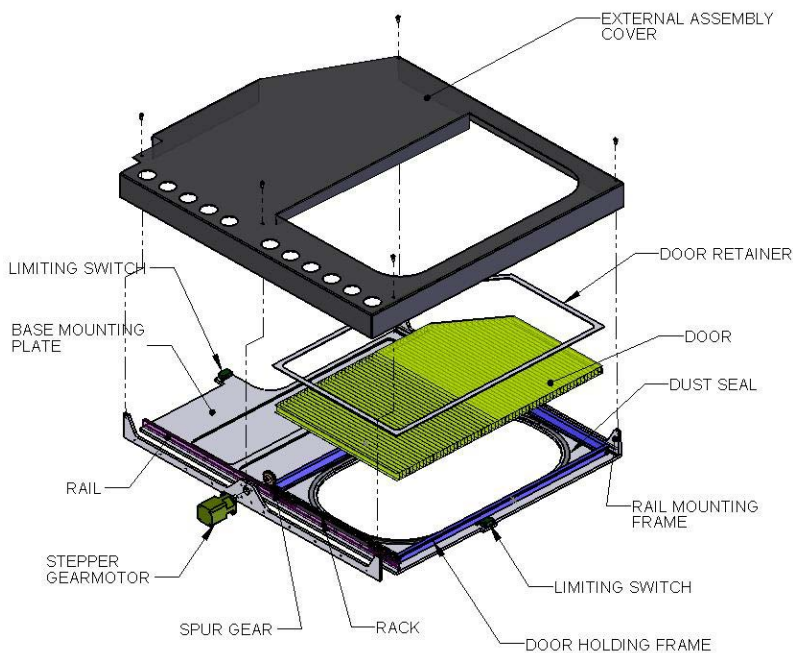
Figure 15: *Dust Cover Assembly Components*

In terms of simulation and prototyping, a sample of the door panel material will be tested during the detailed design phase. It will be supported in a similar fashion to the way the door is supported. The panel sample will be intentionally struck by a length of pipe to simulate WMKO's impact requirement in order to assess the strength of the panel.

Performance of the dust cover is considered nominal if it opens or closes in 1 minute, although faster transit times are possible. The actuation force will be adjusted such that a small margin exists over the force required to operate the door in all applicable gravity orientations. This is to minimize the chance of serious injury.

Because the dust cover is an ambient mechanism, its relative risk is small. It can be maintained and serviced easily, if necessary. The unit is intended to protect the dewar window from catastrophic damage. The strength of the door panel will be thoroughly tested with a prototype prior to fabrication of the final unit.

5.2.1.3 Guider Unit

The MOSFIRE guider unit will be mounted onto the front of the dewar along the snout tube that contains the window as shown already in Figure 13. The design of the dewar front shell and snout tube take into account the need to minimize motion of the guider field with respect to the CSU mounted on the dewar internal structure.

The guider is split into two sub-assemblies which are mounted on opposite sides of the dewar vacuum window. The optical design had to be folded into a Z-shape in order to stay within the Cassegrain space envelope. This approach also keeps the guider components close to the snout, minimizing additional flexure within the guider assembly. The first guider sub-assembly contains a larger doublet lens and the first fold mirror, whereas the second sub-assembly contains the second fold mirror, the rest of the lenses, the filter, and the detector package. This second sub-assembly permits manual focus of the guider, which could be upgraded to motorized focus, if desired.

Lens mounts for the Guider are based on designs utilized for the LRIS red and blue cameras. Each lens will have radial support provided by a series of Delrin dowels which are installed in pockets in aluminum or brass cells. The combination of material selection and dowel sizing results in athermal radial support over the design temperature range. Axial support is provided by "spring-loading" of the lenses against Kapton washers with soft silicone o-rings.

For the fold mirrors we utilize a six-point kinematic definition system designed for supporting and defining LRIS' dichroics and grisms. This design consists of spring-loading the optic against six adjustable hard-points. Polished tungsten-carbide reaction pads are bonded to the mirror substrates to prevent excessive contact stress in the substrate and to help reduce friction. The spring-plungers are Delrin-tipped, to reduce friction. Such a kinematic mount design allows easy adjustment of the mirrors during integration. Force-balance equations used to size the spring-plungers exist from the LRIS work. The performance of the LRIS optics confirms their validity and accuracy. This mount design ensures that the optics will maintain definition throughout the intended temperature range and will re-define their position if disrupted by accelerations.
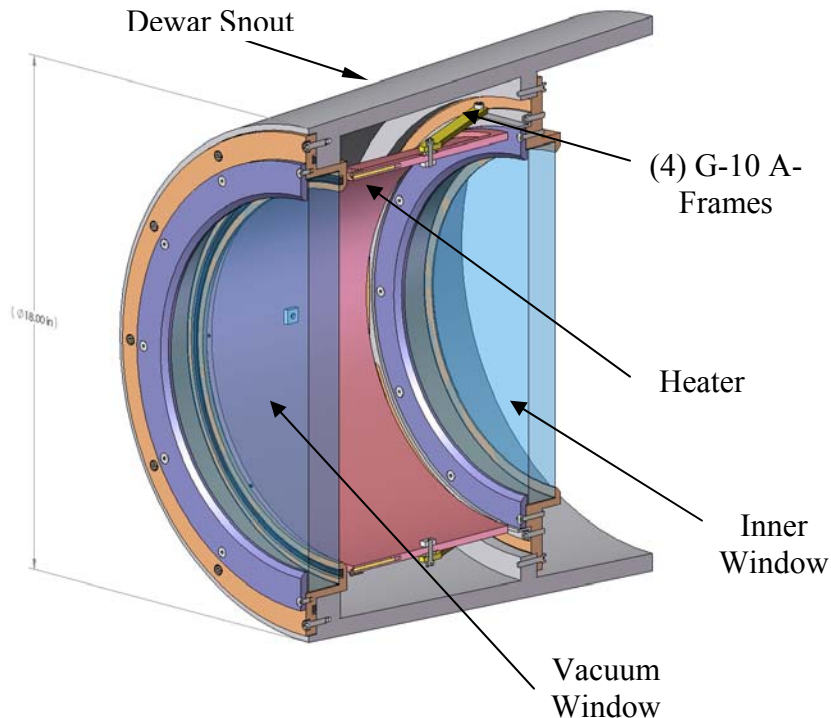
The E2V CCD47-20BT detector will be mounted in a compact dewar provided by WMKO. The aperture plate on the dewar will have to be re-designed to enable the mounting of our field-flattener lens in place of the normal flat window. The guider design includes lenses and mirrors which are comparable to ambient optics previously mounted successfully by members of the MOSFIRE team. Because of this previous experience, the guider assembly is not considered a high risk item.

5.2.1.4 Dewar Window

A major challenge for an infrared instrument such as MOSFIRE with a large field of view is the presence of a large vacuum window that attracts condensation due to radiative cooling to the interior of the dewar. Typically, the solution to this problem has been to blow a continuous stream of dry N_2 over the vacuum window from a reserve tank. But, as window size increases, so does the tendency for the N_2 to become increasingly turbulent and much more likely to mix in moist air. Turbulence may also affect the image quality of the instrument. MOSFIRE will incorporate an alternative approach. External N_2 flow is eliminated and an internal radiator keeps the vacuum window at ambient temperature.

As illustrated in Figure 16, the dewar entrance window is actually a double window with a thicker outer window providing the vacuum seal, and a second inner window serving to help control the thermal radiation with a heater located within the snout tube. This heater consists of a copper cylinder equipped with resistive cartridge heaters. The heater forms the inner lining of the snout tube and balances the heat lost by the front window to the dewar interior. The inner window is at vacuum conditions and acts as a radiation boundary with an intermediate temperature between ambient and the temperature of the internal optical components.

Figure 16: *Double window design.*

Using a snout tube extension of the dewar aids in thermal isolation of the instrument by increasing the separation between the windows and the CSU and by reducing the viewing angle of the window that the CSU is exposed to.

The dewar window design can be broken down into three subassemblies: vacuum window mount, inner window mount, and heater assembly. Both window mount assemblies will mount directly to the snout, however the heater assembly is first bolted to the inner window mount and then both are put in position as one unit. The windows will be fabricated from Infrasil. The vacuum window's diameter is ~ 370 mm in order to accommodate the 6.8′ diameter field of view.

Both analytical and finite element methods were used to optimize the front window thickness. Its thickness affects both vacuum induced stress levels and temperature distributions. Analytical methods were used to determine a safe thickness for withstanding atmospheric pressure. The two cases of a clamped and simply supported window were compared for completeness. This analysis confirmed satisfactory performance in terms of stress and flexure for a vacuum window thickness of ~35 mm. The goal was to keep the window stresses below 500 psi.

Thermal optimization was done with FEA using Algor v18. The goal was to heat the window(s) by radiation to maintain a maximum 2°C differential between the temperature of the center front surface of the vacuum window and the outside ambient. An iterative approach was used. First, a simple model was generated with the heater set at a certain temperature and the resulting temperature model recorded. Then slight changes were introduced between a set of given parameters. After approximately 20 trials, the sensitivity to these parameters was well understood and there was a likely set of optimal conditions that would give the best results. The analysis indicates that a very low power level (~8.4 W) is all that is required to maintain the temperature above the Observatory dome ambient in order to prevent condensation from forming on the outer surface of the window. The inner surface of the inner window stabilizes at a temperature of ~255 K and the resulting heat load on the CSU is estimated to be ~1.4 W. A single window design utilizing a warmed or dried gas purge would have had an estimated load on the CSU of ~0.9 W. The increase of 0.5 W is considered acceptable given the expected increase in reliability of the MOSFIRE heater design.

Performance predictions are summarized as follows:

- Maximum vacuum window stress = 440 psi
- Maximum vacuum window deformation = 25 μm
- Maximum required heater power = 8.4 W

Risk of dewar window condensation has been addressed through detailed analysis studies. The selected heater design provides additional margin since the heater power can be easily adjusted during integration and testing to compensate for any imperfections in the analysis. In addition, the radiative heater design has no moving parts and requires no service.

5.2.1.5   Dewar Shell

MOSFIRE's optics must be maintained at cryogenic conditions and therefore the majority of the instrument must be housed within a vacuum enclosure having a cryogenic cooling system and an internal structure capable of supporting optics. This unit is referred to as the "dewar". MOSFIRE is a Cassegrain instrument which implies that it will experience multiple gravity orientations during usage. As the instrument's guider unit will be located externally on the snout containing the entrance window to the dewar, relative motions between the guider and the internal structure must be minimized. Not only must the dewar's vacuum shell safely resist the atmospheric pressure load in combination with the loads of external components, but also it must have sufficient stiffness between the guider attachments and the internal structure under varying gravity vectors.
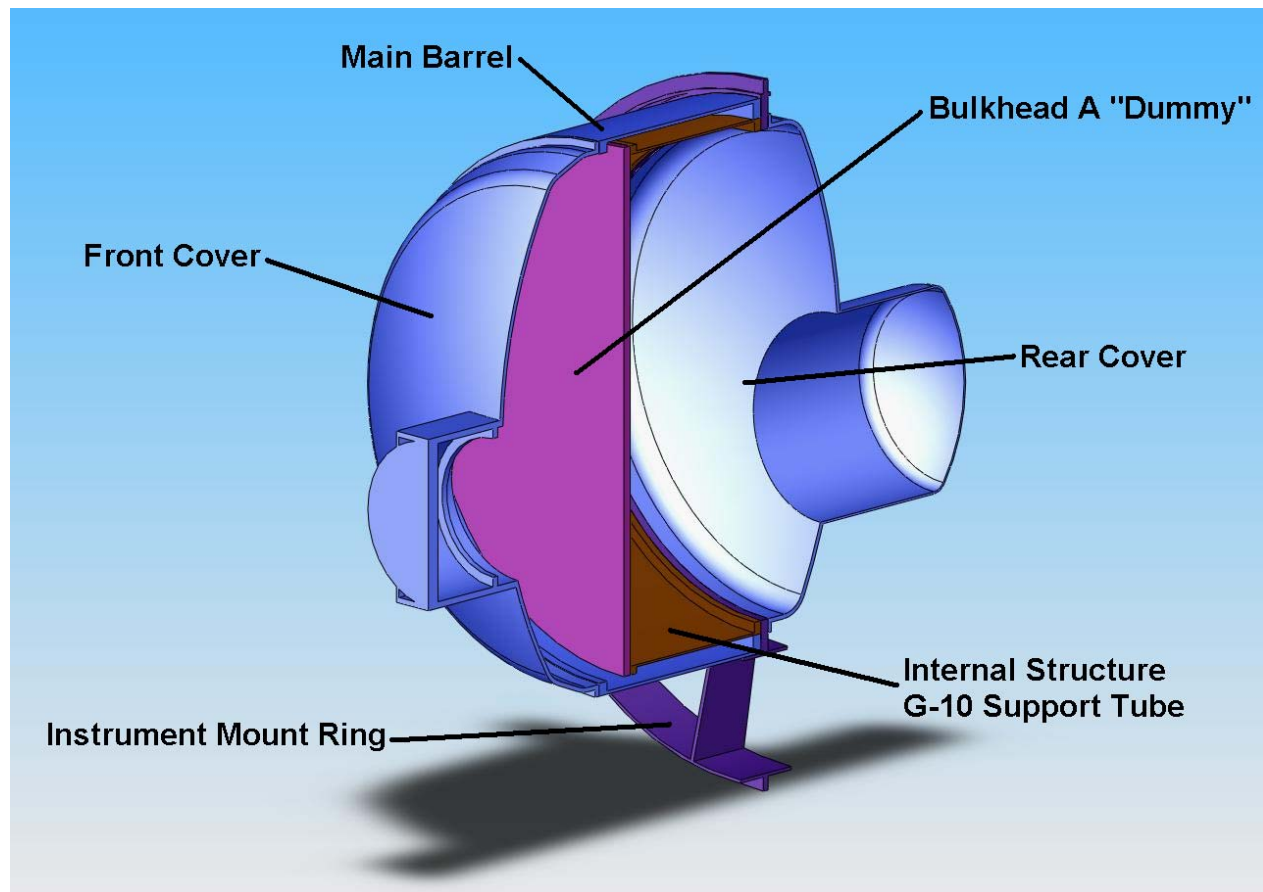
Figure 17: *Cross-section view of the dewar vacuum shell model used for analysis.*

To meet these requirements, a tubular vacuum shell was chosen based on its efficiency under vacuum loads combined with its uniform stiffness under radial bending loads. Likewise, the internal structure support is also tubular. The tubular-shaped shell efficiently fits the space between the cylindrical envelope of the Cassegrain location and accommodates the internal structure. The design is such that both the internal structural support tube and the external dewar barrel have one common end attached to an Instrument Mounting Ring structure (Figure 17). The instrument mounting ring is a welded steel structure which bridges between the instrument and the inner race

of the instrument's Rotator Module. By having both the internal structural support tube and the vacuum shell barrel anchored at the same place, the two tubes sag consistently under radial gravity loads. The dewar has torispherical vacuum end-caps at both ends. Each end cap is removable for servicing, and the intent of the design is to make all of the mechanisms accessible for servicing after removal of either the front or the rear end cap. Both end caps are shaped for vacuum loading efficiency. This shape also helps to minimize the vacuum shell weight in order to fit within the Cassegrain focus weight budget. The front end cap has a cylindrical "snout", or protrusion, extending from it which contains the dewar's double entrance window. The double window design is placed as far forward of the cryogenic Configurable Slit Unit (CSU) as possible to minimize thermal loading on the slit mask. The rear cap on the vacuum shell is similar to the front in design. It is also tori-spherical in shape and has a cylindrical protrusion which houses the flexure compensation system (FCS).

5.2.1.5.1   Design Analysis

General results of the vacuum shell FEA studies are summarized in Table 11. This spreadsheet summarizes the maximum ranges of flexure obtained from the analysis studies which are due to changing gravity vectors. The spreadsheet also includes the maximum stresses for the vacuum chamber and the instrument mounting ring observed in the studies. Results are shown for load cases without atmospheric pressure (vacuum) as well as with it included. All of the results are within the design goals and requirements. Clearly, the vacuum shell stress is dominated by the load due to atmospheric pressure. Our results indicate that, even with 5g's of acceleration, the combined maximum stress would still maintain a safety factor of ~5.

Figure 18 also includes the estimated maximum range of motions for the guider and CSU mounts independently. It is important that the displacements and tilts of the guider and CSU don't deviate excessively from the instrument's rotator axis due to general sagging of the instrument under gravity loads. Analysis indicates that the instrument focal surface will have a maximum radial variation of ~+/-70 μm and a maximum axial variation of ~+/-55 μm. Pointing of the instrument is estimated to vary by a maximum of ~+/-50 μrad. Note that flexure within the CSU mechanism is not included in this assessment.

It should also be noted that flexure of the vacuum shell due to atmospheric pressure is substantial. Radial flexure of the walls was up to 0.1mm and axial flexure was up to ~1mm in certain regions. In general, this flexure is not important in terms of instrument performance. But, some displacements of the vacuum shell are of interest in regards to guider assembly position. Some relative displacement of the axial spacing between the guider and the CSU would be expected due to atmospheric pressure. The analysis predicts ~420 μm decrease in the spacing under vacuum. But, due to the off-axis position of the dewar's window (and the guider) in the Y direction, the front cover flexes in a way which results in 48μm Y displacement and -41 μrad of pitch.

Potentially, the vacuum shell is loaded in a fashion that could cause buckling. A buckling analysis was completed for the six main features of the vacuum shell using elastic stability equations from Roark & Young. All of the features have wall thicknesses which will withstand more than 10 times

the nominal pressure of 15 psi without buckling. In several cases, the safety margin is even greater because material has been added to control flexure.

Maximum Values						
Parameter	**CSU W/Out Internal Structure Flexure**	**CSU With Internal Structure Flexure**	**Guider W/Out Mount Flexure**	**Guider Relative to CSU W/Out IS Flexure**	**Guider Relative to CSU With IS Flexure**	**Design Goal**
Displacements:						
X Displacement (+/- µm)	62.2	62.2	38.7	23.5	23.5	36.3
Y Displacement (+/- µm)	68.6	68.6	65.8	2.7	2.7	36.3
Z Displacement (+/- µm)	49.2	53.7	45.2	4.0	8.5	36.3
Tilts:						
Roll {about Z} (+/-µrad)	0.4	1.5	0.06	0.3	1.4	96.7
Pitch {about X} (+/-µrad)	50.9	46.3	53.65	2.7	7.4	42.5
Yaw {about Y} (+/-µrad)	25.8	25.8	49.03	23.3	23.3	42.5
Stress:	**Value**	**Units**				
Vacuum Chamber W/Out Vacuum	721	psi				
Safety Factor on Yield (6061-T6 Al)	55.5					
Vacuum Chamber With Vacuum	5529	psi				
Safety Factor on Yield (6061-T6 Al)	7.2					
Instrument Mount Ring W/out Vacuum	2859	psi				
Safety Factor on Yield (A 36 Steel)	12.6					
Instrument Mount Ring With Vacuum	4612	psi				
Safety Factor on Yield (A 36 Steel)	7.8					

Table 11: *Summary of Vacuum Shell FEA results.*

The maximum expected range of relative flexure between the guider assembly and the CSU mount surface is indicated at the top of the spreadsheet. This flexure is due to varying gravity vectors.

Again, internal flexure within the guider assembly and the CSU is not included. The design goals are equivalent to 0.1″ of relative motion. The maximum estimated stresses are displayed at the lower left. We adopt a minimum acceptable safety factor of 5.

There were three main risks concerning the dewar design which were assessed during the preliminary design phase. All three risks were interrelated. The risks were: 1) excessive flexure of the external guider, 2) excessive weight, and 3) fabrication difficulties/costs. The FEA addressed the first two risks and validated the dewar's cylindrical design. Guider flexure is manageable and the vacuum shell's weight is within 3% of earlier predictions. To address the third risk, vendors have been consulted and have provided ROM fabrication estimates which are comparable to our earlier expectations.

5.2.1.6   Internal Structure

The Internal Structure of MOSFIRE supports all of the internal sub-assemblies and mechanisms. It also serves as a thermal conduit for uniformly removing heat through the instrument's refrigerators. Floating shields, supported by insulated stand-offs, surround the internal structure.

5.2.1.6.1   Design Description

As with other Cassegrain instruments, the structural design of MOSFIRE must provide sufficiently uniform stiffness to maintain optical alignment through all possible gravity vectors. The MOSFIRE internal structure design primarily consists of two ~1500 mm diameter circular plates or optical benches, joined by a pair of nested, short tubes (Figure 18). This "stubby drum" assembly is suspended inside the cylindrical vacuum chamber by a concentric G-10 fiberglass cylinder which surrounds the internal structure. The thin G-10 cylinder serves as a thermal insulator between the cryogenic internal components and the ambient vacuum shell structure. Each of the optics assemblies and internal mechanisms are attached to one or other of the two optical benches. The tubular shape of the internal structure results in consistent radial flexure of the structure as the instrument is rolled about its cylindrical axis while it's horizontal. The small length to diameter ratio of the structure results in relatively small radial displacements between the two optical benches and between the internal structure and the vacuum chamber as the instrument is rotated from zenith to the horizon.

5.2.1.6.2   Design Analysis

The internal structure was analyzed by FEA methods to estimate the stability of the structure under varying gravity loads (Figure 19). Flexure analysis shows that this structure is very rigid and exhibits generally consistent radial flexure as the instrument rotates about the optical axis. The small length to diameter ratio of the double cylinder construction of the dewar interior serves to constrain displacements between the two optical benches and between the inner structure and the dewar. The full optical effects (both in terms of image motion and image degradation) will be studied further because some flexure motions are likely to counteract others. In the meantime, as a means of approximating the estimated (uncorrected) image motions due to flexure, a pair of

spreadsheets was created (Table 12 and Table 13) which convert the optic component's motion into image motion based on optical component sensitivities obtained from the analysis in §5.1.2.
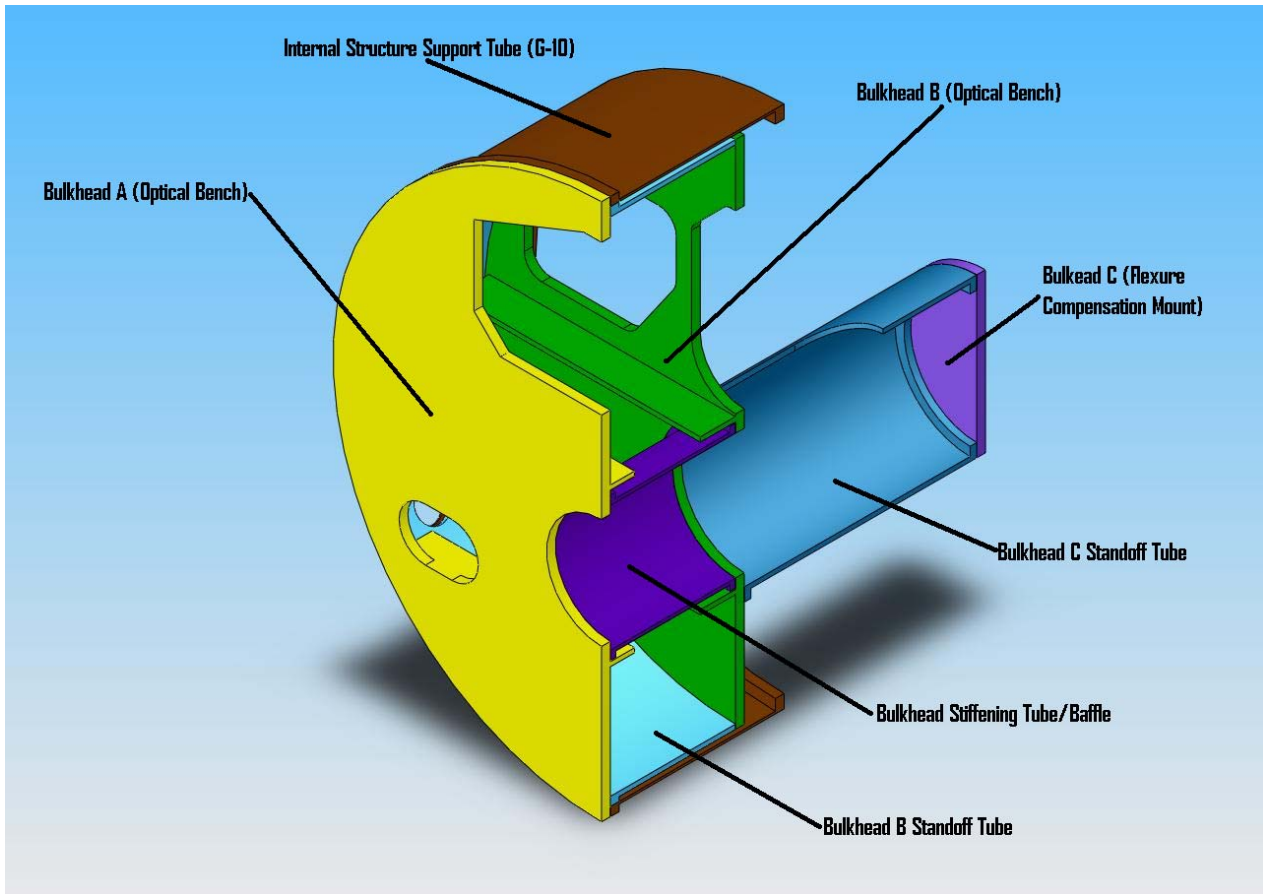
Figure 18: *Cross-Section view of the MOSFIRE internal structure design. All of the optic assemblies and mechanisms are mounted from one of the three bulkheads.*

Our requirement (goal) is ~0.3 (0.15) pixel flexure over 2 hours (Table 5). Assuming that we can reduce the flexure amplitude by 10:1 with a relatively simple tip/tilt mirror, the uncorrected flexure should not exceed 3 (1.5) pixels. The spreadsheet calculations include internal flexure estimates for the grating/imaging mirror mechanism and the flexure compensation system (FCS) which were obtained in separate studies. Internal flexure within the collimator barrel has not been included, but preliminary analysis indicates that the impact on image motion will be negligible. Flexure of the detector mount has also not been included, but is again assumed to be relatively small. Calculations indicate that the maximum correctible flexure-induced image motion will be ~+/-2.5 pixels for full sky coverage. This is due mostly to tilts, with only a small portion due to radial displacements. A more conservative estimate from the first spreadsheet is ~+/- 3.3 pixels, again over the entire sky. Our practical requirement is for any 2 hour period. Thus, the spreadsheet calculations indicate that the formal requirement (0.3 pixels) can be satisfied with 10:1 compensation and that our goal of ~0.1 pixels may be obtained over shorter observing times. It is the grating/mirror turret mechanism that is the major contributor to this flexure motion. Internal flexure within this structure is more than half of the flexure. This mechanism will be stiffened with

new grating and mirror mount designs comparable to the FCS mirror mounts during the detailed design phase.

The uncorrectable image motion due to flexure-induced optical roll motions is estimated to be about +/- 0.06 pixels at the edge of the detector with full sky coverage. The requirement allows more than twice this (+/- 0.15 pixels) over any 2 hour period. Thus, roll flexure nearly meets our goal of +/- 0.05 pixels.

Our proposed flexure compensation system has a tip/tilt stage with a specified range at 77 K of +/- 500 µrads, which is equivalent to +/- 6.2 pixels. Therefore, the preliminary calculations indicate that this stage will have adequate range to compensate for flexure through the telescope's full range of motion. The largest magnitudes of general motion estimated by the FEA are observed in the filter wheel and the pupil mechanism positions. Flexure affects on these mechanisms are not as critical since their contribution to image motion is negligible. Note that the pupil mechanism motion will likely be much less than estimated as the mounting structure included in this analysis has yet to be fully optimized.
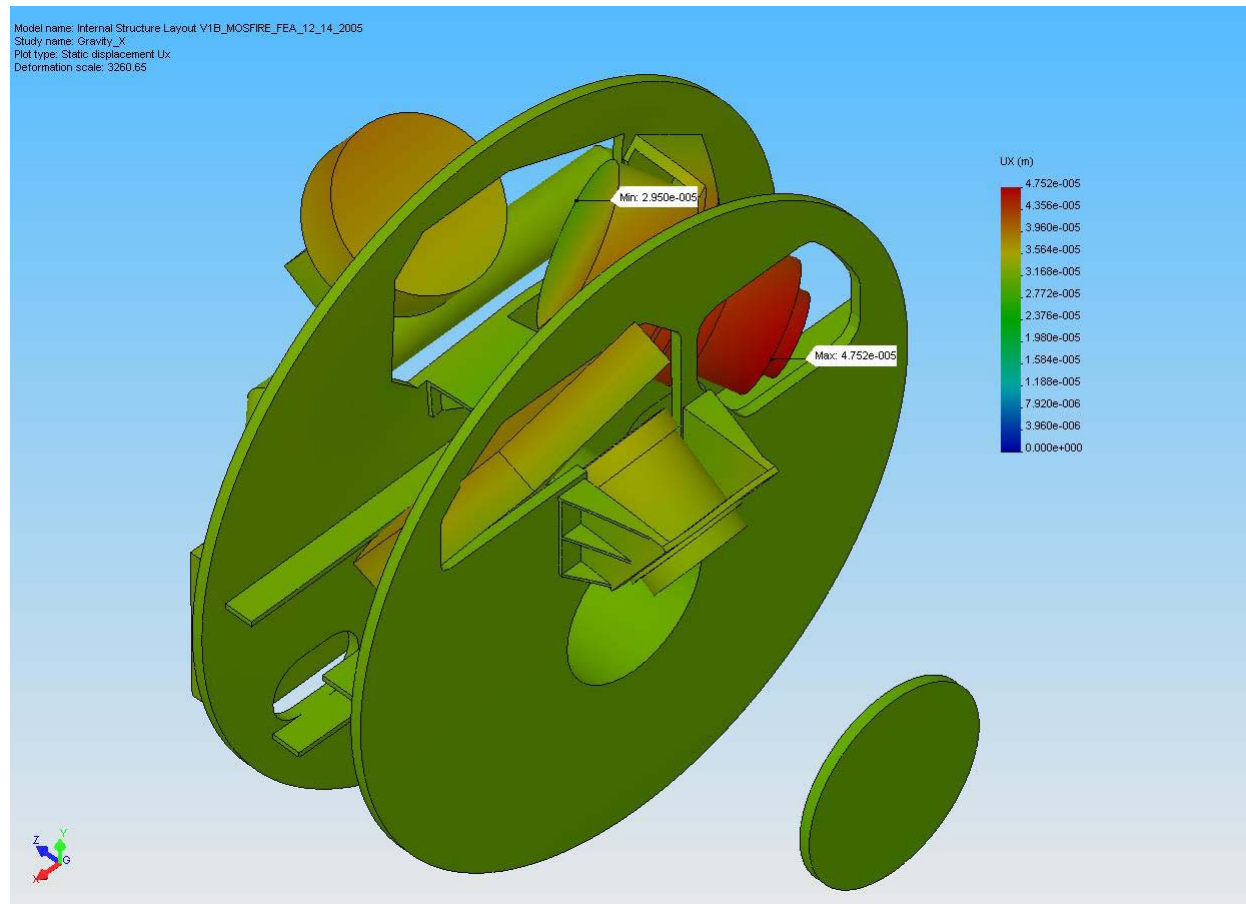
Figure 19: *Example of internal structure FEA displacement results plot. This image shows the X displacement estimate for gravity in X.*

Uncorrected Flexure Estimate- Conservative

Tilt

Component	Estimated Maximum Possible Magnitude +/- µrad	+/- pixels	Comments
Field Lens	11.31	0.001	Tilt Sensitivity: 18000 µrad/pixel
Collimator Mirror Sub-total	12.87	0.159	Tilt Sensitivity: 81 µrad/pixel
Instrument Structure	11.37	0.140	
Mechanism Internal	1.50	0.018	Doesn't include PI stage
Collimator Barrel	7.27	0.004	Tilt Sensitivity: 1800 µrad/pixel (based on lens #6- most sensitive)
Grating & Imaging Mirror Sub-total	91.22	2.534	Tilt Sensitivity: 36 µrad/pixel
Instrument Structure	38.95	1.082	
Mechanism Internal	52.27	1.452	
Camera Barrel	42.30	0.588	Tilt Sensitivity: 72 µrad/pixel (2x imaging mirror)
Tilt Sub-total (+/-):	164.96	3.285	

Decenter

Component	Estimated Maximum Possible Magnitude +/- µm	+/- pixels	Comments
Field Lens	3.24	0.002	Sensitivity: 1800 µm/pixel
Collimator Mirror Sub-total	4.77		Sensitivity: not applicable
Instrument Structure	3.23		
Mechanism Internal	1.54		Doesn't include PI stage
Collimator Barrel	5.90	0.033	@ Barrel Entrance; Sensitivity: 180 µm/pixel (based on lens #6- most sensitive)
Grating & Imaging Mirror Sub-total	15.84		Sensitivity: not applicable
Instrument Structure	10.24		
Mechanism Internal	5.60		
Camera Barrel	14.82		@ Camera Entrance; Sensitivity: not applicable
Decenter Sub-total (+/-):	9.14	0.035	Only includes motions that effect image motion
Tilt + Decenter Total (+/-):		3.319	Goal: +/-0.5 pixel ; Requirement: +/-1.5 pixels (per 2 hours)

Roll

Component	Estimated Maximum Possible Magnitude +/- µrad	+/- pixels	Comments
Field Lens	0.35		Sensitivity: not applicable
Collimator Mirror Sub-total	0.29		Sensitivity: not applicable
Instrument Structure	0.29		
Mechanism Internal			Doesn't include PI stage
Collimator Barrel	0.70		Sensitivity: not applicable
Grating & Imaging Mirror Sub-total	43.56	0.044	Roll Sensitivity: 1000 µrad/pixel
Instrument Structure	9.35	0.009	
Mechanism Internal	34.21	0.034	
Camera Barrel(+ Detector)	19.13	0.019	Roll Sensitivity: 1000 µrad/pixel
Roll Total (+/-):	62.69	0.063	Goal: +/-0.05 pixel ; Requirement: +/-0.15 pixels (per 2 hours)

Axial Spacing

Component	Estimated Maximum Possible Magnitude +/- µm	+/- pixels	Comments
Field Lens	1.68		
Collimator Mirror Sub-total	1.92		
Instrument Structure	1.69		
Mechanism Internal	0.23		
Collimator Barrel	0.19		@ Barrel Entrance
Grating & Imaging Mirror Sub-total	19.67		
Instrument Structure	12.97		
Mechanism Internal	6.70		
Camera Barrel	3.72		@ Camera Entrance
Axial Spacing Total (+/-):	27.18		

Table 12: *Summed estimates of uncorrected image motion resulting from instrument flexure.*

The spreadsheet in Table 12 provides a conservative estimate of the predicted image motion based on simple summation of the maximum magnitudes of component motions without regard to direction.

Uncorrected Flexure Estimates

Tilt

Component	Gravity in +X Relative to Zenith — Pitch Motion (µrad)	(pixels)	Gravity in +X Relative to Zenith — Yaw Motion (µrad)	(pixels)	Gravity in +Y Relative to Zenith — Pitch Motion (µrad)	(pixels)	Gravity in +Y Relative to Zenith — Yaw Motion (µrad)	(pixels)	Comments
Field Lens	-11.314	-0.001	-4.728	0.000	-3.773	0.000	-0.092	0.000	Tilt Sensitivity: 18000 µrad/pixel
Collimator Mirror Sub-total	-11.374	-0.140	-3.949	-0.049	-2.284	-0.028	-0.197	-0.002	Tilt Sensitivity: 81 µrad/pixel
Instrument Structure	-11.374	-0.140	-4.973	-0.061	-3.78	-0.047	-0.197	-0.002	
Mechanism Internal	0.000	0.000	1.024	0.013	1.496	0.018	0.000	0.000	Doesn't include PI stage
Collimator Barrel	-7.266	-0.004	2.790	0.002	-5.891	-0.003	0.106	0.000	Tilt Sensitivity: 1800 µrad/pixel (based on lens #6- most sensitive)
Grating & Imaging Mirror Sub-total	-65.118	-1.809	15.635	0.434	-85.339	-2.371	17.914	0.498	Tilt Sensitivity: 36 µrad/pixel
Instrument Structure	38.952	1.082	-2.705	-0.075	19.191	0.533	-0.356	-0.010	
Mechanism Internal	-104.070	-2.891	18.340	0.509	-104.53	-2.904	18.270	0.508	
Camera Barrel	-15.739	-0.219	-42.296	-0.587	-4.022	-0.056	-27.282	-0.379	Tilt Sensitivity: 72 µrad/pixel (2x imaging mirror)
Tilt Sub-total (+/-)	-110.811	-2.173	-32.548	-0.201	-101.309	-2.458	-9.551	0.116	

Decenter

Component	Gravity in +X Relative to Zenith — Y Motion (µm)	(pixels)	Gravity in +X Relative to Zenith — X Motion (µm)	(pixels)	Gravity in +Y Relative to Zenith — Y Motion (µm)	(pixels)	Gravity in +Y Relative to Zenith — X Motion (µm)	(pixels)	Comments
Field Lens	3.243	0.002	-1.825	-0.001	1.075	0.001	-0.338	0.000	Sensitivity: 1800 µm/pixel
Collimator Mirror Sub-total	3.228		-1.224		2.026		-0.740		Sensitivity: not applicable
Instrument Structure	3.228		-2.763		0.488		-0.740		
Mechanism Internal	0.000		1.539		1.538		0.000		Doesn't include PI stage
Collimator Barrel	-0.141	-0.001	2.673	0.015	0.190	0.001	0.478	0.003	@ Barrel Entrance; Sensitivity: 180 µm/pixel (based on lens #6- most sensitive)
Grating & Imaging Mirror Sub-total	0.908		11.893		10.230		2.358		Sensitivity: not applicable
Instrument Structure	-2.992		7.013		5.450		2.148		
Mechanism Internal	3.900		4.880		4.780		0.210		
Camera Barrel	4.579		-1.448		-1.868		0.299		@ Camera Entrance; Sensitivity: not applicable
Decenter Sub-total (+/-)	3.102	0.001	0.848	0.014	1.265	0.002	0.140	0.002	Only includes motions that effect image motion
Tilt + Decenter Total (+/-)		-2.171		-0.167		-2.456		0.119	Goal: +/-0.5 pixel. Requirement: +/-1.5 pixels (per 2 hours)

Roll

Component	Estimated Maximum Possible Magnitude (+/- µrad)	(+/- pixels)	Gravity in +X Relative to Zenith (µrad)	(pixels)	Gravity in +Y Relative to Zenith (µrad)	(pixels)	Comments
Field Lens	0.351		0.351		0.041		Sensitivity: not applicable
Collimator Mirror Sub-total	0.29		0.289		-0.066		Sensitivity: not applicable
Instrument Structure	0.29		0.289		-0.066		
Mechanism Internal							Doesn't include PI stage
Collimator Barrel	0.697		-0.412		-0.697		Sensitivity: not applicable
Grating & Imaging Mirror Sub-total	43.56	0.044	43.560	0.044	-1.750	-0.002	Roll Sensitivity: 1000 µrad/pixel
Instrument Structure	9.35	0.009	9.350	0.009	1.070	0.001	
Mechanism Internal	34.21	0.034	34.210	0.034	-2.820	-0.003	
Camera Barrel(+ Detector)	19.13	0.019	19.127	0.019	10.780	0.011	Roll Sensitivity: 1000 µrad/pixel
Roll Total (+/-)	62.690	0.063	62.687	0.063	9.030	0.009	Goal: +/-0.05 pixel. Requirement: +/-0.15 pixels (per 2 hours)

Axial Spacing

Component	Estimated Maximum Possible Magnitude (+/- µm)	(+/- pixels)	Gravity in +X Relative to Zenith (µm)	(pixels)	Gravity in +Y Relative to Zenith (µm)	(pixels)	Comments
Field Lens	1.68		3.36		2.25		
Collimator Mirror Sub-total	1.92		3.13		2.04		
Instrument Structure	1.69		3.37		2.28		
Mechanism Internal	0.23		-0.24		-0.23		
Collimator Barrel	0.19		0.24		0.39		@ Barrel Entrance
Grating & Imaging Mirror Sub-total	19.67		39.31		27.35		
Instrument Structure	12.97		25.94		14.32		
Mechanism Internal	6.7		13.37		13.03		
Camera Barrel	3.72		6.83		7.44		@ Camera Entrance
Axial Spacing Total (+/-)	27.18		26.43		19.73		

Table 13: *Estimates of uncorrected image motion from flexure accounting for direction of flexure.*

The second spreadsheet (**Table 13**) provides another and potentially more accurate estimate of the predicted image motion due to flexure. Here, the directions of flexure motions are included for the analysis cases with gravity shifting between zenith and orthogonal horizon directions. The main risks associated with the MOSFIRE mechanical assembly are that it will be too flexible or that it will be too expensive or difficult to manufacture. Flexure performance has been addressed through extensive analysis. Manufacturability concerns have been addressed through interaction with potential fabricators. While the internal structure is large, the design doesn't include any features that are overly difficult to fabricate. ROM cost quotes are consistent with our earlier estimates.

5.2.1.7   Lens Mounts

Lens cells must provide the required mounting tolerances while allowing for differential expansion and contraction during cool down cycles. For large optics like those used in MOSFIRE, typical approaches based on compliant cells can easily result in excessive stress on the optics. A prototype large optic mount based on tangential "flexures" was developed and tested during the KIRMOS program. This mount provided consistent radial and axial motions of the lens element with negligible hysteresis as the mount was rotated and tilted. The same approach will be used for MOSFIRE. The lenses are separated into two groups, the Collimator group and the Camera group. The Camera group has an interface to the Detector Head and the Collimator is subdivided into the Field Lens assembly and the 5-element Collimator Barrel. Figure 20 shows the relative locations.
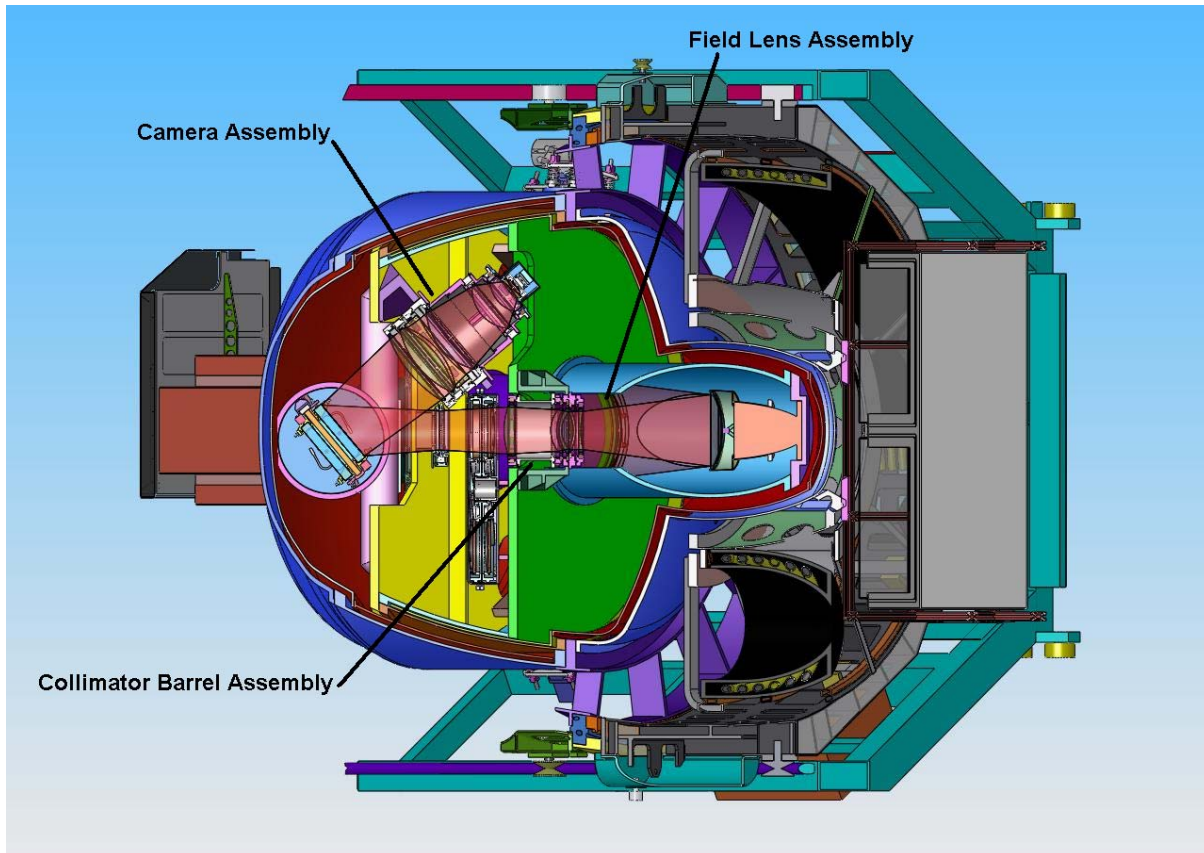
Figure 20: *Partial section view of MOSFIRE through the Collimator and Camera Barrels.*

5.2.1.7.1   Individual Lens Mounts

Each lens will be mounted in a sub-assembly or cell. A typical cell is shown in Figure 21. The lenses are supported by multiple flexures that are attached at one end to the lens cell ring and at the other to the lens itself. Figure 22 shows the basic components that form a flexure assembly. Attachment at the lens is through an epoxy bonded interface pad. The pad material for each lens is a metal which has closely matched CTE properties to the lens material. Table 14 shows the preliminary interface pad selections to match the MOSFIRE optical materials. Interface pads are attached to flexure strips fabricated from beryllium copper sheet utilizing screws. The opposite end of the flexure strips are attached to cylindrical copper inserts with more screws. Each copper insert fits into a pocket in the aluminum cell and is secured in place with screws during assembly.
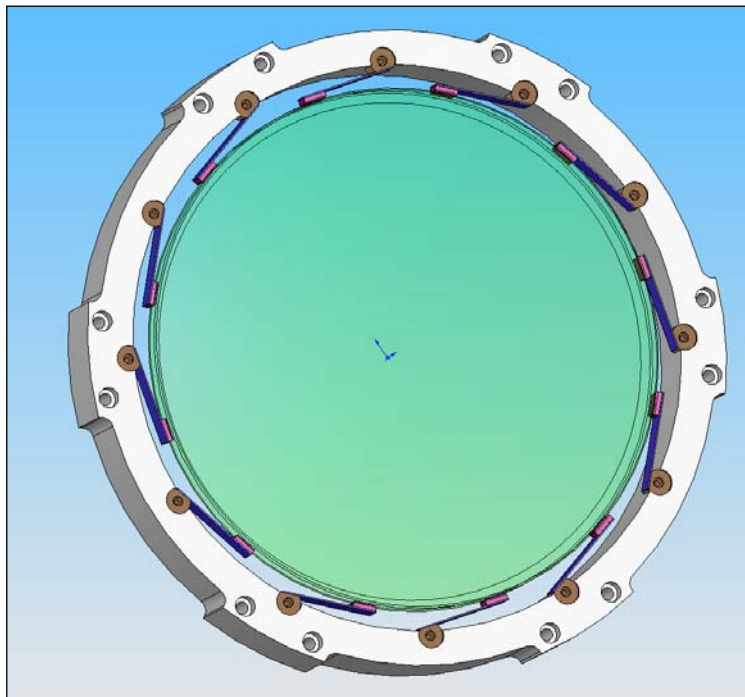
Figure 21: *A representative lens cell assembly with multiple bonded -flexures and mounting ring.*

Figure 22: *Close up view of a typical beryllium copper flexure.*

Lens Material	Lens CTE @ 293K, µm/m-°C	Match Material	Match CTE @ 293K, µm/m-°C
Fused Quartz	0.4	Allegheny Ludlum AL 36, UNS K93600	1.1
Zinc Selenide	7.20	Titanium Alloy Beta-21S	7.06
Calcium Fluoride	18.85	AISI Type 304N Stainless Steel	18.9
		changed from 304 Stainless Steel, UNS S30400	17.3
Barium Fluoride	18.1	Copper, UNS C42500	18.4
S-FTM16	9.0	Various Titanium Alloys	9.0
I-FPL51 (S-FPL51Y)	13.6	Allegheny Ludlum AL 2205™, UNS S31803	13.7
		Special Metals MONEL™ Alloy R-405	13.7
		Beralcast® 363 Beryllium-Aluminum Alloy	13.7

Table 14: *Preliminary interface pad material selections*

Sample bonds utilizing the displayed "match materials" for the first three lens materials have been successfully tested during the KIRMOS preliminary design phase. Other material combinations need to be tested after the material CTE curves are scrutinized further.

5.2.1.7.2 Multiple Lens Cell Assemblies

As mentioned, there will be two sub-assemblies with multiple lens cells, the Collimator Barrel and the Camera Barrel. The alignment and interface methodology of these two units is the same. Figure 23 shows an exploded view of the Collimator Barrel and Figure 24 shows the Camera Barrel. Where distances between individual cells are relatively large, simple spacer tubes fill the gap.

Axial positioning/alignment will be achieved through high tolerance interface surfaces on the lens cell "rings" and radial alignment through high tolerance overlapping steps in the rings. The cells are assembled together with a bolt pattern arrangement. As the design stands, the overlapping steps are shown as a tongue in groove arrangement with the bolt patterns outboard. Through review it has been decided that the design can be simplified by moving the "steps" to the outer diameter of each cell and moving the bolt patterns inboard. This action will simplify machining, and make it easier to achieve the required tolerances, and reduce the overall mass.

In most cases, the required tolerances for parallelism, concentricity, flatness, etc. needed to achieve the required performance are not much more stringent than standard machining tolerances. In a few cases, however, there will be tighter requirements such as interfacing step diameters being held to as little as +/- 0.001in (~25 μm). This level of accuracy is certainly achievable from precision machine shops.
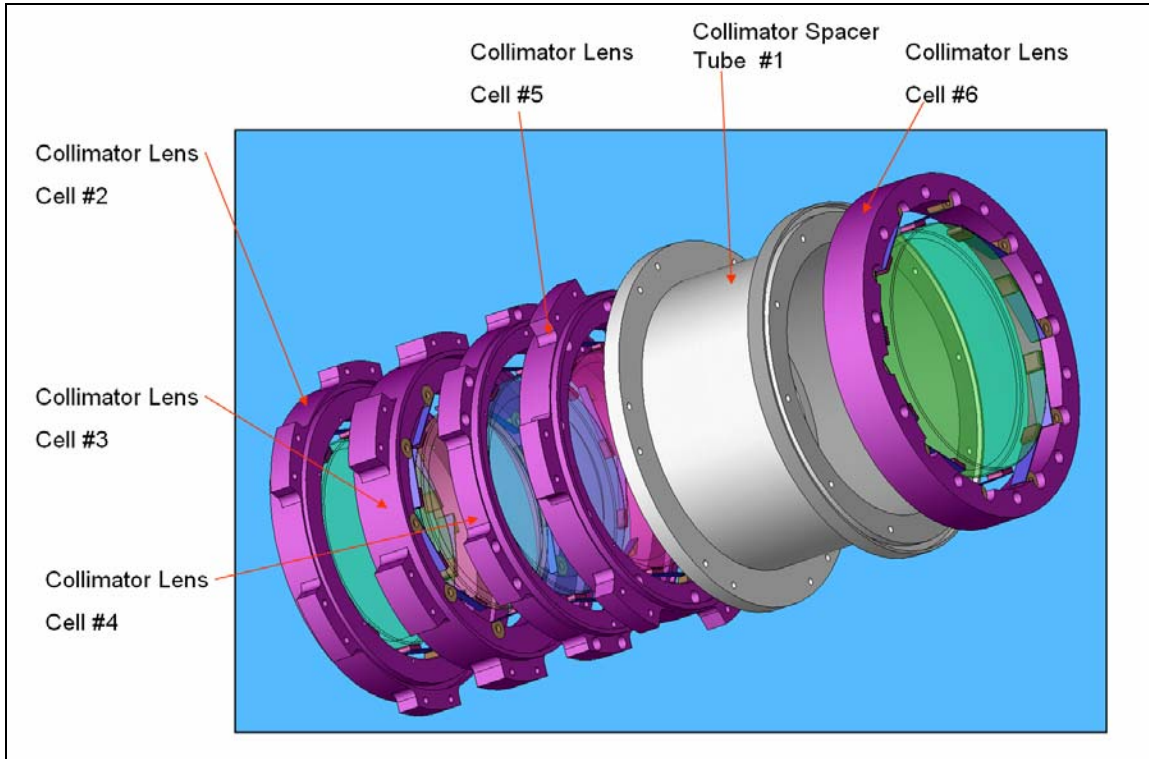
Figure 23: *Collimator Barrel Assembly.*
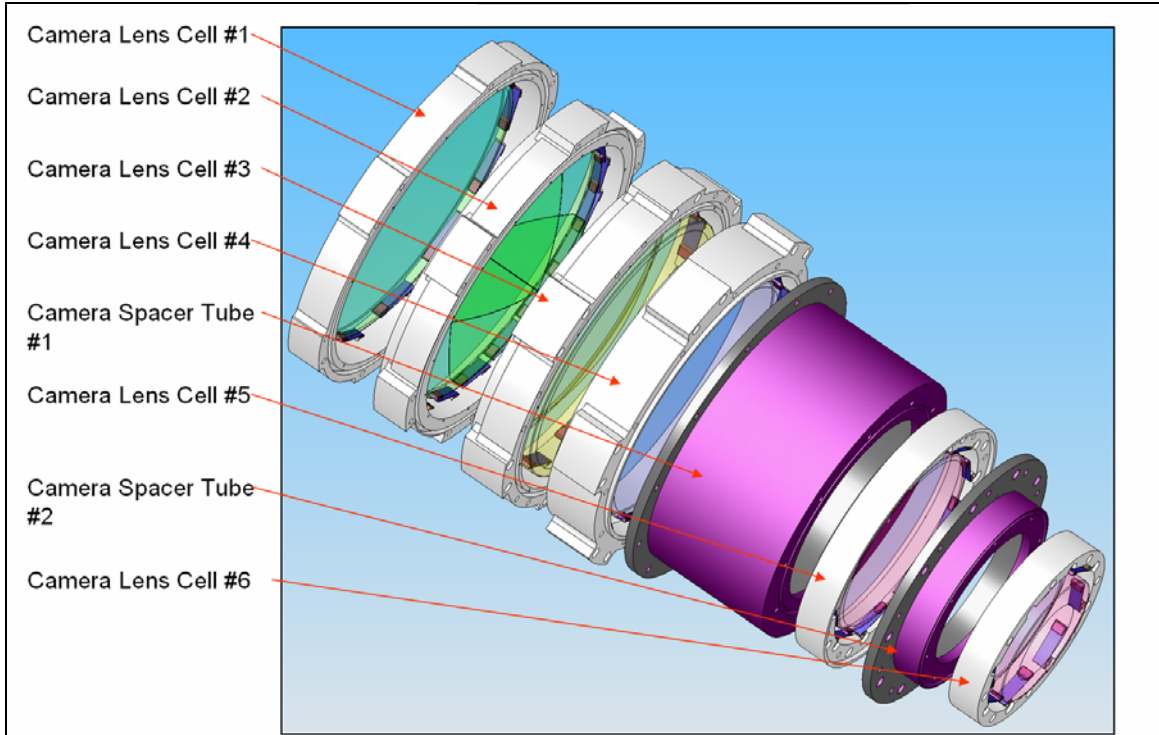
Figure 24: *Camera Assembly.*

Once assembled, the Collimator and Camera units will be light tight along their outer surfaces. However, stray light propagating through the optical system will need to be baffled. Several implementations of various forms of baffles will be used throughout the optical system. One method that will be employed within the two lens barrels is baffle rings as pictured in Figure 25. Structures within the lens assemblies, such as the flexure assemblies, result in surfaces that stray light can reflect off and can result in ghosting and/or the increase in general background radiation. Mounting baffle rings to mask these surfaces precludes this. Additional baffling can be added as necessary. The baffles as well as the internal surfaces of the lens cell "rings" will be painted infrared black using either Aeroglaze Z306 or WZ3301. These paints have been used successfully in NIRSPEC, NIRC2, and OSIRIS.
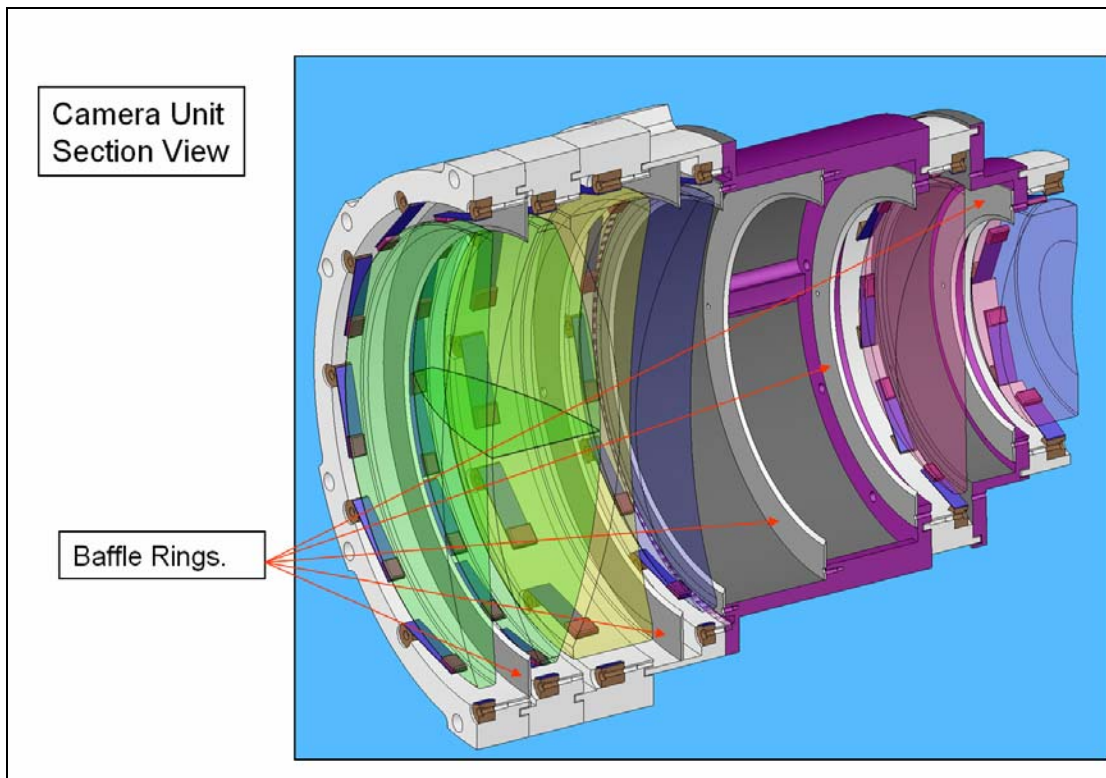
Figure 25: *Light baffles*.

The Collimator and Camera barrels are attached to the instrument structure with mounting brackets (visible in Figure 20). These brackets have precision-machined features which properly align the lens assemblies during integration. Both the collimator barrel and camera assembly have precision, stepped flanges which interface with a precision bore in each mount bracket. This interlocking geometry determines centration and axial position of the optics with respect to the bracket. The base of each bracket has flat surfaces which define a plane and pins which define the position on the plane. These features correlate to machined regions on the main bulkheads of the structure.

5.2.1.7.3 Lens Mount Analysis

The proposed lens mounting method was analyzed extensively in combination with the results of tests on a prototype system during the KIRMOS preliminary design process. Those reports were reviewed early in the MOSFIRE preliminary design in order to determine an analysis strategy that would benefit from and complement this earlier work with the end result being full confidence in the approach for all of the MOSFIRE lenses. The reduction of lens dimensions in MOSFIRE relative to the size of the KIRMOS prototypes meant that the suitability of the approach for smaller lenses had to be verified. MOSFIRE also includes different lens materials, so the suitability of the mount approach had to be verified for these new materials. The KIRMOS prototype tests also revealed some interesting bond edge issues which required further study to understand completely. Documentation from the KIRMOS project is available to the MOSFIRE team and relevant documents are posted on our web site with MOSFIRE Design Notes.

In order to address the issues mentioned, the bonded-flexure mount design was analyzed in two ways. One set of studies analyzed fully mounted lenses. This analysis predicted flexure and stress levels within the structure, and estimated bond reaction forces for the sizes, shapes, and materials to be used in MOSFIRE. The lenses were analyzed in perceived order of risk based on size or geometry until enough lenses were analyzed to indicate that the rest of the lenses would present no mounting problems by inspection. Another set of studies analyzed the performance of a single bond in detail in order to better understand the effects of thermal contraction on the bond interface-particularly at the interface pad perimeter. In both cases, the analysis results were compared to analytical predictions and to the KIRMOS prototype tests.

5.2.1.7.4 Lens Cell Assembly Analysis

FEA of the preliminary designs of the lens cells was used to predict lens flexure and maximum stresses in the assembly components under both gravity and thermal loads. Since inclusion of the thin adhesive layer was not practical for these multi-flexure analysis models, the models were used to predict maximum reaction forces at the bond interfaces instead. These estimated reaction forces were then compared to empirical data from destructive bond strength tests which were completed during KIRMOS' preliminary design phase. Four MOSFIRE lenses mounted with the bonded-flexure approach were analyzed in detail before it was apparent that the remaining lenses could be accurately and safely supported using this approach. The four critical lenses studied included: the largest and heaviest lens (Collimator lens #1); the second heaviest lens (Camera lens #2) which also has one of the smallest edge girdles; a small, thin meniscus lens (Collimator lens #3) which limited the number and size of flexure assemblies; and, a second small meniscus lens (Collimator lens #4) which was mounted in close proximity to the previous lens. Successful mount designs for these lenses explored the limits of the parameters that have an influence on the viability of the flexure mounting approach. The conclusions of this analysis, listed in Table 15, show that the resulting displacements and flexure from the mount designs are all comparable and well within acceptable values.

	Collimator			Camera
	#1	**#3**	**#4**	**#2**
Max. Lens Decenter (at center), μm	0.4396	0.2498	0.1859	0.3754
Max. Lens Axial Displacement (at center), μ m	2.4322	2.0025	1.4435	1.8165
Max. Lens Tilt, μrad	0.9604	4.4001	3.9596	0.1184
Max. Change in Radius 1, in	-0.004	-0.0003	0.0000	-0.0039
Max. Change in Radius 2, in	-0.0228	0.0000	0.0002	-0.0051
Max. Stres in Lens @ 1g, psi	138.6	101.8	97.5	137.6
Max. Stress at Clear Aperture @ 1g, psi	39.2	23.4	26.0	50.5
Max. Stress in Pad @ 1g, psi	2855.0	1527.5	1759.5	1816.0
Max. Stress in Flexure @ 1g, psi	6956.9	10474.8	9546.7	5321.2
Reaction Force Vector @ Plug, 293K, -1g Y				
magnitude, lb	2.1862	0.4969	0.3945	2.0512
θ, degrees	179.68	178.98	179.54	0.03
φ, degrees	90.04	90.05	90.01	90.03
Reaction Force Vector @ Plug, 293K, -1g Z				
magnitude, lb	1.1164	0.2574	0.2155	1.0538
θ, degrees	-90.45	-90.10	-90.05	90.53
φ, degrees	90.14	90.13	90.54	89.96
Reaction Force Vector @ Plug, 120K, 0g				
magnitude, lb	0.0143	0.3270	0.3540	0.4728
θ, degrees	0.00	-0.70	0.05	0.00
φ, degrees	8.82	13.72	15.64	8.23
Reaction Force Vector @ Plug, 120K, -1g Z				
magnitude, lb	1.4448	0.4171	0.3456	1.1523
θ, degrees	-82.80	-72.35	-69.54	86.32
φ, degrees	51.07	40.38	37.04	66.05

Table 15: *Relevant FEA results for the collimator and camera lens mounts.*

Note that clear aperture stresses are required to be < 200 psi to ensure that aberrations are not induced into the optics. Flexure predictions from the FEA studies can be better assessed when correlated to expected image motion. Table 16 shows a spreadsheet which is used to convert the estimated lens motions to image motion based on optical de-center/tilt sensitivity calculations (§5.1.2). The axial spacing flexure estimates are compared to the +/-10 μm goal established by the optical designer and estimated changes in the radius of curvature are compared to the original radius. Image motions can then be compared to overall uncorrected image motion requirements

and goals. The results for the four lens-mounts analyzed indicate a worst-case contribution to image motion of 1% of the requirement (camera lens #2). All of the other lenses analyzed contribute an order of magnitude less to image motion. By inspection of the remaining lenses not analyzed in detail, it is apparent that this 1% value is not likely to be exceeded.

The worst case axial spacing change due to flexure is ~1/4 of the goal for each individual lens. Again, based on inspection of the remaining lenses which weren't analyzed in detail, this value is not likely to be exceeded. The worst case radius change resulting from gravity effects is 0.04%, which is negligible. Again, inspection of the remaining lenses which were not analyzed indicates that this value is not likely to be exceeded.

Uncorrected Flexure Estimates				
Tilt	**Estimated Maximum Motion**		**% of Requirement** **(+/- 1.5 Pixels)**	
Component	**µrad**	**pixels**	**%**	**Comments**
Collimator Lens #1	0.9604	0.0001	0.004	Tilt Sensitivity: 18000 µrad/pixel
Collimator Lens #3	4.4001	0.0020	0.130	Tilt Sensitivity: 2250 µrad/pixel
Collimator Lens #4	3.9596	0.0007	0.044	Tilt Sensitivity: 6000 µrad/pixel
Camera Lens #2	0.1184	0.0002	0.013	Tilt Sensitivity: 621 µrad/pixel
Decenter	**Estimated Maximum Motion**		**% of Requirement** **(+/- 1.5 Pixels)**	
Component	**µm**	**pixels**	**%**	**Comments**
Collimator Lens #1	0.4396	0.0017	0.114	Decenter Sensitivity: 257 µm/pixel
Collimator Lens #3	0.2498	0.0015	0.102	Decenter Sensitivity: 164 µm/pixel
Collimator Lens #4	0.1859	0.0022	0.145	Decenter Sensitivity: 86 µm/pixel
Camera Lens #2	0.3754	0.0136	0.904	Decenter Sensitivity: 28 µm/pixel

Axial Spacing	**Estimated Maximum Motion**		**% of Goal** **(10 µm)**	
Component	**µm**		**%**	**Comments**
Collimator Lens #1	2.4322		24.322	
Collimator Lens #3	2.0025		20.025	
Collimator Lens #4	1.4435		14.435	
Camera Lens #2	1.8165		18.165	

Radius Change	**Estimated Max Change**	**Initial Radius**	**% change**	
Component	**µm**	**mm**	**%**	**Comments**
Collimator Lens #1 Surface #1	-10.1600	547.5947	-0.002	
Collimator Lens #1 Surface #2	-579.1200	-4438.9518	0.013	
Collimator Lens #3 Surface #1	-7.6200	-150.9766	0.005	
Collimator Lens #3 Surface #2	0.0000	-137.6240	0.000	
Collimator Lens #4 Surface #1	0.0000	92.6744	0.000	
Collimator Lens #4 Surface #2	5.0800	130.6669	0.004	
Camera Lens #2 Surface #1	-99.0600	302.6267	-0.033	
Camera Lens #2 Surface #2	-129.5400	-319.5752	0.041	

Table 16: *Estimated maximum lens motions vs. uncorrected image motion requirements & goals.*

Stress and reaction forces derived from FEA studies can also be better assessed when correlated to established material properties and strength test data. Table 17 shows a spreadsheet which is used to compare the maximum values obtained from the analysis to pertinent measures of the strength of the respective materials. For lens stress, the thermal stresses that develop in the bond area were not included because this analysis was handled separately. Instead, the maximum stress is based on gravity loads and includes the stress in the immediate bond area. The maximum predicted lens stress occurs in the largest and heaviest lens (Collimator #1). The stress is significantly below the established lens material safe limit of 500 psi under static loading. However, the MOSFIRE team

has established a 5g design goal (for shipping and handling) and two of the analyzed lenses fall below this level. These peak lens stresses occur at the sharp corners of the interface pad perimeter and are likely over-estimated to some degree. The reaction force safety factors which are based on empirical test result data indicate that this is true.

Bond reaction forces compare the forces obtained from the FEA studies to bond prototype tests in which the bond material was tested to failure. Sample bonds were fabricated utilizing appropriate lens and interface pad materials. The samples were then loaded in a manner comparable to the way bonds are loaded in the lens mounts, and the loads increased until the bonds failed. Load cells monitored the loads. Tests were performed at both room and cryogenic (~140 K) temperatures. Comparing the prototype results to the predicted reaction forces, it appears that the lens mounting approach has adequate margin of safety for the mounts analyzed.

Maximum Stress & Reaction Force Estimates

Lens Stress	Estimated Max Stress	Maximum Allowable	Factor Of Safety	
Component	psi	psi		Comments
Collimator Lens #1	138.6	500	3.6	Stress level indicates only 3.6 g acceleration survivability
Collimator Lens #3	101.8	500	4.9	Meets 5 g acceleration survivability goal
Collimator Lens #4	97.5	500	5.1	Meets 5 g acceleration survivability goal
Camera Lens #2	137.6	500	3.6	Stress level indicates only 3.6 g acceleration survivability

Flexure Stress	Estimated Max Stress	Yield Stress	Factor Of Safety	
Component	psi	psi		Comments
Collimator Lens #1	6956.9	190000	27.3	Meets 5 g acceleration survivability goal
Collimator Lens #3	10474.8	190000	18.1	Meets 5 g acceleration survivability goal
Collimator Lens #4	9546.7	190000	19.9	Meets 5 g acceleration survivability goal
Camera Lens #2	5321.2	190000	35.7	Meets 5 g acceleration survivability goal

Bond Reaction Force	Estimated Max Reaction Force	Pull-Test Failure	Factor Of Safety	
Component	lb	lb		Comments
Collimator Lens #1 (CaF2)	2.19	56.7	25.9	Meets 5 g acceleration survivability goal
Collimator Lens #3 (ZnSe)	0.50	43.0	86.5	Meets 5 g acceleration survivability goal
Collimator Lens #4 (Fused Quartz)	0.39	55.5	140.7	Meets 5 g acceleration survivability goal
Camera Lens #2 (CaF2)	2.05	56.7	27.6	Meets 5 g acceleration survivability goal

Table 17: *Comparison of the maximum estimated stresses and reaction forces obtained in the studies to appropriate bench-mark data.*

In this analysis the lens and flexure maximum stresses result from gravity loads. The bond reaction force results include the effects of thermal contraction and the bond reaction force pull-test data is obtained based on the materials bonded.

5.2.1.7.5 Single Bond Analysis

This study analyzed the bonded pad geometry for the FCS mirror supports, but the results are applicable to the lens bonds, as well. Thermal effects were studied on the bonded interface between a single mirror pad and the mirror substrate. This study consisted of a single 12.7 mm diameter x 2.5 mm thick invar plate bonded to a fused silica substrate. In the analysis, typical material properties, such as CTE and Young's modulus and their variation with temperature based

on available data, were used. Some model parameters were varied in order to understand trends due to parameter changes. Results were obtained that appear to correlate well to prototype bond tests, even though they do not give a definitive answer to the maximum stress levels in the bond components. We confirmed the importance of minimizing excess adhesive around the pad.

Excess adhesive is unconstrained by the pad, and can rupture the substrate material as the adhesive contracts if the adhesive is stronger than the substrate material. Some of the prototype samples confirm this, as excess adhesive around the bond joints "chunked" out the sample substrates while the bond area under the pads remained intact. Our analysis predicts that peak stresses occur in the immediate vicinity of the discontinuities of sharp model edges around the perimeter of the pads but drops to safe levels within a couple of mesh elements away from the sharp corners. Near the edges of the pad the peak stresses increase towards infinity as the mesh density increases towards infinity–a property of FEA. The uncertainty in the analysis lies in how many mesh elements away from the sharp edge does one start to predict realistic stress levels. Brittle fracture and crack energy come into play and FEA does not adequately simulate this when the element sizes get infinitely smaller. FEA runs without the adhesive layer included indicates stress levels in the bond region of a few hundred psi throughout the entire bond interface. Addition of a "membrane" layer of adhesive with zero thickness brings the peak stress at the perimeter of the bond up to a few thousand psi while the stress in the center of the bond remains low. As the adhesive thickness is increased up to 0.25 mm, the stress in the perimeter region continues to rise in a roughly linear fashion to a few 10,000 psi, but the stress in the rest of the bond area remains at a few hundred psi. So, the analysis indicates that minimal controllable adhesive thickness is also desirable. This result was also observable in prototype bond tests. Prototype tests showed good bond pull-strength with 0.13 mm bond thickness, but bond failure under thermal cooling (without load) with 0.25 mm thick bonds. While this study of the bond geometry didn't reveal the actual stress levels in the perimeter of the bonds with certainty, it did help to determine what to test next in order to improve confidence and safety margins in the bond technique.

5.2.1.7.6   Prototype Testing

During the detailed design phase we will build and test one or more lens cells. We will build on the experience already gained with the use of bonded flexures to mount the large field lens for KIRMOS.

5.2.1.7.7   Lens Mount Assembly

Lens mount assembly and disassembly procedures will be developed during the detailed design phase. Jigs will be made to handle the installation of a lens into its cell and the bonding of fixtures to the lens girdle. Lens cells are easily handled and stacked into the camera barrel. Similar techniques have been developed by this team to handle smaller lenses in other Keck instruments.

5.2.1.8   Mechanisms

5.2.1.8.1   Grating/Mirror Exchange Turret

MOSFIRE provides both imaging and spectroscopic observing modes and this is accommodated by interchanging a plane mirror and a reflective grating in the collimated portion of the MOSFIRE optical path. MOSFIRE is designed to use a fixed grating, so the method used to interchange the grating and mirror must be highly repeatable. This is accomplished using a turret mechanism.
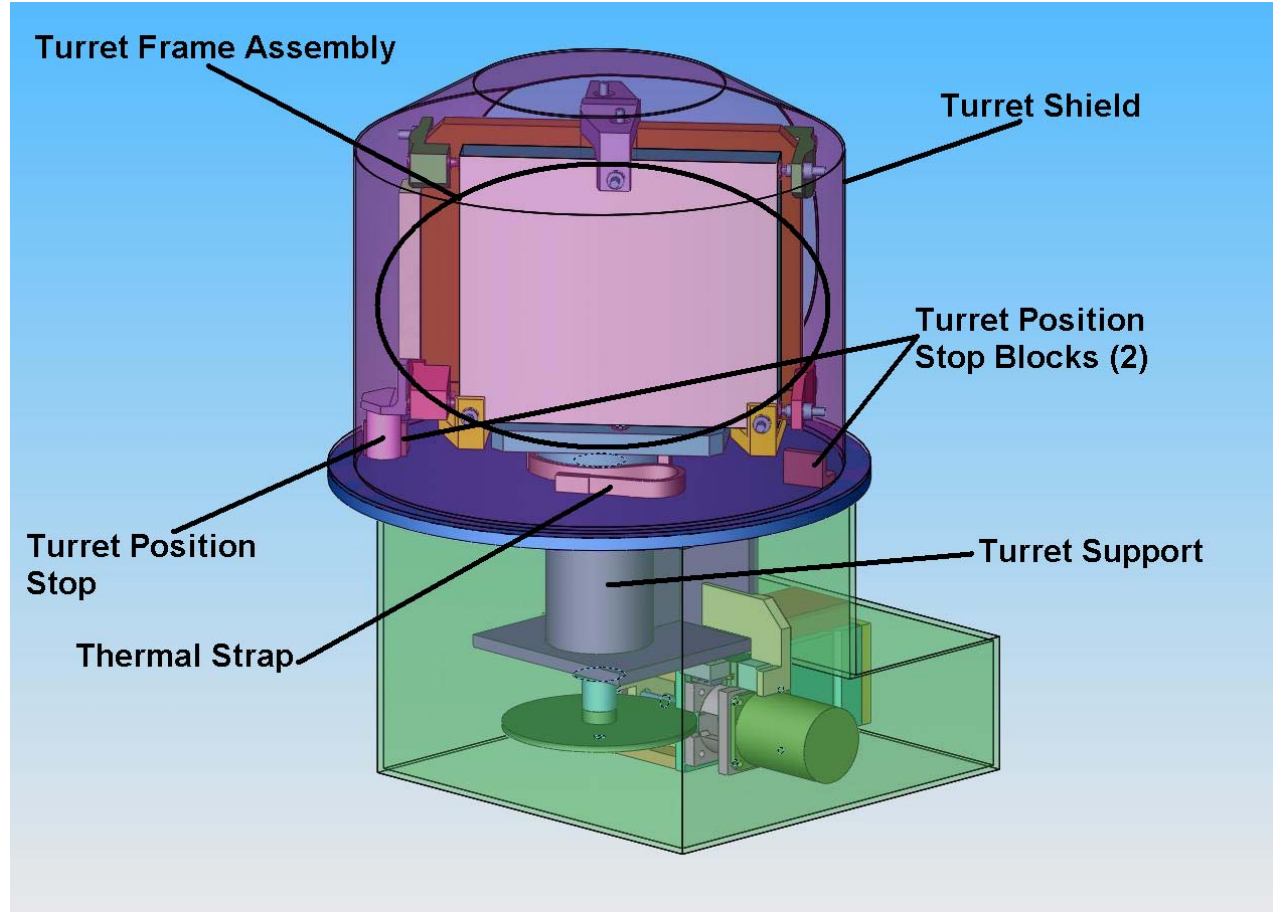
Figure 26: *Grating/mirror exchange mechanism.*

The grating/mirror exchange mechanism consists of a turret assembly and a drive assembly. The turret assembly contains the frame assembly which supports the grating and mirror. The frame assembly is attached to the end of a spindle, or shaft. The spindle is supported by a pair of cryogenically-prepared deep-groove ball bearings (Champion CS6008BBRT-9). The bearings are retained in an aluminum hub structure while the spindle is constructed of stainless steel to match the bearing race construction. Bearings will be pre-loaded to compensate for the thermal differential contraction of the materials. These bearings are substantially over-sized relative to the turret loads to allow for a thicker, stiffer shaft which minimizes turret flexure under varying gravity vector loads. The drive system for the turret is connected to the other end of the spindle.

Layout of the turret assembly can be seen in Figure 26. This image also shows the two turret position stop blocks which define the deployed optics, the thermal straps which help cool the moving turret frame assembly, and the turret shield. The thermal strap design is borrowed from an earlier instrument (NIRC2). Straps provide a conductive path to help cool the rotating components of the turret during instrument cool down.

An aluminum structure provides the rotating-turret frame and contains provisions for mounting the grating and the imaging mirror in a back-to-back configuration. For turret balance purposes, the grating and the imaging mirror will likely be fabricated to the same dimensions despite slightly differing clear aperture requirements. The optics mount in a back-to-back configuration which helps minimize turret space requirements. Each element is positioned with a unique angle to the incoming beam when deployed, while also maintaining the same distance to the previous optical element. Their centerlines are slightly offset from each other and relative to the turret axis to compensate. This mounting arrangement creates a slight out-of-balance condition for the turret. Consequently, the turret position-stop is located to help counteract this balance condition, but an additional small counterweight mass is required to re-balance the turret frame assembly.

Both the grating and mirror are depicted mounted with a spring-loaded, six-point definition system similar to designs incorporated in previous instruments. This mount approach was invalidated during the preliminary design phase based on friction test results. Tests indicated that the low-friction plastic defining point components have substantial increases in friction at MOSFIRE's intended operating temperature. Instead, the grating and mirror will be mounted utilizing the bonded tripod mount that was design for the FCS mirror. The grating and imaging mirror are of comparable size to the FCS mirror, so the analytical results are applicable. Details of this mounting approach are found in the FCS section. The turret frame will be modified for these mounts in the detail design phase. Adjustment of the grating and mirror yaw angle will be done via adjustment of the turret stop blocks. Pitch will be adjusted with shims.

A worm drive assembly connected to the lower end of the spindle is used to operate the grating turret mechanism (Figure 27). This worm drive system is based on the grating/mirror exchange design used in the NIRSPEC instrument. The worm gear is stainless steel with 32 pitch and 14.5 pressure angle. The worm is constructed of UHMW polyethylene and is supported on a 416 stainless steel shaft by a pair of cryogenically-prepared deep-groove ball bearings (Champion CSR3BBRT-9 & CSR4BBRT-9). These bearings are also axially pre-loaded to compensate for variances in material thermal contraction. The worm shaft is connected to a cryogenically prepared NEMA 23 stepper motor via a flexible coupling and the entire worm drive assembly is mounted on a flex-mount frame. The drive assembly utilizes a pair of symmetrically-mounted compression springs to pre-load and define the turret frame assembly against the turret definition stop blocks. Two pairs of symmetrically-located switches (Honeywell Microswitch #11HM1) are utilized to stop the drive motor and report the drive's current position.

The grating/mirror exchange mechanism uses a simple drive "wind-up" method to accurately re-position the two optics into their defined positions. This method is possible since there are only two, "end-of-travel" positions required of the mechanism. In addition, this method eliminates the need for high precision of the drive-train components or extremely high accuracy in the

switches/interlocks. It also accommodates wear of the drive train components without loss of position accuracy.
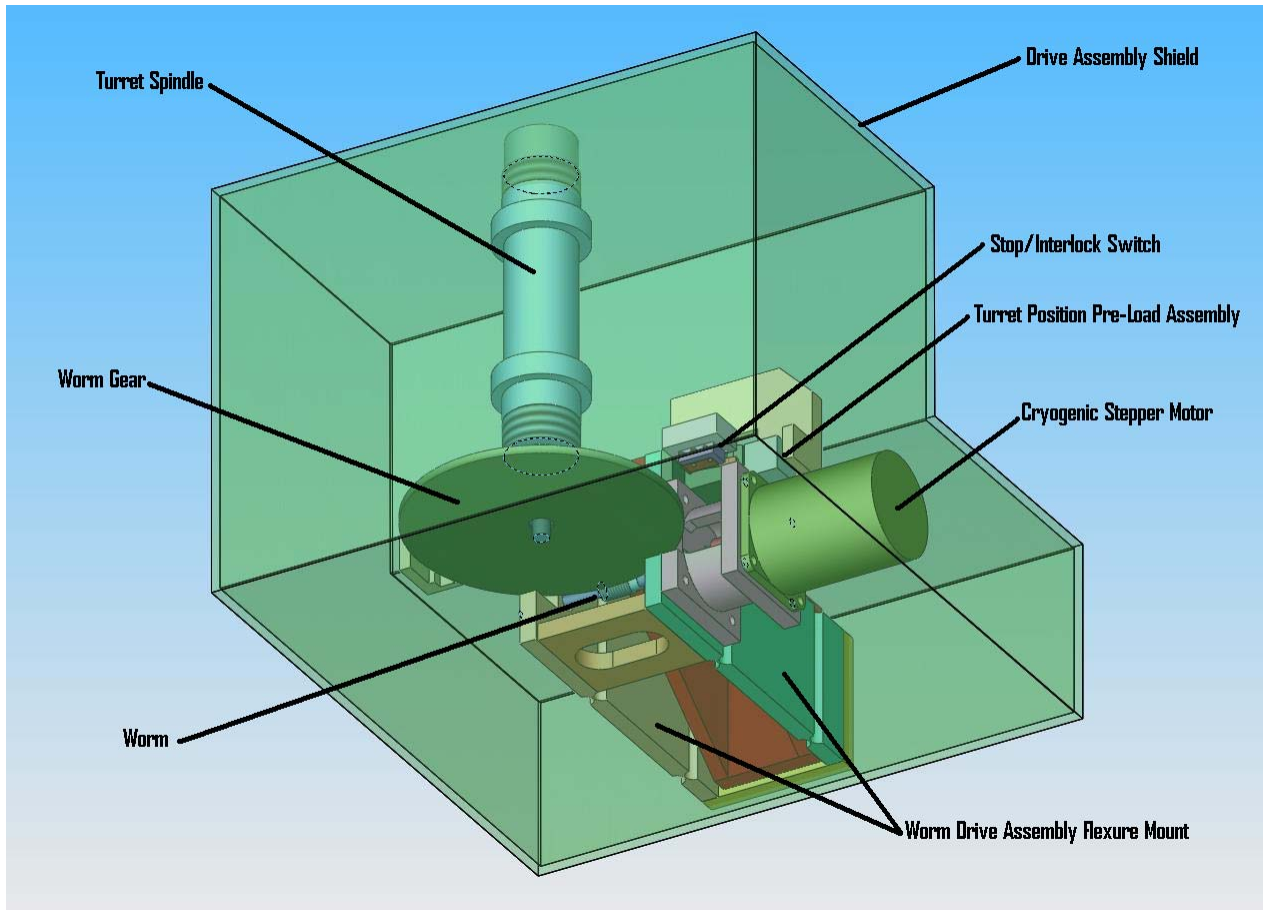
Figure 27: *Grating/mirror exchange mechanism worm drive components.*

When the instrument operator wishes to switch between instrument modes (imaging/spectroscopy), the correct optic is selected (grating/mirror). If the incorrect optic is in position based on the state of the grating/mirror exchange mechanism's two interlock switches, the mechanism's motor is driven in the proper direction for a pre-determined number of steps. The motor then decelerates and slowly creeps until the motor stop switch is actuated. Through this process, the motor is turning the worm, which in turn is turning the worm gear. The worm gear spins the turret through the 157.4 degrees of rotation between the two optical deployment positions. The optical design requires an offset of 22.6 degrees between the grating angle and mirror angle. As the turret slows down near the deployment position, the turret's stop engages one of the two fixed stop blocks which define the mirror or grating position. The turret can no longer rotate in this direction, so the turret, spindle, and worm gear stop rotating. However, the worm and motor continue to turn, and this action causes the worm drive assembly to translate tangential to the worm gear. The drive assembly's motion is constrained to tangential motion by the flex mount. Tangential motion compresses the drive pre-load spring in that direction by approximately 1 mm. At that point, the stop switch is activated- shutting off the motor. The worm drive won't back-drive, so the turret is

loaded against a fixed definition block with a consistent and sufficient force to accurately define the deployed optic. The position of the turret is indicated by an interlock switch which is adjusted to activate slightly before the corresponding stop switch. A second switch is used in this fashion to ensure that the interlock switch is definitively engaged regardless of temperature, gravity orientation, or creep within the drive. The stop switch may disengage under any of these conditions in between mode changes, but its job of stopping the motor has already been done. The pre-load spring is sized so that these small position effects don't appreciably alter the amount of pre-load and, thus have negligible effect on the optic's position. When the drive is reversed to deploy the other optic, a symmetrical set of pre-load components and switches are activated. Figure 28 is a plan view of the grating turret.
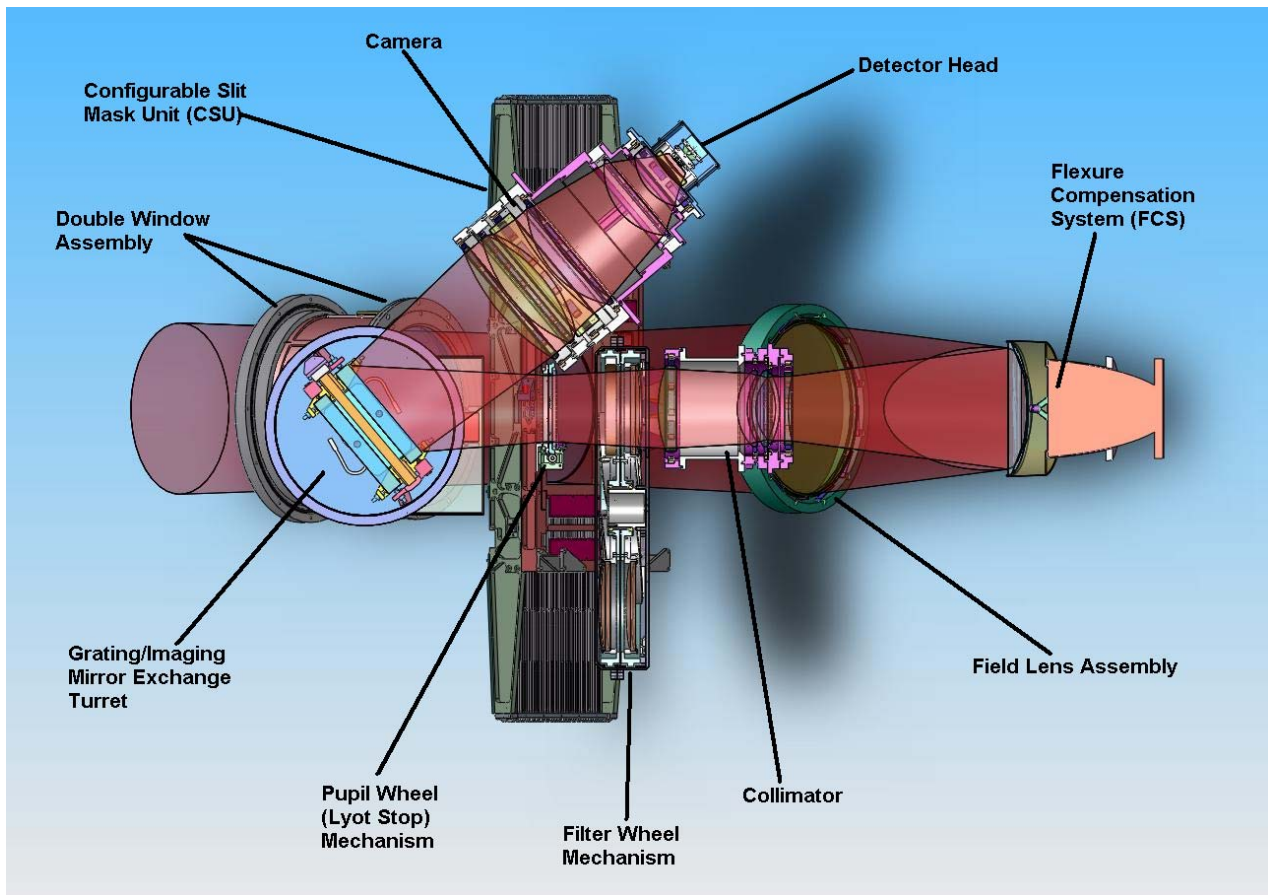
Figure 28: *View of MOSFIRE's optical system components with the grating/mirror turret mechanism set for spectroscopic mode.*

The turret frame and spindle were analyzed using FEA to predict the internal flexure within the structure. Although the analysis was based on a six-point kinematic mount scheme which has now been abandoned, it indicated that most of the optical motion was due to flexure in the spindle itself. Our plan is to base the current grating and mirror mounts on the FCS mounting scheme which has been shown to be very rigid. The spindle flexure will continue to limit the grating and mirror motions. Thus, the turret analysis results are considered valid for MOSFIRE's flexure budget.

Analysis indicated that the mechanism's contribution to instrument flexure is small enough to meet our uncorrected flexure requirements. The grating mechanism's flexure is a major portion of the overall flexure, so further reductions of flexure in this mechanism will have a strong impact on reducing overall instrument flexure levels. The re-design of the mirror and grating mounts provides an opportunity to further reduce flexure without adding appreciable weight to the assembly.

Performance Predictions
- Exchange time: <30 seconds
- Position accuracy: <6 µrad (~0.16 pixels)
- Position repeatability: <6 µrad (~0.16 pixels)

5.2.1.8.2   Double Filter Wheel

MOSFIRE's filter wheel design is based on the proven stepper motor drive units used in OSIRIS, scaled in diameter to accommodate the larger filters required. As shown in Figure 29 the design incorporates a double wheel. The volume available for the mechanism and the necessary filter size are the dominant drivers for the configuration. Our preliminary design accommodates filters up to 180 mm in diameter. This provides ample area for the required clear aperture (~155 mm) and mounting requirements. Each filter will be mounted in an individual cell or mounting assembly which will provide the angular tilt with respect to the optical path and will facilitate the handling of the filters when not mounted to the wheel. Volume constraints dictate a wheel diameter no larger than 25 inches. This size can accommodate six (6) mounted filters. MOSFIRE will require at least five or six different filters as a bare minimum. To accommodate future requirements we have decided to have two filter wheels in a stacked configuration. Each wheel will have positions for 5 optical elements (filters, blanks, etc.) and one open position.

Filter wheels will be edge driven. Custom gear teeth will be cut into the edge of each wheel. They will be driven by stepper motors and spur gears. A 20 pitch gear is included in the preliminary design. The spur gear in the current design is 2 inches in diameter. With this ratio any filter move should be accomplished in less than 20 seconds. The gear pitch is relatively coarse to allow enough back-lash for the detents to engage. We intend to use stepper motors that are modified for cryogenic use. A major factor in selecting internal motors instead of external "warm" motors is that the locations of the mechanisms within the structure would require very long and complicated drive shafts. The design and implementation of these shafts was considered riskier than utilizing cryogenic motors, especially given their successful application in NIRSPEC and OSIRIS.

Each wheel will be supported by and revolve around a central hub using a stainless steel, 4-point-contact ball bearing available from Kaydon Corp. Using a 4-point-contact bearing allows us to support both the radial and axial loads using a single bearing per wheel. Positional accuracy and repeatability will be provided by detents. Positional feedback is achieved using three micro switches for each wheel and a series of activators that give a unique binary pattern for each individual position. This approach was tested and used in the OSIRIS instrument.

The large wheels have a fairly tenuous thermal conduction path to the static housing surrounding them. The only path is primarily through the ball bearings. Therefore, the wheels will cool down largely through radiation. In order to achieve the most efficient cool down we will have to ensure that the filter wheel module mounting brackets provide adequate conduction. In order to expedite the cooling of the wheels themselves there is a thin static plate mounted between the wheels and attached to the housing. This essentially doubles the "cold" surface area for the wheels to radiate onto and therefore almost halves the cool down time.
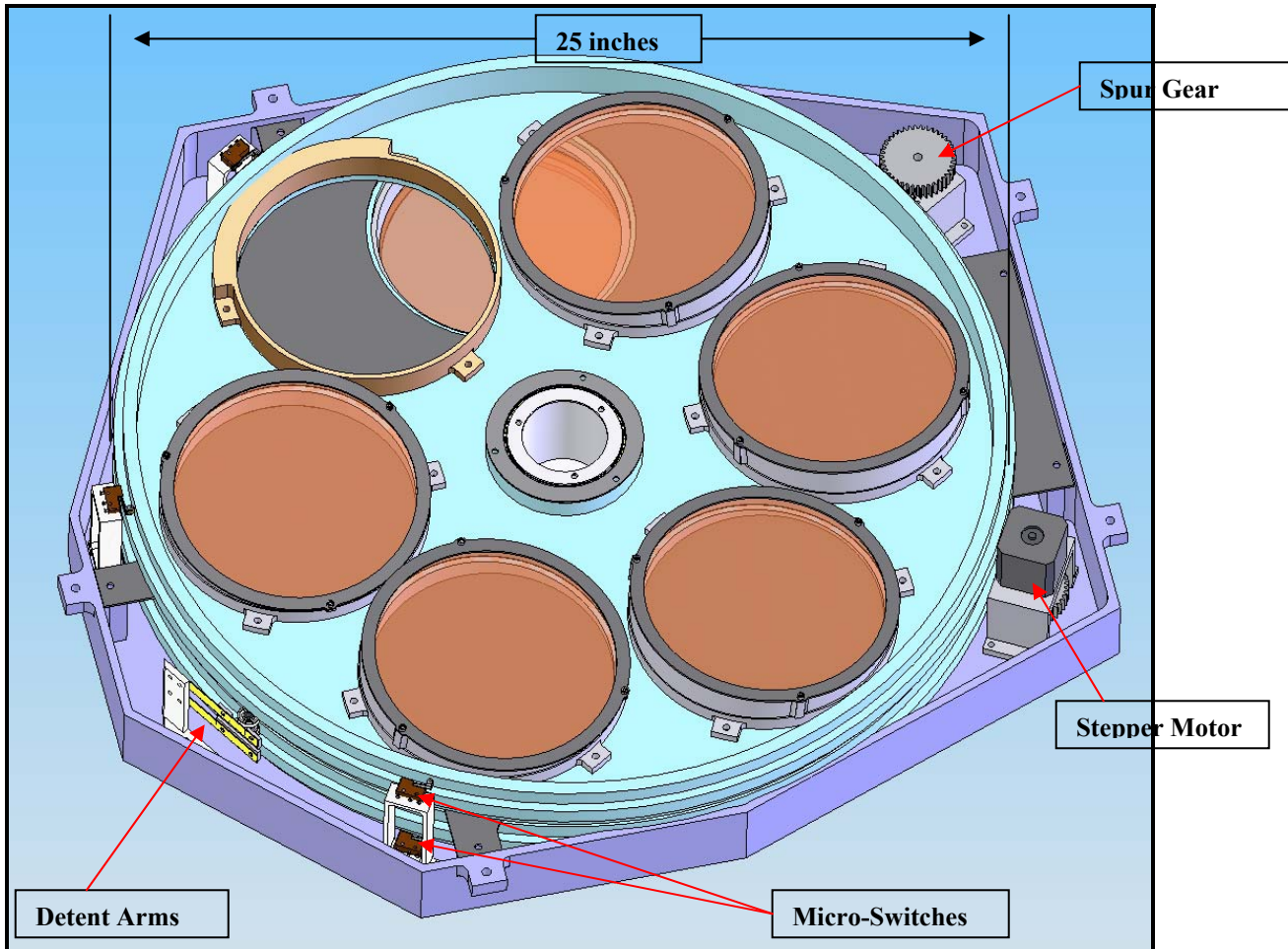
Figure 29: *Dual filter wheel with cover removed.*

Minimal calculations were done for the filter wheel mechanism during the preliminary design due to its heavy reliance on details from previously built designs. There is enough heritage with similar mechanisms that these are not pressing issues. A simple hand calculation shows the maximum flexure of the wheel housing from the mass of the wheels and a 180 degree shift in gravity vectors to be approximately 0.001″. This is well within requirements for positioning and stability for a filter mechanism. This is also a worst case condition that the mechanism will never see in actual use. In the detailed design phase, additional analysis will be done to verify adequate flexure

performance, optimize gear pitch and size, and verify motor choice. Based on its reliance on previously built and tested mechanisms, this mechanism is considered a low risk device.

5.2.1.8.3   Pupil Wheel

MOSFIRE requires a cold Lyot stop in the H and K bands to suppress stray thermal radiation from the telescope. Because the Keck telescope pupil is hexagonal, this stop should also be hexagonal to maximize throughput. The design of a hexagonal stop is further complicated by the fact that the stop must rotate to compensate for the action of the instrument rotator.

The MOSFIRE pupil wheel is shown in Figure 30. Two stop modes will be available using an adjustable iris. For the longer wavelengths, the iris will close to "K" band position and then the mechanism will rotate at the prescribed rate to track the hexagonal image of the primary. Figure 30 shows the mechanism with the iris closed to this configuration. In Figure 31 you can see the iris blades in detail. There are 6 blades currently forming a simple hexagon. The final size and shape of the iris will be determined in the detailed design phase. In this mode the mechanism can provide clockwise and counter clockwise rotation on the order of 300 degrees. To function properly as an optical baffle, the iris blades will be painted InfraRed black using something like Aeroglaze Z306 or WZ3301. These paints have been used successfully in NIRSPEC, NIRC2, and OSIRIS. For the shorter wavelength's mode, the mechanism rotates into a stop, the iris opens completely, and the mechanism engages another stop as a home position.

Again, two 4-point-contact ball bearings available from Kaydon Corp. will be used as rotational bearings. This type of bearing has also been used in NIRC2. Because of the relatively large diameter of the bearings and the fact that they are of steel construction we have decided that the majority of the assembly will be fabricated from 416 Stainless Steel. The coefficient of thermal expansion (CTE) of this material is similar enough to the ball bearing's CTE that no additional compensation for differential expansion is needed for the interface between the bearings and housing.

As with the filter wheel, the pupil mechanism will be driven with a stepper motor that has been modified for cryogenic use. Once again, the location of the mechanism and heritage from OSIRIS were the key factors in selecting cryogenic motors.
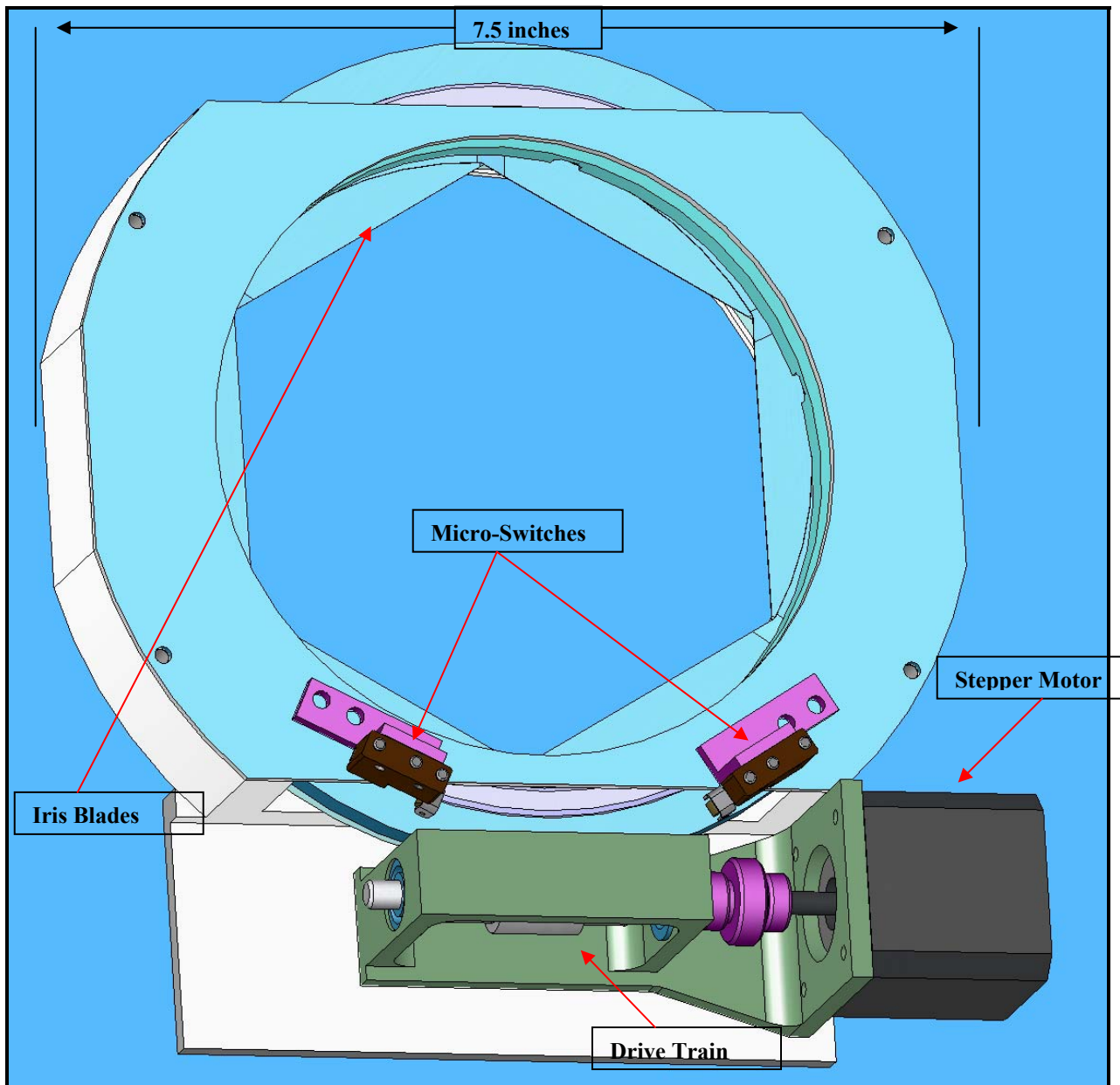
Figure 30: *Pupil Mechanism components.*
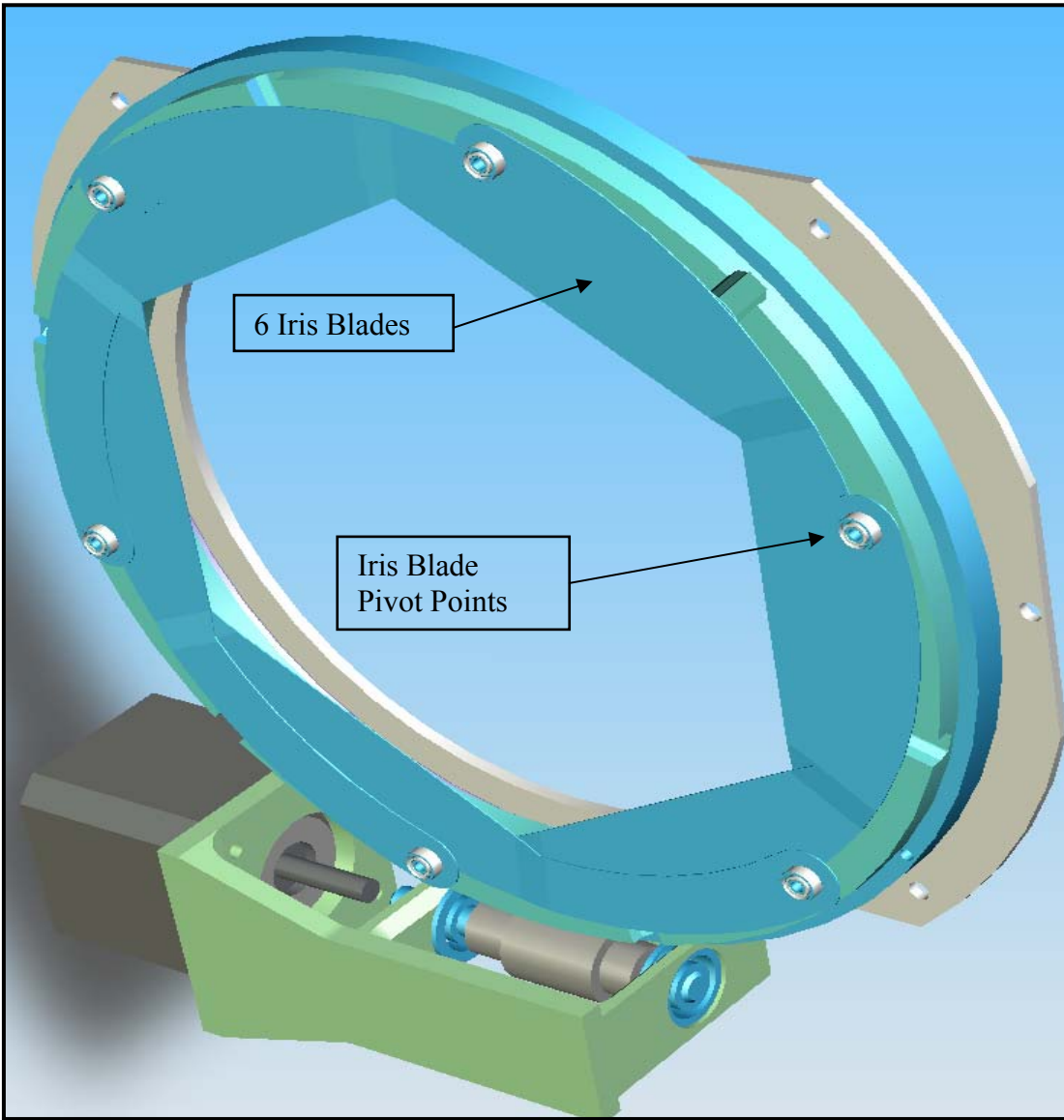
Figure 31: *Pupil mechanism iris blade detail.*

We will likely use motors from a company called MRC. These motors have been tested at CIT and demonstrated a lifetime of at least 20 years. The mechanism will be edge driven using a worm and worm gear (see Figure 31). This drive train is very similar to the one used in the MOSFIRE grating turret mechanism and has been used several times in previous UCLA instruments (OSIRIS, NIRSPEC). By setting the backlash between the worm and worm gear properly and by using accurate tolerance techniques during fabrication, the positioning and stability requirements of the mechanism can be maintained without additional measures.

The pupil mechanism will have a "Home" position defined by a hard stop. In the "Home" position the iris is open to the shorter wavelength mode. Positional feedback at the "Home" position is achieved using a micro switch. Previous experience has shown that such a hard stop provides an

adequate datum for positional calibration. The distance from the "Home" position to the iris closed to "K" position will need to be calibrated. The mechanism can then be rotated to the proper position in the field by simply counting steps. A second micro switch can either serve as a redundant "Home" feedback or as some intermediate feedback point.

In the long wavelength mode (iris closed to "K" and pupil rotating) the stepper motor will probably be running continuously. This will result in a heat source that will need to be attached to a heat sink. To avoid unacceptable heat transfer into the mechanism itself or other structure close to the optical path, the stepper motor will be connected with flexible copper straps to the nearest Aluminum bulkhead of sizeable mass.

5.2.1.8.4   Flexure Compensation System

In order to meet the MOSFIRE design goal of <0.1 pixel of residual image motion due to flexure, an active flexure compensation system (FCS) has been provided. This design utilizes a piezo actuator driven tip/tilt mirror mounted in a standoff tube attached to the rear optical bench as shown in Figure 14. Flexure correction will be implemented using a look up table based on telescope elevation and instrument rotator angle. Previous experience with similarly sized Cassegrain instruments (Kibrick et al. 2000, 2003) has shown that a 10:1 reduction in image motion is possible with such a system. For MOSFIRE, the instrument optics must be cooled to cryogenic temperatures (~130 K), so the flexure compensation system must be compatible with cryogenic conditions.

MOSFIRE's flexure compensation system is based on a custom version of a piezo tip/tilt platform to be designed and manufactured by a vendor named PI (Physik Instrumente). A similar system has recently been built for NIRES and is just beginning testing. Experience gained from the NIRES system will benefit the design of the MOSFIRE system. The layout of the flexure compensation system assembly is shown in Figure 32. Basically, the tip/tilt platform, which has a 266 mm diameter mirror mounted from the platform's load plate, consists of three low-voltage piezoelectric linear drives which will support the load plate in a tripod fashion. The platform itself will operate closed loop with feed-back from capacitive sensors. The tripod drive arrangement allows a level of redundancy in the system design since the platform could still operate through a portion of its range should one of the linear drives fail.

The mirror mount design is also based on a tripod layout. For the mirror itself we plan to use CLEARCERAM-Z, which is an ultra-low expansion glass-ceramic material. Attachment of the mirror to the load plate will be by means of three flexure assemblies which form a tripod. The flexure assemblies consist of a cylindrical mirror pad which is bolted or pinned to an A-frame shaped flexure. The flexure components and the load plate will be constructed of invar so that their thermal contraction closely matches the mirror substrate. The flexure assemblies are designed to allow for the relatively small differential radial contraction between the mirror substrate and the load plate without breakage of the mirror substrate. At the same time, they provide accurate location of the mirror with minimal flexure as the assembly experiences varying gravity vectors. The mirror mount flexures are attached to the mirror substrate with a bonded joint and 13 mm diameter round CTE-matched invar pads are bonded to the substrate with a ~125 μm filled-epoxy

joint (Armstrong A-31). This bonding approach has been prototyped and strength-tested to establish safety margins for various substrate/pad combinations.

The FCS assembly includes two additional components. First, there is an aluminum shield which surrounds the back side and edge of the mirror. This shield will help cool the mirror by radiation coupling to the exposed substrate surfaces. In addition, the shield is designed to constrain the mirror from separating from the assembly in the unlikely event that any of the bond joints fail. A second additional component of the FCS is a counterweight "sleeve" which is suspended from the load plate. The counterweight places the CG of the supported load at the pivot point of the tip/tilt platform.
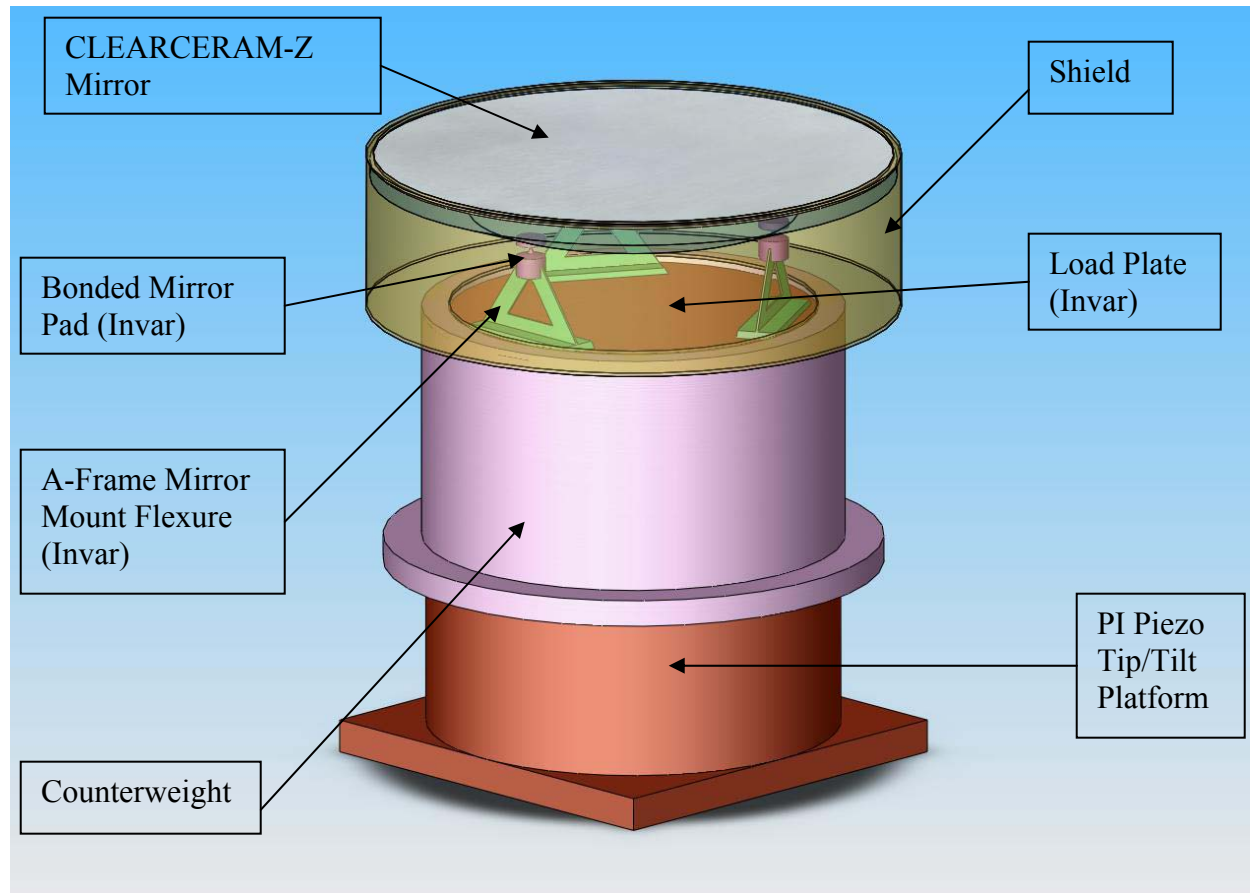
Figure 32: *Preliminary design of the flexure compensation system assembly. The shield is shown transparent so that the mirror mount components can be seen.*

Preliminary analysis indicates that the bonded, tripod mirror mount design provides sufficient rigidity to meet our flexure budget goals for this structure. Analytical results are summarized in Table 18. In addition, the design is estimated to safely withstand a minimum of 5 g's of acceleration in all directions under cryogenic conditions. Estimates of mirror distortion under combined loads (thermal & gravity) indicate one extreme gravity orientation where the distortion

may be marginal relative to our goal. One edge of the mirror "curls" by ~0.34 μm (see Figure 33) while the goal is deformation <0.25 μm. Further optimization of the design parameters (pad location, flexure thickness, etc.) during the detail design should bring the maximum deformations within our goal. A concern is that the tripod design does not provide sufficient cooling paths to cool the mirror to operating temperature in the same time as the rest of the instrument through conduction alone. However, radiative coupling between the mirror substrate and the surrounding metal structure can reduce the mirror cool down time to match the rest of the instrument.

Summary of Extreme Values		
Parameter	**Value**	**Unit**
Maximum Axial Displacement	**12.37**	µm
Maximum Axial Thermal Displacement	12.19	µm
Maximum Axial Gravity Displacement	0.23	µm
Maximum Radial Displacement	**1.59**	µm
Maximum Radial Thermal Displacement	0.01	µm
Maximum Radial Gravity Displacement	1.54	µm
Maximum Tilt		
Ambient Conditions (298 Kelvin)	2.32	µrad
Operating Conditions (120 Kelvin)	1.50	µrad
Maximum Mirror Surface Deformation	**0.34**	µm
Minimum Bond Strength Safety Factor		
Shear Strength	15	
Tensile Strength	5	
Minimum Support Component Safety Factors		
Flexure Stress	8	
Flexure Buckling	44	

Table 18: *Summary of the preliminary FCS static analysis results.*

5.2.1.8.5   Performance Predictions

- FCS correction range: +/-500 µrad (+/- 6.2 pixels) @ 77 K

As discussed in the instrument flexure section, the current conservative estimate of maximum image motion is +/- 3.3 pixels for complete sky coverage. Thus, the predicted FCS range is nearly twice the expected range needed.
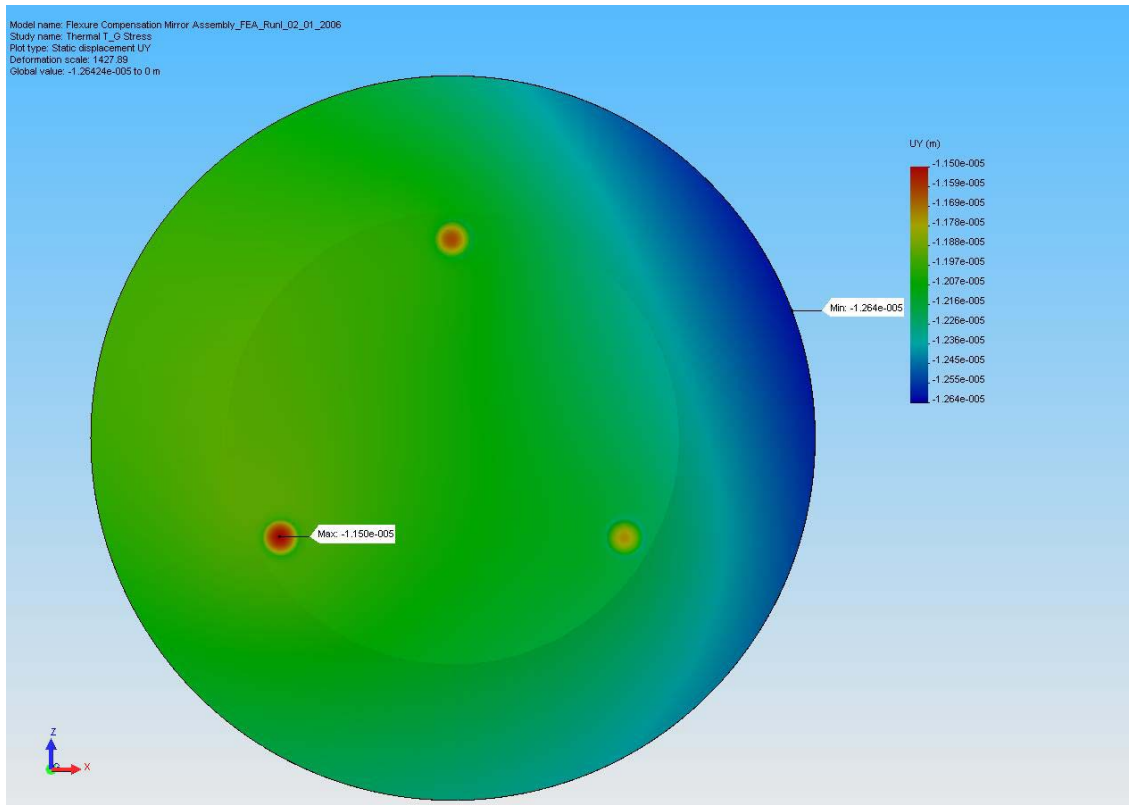
Figure 33: *Axial displacement plot from the analysis load case which produces the maximum surface deformation (0.34 μm).*

Figure 33 reveals that the estimated value slightly exceeds our maximum deformation goal of 0.25 μm. This effect may be controlled by further optimization of assembly/component parameters such as component dimensions or support spacing.

The highest risk aspect of the FCS system is the bonded flexures which support the mirror. The bonding approach will be used for the lens mounts, as well as the other optic flats in MOSFIRE. Starting during the KIRMOS preliminary design, extensive analysis and prototyping has occurred in order to validate the bonding technique and reduce the risk. More information on these risk mitigation efforts was detailed in the lens mount section.

5.2.1.8.6   Detector Head/Focus Assembly

The images and spectra produced by the MOSFIRE optics will be captured by a Rockwell Hawaii 2-RG detector. This detector is 2048 by 2048 pixels, and has an ASIC chip controlling it and interfacing it to our acquisition system. The ASIC chip will be located close to the detector, inside the vacuum chamber, so its mounting must be considered, as well. The detector will have a mechanism to move it to keep the images in focus for different wavelength ranges. The final lens of the camera optics, the field flattener, is located very close to the detector, so it will be mounted as part of the detector head and move with the detector.

The design is partially based on the detector head of the FLITECAM instrument, in which a vendor-supplied detector mount was enclosed in an outer shell, thermally isolated by G10 tabs, and cooled from a cold finger from a liquid Helium tank. In MOSFIRE we will provide a dedicated CCR head (probably a CTI Cryogenics model 22) which will cool only the detector head.

Figure 34 shows a cutaway view of the whole detector head assembly. This module contains the detector, field-flattener lens and a piezo-driven focus mechanism. The detector itself is supplied on a molybdenum alloy substrate, with threaded holes for four legs. The legs are threaded at both ends with spacers (thick washers) in the middle. The legs attach to a block of similar molybdenum material (to avoid thermal mismatch when we cool everything down). The temperature sensor and heater are attached to the back of this block. The block is then interfaced to the focus mechanism via G-10 A-frames. The focus mechanism, supplied by Physik Instrumente, is a piezo-driven actuator in the form of a small (50 mm square by 17.5 mm thick) block, with one square face forming the mounting surface. Attached to the front surface of the block and enclosing the detector is a box structure. A plate holding the mount for the field flattener lens forms the front of this box. The focus mechanism is to the rear of the outer enclosure, which is a box with a circular flange. This flange attaches to the rear of the camera tube. For handling, a temporary front cover is available.
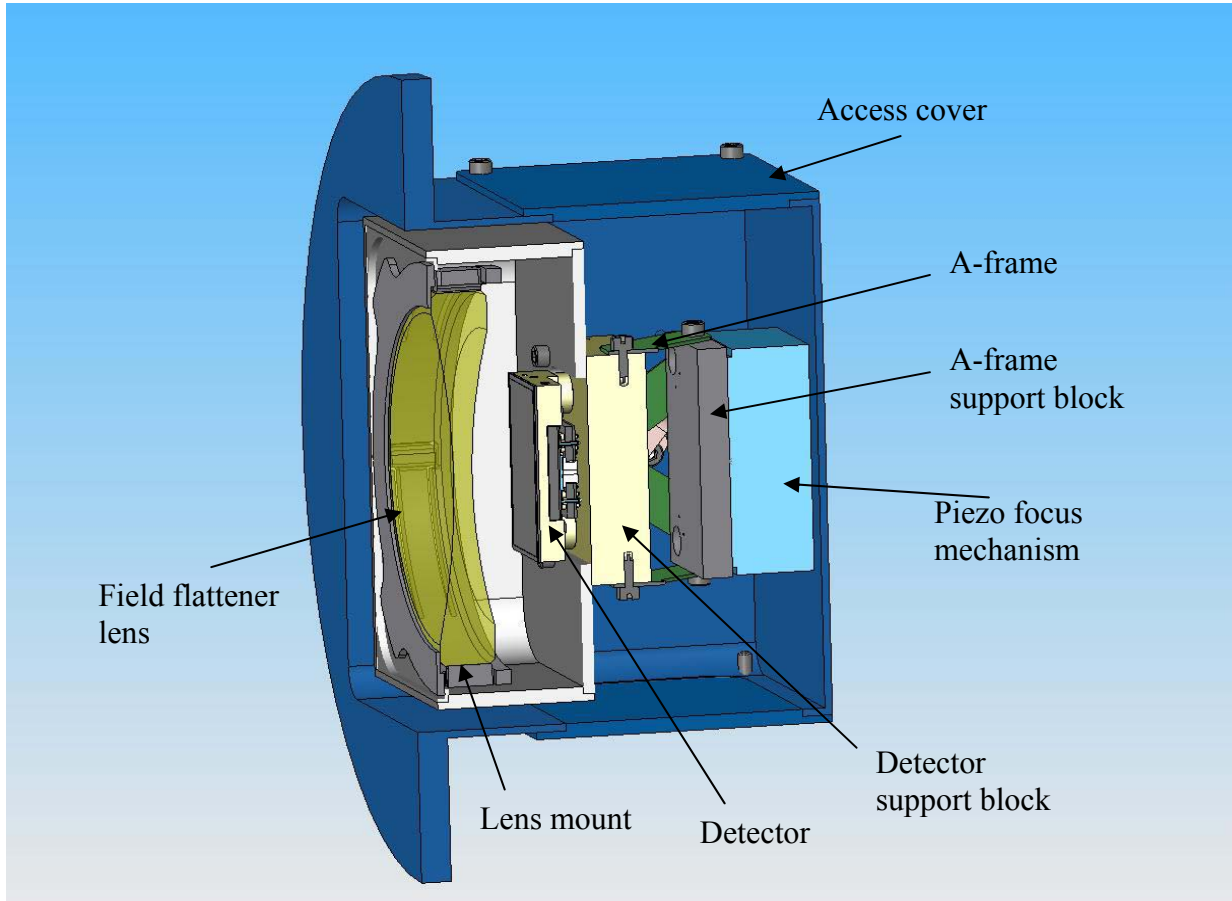
Figure 34: *Detector Head cut-away view showing the field-flattening lens and focus mechanism.*

To allow detectors to be mounted closely butted against each other, the detector runs close to three of the edges. Each of these edges has a pattern of one tapped and two plain blind holes, allowing attachment of a handle to make it easier to place the detector without risk of accidentally touching the delicate surface. On the fourth edge the connections to the silicon multiplexer interface to a ceramic block which is mostly underneath the molybdenum alloy block, with a slim extension wrapping up around the edge. Wire bonds from the detector go to pads on the top edge of the wrapped around part. A flexible printed wiring strip connects to a grid pattern of pins on the underside of the ceramic block. All necessary connections to the detector are brought out to a connector on the other end of the strip. The detector and molybdenum alloy block are shown in (Figure 35).
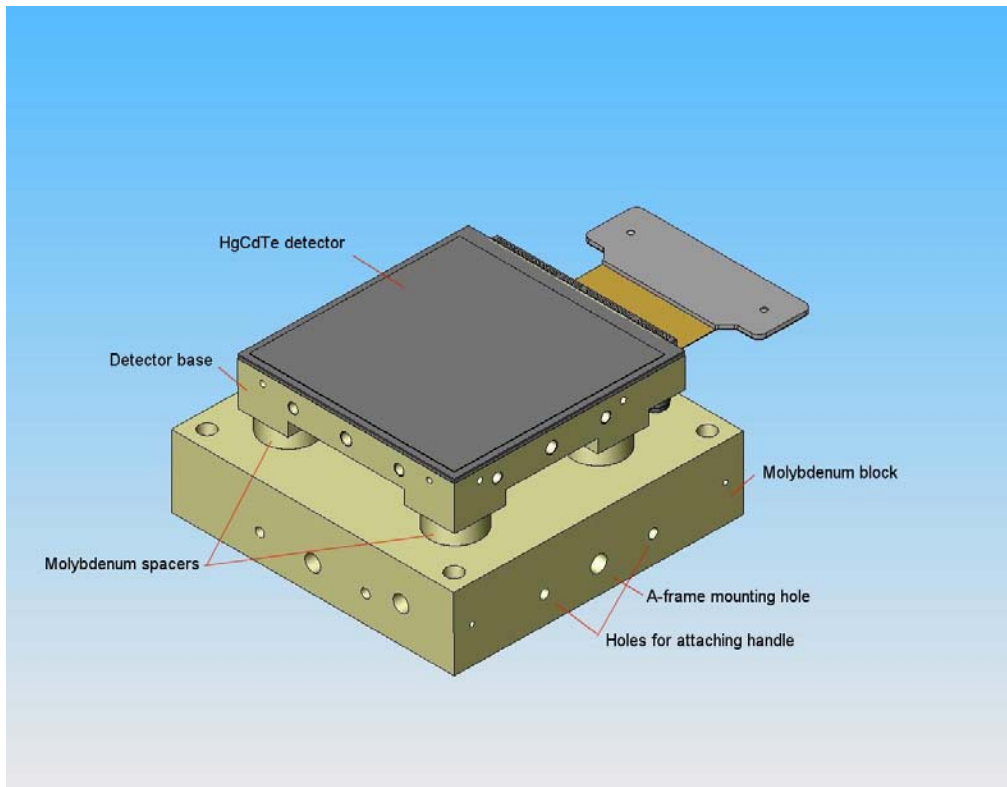
Figure 35: *The 2K x 2K Rockwell detector mount.*

The alloy used for this block (TZM 634) is the same as the detector substrate so that there is no CTE mismatch. GL Scientific recommend a mounting pattern in which one hole is a snug fit to the leg, one hole is slotted (short dimension the same as the diameter of the snug fit hole), and the two remaining holes are slightly oversized. The legs go through these holes and are fixed by nuts on the back. In the edge of the mounting block the hole-pattern found on the edge of the detector block is duplicated so that the same style of handle can be used to manipulate the two parts when they are mated. The central hole of these hole-patterns is also the attachment hole for the G-10 A-frames which stand the detector assembly off from the focus mechanism. Other features of the interface block are a temperature sensor and heater on the back, and a tapped hole for the thermal strap connected to the auxiliary CCR head. The base of the lens mounting box attaches to the top

of the interface block. At present this interface is drawn as a simple one with the box base secured flat to the top of the block. During the detailed design phase features will be added to ensure a light-tight seal.

A three-part box encloses the detector. The base plate interfaces to the front of the detector interface block, behind the detector. A square tube attaches to the base and extends forward of the detector. The front plate sets in a recess in the front of the square tube. The front plate in turn has a cutout and recess for the lens mount that carries the field flattener lens. The base plate has a cutout for the electrical connector on the detector flex circuit. This connector must be attached to the base plate once the detector has been mounted to the interface block, before the tube section is added.

The lens mount is a finger-type mount (Figure 36) as used in FLITECAM. It has a flange around the front which mates with the recess in the front plate of the lens tube, with four tabs for mounting screws. The lens itself then sits down inside the lens tube once the mount is installed. This means no light can enter the lens tube except through the lens. A cover is available which will protect the lens when the assembly is not installed in the instrument. This cover also forms a base for the detector/block/lens tube assembly once it is assembled. The assembly with the cover installed can be placed lens side down for attachment of the rest of the detector head.
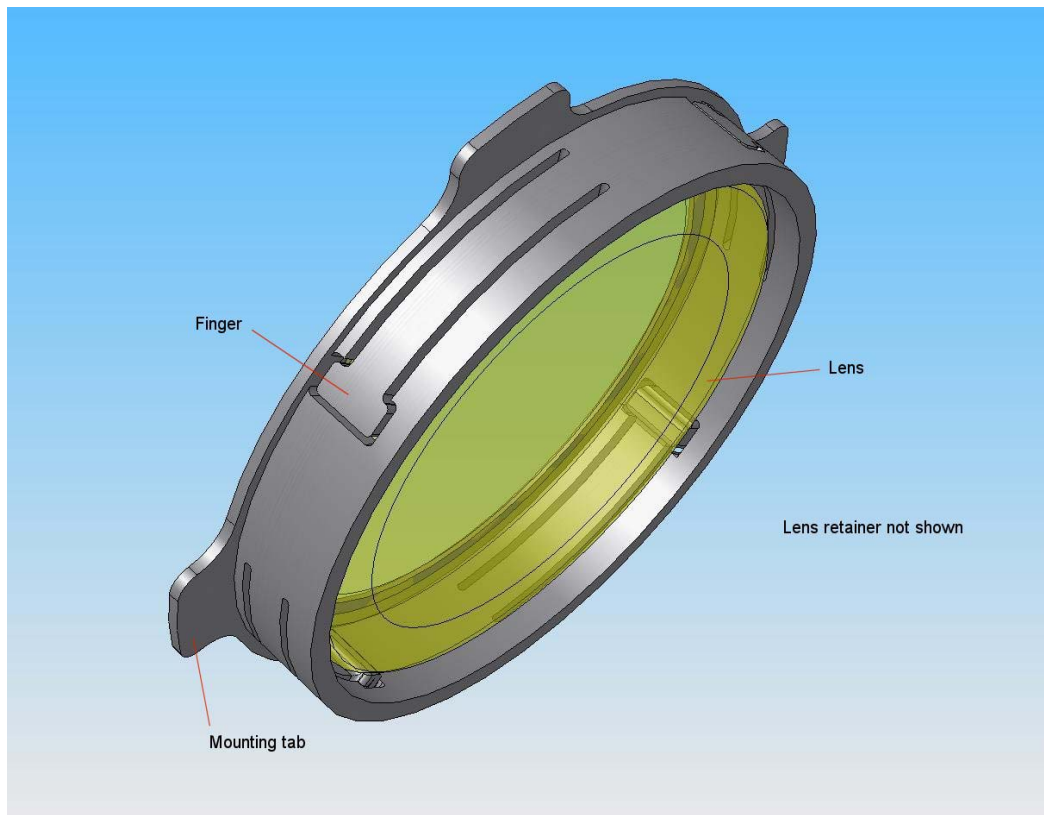
Figure 36: *Field flattener lens and the finger-style lens support tabs.*

The detector interface block is mounted from the A-frame interface block by four G-10 A-frames. The A-frames provide thermal isolation between the detector assembly at ~70 K and the rest of the system at ~120 K. This layout allows for a CTE differential between the molybdenum alloy detector interface block and the aluminum alloy block. Each A-frame will flex equally as the detector assembly is cooled and contracts, maintaining the detector's location and center.

The proposed focus mechanism is a piezo-driven flexure-type actuator from Physik Instrumente (PI), model P-622.ZCD. Physically it is a square, flat block 50 mm square by 17.5 mm thick with a slightly raised mesa in the middle. This mesa part moves (pistons) through a range of 250 μm under control of an external controller. It has capacitive position feedback so motion is closed-loop, enabling control to 1 nm precision and repeatability. Because it is a precision flexure it doesn't go off-center or tilt when moving. Tilt is typically 30 μrad.

The outer shell of the assembly is an approximately cubic box (4.5 in square by 3.25 in high) with access hatches in two opposing faces, and a circular flange (7.0 in diam.) which attaches to the rear of the camera lens barrel. Located on one of the sides without an access hatch is the thermal feed-through assembly. Electrical connectors for the detector are on the opposite face. Connections to the heater and temperature sensor, and to the focus mechanism, are on the rear face.

As shown in Figure 37 the thermal feed-through structure has a thin G-10 disk, loosely clamped at its edge where it is attached to the outside of the outer shell. The disk has a two-part copper plug through its center, forming the cooling path through the outer shell. The plug components are flanged and mate so that they too only loosely clamp the inner edge of the hole in the disk. Thus the plug is isolated from thermal contact with the outer shell. The hole in the outer shell through which the plug passes is only just larger than the plug, so that it blocks any thermal radiation coming through the G-10 disk. A thermal strap of multiple thin sheets of copper foil connects the plug to a copper pillar screwed into the molybdenum block supporting the detector. This strap is formed into a "J" shape so that it can flex to deal with thermal contraction of the molybdenum block without introducing stress. The outside thermal link to the CCR head will have a similar geometry, and will be the part tailored for thickness or width to adjust the base temperature of the detector head.

Heat flow along the A-frames was calculated as 0.009 W per leg. This estimate is based on anticipated temperatures of 77 K for the detector and 120 K for the instrument structure. For four support legs, the total load is estimated to be 0.056 W.
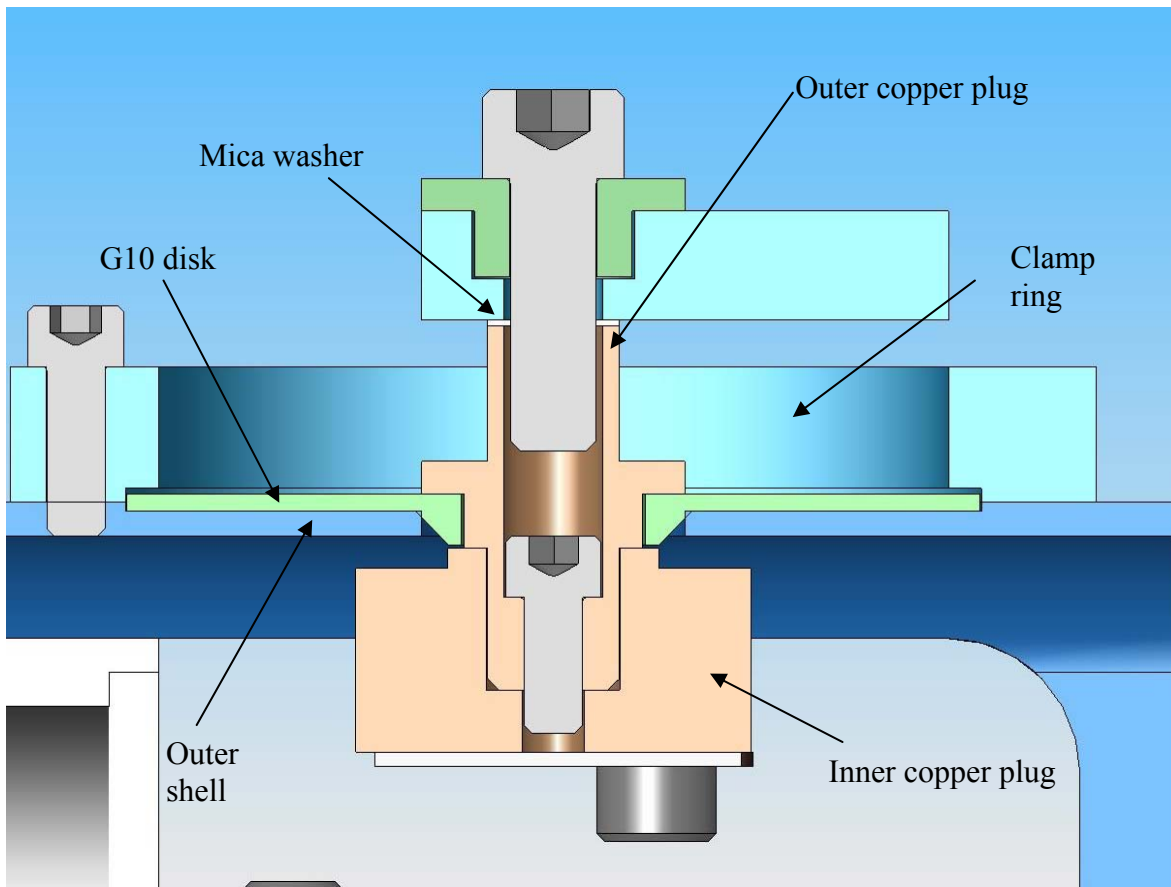
Figure 37: *Thermal feedthrough structure for detector head with electrical isolation.*

5.2.1.9   Configurable Slit Unit

A Configurable Slit Unit (CSU) has been chosen chiefly to eliminate the difficulty, risk, and expense of moving sets of masks to and from a vacuum, cryogenic environment on a daily basis. In addition to meeting the requirements derived from the science case, extremely high reliability is paramount. For this reason, a vendor that had experience in producing such a device was sought. We have identified the Swiss company, CSEM, as the proposed vendor for several reasons. Foremost is that they have produced and extensively tested a prototype configurable slit mask at cryogenic temperatures. The prototype (Henien et al. 2003) was built for the European Space Agency (ESA) as a candidate for the slit mask on NIRSpec, an instrument to be installed on the James Webb Space Telescope (JWST). The prototype is shown in Figure 38. Tests have shown that the ESA prototype is accurate and reliable (P. Spanoudakis et al. 2004). Face to face discussions with the engineering team at their site and inspection of examples of their work indicate that the engineering design and workmanship are of a very high quality. CSEM was placed under contract in October 2005 to begin the development of a CSU that meets our requirements for larger field of view and operation under all orientations at the Cassegrain focus. CSEM has now produced a revised design and a prototype as documented in CSU Design and

Analysis Report dated March 22, 2006 (Doc. No. RSM.CSE.RP01). Other CSEM documents are listed in the Appendix and posted on the MOSFIRE web site.
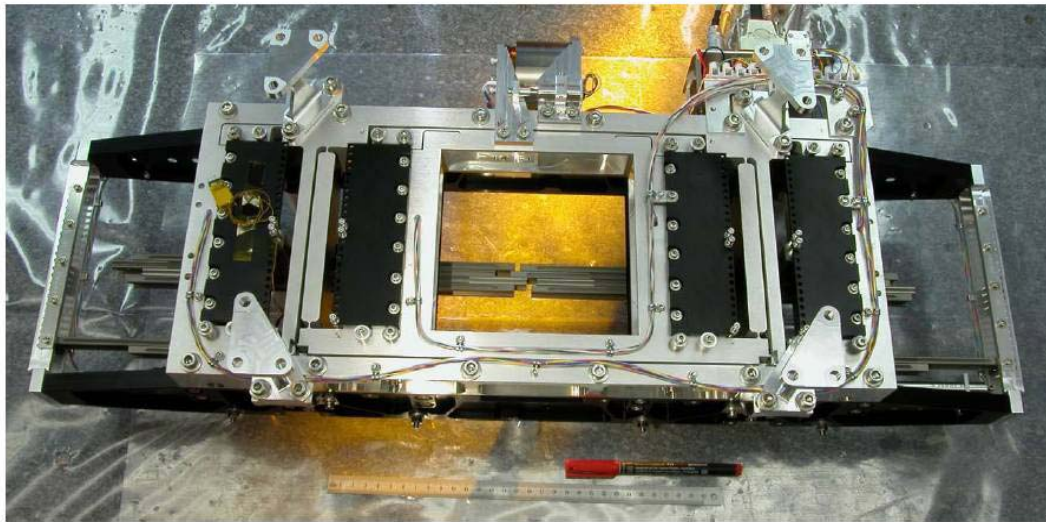
Figure 38: *A prototype CSU developed by CSEM for ESA. Only a few slit bars are installed.*

The notable design changes from the JWST mechanism that have been or will be implemented for the MOSFIRE instrument are as follows:
- Increase the field of view from 137 x 137 mm to 262 x 262 mm
- Flexible and Rigid Wheel Replacement by miniature crossed rollers
- Simplification of Clutch Mobile Connections
- Replacement of titanium by aluminum in all mechanical parts
- Optimization of the Masking Bar design
- Implementation of a 2 step coarse mode (increased speed)
- Improvement of Coil and Magnet performance and fastening

The CSU is designed to simultaneously displace masking bars across the FOV to mask unwanted light. A slit is formed at a designated position within the FOV by approaching two opposite bars and maintaining a distance between them to create a rectangular slit. The end of each bar carries a slit jaw whose height is set to approximate the curvature of the Keck Telescope focal plane. A set of approximately 45 bar pairs will be used to form the MOSFIRE focal plane mask. The sides of the bars are convoluted so that light is prevented from passing between adjacent bars. The bars that form one side of the slit can be moved independently of those that form the other side, so that any width of slit can be formed, up to a completely open imaging field when the bars are fully retracted. Bars on one side form an identical assembly to those on the other. The masking bars are displaced across the FOV using incremental steps (inchworm principle) where a number of oscillating steps are required to displace the masking bars. A voice-coil actuator on an indexing stage provides the motion to move the bars from opposite sides simultaneously. A common position sensor (LVDT) keeps track of all relative movement of bars with respect to the fixed

reference frame. All bars can be displaced at the same time or individually, as is the case when final slit position is to be achieved. Additional information may be found at the CSEM website[1].
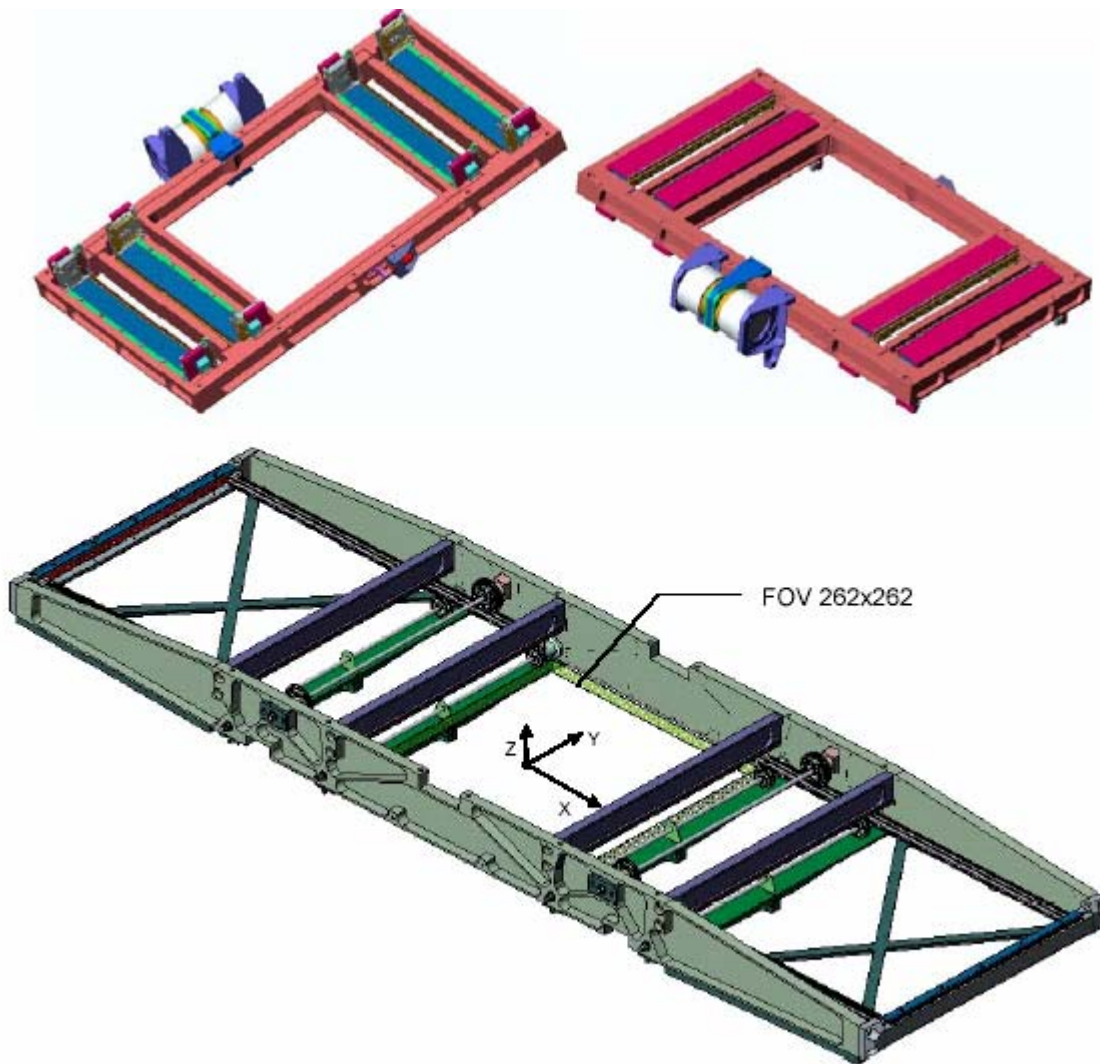
Figure 39: *Two major CSU sub-assemblies: the Indexing Stage (top) and Support Frame (bottom)*

The ratchet and brake clutch actuators are used to engage and block the masking bars during the incremental movement of the indexing stage. Clutches are assembled in a side-by-side array to create a sub-assembly capable of addressing all bars in parallel or individually. The masking bars are held within the support frame and are guided using rollers on bushings (Figure 39).

Some of the details of the mechanism are shown in Figure 40. The masking bars are guided using three wheels; two rigid wheels and a radially-flexible wheel which is used to pre-load the sub-assembly. The entire support shaft of the flexible pre-load wheel is adjustable in the Z-direction.

---

[1] http://www.csem.ch/fs/micro_mechatronics.htm follow links to mechanisms and then mechanical slit mask

The masking bars are guided using three cross roller pairs; two rigid pairs and a spring-loaded pair which is compliant in the Z-direction. The rollers ride on a pair of angled surfaces machined along the top and bottom lengths of each bar. On the upper surface, the bars are machined to provide a tooth profile that engages with the Ratchet Clutch to provide motion. Tooth pitch is 1.2 mm.
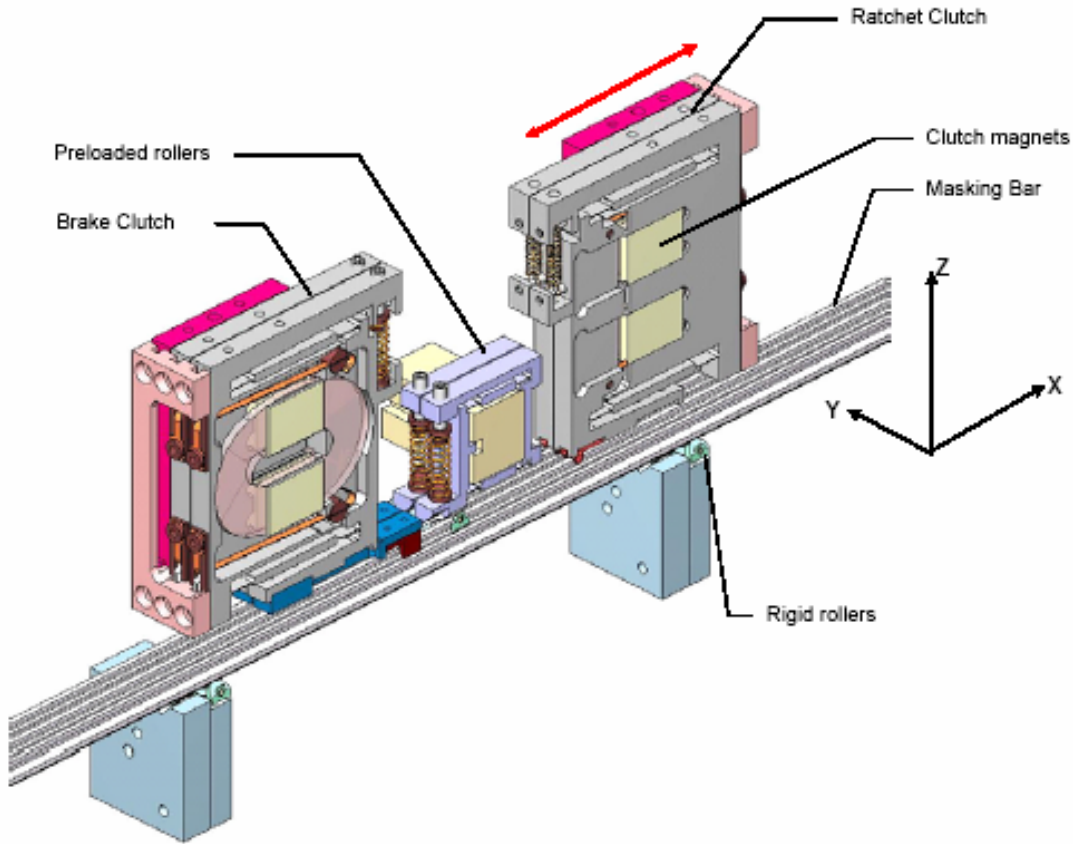
Figure 40: *Modified masking bars and guide wheels for MOSFIRE.*

There are two mechanisms associated with each bar: a brake which holds the bar's position by friction and a mover (called the ratchet clutch) which inserts a sapphire claw between the two teeth nearest it on the bar's edge. A coil of wire moving in a magnetic field actuates each of these mechanisms. By energizing a bar's brake coil, the brake for that particular bar can be released, and by energizing a bar's mover coil, the mover claw for that bar is inserted. With this design, any configuration of bars that have their mover claws engaged and their brakes released can be moved by up to one tooth pitch. The configurations for each side are independent.

5.2.1.9.1   Operating Modes

When all the bars are in-phase, any number of bars can be moved one step in any direction at each cycle. This is called Mode 1: Discrete in-phase group motion and it allows the bars to move quickly to the vicinity of their exact target position. The bars can be moved within single steps only by individual actuation of one bar. This is Mode 2: Continuous out-of-phase individual motion and leads to the slit position accuracy and slit width accuracy requirements of the

mechanism. Figure 41 shows the sequential movement of one pair of bars: modes 1-2-1, and represents the state of the system after one consecutive cycle time (top to bottom).
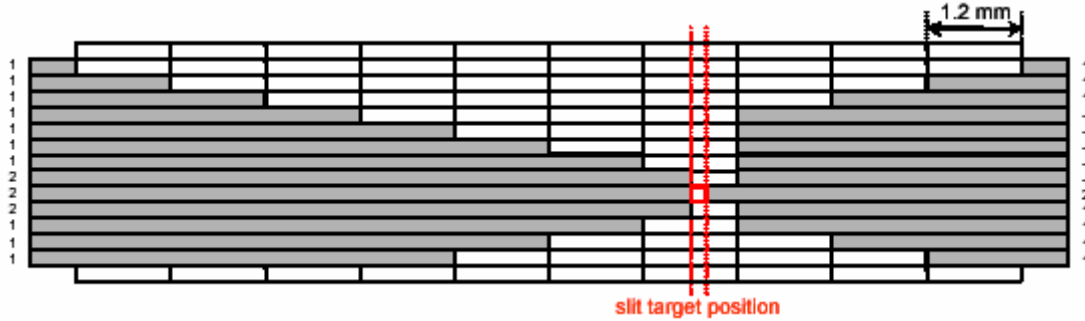
Figure 41: *Sequential movement of one pair of bars: modes 1-2-1*

There is also a masking bar initialization mode which is meant to retract all bars to the FOV open position in the case where total position information of the bar is lost (memory loss, power loss). Each bar is activated individually and retracted to its end-stop position.

If all of the bars are retracted so the mask is open and it is desired to form a pattern of slitlets, the following efficient sequence of motion would be used. All the mover claws would be engaged and all the brakes released. The frame for all the movers would be moved one tooth pitch, the brakes engaged and the claws disengaged. The frame would be moved by one tooth pitch while all of the bars are held by the brakes. This sequence would continue until a bar was within one tooth pitch of its final destination. On the next frame move, the frame motions would be halted when this bar was at its exact destination, its brake engaged and its claw released. This bar would be left in its desired position, and the sequence would then be continued until all of the bars were properly positioned. By this means, the time to configure all of the bars is less than the time needed to move one bar across the field. The worst case full reconfiguration is from a fully open FOV, to a set-up with all 45 bars all the way across to one side and then back to the fully open position. Typically, to go from one mask set-up to another, including imaging mode, takes 2.5 minutes.

CSU development program consists of two phases. The first phase, currently in progress, has the objective of developing a prototype of the MOSFIRE CSU mechanism incorporating changes for the larger field of view and the needs of ground based operation such as a variable gravity orientation. CSEM refers to this prototype as the EUX model.
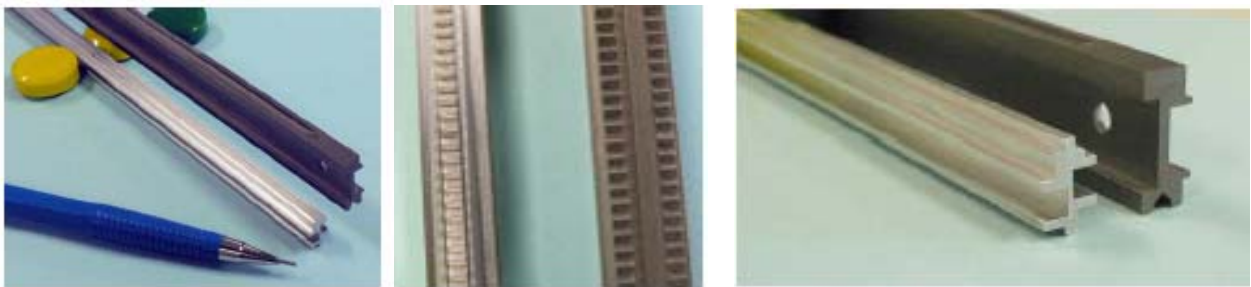
Figure 42: *The new EUX bar (bare aluminum) alongside the previous larger bar (darker finish) developed for JWST. The rightmost pictures show the bar profile and drive grooves.*

5.2.1.9.2   Bar profiles

To block out the incoming light, the bars incorporate a masking shoulder which determines the fill factor of the mechanism. The bar profile has been optimized to reduce mass and maintain lateral stiffness. Each aluminum bar is 10 mm by 445 mm. A tribology surface coating 20 m Ni-PTFE improves friction properties and is applied on all surfaces. This coating also limits the amount of light reflected between bars. The bars are coated with an additional layer of gold on the face exposed to the sky. To reduce the mass of the masking bar a detailed trade-off study was carried out to find the preferred shape (see Figure 43).
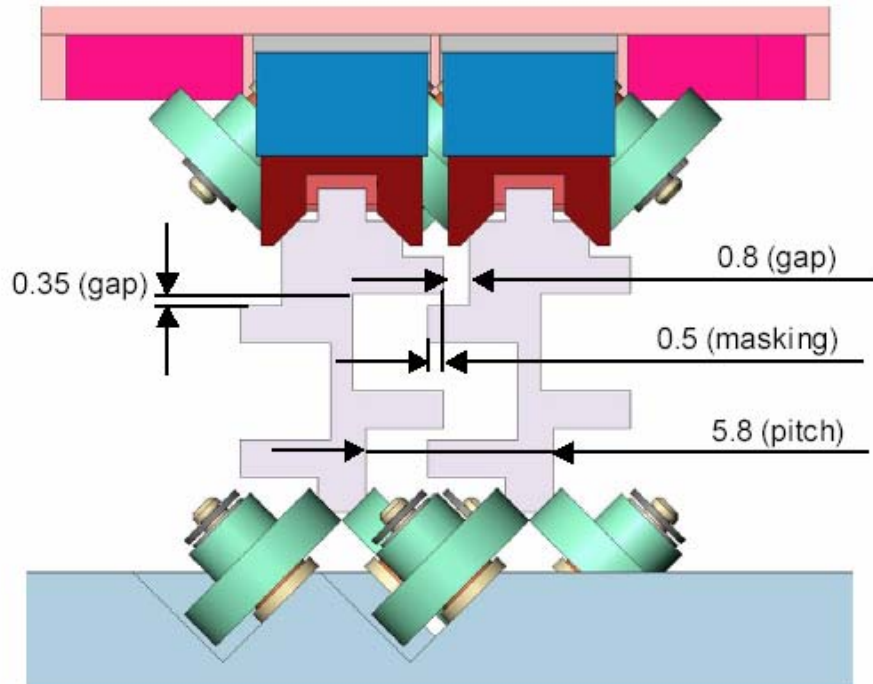
Figure 43: *Guide wheel and bar detail.*
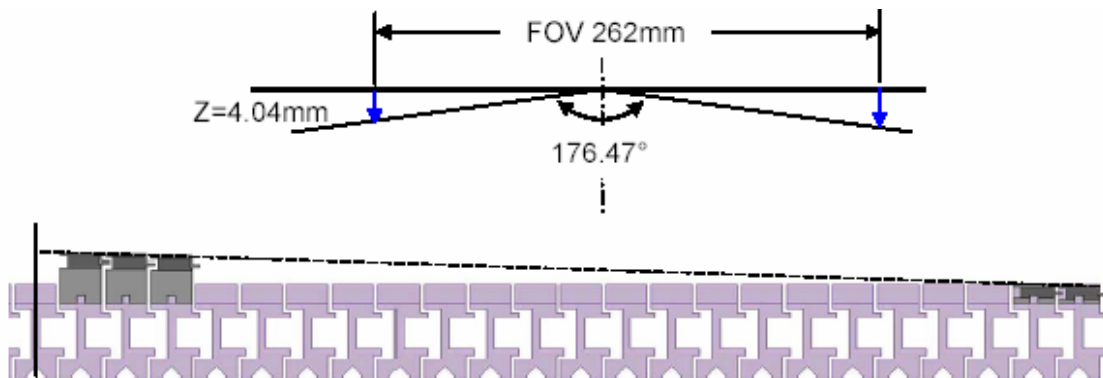
Figure 44: *Knife edge added to the tip of the bar to compensate for field curvature.*

Because of the field curvature of the Keck telescope, the MOSFIRE focal plane is not planar. A practical solution is to approximate the spherical radius of curvature (2.124 m) by two flat planes with an angle of 176.47°. The change in height (Z) from one end of the MOSFIRE FOV to the center is 4.04 mm. There are 22 bars on each side of the central bar and so the change in height between bars is 0.18 mm. A knife-edge is added to the top of each bar as shown in Figure 44.

The EUX prototype mechanism shown in Figure 45can index two bars across the field of view. A test campaign at both room temperature and cryogenic temperature will permit evaluation of all critical parameters. Moreover, the prototype will be fully representative of all critical components (ratchet and brake clutches, guide rollers, limit switches, actuators and sensors) as well as interfacing with the control system and electronics.
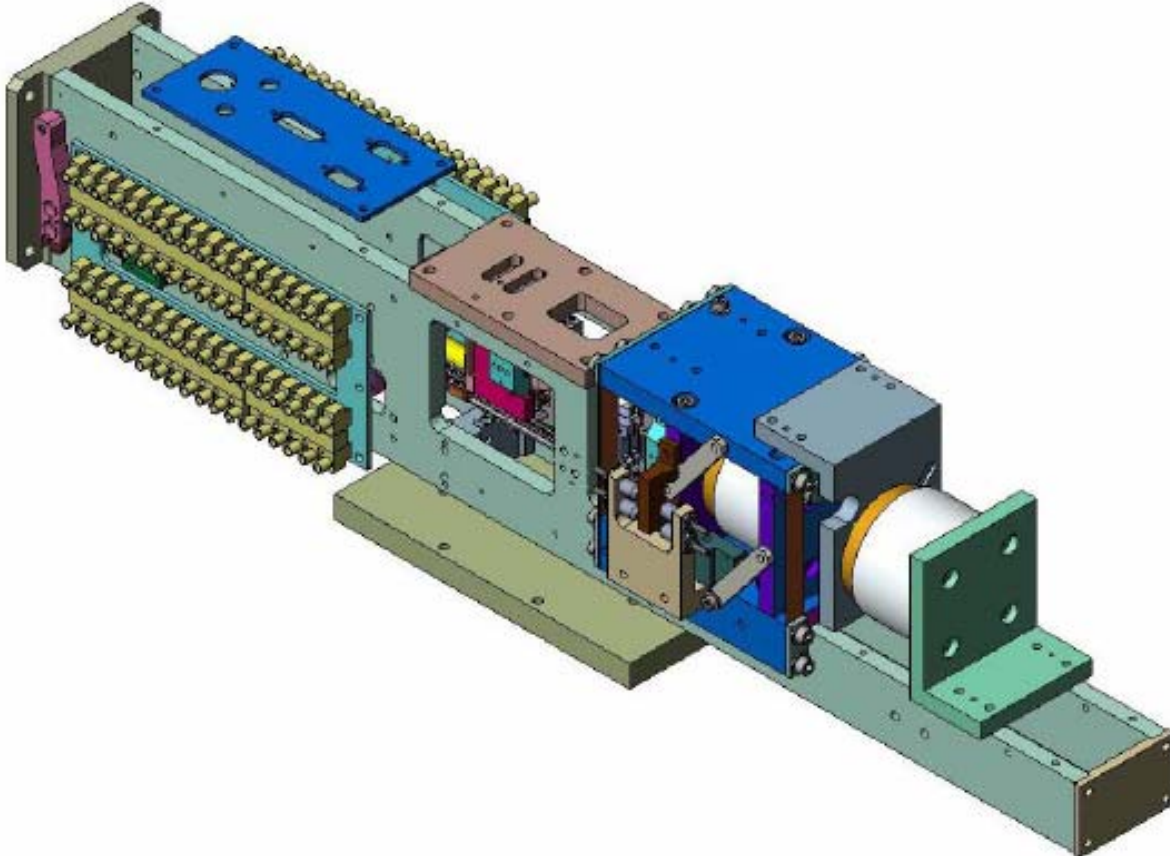
Figure 45: *The EUX prototype*

The EUX will evaluate all performance requirements with respect to bar positioning, initialization functions and operation in both horizontal and vertical positions. An electronic system was developed for control of the CSU. The control software runs on a commercial off-the-shelf controller card purchased from dSpace. Electronic hardware is divided into two racks, a control rack including the intelligent motion control system, and an amplifier rack to drive the brake and

ratchet clutches. The dSpace DS1104 card is mounted in a mini-PC with its own power supply. The prototype control electronics rack used during tests is shown in Figure 46.

Figure 46: *The prototype control electronics rack during bench tests. This unit will be mounted with the MOSFIRE electronics at the rear of the instrument.*

Extensive testing has been carried out on the electronics control rack in preparation for testing the two pairs of bars in the EUX model. Fabrication of EUX parts is almost complete (Figure 47). Testing will be done at cryogenic temperatures in a large test chamber at CERN.
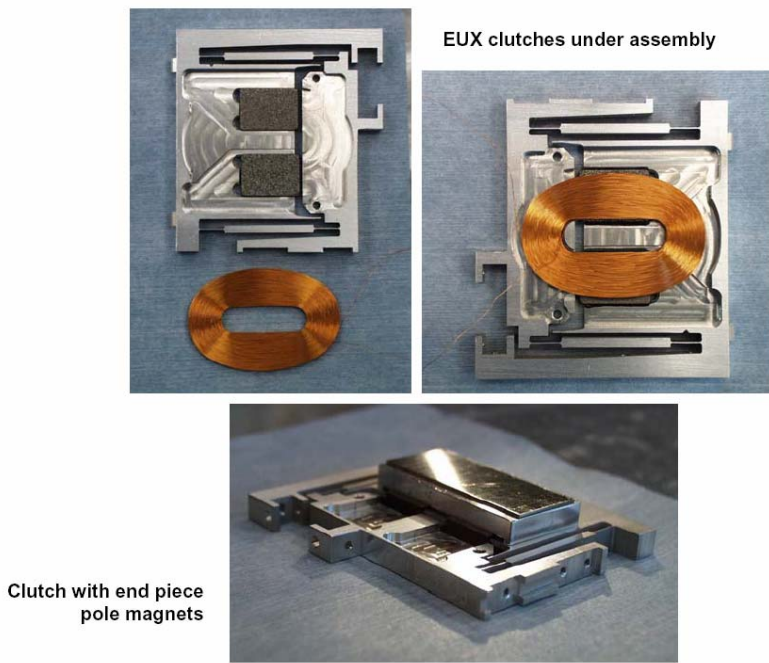
Figure 47: *New clutch assemblies recently built for the EUX prototype.*

During the initial study phase a specification was provided to CSEM and a detailed compliance matrix was developed which shows that in principle, all our requirements can be met. CSEM offered a firm fixed price for the CSU that also includes control electronics and low-level software. Over the lifetime of this instrument, the operational cost-savings from the elimination of mask fabrication and cryogenic mask exchanges will significantly mitigate the large capital expenditure. CSEM have given a delivery date of May 2008 for the completed 45-bar unit.

A similar concept is being employed for the EMIR instrument for the GTC. The EMIR team has contracted a Dutch company to develop a competing mechanism to that of CSEM. A 2-bar prototype is nearing completion, and thus CSEM may not be the only source of this technology.

5.2.1.10   The MOSFIRE Cryogenic System

For proper operation, MOSFIRE must be a cryogenic instrument. The instrument layout and internal structural design must be compatible with cryogenic conditions. Space, weight, and service restrictions at the intended Cassegrain mount location of Keck I also influence the instrument design. MOSFIRE's structural and thermal systems design achieves a balance of these considerations, while also meeting instrument stability (flexure) goals.

For example, the layout of the internal structure was chosen to achieve balance between structural flexure and thermal design considerations. The concept of two stout, circular bulkheads separated by a pair of concentric, stubby tubes has been shown to perform equally well in minimizing flexure and minimizing thermal gradients within the structure. The aluminum internal structure is supported inside the vacuum chamber by a thin-walled G-10 tube. This tube serves as an insulator, resisting thermal conduction between the internal structure and the vacuum chamber structure while also serving as an efficient, stiff support.

The entire internal structure is surrounded by a cooled, floating shield constructed of ~6 mm thick polished aluminum sheet. This shield will reduce the radiation load on the internal surfaces and reduce thermal gradients within the internal structure. The large external faces of the internal structure will be covered with a thin covering of MLI in order to increase their reflectivity and reduce the emissivity of the surfaces. Additional MLI could be added to the external surface of the shield if necessary. The entire internal structure of MOSFIRE will be cooled by a pair of single-stage, closed-cycle refrigerators. CTI-Cryogenics Model 1050 refrigerators will be used. The refrigerator heads will penetrate the cylindrical portion of the vacuum chamber, the shields, the G-10 support tube, and the internal structure at a location between Bulkheads A and B. They will be positioned ~120 degrees apart around the tube in order to provide equal cooling through both large bulkheads which will serve as conduits for removing heat uniformly from the structure's extremities. Each refrigerator head will have copper thermal straps bridging to each bulkhead. The straps will be based on a design fabricated for NIRC2 (Figure 48). Approximately 48 of these straps will be necessary (24 per refrigerator). The total cross-sectional area of the straps can be adjusted by design to minimize the temperature gradients between the bulkheads. A dual speed controller will be used to extend the lifetime of the cold heads once the operating temperature is reached.
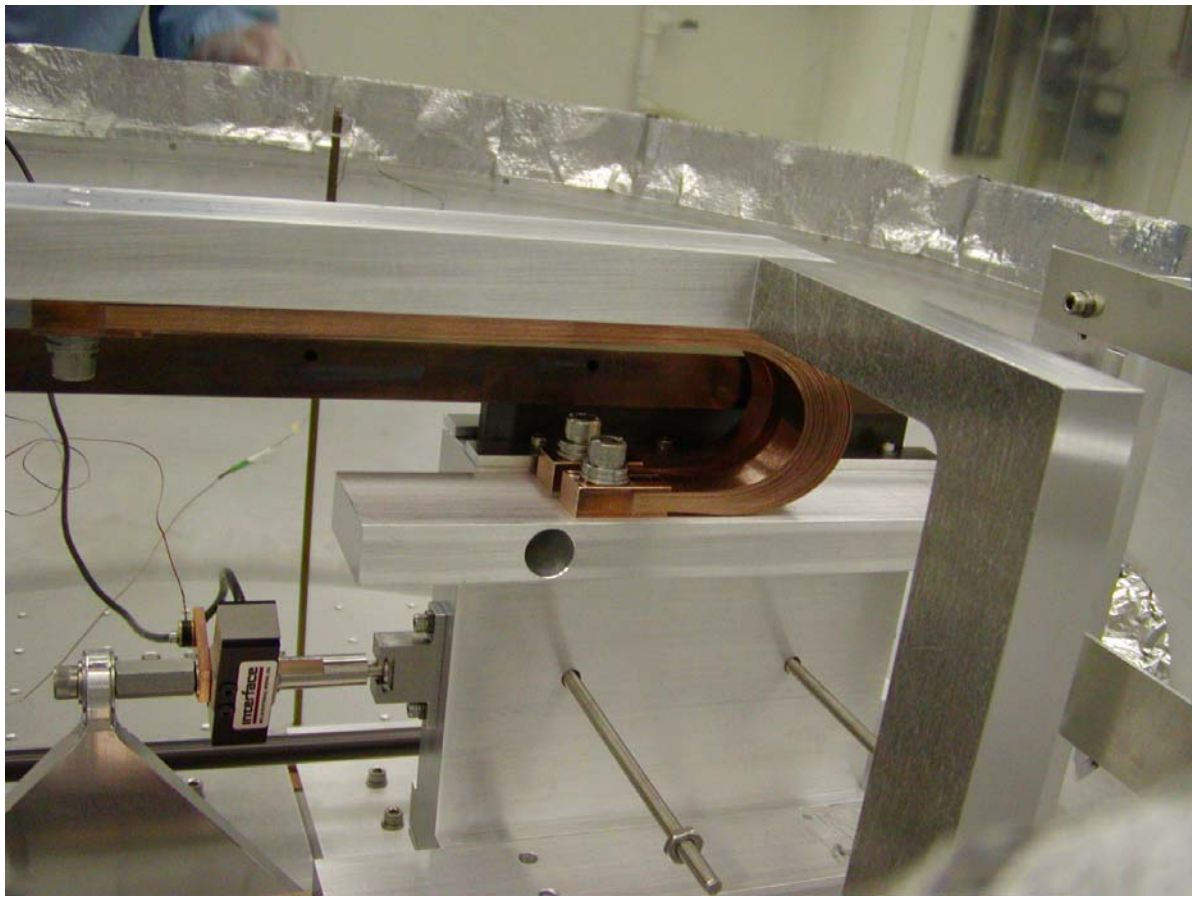
Figure 48: *NIRC2 flexible thermal strap design.*

In Figure 48 a pair of spare NIRC2 straps is visible in this image of a test assembly. The straps consist of many layers of copper sheet which are fused together at each end of the strap.

A third, smaller refrigerator will be used to cool the detector. A two-stage CTI-Cryogenics Model 22 refrigerator has been selected so that the getter can be cooled from this refrigerator as well. This refrigerator will also be mounted to the cylindrical portion of the vacuum chamber immediately in front of the instrument's rotator bearing location. The refrigerator's head will protrude into the instrument just behind Bulkhead B near the detector head.

Figure 49 depicts the general refrigerator mount design for MOSFIRE. The mount design is based on mounts utilized for both NIRC2 and OSIRIS (Figure 50). Since MOSFIRE is located at the Cassegrain mount location, the mount concept had to be modified to work in multiple gravity orientations. This is achieved by re-sizing the compression springs to handle lateral loads and by ensuring that the assembly's CG is centered between the springs.
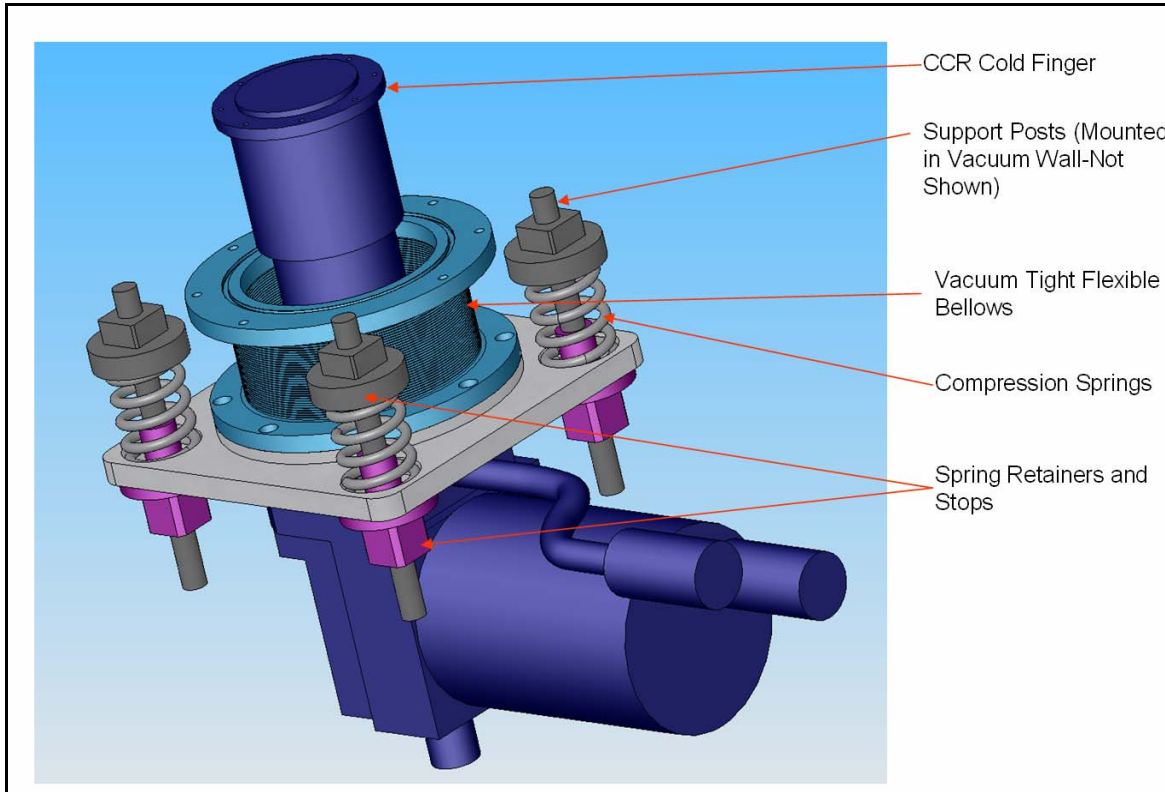
Figure 49: *CTI CCR Head and low vibration mounting system.*
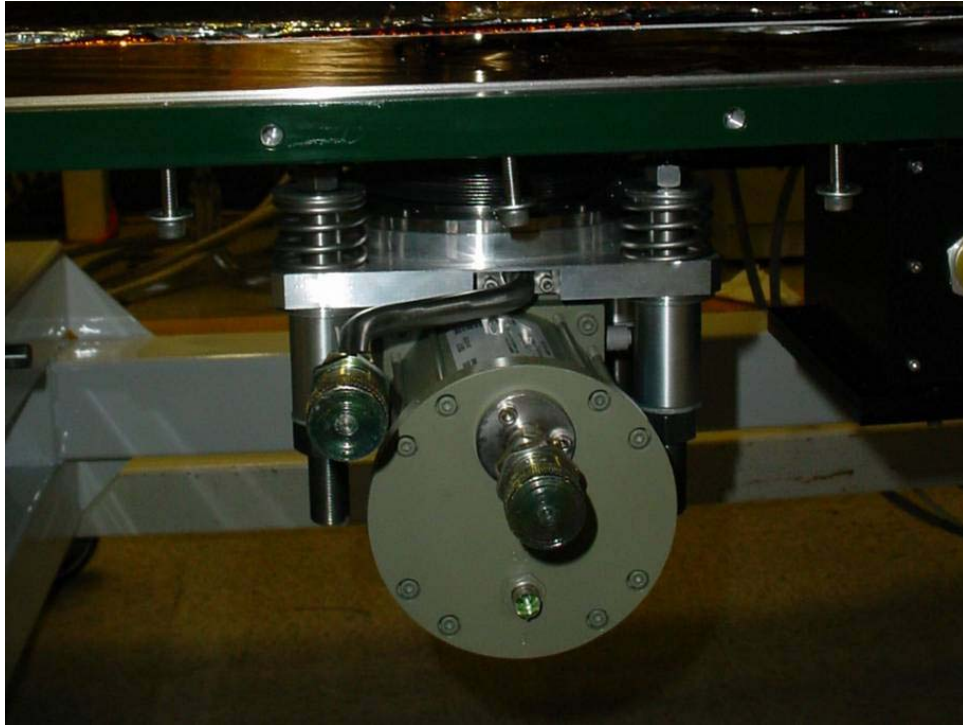
Figure 50: *CTI CCR head installed on OSIRIS.*

The internal structure of the instrument was analyzed utilizing FEA to assess the thermal performance of the design. The preliminary analysis results indicate that the instrument layout will result in a sufficiently uniform temperature distribution among the optics. Form the analysis we conclude that the structure's temperature can be lowered from ambient condition to <130 K in ~7.5 days. This cool down time can be achieved with a pair of 150 W refrigerators without LN2 assistance. These refrigerators can be fed by a single pair of supply lines serviced by a single compressor, as is the case for NIRSPEC and NIRC2. For the preliminary analysis model, the main instrument shield wasn't included, but its effect was simulated by the application of the loads to the analysis model. A more detailed thermal analysis which includes the surface to surface radiation interactions between the vacuum chamber, shield, and internal structure will be completed during detail design in order to verify the required shield thickness.

Our thermal analysis included both steady-state and transient studies. From the steady-state analysis we determined the estimated temperature distribution within MOSFIRE under operating conditions. The restraints and loads used in the simulation are listed below. Figure 51 shows the location of the loads on the analysis model.

Restraints:

- Internal Structure Support Tube: Fixed Temperature= 295 K on chamber interface surface

Loads:

- Window Load on CSU Dummy: +2 W on front face of CSU dummy.

- Window load on front baffle/shield: +63 W on front face of bulkhead.

- Vacuum chamber radiation on internal structure: T=295 K; Emissivity = 0.02; View Angle = 1; applied on external surfaces of main tube structure (5).

- Refrigerator Power (negative): -30.25 W at each cold head interface (2 per bulkhead).
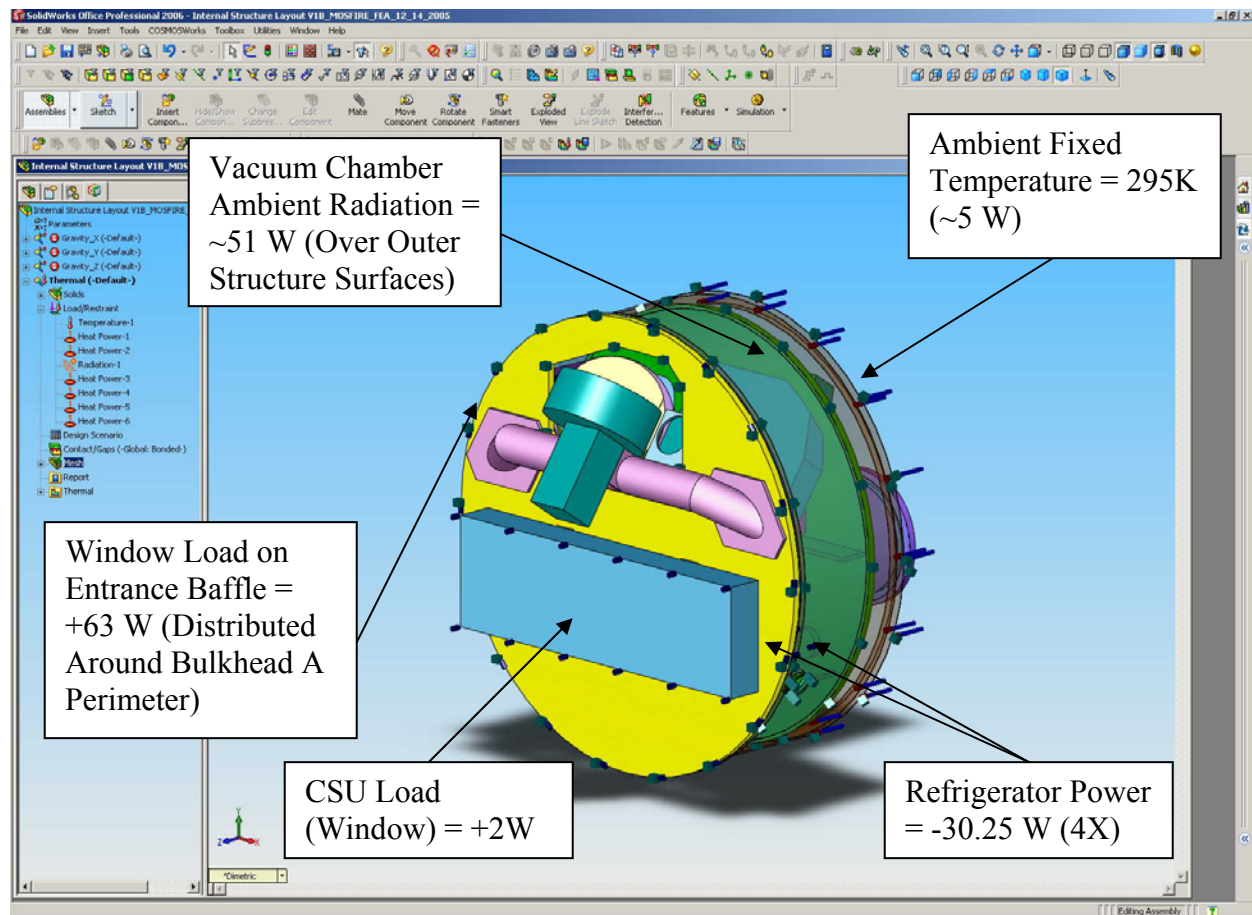
Figure 51: *Preliminary steady-state thermal analysis loads and constraints.*

The loads and constraints indicated above represent the final iteration of the analysis. Window loads were calculated utilizing radiative heat transfer equations. At the CSU the load is approximately 2 W, and was applied to the front face of the CSU "dummy". The window load on the front shield/baffle was applied to the perimeter of Bulkhead A since the shields were not included in the preliminary analysis model. The value of the load is derived from subtracting the CSU load from the entire estimated window load (65-2 = 63 W). In reality, the shield will actually have straps connecting it near the main refrigerator straps so that the heat only passes through a small region of the bulkhead instead of passing from the entire perimeter of the bulkhead to the refrigerator locations. The ambient radiation load was applied directly to the large outer surfaces of the internal structure since the shields weren't included. We set the internal structure emissivity fairly low to compensate for the lack of a shield in the analysis. Refrigerator power was connected to a pair of thermal strap attachment features on both of the large bulkheads. These attachment locations are positioned to evenly distribute the heat removal through the structure.

The analysis was iterated to determine the power required to maintain temperatures throughout the structure of less than 130 K. Table 19 and Figure 52 show the results of the final iteration. The

analysis predicts that two refrigerators removing 61 W each will maintain the entire structure below 130 K. The estimated gradient in the entire structure is ~9 K. The estimated gradient among all of the optic components is ~3 K. Within an individual optic sub-assembly, the maximum estimated gradient is ~0.5 K. The sub-assembly gradients will be relatively small based on the general method of mounting them. Optics assemblies are mounted so that they generally don't bridge large gradients in the structure and become conduits for heat from other parts of the structure. Proper selection of the locations of the main refrigerator thermal strap attachments to the bulkheads also minimizes gradients within the optic sub-assemblies.

Previous experience suggests that radiation among components within the structure will help to reduce the gradients below the estimates resulting from this preliminary analysis. Also, since this preliminary analysis didn't include a realistic representation of the shields, the gradient within the structure will likely be less since more heat will be taken out of the instrument through the shields rather than through the internal structure.

Load Case 3: Thermal Steady State- 61W & 61W				
Component/Location	**Maximum Temp (K)**	**Minimum Temp (K)**	**Range (K)**	**Comments**
CSU Dummy	124.9	124.6	0.3	Crude Model
Field Lens Mount	124.2	123.7	0.5	Mount Surface
Flexure Compensation Mount	125.2	125.1	0.1	Mount Surface
Collimator Barrel Dummy	124.4	124.3	0.1	Solid Bar
Filter Wheel Dummy	124.5	124.3	0.2	Crude Model
Pupil Mechanism Mount	125.5	125.5	0	Mount Surface
Grating Mechanism Dummy	126.3	126.3	0	Solid Bar
Camera Barrel Dummy	126.4	126.1	0.3	Solid Bar
Optic Component Range	126.4	123.7	2.7	
Maximum Structure Temp	129.5	Kelvin		Top of Bulkead A
Minimum Structure Temp	120.7	Kelvin		Bottom of Bulkhead B
Maximum Range	8.8	Kelvin		

Table 19: Tabulated results of steady-state thermal analysis.
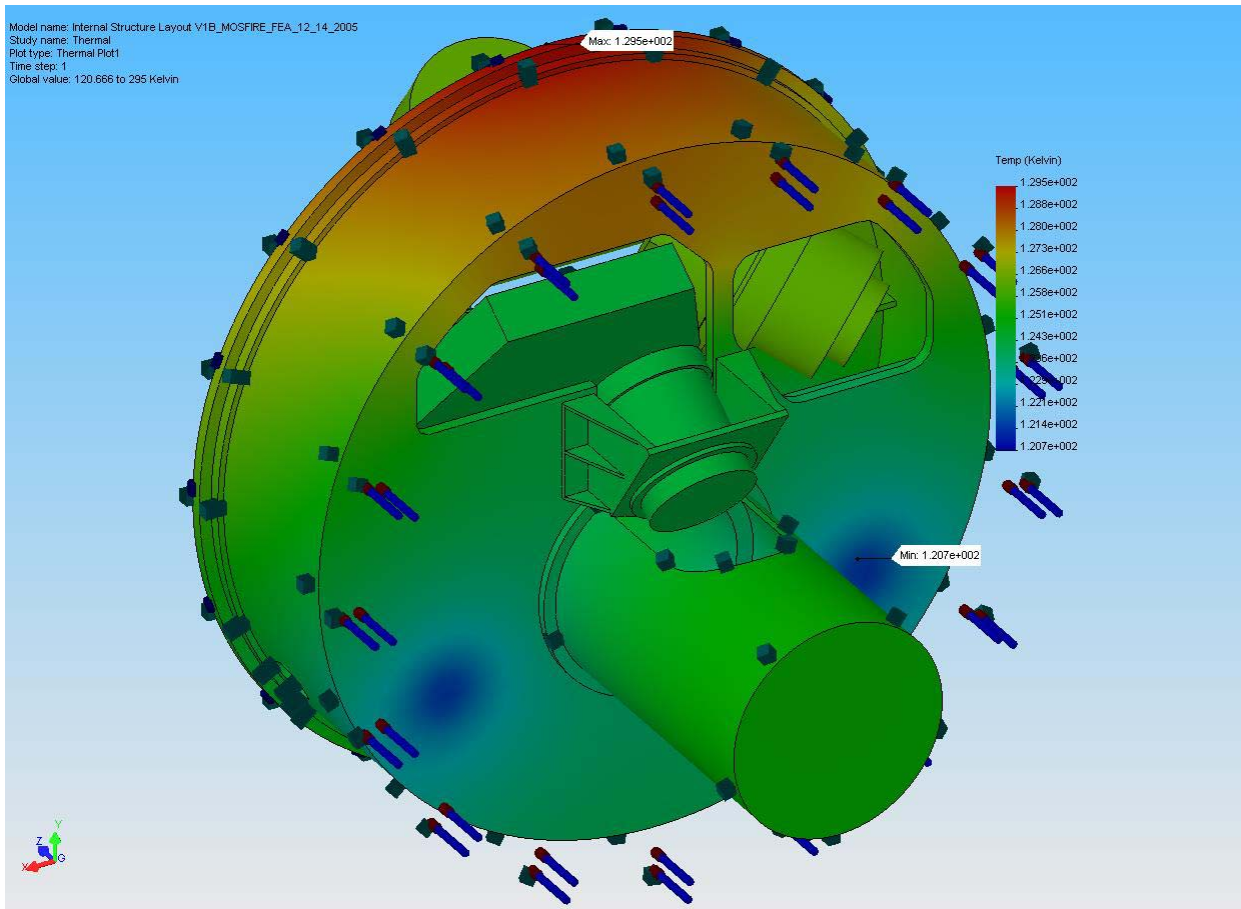
Figure 52: *Rear ¾ view of the steady-state analysis temperature plot. The locations of two of the refrigerator attachment point on Bulkhead B are apparent.*

Based on the relative positions of the refrigerator heads and the two main bulkheads, thermal straps can be sized for given temperature drops between the heads and the structure utilizing a thermal conductivity equation. The instrument weight budget and the refrigerator performance characteristics factor into the selection of the temperature drop. The thermal conductivity equation is:

$$Q = \frac{A}{L} \cdot (I1 - I2)$$

Where

$$A = w^2$$

From the steady state analysis results, the bulkhead temperature, the heat load per strap, and the approximate length of the straps were known:

- T1= 120 K
- Q= 30.25 W
- L= 10 in = 25.4 cm

Square cross-sectioned copper straps were assumed for the calculations. The thermal conductivity integrals for a range of temperatures were obtained from tabular data. Several temperature drops were assumed, and the resulting strap weight and refrigerator performance at the given temperatures were compared. A temperature drop of 20 K was selected for the preliminary design. This drop requires copper straps of ~1.25 inches square, and the straps will weigh ~8.1 lbs each.

Given a 20 K drop, the required refrigerator head temperature is 100 K. The chosen refrigerators can remove ~120 W each at 100 K. Since only 61 W is required per head to maintain steady-state conditions, MOSFIRE will have plenty of cooling power margin, and the heads can be operated at reduced speeds. This should help prolong their life.

A conservative estimate of the instrument cool down time was obtained utilizing the results from the previous calculations. The refrigerators will always be able to remove at least 120 W each down to the desired operating temperature. Using this power capacity, a preliminary transient thermal analysis was done to determine the time to bring the warmest part of the structure below 130 K. The preliminary estimate based on the simulation assumptions is ~7.5 days.

5.2.1.10.1   Performance Predictions

- Steady-state power requirement: 122 W
- Cool down time: 7.5 days to <130 K
- Maximum structure temperature gradient: 9 K
- Maximum optic component temperature distribution: 3 K
- Maximum optic sub-assembly temperature distribution: 0.5 K

Initially, we had a concern about supplying CCR lines for more than one pair of 150 W cold heads. Conservative analysis indicates that no more than two 150 W cold heads will be required to cool the instrument. There was also concern whether the cold heads could cool the instrument in the time required without supplementary cooling (LN2). Again, conservative analysis also indicates that the pair of cold heads will be able to cool the instrument within the desired time.

5.2.1.11 Cable Wrap and Rotator

The cable wrap (see Figure 53 & Figure 54) is the structure that safely manages the cables and hoses that connect between the instrument and the module as the instrument is rotated about the telescope axis during operation. The rotator is also shown in the figures. The rotator is a modular assembly containing the mechanisms required to rotate the instrument about the telescope's optical axis.

MOSFIRE's cable wrap design is based on the same "serpentine" concept created for KIRMOS in collaboration with engineers at IGUS, a manufacturer of cable wrap components. The design allows nearly 540 degrees of rotation (+/- 270). The cable wrap assembly basically consists of a plastic chain (carriage) which encases the required hoses and cables. The chain protects its contents and helps limit the direction and degree of bending that can occur. The end of the chain near the instrument's axis is attached to a drum-shaped guide (spindle) which rotates with the instrument. The other end of the chain is fixed to a stationary cylindrical drum (outer guide) which is secured to the rotator module. This outer guide constrains and helps support the chain as it moves through its range of motion. A carriage tray is also attached to the outer guide to help support the chain when the instrument's axis is vertical with respect to gravity.

This type of wrap assembly is called a "serpentine" style wrap. The wrap's components were sized based on preliminary assumptions of the size and quantity of its contents. In addition, for optimal serpentine style wrap operations, all of the carriage's contents should be aligned with the carriage neutral axis to eliminate repeated rubbing friction between the contents as the carriage reverses its bend during operation. This can cause binding and wear damage to the carriage contents. The carriage is constructed of a low-friction plastic to minimize friction effects on the carriage's contents. The cross-section of the carriage was determined predominantly on the anticipated maximum size and number of cold heads required to cool the instrument. The cold head hoses are the largest items to be managed by the carriage and they have the largest minimum bend radius.
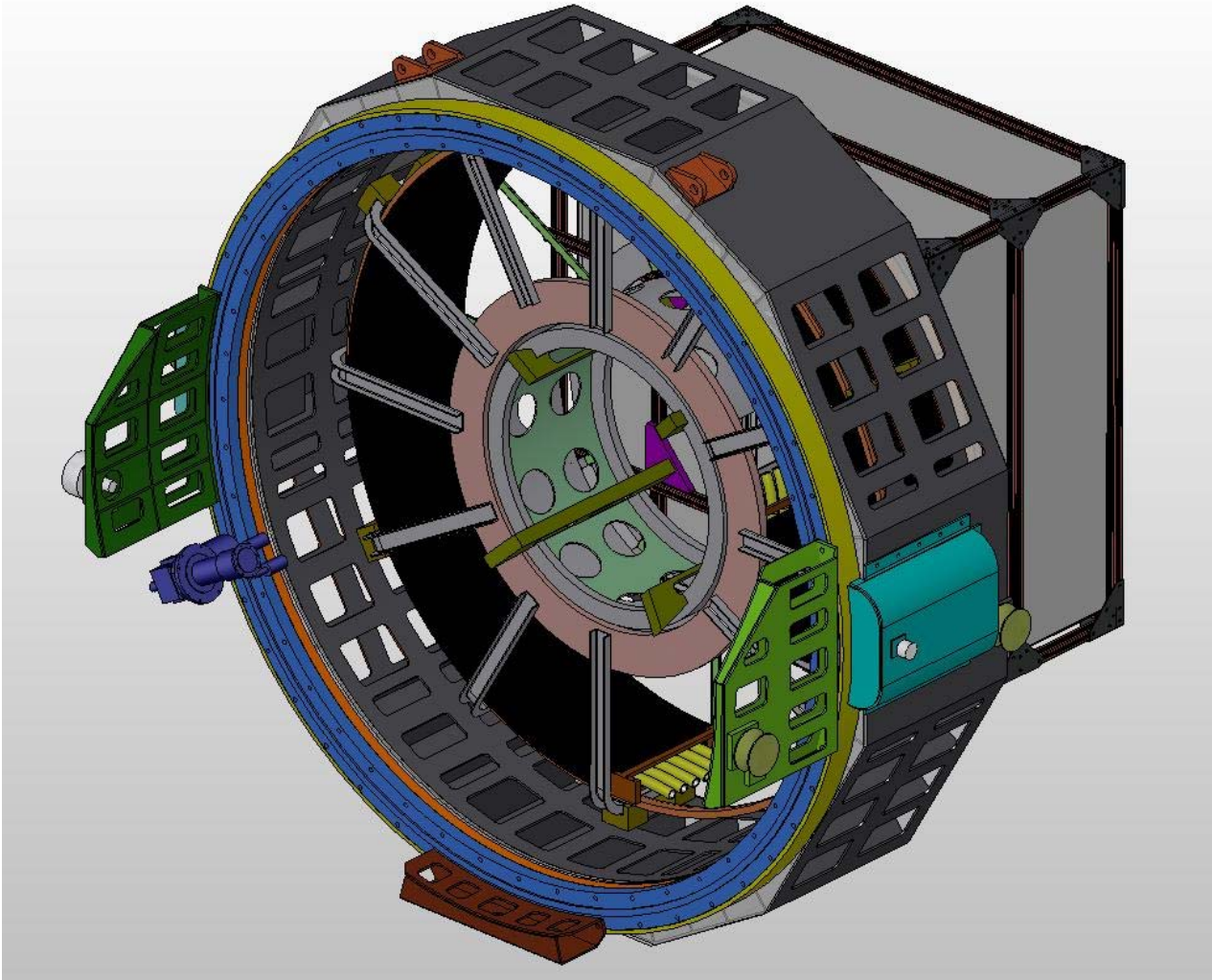
Figure 53: *Front ¾ view of the cable wrap and electronics rack assemblies. The rotator module is included in this view.*

For the conceptual design phase, two Cryomech AL-300 300 W cold heads were chosen for sizing the lines. These cold heads each required their own pair of refrigerant lines. During the detail design phase, thermal analysis revealed that a pair of smaller 150 W heads would provide sufficient cooling. These cold heads can be supplied by a single pair of refrigerant lines, so the cable wrap preliminary design has the capacity for an extra pair of refrigerant lines. The carriage size will likely be reduced to eliminate these extra lines during detail design. The chosen hose carriage was selected with the assistance of Igus. The interior of the carriage is separated into 9 compartments. Four compartments contain the two cold head flexible hose pairs. Two compartments hold a pair of heat exchanger lines – supply and return. A heat exchanger will be required to remove any heat generated by the instrument electronics from the instrument so that it doesn't escape into the dome. The heat exchanger lines are assumed to be equivalent in size to the cold head return lines, for now. One compartment will contain the power cable for the instrument.
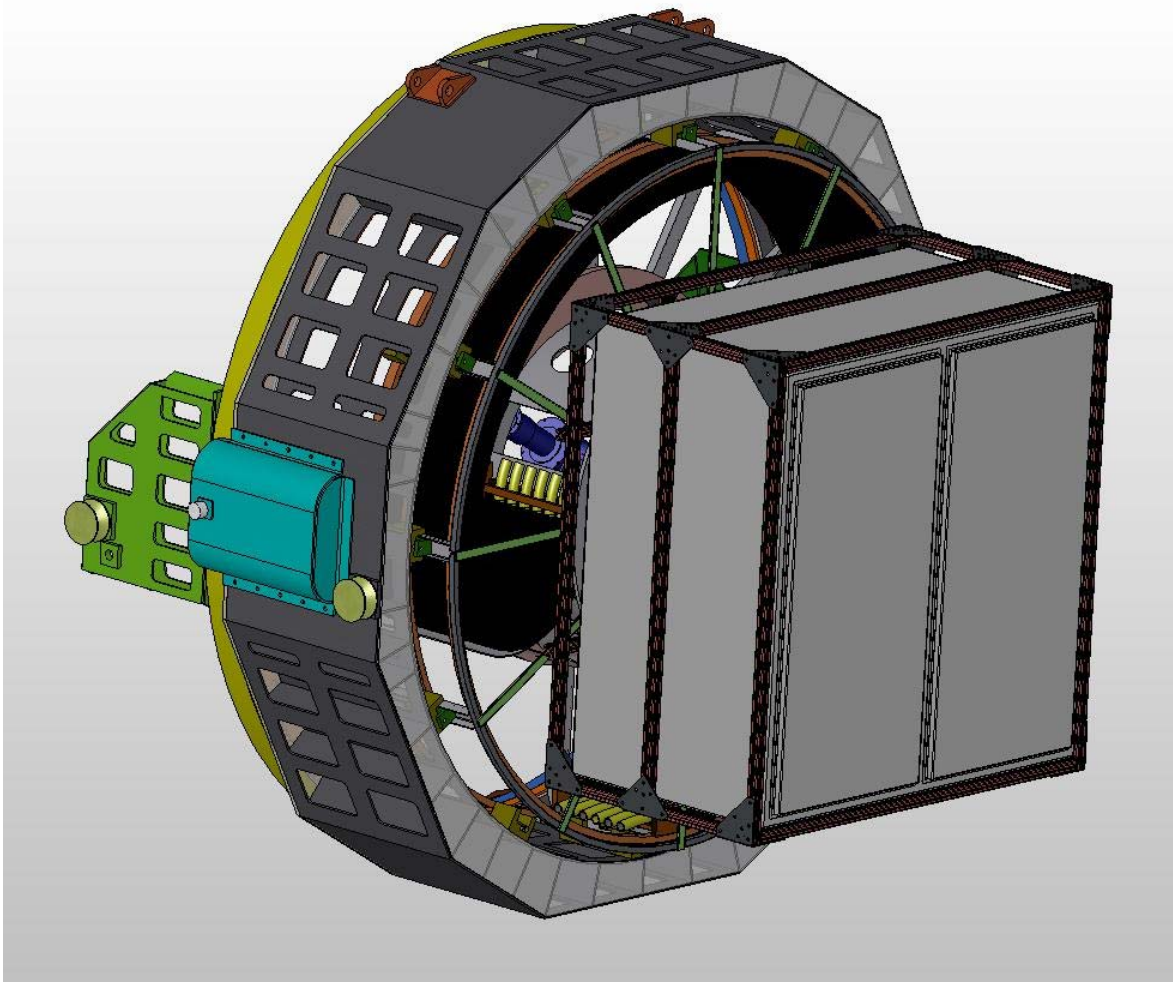
Figure 54: *Rear ¾ view of the cable wrap and electronics rack assemblies.*
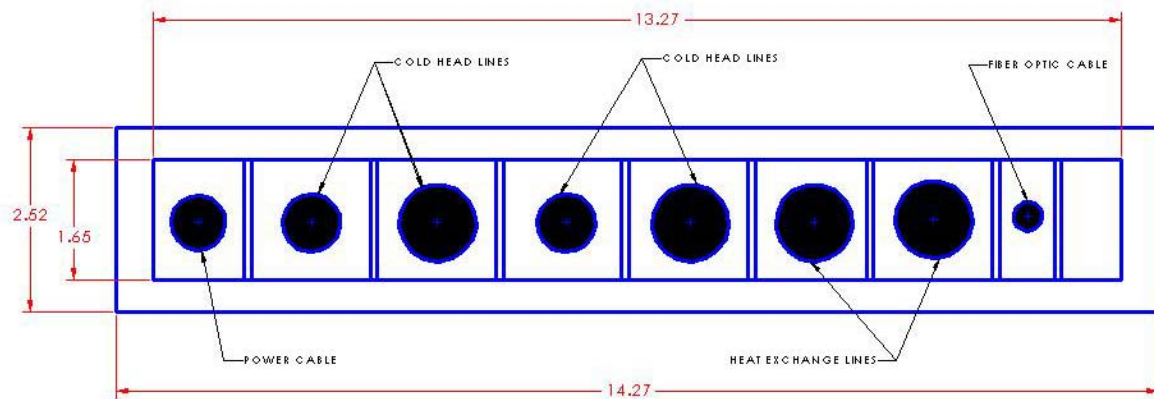
Figure 55: *Cross-section view of the preliminary cable wrap carriage.*

There is a compartment for fiber optic cabling and one compartment is a spare. Figure 55 depicts the carriage cross-section layout.

In order to provide access to the rear cover of the dewar, if necessary, the cable wrap and the electronics rack are designed to be removable with relative ease. The electronics rack assembly will be supported from the central hub of the cable wrap assembly since the electronics rack must rotate with the instrument and the central hub. The central hub of the wrap encases the cylindrical protrusion which extends from the dewar's rear cover. The hardware for attaching the electronics rack to the hub will be located so that it is accessible, as will all of the connections to the electronics rack. When access to the rear cover is required the electronics rack will be disconnected and removed first. This will provide access for disconnecting the cable wrap contents at both the instrument and the module. The hub can then be un-bolted from the rear cover protrusion, and the stationary, outer guide structure for the wrap can be un-bolted from the rotator module. The cable wrap will be designed to be self supporting so that it can be removed from the instrument without collapsing. The size and weight of these structures will require special handling fixtures and the use of an overhead crane.

The instrument dewar mounts to a bearing in the rotator module. The rotator module also contains the mechanisms required to define the instrument at the telescope's Cassegrain focal station and it also provides an interface to the instrument handler. MOSFIRE's rotator module will be a copy of the basic design used for LRIS and ESI, possibly with some improvements. For example, the drive system will likely need to be upgraded to provide additional torque for handling the loads from the large cable wrap. The module structure must also be modified with the attachment points for the stationary portions of the cable wrap guides. Quick-disconnect panels must be integrated into the module structure at the proper locations for the cable wrap connections.

5.2.1.11.1   Performance Predictions

- Instrument rotation range: ~+/- 270 degrees

The wrap and rotator module are considered low risk assemblies. The module is a copy of existing hardware. A similar serpentine wrap design has been used on IMACS. A small prototype was fabricated and tested during the KIRMOS preliminary design phase.

5.2.1.12   Instrument Handler

The handler is an Observatory standard assembly that supports the instrument when it is not mounted on the telescope and provides for moving the instrument to and from its storage position. MOSFIRE's instrument handler will be a copy of those previously designed and built for earlier Cassegrain instruments at WMKO (e.g. LRIS, ESI).

5.3   Electrical/Electronic Design

The MOSFIRE electronics consists of two major component groups, the MOSFIRE instrument electronics located in the electronics racks mounted on the instrument, and the MOSFIRE computer rack containing the instrument host computer and data storage disks located in the Keck I computer room. The host computer communicates with the instrument electronics via a dedicated 100Base-TX network.

The instrument electronics are housed in a pair of EIA 19 inch rack cabinets meeting the NEMA-4 specifications (continuous hinges and clamped gasketed doors, interior protected from dripping water, sprayed water and ice formation on the exterior of the cabinet). The arrangement of the electronics cabinets on MOSFIRE is shown in Figure 56.
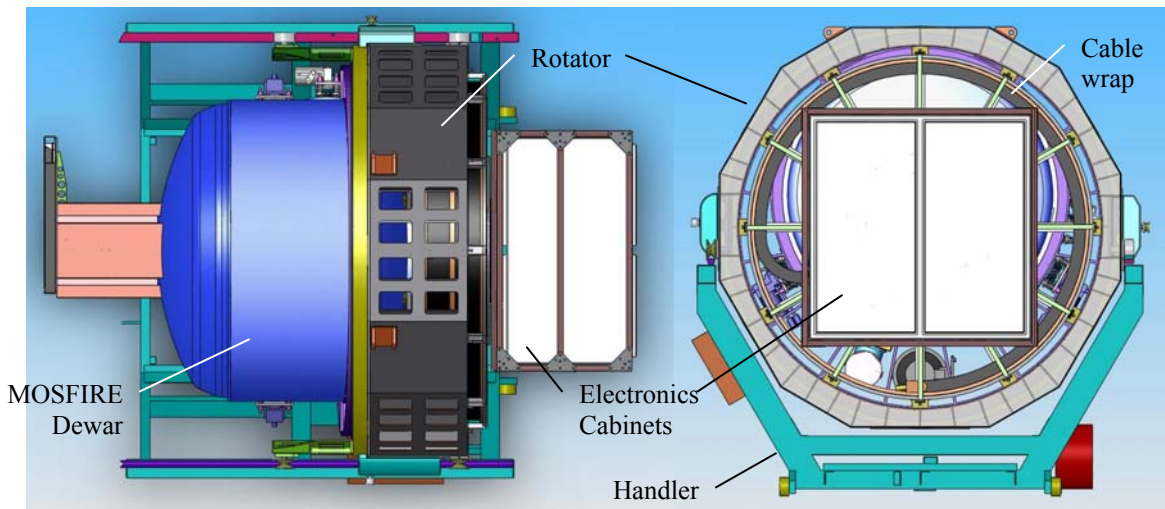
Figure 56: *MOSFIRE Electronics Cabinets*

The left side of the figure shows a top view of MOSFIRE with the electronics cabinets shown in white near the center. The right side of the figure shows a rear view of MOSFIRE.

Interconnections between the MOSFIRE dewar and the electronics cabinets are made via connector panels mounted on the side of the electronics cabinets and on the lower outside portion of the main dewar shell. Connections from the instrument to the Observatory systems are made though the instrument cable wrap to an instrument interconnect panel mounted on the instrument rotator. This panel is located on the stationary outer portion of the rotator while the dewar, cable wrap and electronics cabinets are mounted in the rotator bearing and move as a unit during observing.

A block diagram of the instrument interconnections is shown in Figure 57. The instrument is supplied with filtered 120 Vac power from the Observatory uninterruptible power supply (UPS). Data communications with the host computer is provided by a 1000Base-SX fiber optic link connecting two 10/100Base-TX switches, one in MOSFIRE instrument electronics rack number 1,

and one in the MOSFIRE compufer rack in the Keck I control room. The two switches form a single private 100Base-TX network for the instrument.

Figure 57 also shows the connections for glycol cooling on the instrument and the CCR head helium connections and power connections. A glycol pressure control module mounted on the instrument rotator next to the instrument connector panel provides for glycol connections. Glycol flow is distributed via a manifold to heat exchangers located in each electronics rack.

There are three CCR heads on the instrument, two primary heads to cool the instrument optical benches and a separate smaller head to cool the science detector. The high-pressure helium flow is split via a manifold to the three CCR heads. The two primary CCR heads are powered from the same control output on the compressor while a separate controller is provided for the smaller CCR.

The instrument guider will use a CCD camera head and electronics supplied by WMKO as part of its new guider development project. The guider will use a fiber optic connection for data and control, and will be supplied with 120 Vac power from the instrument UPS power.

The instrument rotator is controlled via a servo amplifier in the Keck I computer room. Definition of the instrument at the Keck I Cassegrain position is controlled by a local controls system on the telescope. Both the rotator and the local controls interface are connected via the instrument interconnect panel.

The instrument interconnect panel and the glycol module interface with the Cassegrain position connector panels when MOSFIRE is installed in the Keck I telescope, and with the storage position connector panels when MOSFIRE is stored on the Keck I Nasmyth deck at position RT1.

5.3.1   Instrument Interconnect Panel

The MOSFIRE instrument interconnect panel provides for the connections between the MOSFIRE instrument and the Observatory systems. The panel includes the connections listed in Table 20.

Connect #	Function

J1	Fiber Optics:
	   1000 Base-SX 62.5/125 m multimode optical fiber (RX & TX)
	   Guider optical fiber

J2	Instrument Power
J3	Detector CCR Power
J4	Primary CCR Power
J5	Guider Power
J6	Local Controls Interface for Cassegrain Defining Points
J7	Rotator Power and Control
He In & He Out	CCR Helium Supply and Return

Table 20: *MOSFIRE Instrument to Observatory Interconnections*
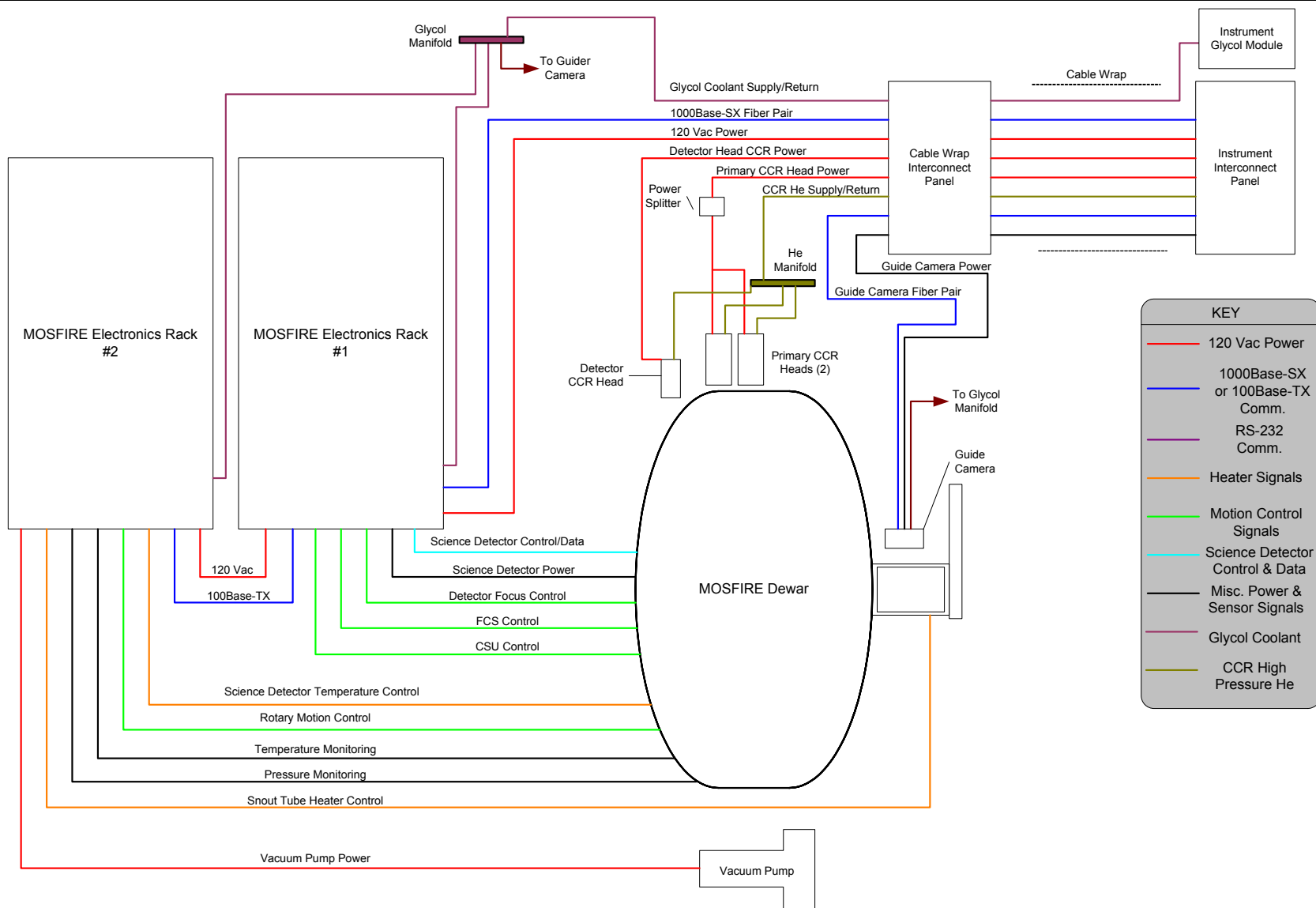
Figure 57: *MOSFIRE Interconnection Diagram*

5.3.2   MOSFIRE Instrument Electronics

MOSFIRE instrument electronics are shown in greater detail in the block diagram of
Figure 58. All of the electronics with the exception of the science detector ASIC and Jade 2
interface module (see §5.3.2.1) are located in two EIA 19 inch rack cabinets. Each rack cabinet is
cooled via a glycol heat exchanger equipped with fans to circulate the air within the cabinet.

MOSFIRE's instrument electronics are based on many of the same off the shelf electronic
components used in OSIRIS. The temperature controllers, vacuum gauge controller and terminal
servers are components standardized by WMKO, and the instrument's network architecture and
motion control systems are very similar to those used on OSIRIS.

The main components of the MOSFIRE instrument electronics are the science detector system, the
motion control systems (rotary mechanisms, FCS, detector focus and the CSU), the thermal
management systems, the housekeeping systems (temperature monitoring, pressure monitoring and
power control) and the data communications system.

All of the major MOSFIRE electronics components are listed in Table 21. With the exception of
the CSU controller all of these hardware components are commercial off-the-shelf products, and
each component requiring software control comes complete with firmware and a documented API.
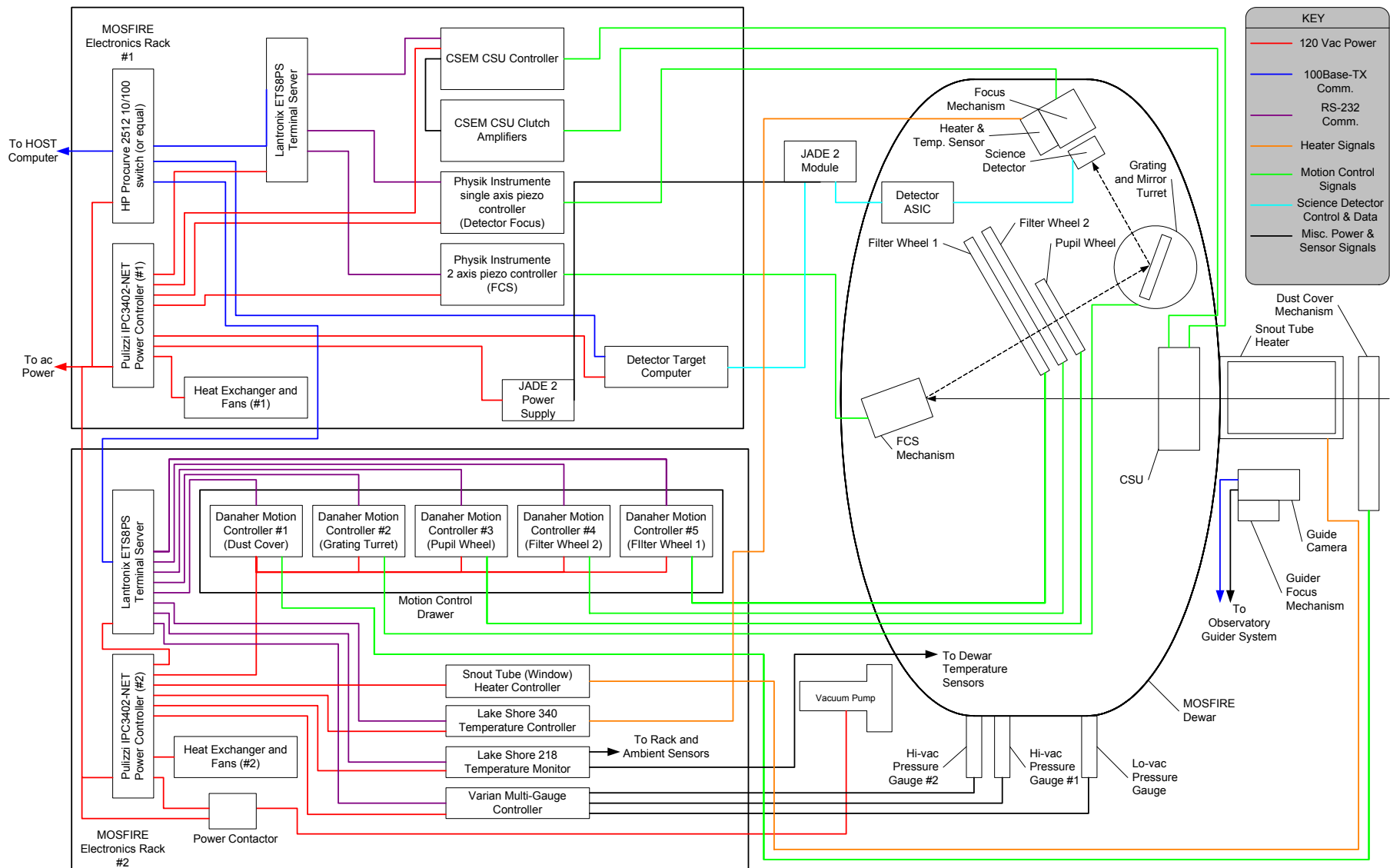
Figure 58: *MOSFIRE Electronics Block Diagram*

Function	Instrument Electronics Component	Control/Data Interface
Science Detector		
Detector	Rockwell HAWAII-2RG 2048×2048 HgCdTe Infrared Array	Discrete digital + analog I/O
Detector Controller	Rockwell ASIC + Jade 2 interface Card	Proprietary + USB 2.0
Detector Power Supply	5 Vdc Regulated Power Supply	Not required
Detector Target	1U rack mount Windows XP server	100Base-TX CAT-5 & USB 2.0
Motion Control		
Rotary Mechanisms (5)	Danaher Motion Controller	Serial RS-232
Flexure Compensation System	Physik Instrumente Two-Axis Piezo Controller	Serial RS-232
Detector Focus Mechanism	Physik Instrumente Single Axis Piezo Controller	Serial RS-232
Cryogenic Slit Unit	CSEM Custom CSU Controller	Serial RS-232
Thermal Management and Control		
Detector Temperature Control	Lake Shore 340 Temperature Controller	Serial RS-232
Snout Tube Heater Control	Off the shelf automatic heater controller	Not required
Housekeeping		
Temperature Monitor	Lake Shore 218 Temperature Monitor	Serial RS-232
Pressure Monitor	Varian Multi-Gauge Controller	Serial RS-232
Power Control	Pulizzi IPC3402-NET Power Controller	100Base-TX CAT-5
Vacuum Pump Control	TBD	Via Pulizzi IPC
Data Communications		
Network Switch	HP Procurve 2512 10/100 Switch with gigabit SX transceiver	100Base-TX CAT-5 UTP & 1000 base TX Fiber Optic
RS-232 Terminal Servers (2)	Lantronix ETS8PS Terminal Server	100Base-TX CAT-5 & RS-232

Table 21: *MOSFIRE Instrument Electronics Components*

5.3.2.1   Science Detector and Detector Controller

The MOSFIRE team has selected the Rockwell Scientific Hawaii2-RG 2K x 2K HgCdTe array with 18 μm pixels and a 2.5 μm cut-off wavelength. This is the same device architecture being developed for JWST and ground-based users will benefit from the considerable development work undertaken to solve many difficult requirements such as charge persistence, QE, noise, dark current and delamination. Recent proprietary data presented to us by Rockwell suggests that excellent progress has been made in all these factors and that our performance goals will be achieved. Fowler-sampled H2-RG devices have yielded <5 e$^-$ noise rms and dark currents of < 0.005 e$^-$/s.

Rockwell is now offering H2-RG devices with an Application Specific Integrated Circuit (ASIC) that implements all of the detector readout functions. The ASIC provides clocks and bias voltages to the detector and digitizes the detector outputs. The ASIC is packaged separately on a small board that is located inside the dewar next to the detector head.

Many other groups are also adopting the ASIC for instruments that will be completed prior to MOSFIRE. The Rockwell ASICs are also being used for the JWST instruments.

To enable our team to become familiar with the operation of these devices we obtained a prototype ASIC chip, interface card and software (shown in Figure 59) in February 2006, and we are working closely with Rockwell staff to develop the ground-based packaging of the ASIC. The detector will also require temperature control and this will be provided by an implementation similar to that used in OSIRIS, which is based on a standard Lake Shore temperature controller.
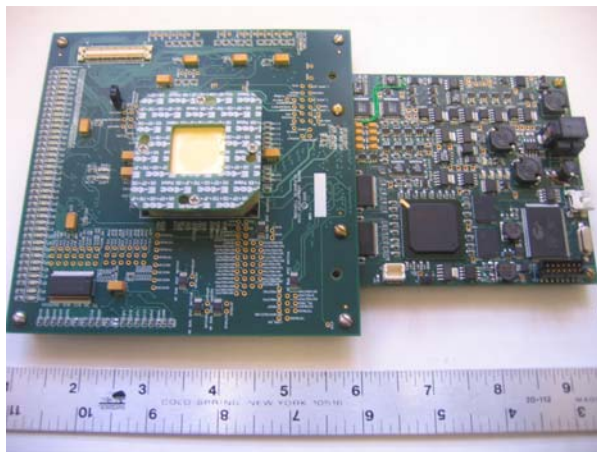
Figure 59: **The Rockwell ASIC.**

The ASIC is mounted in the center of the large breadboard. This is a fully functional model suitable for program development but not intended for cryogenic use. The final ASIC will be mounted in a much smaller enclosed module. The printed circuit card on the right is the Jade-2 interface board provided by Rockwell.

Figure 60 is a block diagram of the hardware and software components of the MOSFIRE detector system. This system consists of the detector, detector controller, interface components, two computer systems (the MOSFIRE host and the detector target) and the software modules required to control and read out the science detector.

The Rockwell ASIC uses a proprietary interface to a module called the "Jade 2", also supplied by Rockwell. The Jade 2 provides power conditioning for the H2-RG and the ASIC and a USB 2.0 compliant interface to the detector target computer. All of the detector control communications and read out data are transferred over the USB 2.0 interface. The ASIC is designed to be installed in the dewar near the detector and operates at cryogenic temperatures. The Jade 2 module will be located outside of the dewar in the instrument electronics racks or mounted on the outside rear wall of the dewar.

Rockwell uses a third party USB driver (Bitwise Systems QuickUSB) and their own hardware abstraction layer (HAL), which translates application commands into driver specific commands, hiding USB-specific driver detail from a higher-level application layer. The HAL in turn uses a second Rockwell supplied software component called the "COM DLL" to communicate with the HAL using the Microsoft .NET web service. The COM DLL application allows third party software to interface to the HAL and in turn to the ASIC via USB and the Jade 2.
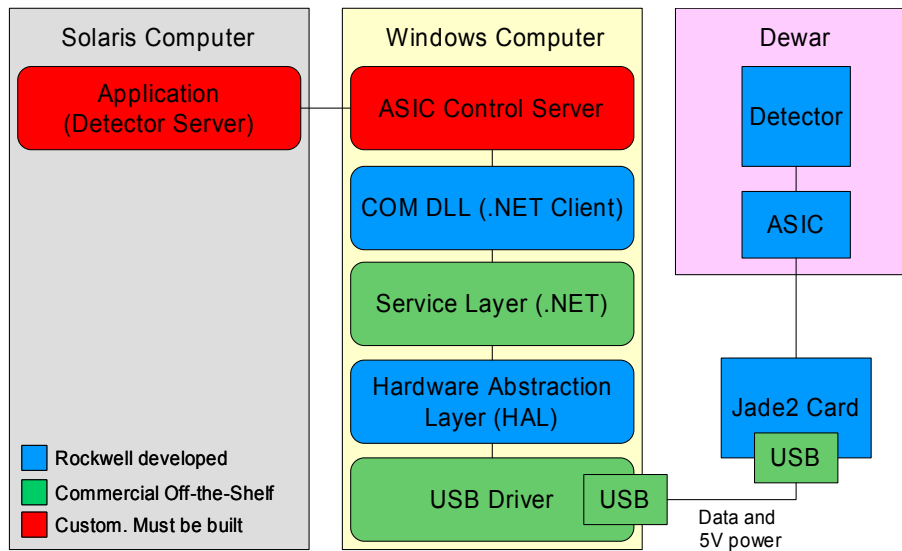
Figure 60: *MOSFIRE Detector System*

A computer running Windows XP is required to run the USB driver, HAL software and COM DLL. This computer will be a flash drive equipped rack mount computer located in MOSFIRE electronics rack 1 and will function as the detector target. This target computer will be located on a private network within the instrument and it will not be accessible via network communications except through the MOSFIRE host computer. The system will not require the use of less secure applications such as web browsers, reducing the need to implement frequent security updates.

5.3.2.2   Motion Control

MOSFIRE has 5 rotary motion axes driven by two phase bipolar stepper motors. Each of the rotary mechanisms is equipped with limit switches that are interfaced with the corresponding motion controller. Each motion axis is controlled by a Danaher/Pacific Scientific P70360-PNN indexing motion controller.

The Danaher motion controllers are mounted in an EIA 19 inch rack mount drawer with internal power distribution for the 5 motion controllers. Fan cooling will be provided if required to ensure adequate air circulation within the drawer. Each of the motion controllers will operate with low duty cycles so power dissipation will be minimal.

The two Physik Instrumente (PI) piezo controllers are self contained rack mount units. The CSEM controller consists of two rack mount units, one for the controller and one for the clutch amplifiers.

Table 22 describes the Motion control requirements for MOSFIRE in greater detail.

Mechanism	Description
Rotary Motion	
Dust Cover	A linear stage that slides a cover over the window when instrument is not in use, two positions (on/off)
Filter Wheel 1	Edge-driven wheel with 6 positions, including an open position
Filter Wheel 2	Same as filter wheel 1, the two wheels provide for a total of 10 filters
Pupil Rotator Wheel	Used when working in the K band. A hexagon shaped mask serves as a Lyot stop, and rotates to match the rotation of the telescope pupil as an object is tracked across the sky. The mask is formed using an iris which is open for all other wavelength bands
Grating-Mirror Exchange	The spectrometer diffraction grating and imaging fold mirror are mounted back-to-back on a turret. The mechanism rotates turret approximately 180 degrees to two hard stopped positions
Piezo Controllers	
Flexure Compensation System	Two-axis stage that compensates for flexure in the instrument due to a varying gravity vector. Uses a lookup table based on positioning information from the telescope drive system.
Detector Focus	Single-axis piston stage that adjusts the detector focus based on filter selection.
Cryogenic Slit Unit	Cryogenic adjustable slit mask, comprised of a set of ~45 pairs of bars

Table 22: *MOSFIRE Motion Control Requirements*

5.3.2.3   Thermal Management and Control

The science detector operating temperature is controlled by a closed loop temperature control system using a Lake Shore Cryotronics, Inc. model 340 temperature controller, a diode temperature sensor and a resistive heater located on the detector mounting block.

The snout tube heaters are resistance type cartridge heaters controlled by a closed loop temperature controller also using a diode temperature sensor. The exact make and model of the snout tube heater controller is TBD.

5.3.2.4   Housekeeping

The MOSFIRE instrument housekeeping functions include electronics rack, dewar and ambient temperature monitoring, dewar pressure monitoring and instrument power control.

Temperature monitoring is provided by a Lake Shore Cryotronics, Inc. model 218 and diode temperature sensors deployed at various locations in the dewar and one sensor located in each equipment rack. A temperature sensor is also provided for ambient temperature monitoring.

Pressure monitoring is provided by a Varian Multi-Gauge controller. This controller is equipped with two high vacuum gauges (Varian IMG-100) one as the primary high vacuum gauge and one as a backup. A low vacuum gauge (Varian ConvecTorr gauge tube) is also provided.

AC power is input to electronics rack 1 and then distributed to the AC power controllers. AC power control for the MOSFIRE electronics is performed by Pulizzi IPC3402-NET power controllers. Each distribution unit provides 8 outlets, and these are assigned as shown in Table 23.

Electronics Rack #1	Load	
Pulizzi Output #	Description	Typical Wattage
1	HP Procurve 2512 Switch	36
2	Lantronix ETS8PS	12
3	CSU Controller	80
4	Detector Focus Controller	50
5	FCS Controller	50
6	Detector Target Computer	550 (max.)
7	Jade 2 Power Supply	15
8	Heat Exchanger Fans	32
Electronics Rack #2	Load	
1	Lantronix ETS8PS	12
2	Rotary Motion Control Drawer	75
3	Snout Tube Heater Controller	15
4	Lake Shore 340 Temperature Controller	190
5	Lake Shore 218 Temperature Monitor	18
6	Varian Multi-Gauge Controller	120
7	Heat Exchanger Fans	32
8	Vacuum Pump Contactor	5

Table 23: *MOSFIRE AC Power Distribution*

An AC operated power contactor controlled by an output on the power controller in rack 2 will be provided for control of the vacuum pump. This will isolate the high power motor load from the filtered power provided by the power controller.

5.3.2.5 Data Communications

A Hewlett Packard Procurve 2512 10/100Base-TX switch equipped with a 1000Base-SX transceiver is used to provide TCP/IP communications for the instrument electronics. The 1000Base-SX transceiver provides a gigabit link to a second Procurve 2512 located in the MOSFIRE computer rack in the Keck I control room. The two switches form a single private 100Base-TX network for the instrument.

The switch located in electronics rack 1 on the instrument communicates with the detector target computer, two Lantronix ET8PS terminal servers (one in each rack) and two Pulizzi IPC3402-NET power controllers (one in each rack).

The switch located in the MOSFIRE computer rack communicates with the MOSFIRE host computer and provides access to the instrument private network from the Keck I control room.

RS-232 communications is used for control of the other MOSFIRE electronics components, and two terminal servers allow control of these devices via the MOSFIRE private network using TCP/IP.

5.3.3   Guider

WMKO is currently developing new guide cameras and telescope guiding software as an upgrade to the Observatory's current guiding system. We plan to use this new system for the MOSFIRE guider (detector, electronics and software).   The MOSFIRE focus mechanism will also be controlled by the Observatory guider system. The requirements of the MOSFIRE guider optics are being taken into account as the Observatory's new guiding system is designed.

The guider communicates with the Observatory guider control computer using a 100Base-TX network connection over a fiber optic link. A fiber optic transceiver located in the MOSFIRE computer rack interfaces the guide camera to the Observatory guider private network.

5.3.4   MOSFIRE Instrument Computers Overview

WMKO has standardized on computers running the Sun Solaris operating system as the primary platform for instrument host computers. The final selection of server computer will not be made until the third year of the project, so it is possible that the model number and feature set will change when the computer is actually purchased.

The MOSFIRE computer architecture consists of three main computers and two switches: an instrument host computer, a detector host computer, and a detector target computer. The detector target computer's responsibility is to run the MOSFIRE ASIC Server and Rockwell ASIC control software. This system will run Windows XP Professional and will reside in the instrument electronics cabinet. The detector host computer will run the Detector Server and connect to a storage array for data. The instrument host computer will run everything else. These latter two systems will run Solaris and reside in the Keck computer room. All network devices are connected through two private network switches: one at the instrument, one in the Keck computer room. The switches will be connected through the telescope wrap with a fiber connection. Access to the private network will be through the Keck public network to a secondary network adapter on the instrument host computer.

Figure 61 illustrates the MOSFIRE Private Network:
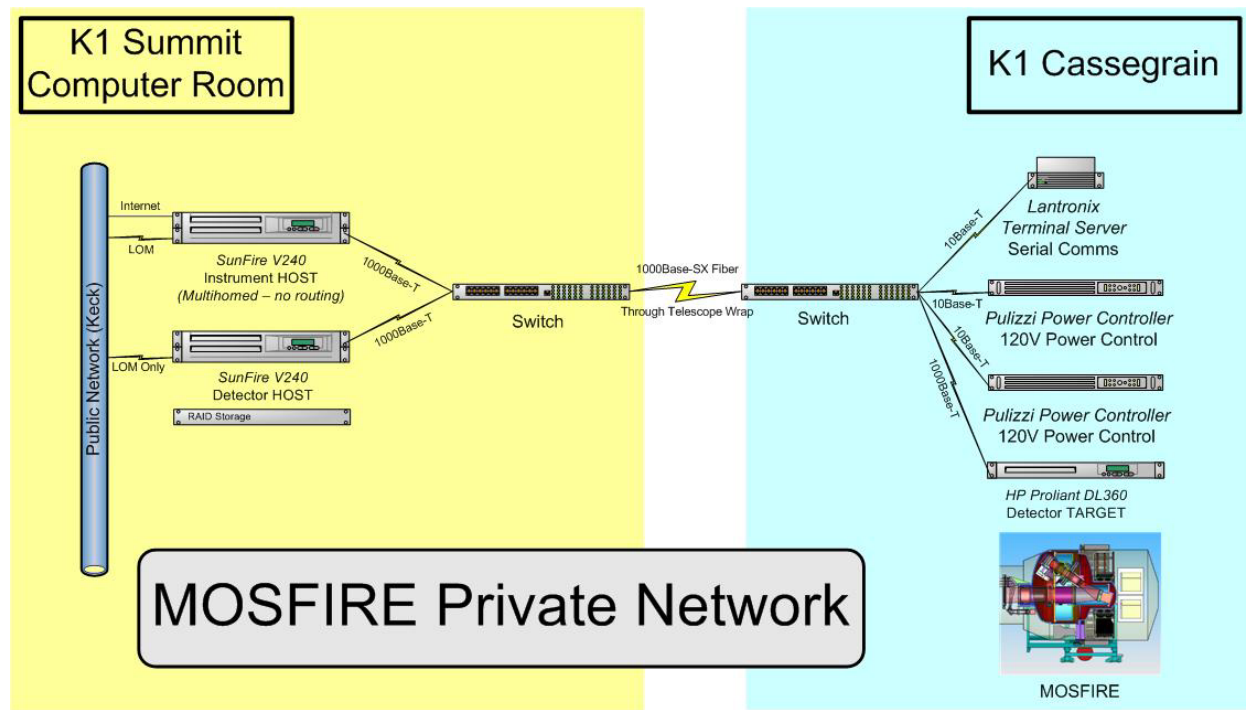
Figure 61: *MOSFIRE Computer Network*

5.3.5 Design Practices

The details of the MOSFIRE instrument interconnections and electronics rack layouts will be finalized during the detailed design phase. All signal and control interconnections will use fully shielded cables with 360º grounding backshells. A Faraday shield design will be employed for the dewar to electronics rack inter connections. The dewar electronics racks are RF tight designs with full EMI gaskets and ground straps between the hinged access doors and the rack cabinet body.

Signal DC grounding will be designed to ensure that low level signal reference points are not subjected to ground loops.

5.4   Software

MOSFIRE is a third generation Keck instrument and can therefore inherit a wealth of existing software infrastructure, and benefit from previous experience developed in setting and refining requirements. Most significantly, MOSFIRE will benefit from a polished and robust client-server architecture, which facilitates distributed processing and remote observing. This framework was started with NIRSPEC and NIRC2, and was most recently refined in the implementation of the OSIRIS instrument software. This server architecture offers many features that have become standard practice for infrared instruments at WMKO. Each instrument server is compliant with the Keck Task Library (KTL), which uses remote-procedure calls (RPCs) in a WMKO standard framework for network communications. Standard WMKO keywords are used as the main applications programming interface (API), and simple clients, such as "show" and "modify" facilitate easy scripting. By using existing KTL interfaces to other popular languages such as Java, IDL and Tcl, a diverse range of user interfaces can be implemented.

MOSFIRE will make extensive use of software developed for OSIRIS, the most recent instrument delivered to WMKO (first light February 22, 2005), including server frameworks, GUI components, and client-server interface tools. In addition, the pressure monitor, power control and temperature servers will be identical to the servers implemented for OSIRIS.   The flexure compensation system (FCS) server will also be reused, in this case from another instrument currently being developed, NIRES, which is using a flexure correction approach very similar to the MOSFIRE design.

The only completely new software components are the interface to the Hawaii-2RG ASIC and the server for the CSU. Both of these components will require significant development effort, but overall the software for MOSFIRE does not present major technical or schedule risks.

Software effort will be distributed among three programming groups, the OIR group at CIT, the IR Lab group at UCLA and the software development group at WMKO. This collective team brings many years of experience in developing instrumentation software at WMKO.

5.4.1   Software Architecture

At the highest level the MOSFIRE software is based on three software layers, a low level server layer, the KTL layer, and a user interface layer, which provides a graphical user interfaces (GUIs). These layers are illustrated by the block diagram shown in Figure 62.

The server layer consists of a generic server module that is configured by a hardware dependent function library to control each MOSFIRE hardware subsystem though a variety of hardware interfaces (Ethernet, RS-232, etc.).

The KTL layer is a standard WMKO software component that is used in every instrument at the Observatory. This layer is implemented as a set of library routines to provide keyword control of the servers. Instrument specific keywords are defined in a keyword list. Common practices and

standards exist for the development of keyword lists, and the keyword lists for MOSFIRE will be based on existing keyword lists. An important feature of this architecture is that the MOSFIRE hardware can be controlled and tested using keywords and keyword scripts once the servers are complete. This avoids the interdependencies between hardware assembly/test and user interface development, which often lead to development schedule problems.
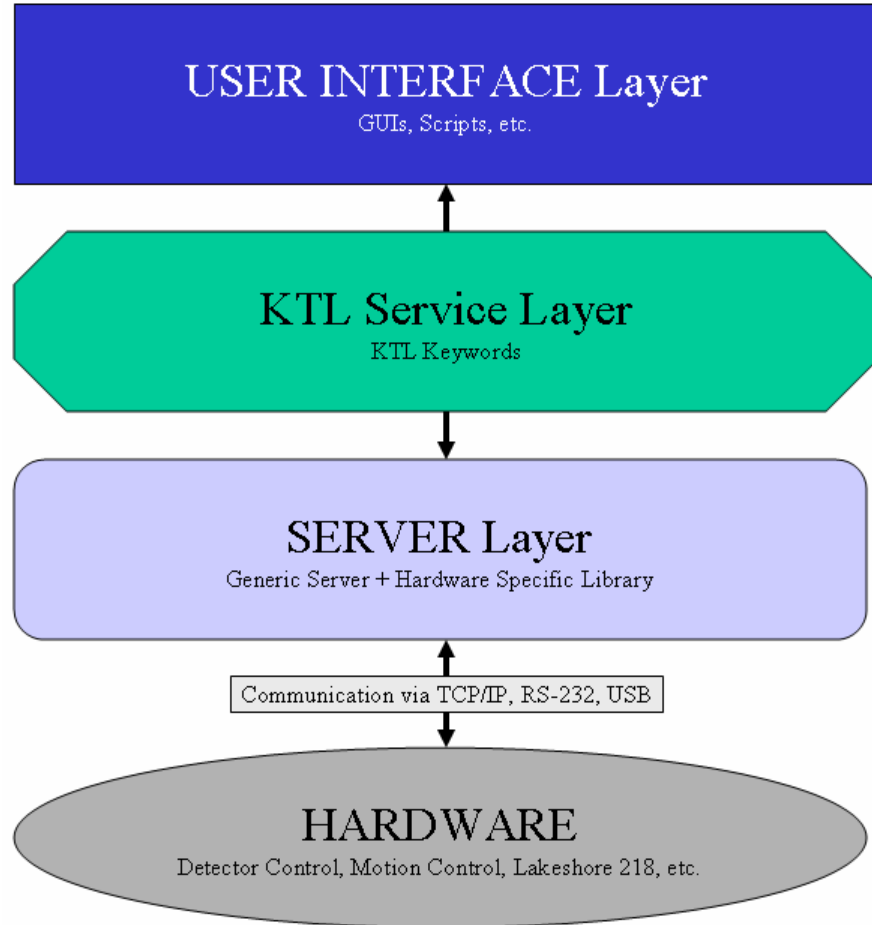
Figure 62: *MOSFIRE Software Layers*

5.4.2 MOSFIRE Software Modules

The MOSFIRE software is made up of three kinds of software modules. Two of these correspond to the server and user interface layers shown in Figure 62. The third kinds of modules are related applications, the CSU configuration software and the image viewing software. All the MOSFIRE software modules are shown in Figure 63.
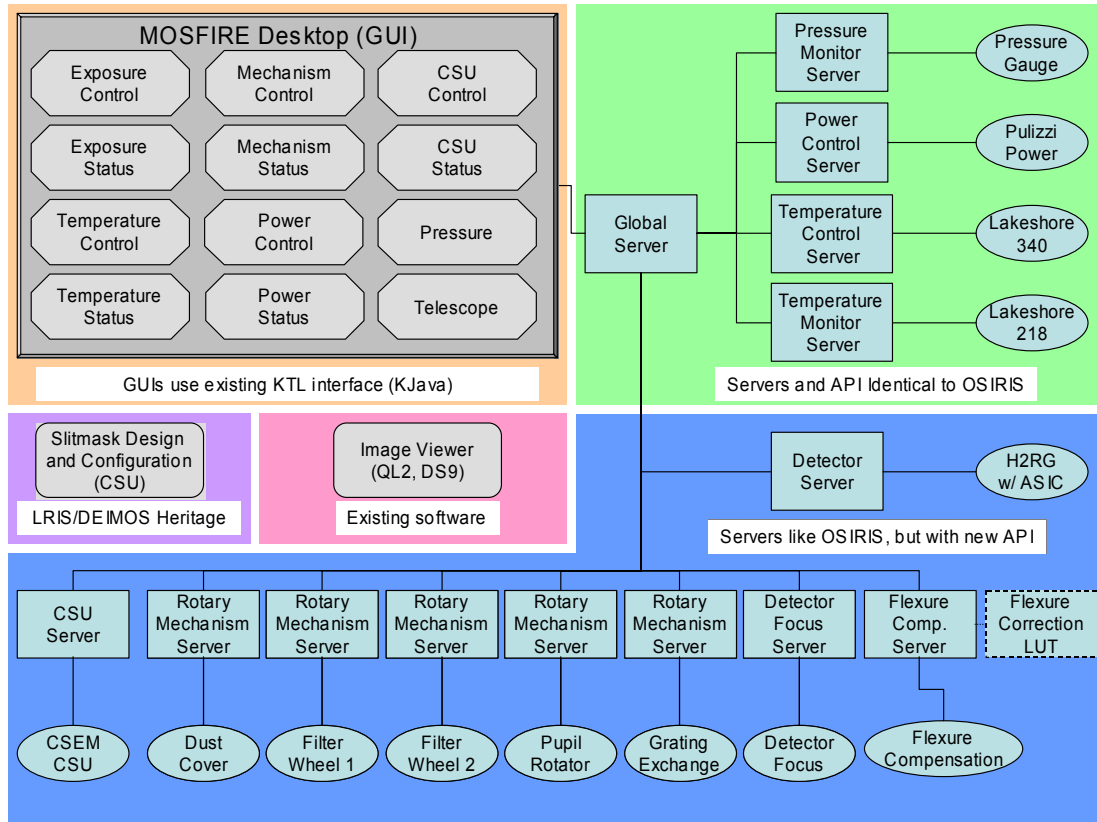
Figure 63: *MOSFIRE Software Modules*

5.4.2.1 Servers

The MOSFIRE servers are based on the WMKO KTL layer. Included in KTL is a methodology for implementing keyword servers. These keyword servers maintain a list of keyword-value pairs. Some keywords are status keywords, updated as the hardware changes (e.g. a temperature reading); some keywords are functional keywords that execute some action when set to appropriate values (e.g. setting a "go" keyword to 1 to start an exposure); and some keywords are utility keywords used to define system parameters or information (e.g. location of temperature sensor 1).

All servers (except the ASIC server) use a common KTL server framework called `rpcKey_server`, a distributed, RPC-based, client-server infrastructure written in C. This framework isolates all details associated with the RPC communications scheme and the network and transport layers below it from the developer. The developer is responsible only for the application code loaded via shareable libraries and configuration files, both of which define the behavior of the server.

The server framework features the creation of iterative forked processes, each of which iterate at a constant, keyword-defined rate. These processes are used for checking status of hardware, polling hardware for current readings (e.g. temperatures), or probing another server. Each component of

the MOSFIRE instrument electronics that requires software control will have a server instance, referred to as a hardware server. For each MOSFIRE hardware server, the MOSFIRE software team then only needs to implement the hardware specific library that handles the actions of the keywords and bind it to the framework server process.

The MOSFIRE hardware servers are listed in Table 24.

Acronym	Name	Description
MDS	MOSFIRE Detector Server	Provides controls to configure, start, and abort exposures through the ASIC Server.
MAS	MOSFIRE ASIC Server	Controls the Rockwell ASIC, and through the ASIC controls the science detector. Runs on Windows machine. Based on RMI, not KTL.
MRMS	MOSFIRE Rotary Mechanism Server	Controls mechanisms that use one-axis spinning motors, such as wheels, slides, and turrets. For MOSFIRE, the rotary mechanisms are the filter wheels, the pupil rotator, the dust cover, and the grating-mirror exchange.
MFCS	MOSFIRE Flexure Compensation Server	Controls Tip/Tilt Mechanism Controller.
MDFS	MOSFIRE Detector Focus Mechanism Server	Controls Piezo Mechanism Controller.
MCSS	MOSFIRE CSU Server	Controls CSU.
MTMS	MOSFIRE Temperature Monitor Server	Controls LakeShore 218 temperature monitor.
MTCS	MOSFIRE Temperature Control Server	Controls LaksShore 340 temperature controller.
MPRS	MOSFIRE Pressure Monitor Server	Controls pressure gauge(s) via Varian Multigauge Controller.
MPWS	MOSFIRE Power Control Server	Controls Pulizzi power controller.

Table 24: *MOSFIRE Hardware Servers*

Because of the use of common hardware, the four houskeeping servers (MTMS, MTCS, MPRS, and MPWS) will be identical to their respective OSIRIS housekeeping servers. The Mechanism Servers will also be similar to the OSIRIS Motor Server, but will use a different motor controller. Therefore, as with the Detector Server, much of the functionality and many of the algorithms can be reused. Coding effort will be substantially reduced, being directed toward modifying the portion of the code that interfaces with the API of the new hardware components.

The MOSFIRE ASIC Server is unlike the other servers in that it is not built upon the KTL framework. This server runs on a Windows machine, and is solely responsible for providing a

translation layer between the legacy C code of the MDS and the Rockwell proprietary ASIC control software. It does so using a set of Java technologies, including Java Native Interface (JNI) and Remote Method Invocation (RMI). More information can be found in the Interfaces section below.

In addition to the hardware servers there is another server, called the MOSFIRE Global Server (MGS). This server provides a single point interface from the GUIs to the hardware servers. In this way, a GUI only needs to talk to the MGS, rather than interfacing with multiple servers. The MGS also facilitates the creation of "coordinated keywords" that allow a single keyword command to the MGS to coordinate the actions of multiple hardware servers.

5.4.2.2   User Interfaces

User interfaces for MOSFIRE consist of GUIs, scripts, and KTL clients. KTL RPC clients are the simplest of user interfaces to the server level. There are four clients that are commonly used to access server keywords: `show`, which can get the value of a keyword from a server; `modify`, which can set the value of keyword; `cshow`, which watches a keyword and prints out the new value when it changes; and `xshow`, which is like cshow, but is displayed in a Tcl/Tk dialog. KTL clients are part of the KTL library, and are reliable engineering tools that quickly and directly interface with any server.

Scripts are built using these KTL clients. They are C-shell scripts that use `show`, `modify`, `waitfor`, and other tools to automate a sequence of actions. Scripts are broken down into three categories:

- Control scripts: These scripts are used to control the instrument, such as configuring the mechanisms and automating exposure sequences.

- Operations scripts: These scripts are used by the observatory staff to prepare the instrument and user environment for observing. Scripts are also used to automate initial software installation and configuration.

- Run scripts: These scripts do not manipulate server keywords but instead they are used to start and stop the various server and GUI components of the system.

While the KTL clients and scripts can be used to fully control the instrument, this approach can be clumsy and non-intuitive for new users. Therefore, a set of Graphical User Interfaces (GUIs) will serve as the primary user interface for the instrument. GUIs will provide visual status information and interactive dialogs to control the instrument and take exposures.

The MOSFIRE GUIs will be written in Java. This is primarily for commonality with the OSIRIS software package, so that MOSFIRE can take advantage of the OSIRIS heritage and development experience. A Java KTL interface, called `KJava`, was created for OSIRIS to allow access to the servers, and MOSFIRE will use this interface as well.

The MOSFIRE GUIs are listed in Table 25.

Acronym	Name	Description
MECGUI	MOSFIRE Exposure Control GUI	Sets up exposures (integration time, coadds, etc.) and starts and aborts them.
MESGUI	MOSFIRE Exposure Status GUI	Tracks the progress of an exposure, showing parameters of current exposure and remaining integration time.
MMCGUI	MOSFIRE Mechanism Control GUI	Controls the mechanisms of the instrument. Only filter and observing mode (imaging or spectroscopy) options are provided, and the two filter wheels, pupil wheel, grating turret, and focus mechanisms are moved according to those two parameters.
MMSGUI	MOSFIRE Mechanism Status GUI	Shows the status of each MOSFIRE mechanism, except the CSU.
MSCGUI	MOSFIRE CSU Control GUI	Provides controls to configure the CSU.
MSSGUI	MOSFIRE CSU Status GUI	Shows current position of bars in CSU.
MTCGUI	MOSFIRE Temperature Control GUI	Provides controls to set MOSFIRE dewar and science detector operating temperature.
MTSGUI	MOSFIRE Temperature Status GUI	Shows current temperatures at various locations in the instrument.
MPRGUI	MOSFIRE Pressure Status GUI	Shows current dewar pressure.
MPCGUI	MOSFIRE Power Control GUI	Provides controls to turn on and off power of selected components.
MPSGUI	MOSFIRE Power Status GUI	Displays power status of selected components.
MTGUI	MOSFIRE Telescope GUI	Provides controls to the telescope drive and control system, such as offsetting and control of the instrument rotator.

Table 25: *MOSFIRE GUIs*

MOSFIRE GUIs will be designed using the Model-View-Controller (MVC) framework. The MVC separates the data model of a program, the user interface (the view), and the communication between them (the controller) into logical components. The model encapsulates all of the properties of the program, and handles the interaction between them. This is the core of the program, and is usually quite stable. The view, on the other hand, often undergoes changes to suit the end user's preferences. The MVC allows for the view to change quite significantly, yet the core logic of the program, stored in the model, remains the same. It also allows for multiple views to represent the same model.

The MVC implemented in our Java programs is event-driven. Events for MOSFIRE are usually triggered in one of two ways. One way is by user interaction with the GUI, such as pressing a button. The other way is when a keyword value changes. This event is propagated using KJava from the server, to the model, which has registered itself to the server as a listener of keyword value change events. When the model itself changes, usually another event is triggered to notify the view of the change, and the view represents this change in the prescribed visual manner.

5.4.2.2.1   The MOSFIRE Desktop

The MOSFIRE GUIs will run within a desktop environment called the MOSFIRE Desktop. The MOSFIRE Desktop is a virtual desktop that consists of an empty dialog or frame that will contain most of the MOSFIRE GUIs (Figure 64). It will manage the creation and destruction of the other GUIs, and provide a toolbar for launching them. It will have the ability to create groups of GUIs to be managed together, so that they can be launched and destroyed with one click. Additionally, groups of GUIs can be moved around the desktop while maintaining the positional relationships between the members of the group.
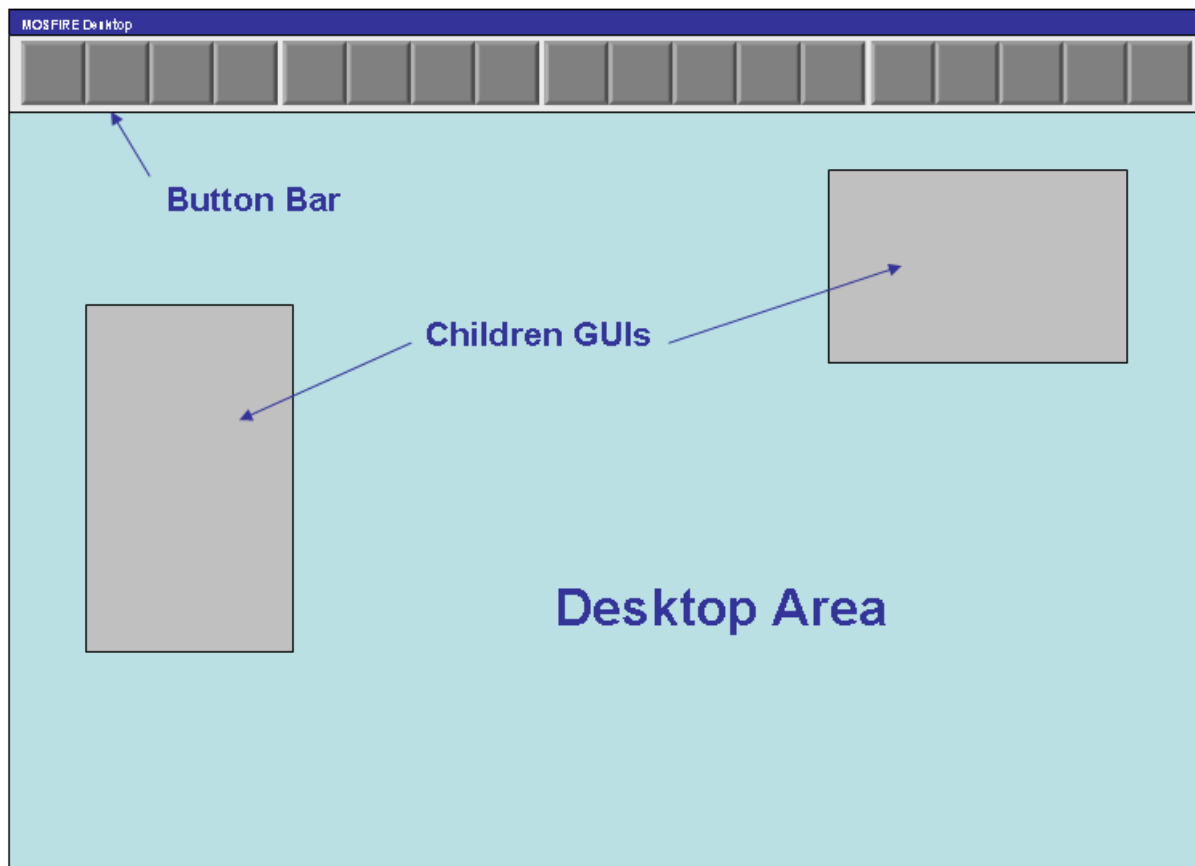
Figure 64: *MOSFIRE Desktop*

This program will also have the responsibility of connecting to the instrument servers via a KJava connection to the MOSFIRE Global Server. The desktop will receive updates as keyword values of the global server change, and maintain its own list of these values, which are broadcasted to the child GUIs for their disposal. However, child GUIs of the MOSFIRE Desktop will have the ability to make their own connection to a server, so that they can be run, fully featured, independently, outside the MOSFIRE Desktop environment.

5.4.2.2.2   Status GUIs

MOSFIRE will use one set of GUIs to monitor the status of the instrument. Each one is read-only. They work by monitoring keyword values, receiving KJava callbacks whenever a keyword changes value. For most items, the value is simply displayed as text. Some items can optionally be displayed graphically. Regardless of the visualization, the underlying model which handles the actions taken when a keyword changes is the same. This is the power of the MVC architecture.

As an example, consider the status of a power outlet. When the power is turned on in the server, the keyword representing the power status, say `pwrstat1`, changes value from 0 to 1. The keyword in the power server is reflected as a meta-keyword in the global server. When the meta-keyword changes value, an event is triggered to all registered listeners. For MOSFIRE, the MOSFIRE Desktop will have registered as a listener. The `KJavaCShowCallback` function is called, saying that `pwrstat1` has a new value of 1. The Power Status GUI will have registered with the Desktop as being interested in the `pwrstat1` keyword, and will be notified of the change. The model of the MPSGUI will set its internal member variable representing the status of the first outlet to "on" or "true" (since it is a boolean state). Now, the Controller registers itself as interested in a change of the value of the member variable (not the keyword) of the model, and it is notified using Java `PropertyEvents`. It, as an inner class member of the View, tells the View that the value has changed. The View then decides how to visually represent the change to the user. One view could simply be a text label saying "On" or "Off". Another, used in OSIRIS, is a button that turns bright green when on, and a dark green color when off, resembling a light.

5.4.2.2.3   Exposure Status GUI

The MOSFIRE Exposure Status GUI (Figure 65) is responsible for displaying information about the current or last exposure taken with the instrument. It will show the following information:
- Integration time (per coadd)
- Number of coadds
- Sampling mode
- Number of reads / read pairs
- Filename
- Object name
- Frame comment
- Exposure progress (percentage complete, time remaining)
- Dither pattern progress (frames complete/remaining)

A progress bar will be used to graphically show exposure progress.
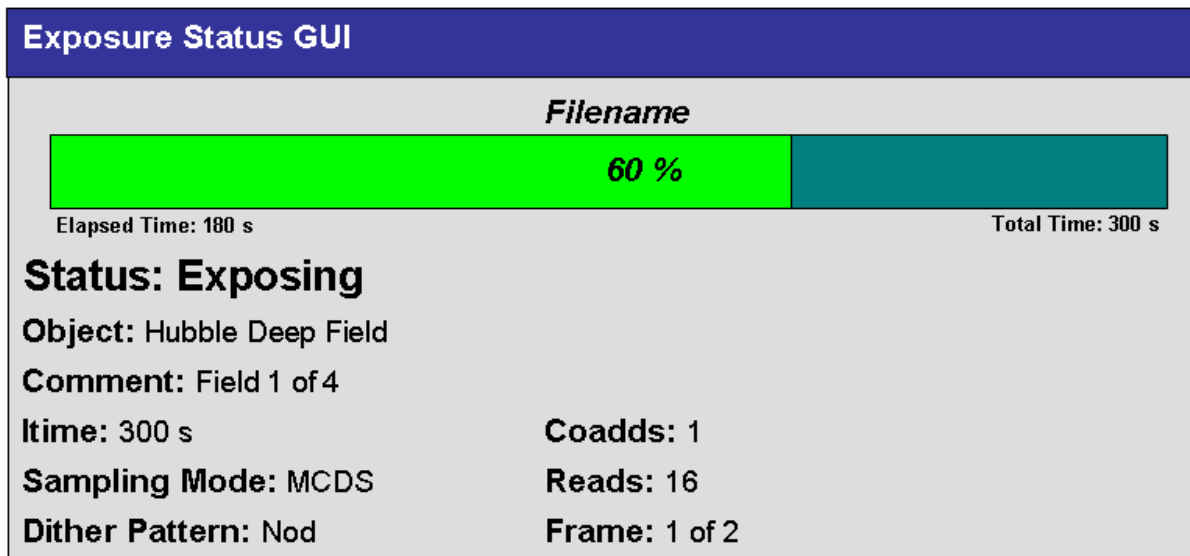
Figure 65: *MOSFIRE Exposure Status GUI*

5.4.2.2.4 MOSFIRE Mechanism Status GUI

A Mechanism Status GUI (Figure 66) will be used to show status information for a mechanism. An instance of this GUI will be used for each mechanism in the instrument. It will give the current mechanism status (Moving, Lost, Error, etc.), current position, and target position. A graphical representation of the mechanism will also be displayed, and animated to reflect the motion of the mechanism when appropriate. Detailed information, such as switch status, will be available via a menu option or some other hidden mechanism.
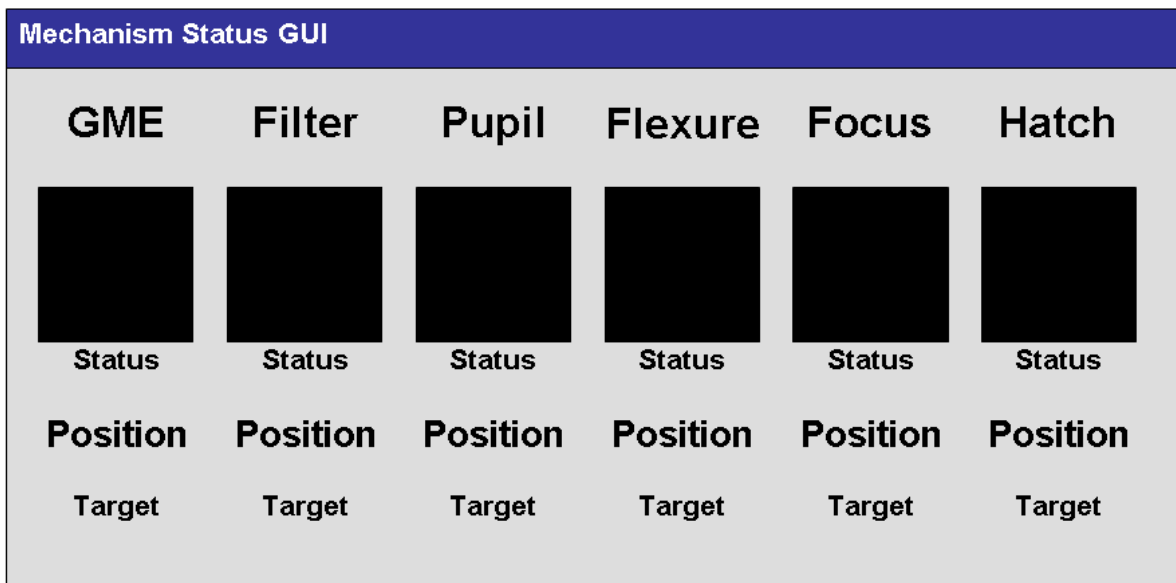
Figure 66: *MOSFIRE Mechanism Status GUI*

5.4.2.2.5 Temperature Status GUI

This GUI (Figure 67) shows the temperatures as monitored by the MOSFIRE Temperature Monitor and Control Servers. It will simply display the values as text to the screen, with the sensor location prefacing the value.

5.4.2.2.6 Pressure Status GUI

This GUI (Figure 67) will show the current pressure of the dewar, as monitored by the MOSFIRE Pressure Server. Like the MTSGUI, it will display the value as text.

5.4.2.2.7 Power Status GUI

This GUI (Figure 67) will show the status of each of the outlets in the power controller as controlled by the Power Servers. It will use a set of lights, as described in the example above, each labeled with the function of the outlet.
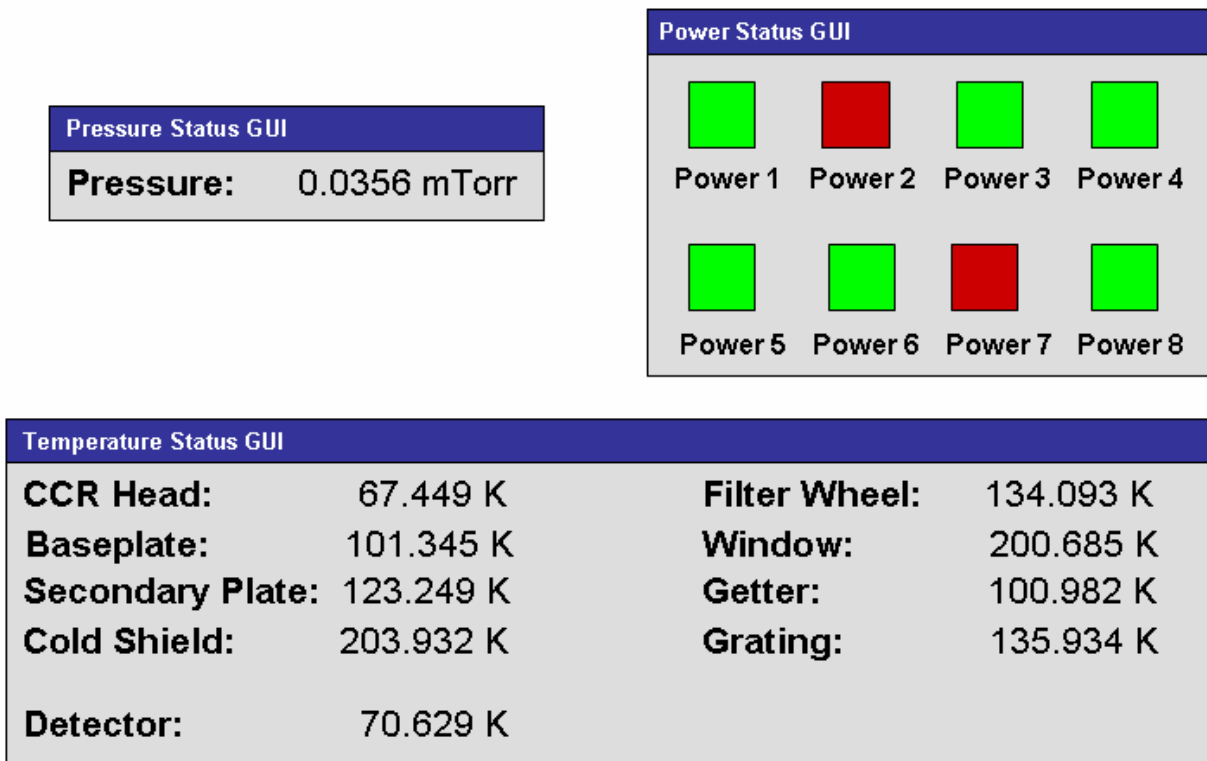
Figure 67: *MOSFIRE Temperature, Pressure, and Power Status GUIs*

5.4.2.2.8 CSU Status GUI

The MOSFIRE CSU Status GUI (Figure 68) is responsible for reporting the positions of the slits in the CSU. This can be done a number of ways, but we will feature two of them. One will be a

simple list of positions and widths for each row. It will be shown as a table in a scrollable viewport. The other method is graphical, showing the field of view and each slit within it. The sides of the field of view will be colored differently to depict the regions where slits would not get full spectra coverage. The slits may be exaggerated in width, to make it clearer where they are. There will be a zoomed in drawing of a single row available, so that when a user clicks on a row, that row is visualized in a larger view, showing the true width of the slit.
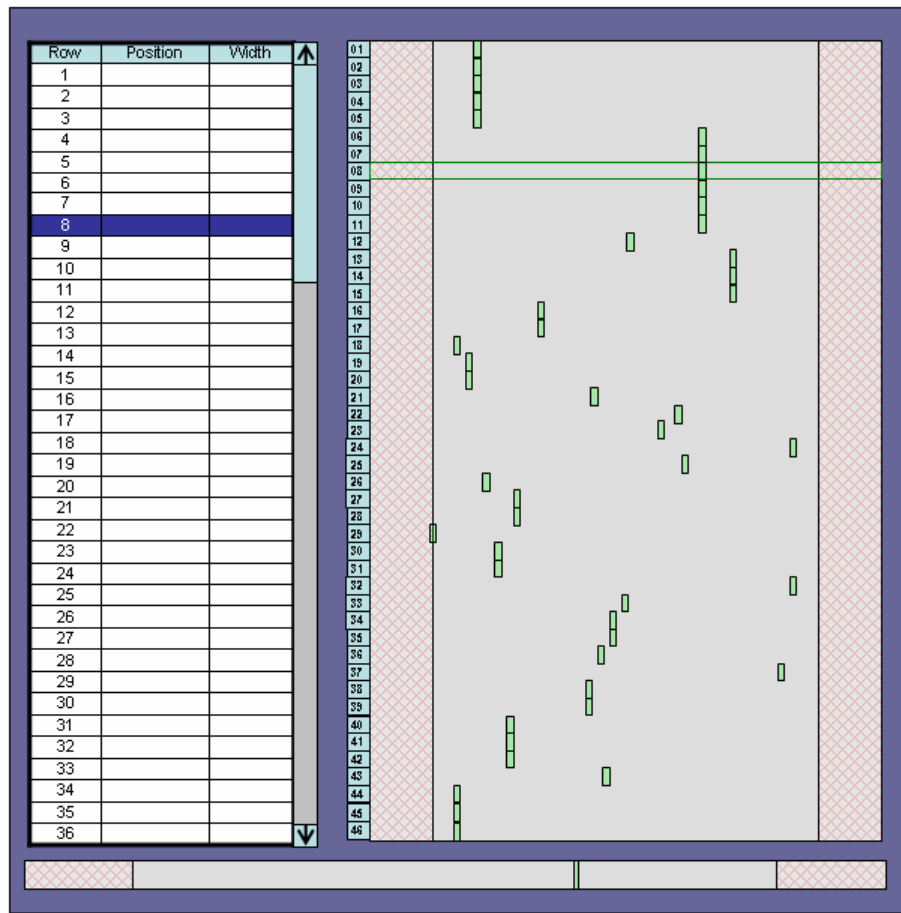
Figure 68: *MOSFIRE CSU Status GUI*

5.4.2.2.9   Control GUIs

Control GUIs are used to create action in the instrument, from switching on power to something, to moving mechanisms, to taking exposures. They will use KJava `modify` calls to set keywords in the Global Server. These calls will be routed through the MOSFIRE Desktop. As the instrument changes configuration, the Status GUIs will update to reflect this new information, leaving the control GUIs free to set up the next setting. The control GUIs know very little about the current state of the instrument, except what is needed to present the proper options to the user.

5.4.2.2.10   Exposure Control GUI

The MOSFIRE Exposure Control GUI (Figure 69) provides to the user controls to set up and take an exposure. This includes the following controls:
- Integration Time
- Number of Coadds
- Sampling Mode
- Number of Reads
- Object Name
- Frame Comment
- Filename controls (including data directory)
- Dither Pattern

It is possible that the sampling mode and number of reads will be predetermined for the user. If this is the case, these controls would not be included in this GUI. A filename will automatically be generated for the user, but this GUI would provide controls to alter the filename, if desired, and set the output directory for raw files. This GUI will also provide buttons to start and abort an exposure or dither pattern sequence. A dither pattern sequence is a set of frames that are combined together during data reduction to increase field of view or reduce noise. The Exposure Control GUI will provide controls to define a dither pattern and execute it. Once executed, progress through the dither pattern can be monitored in the Exposure Status GUI.
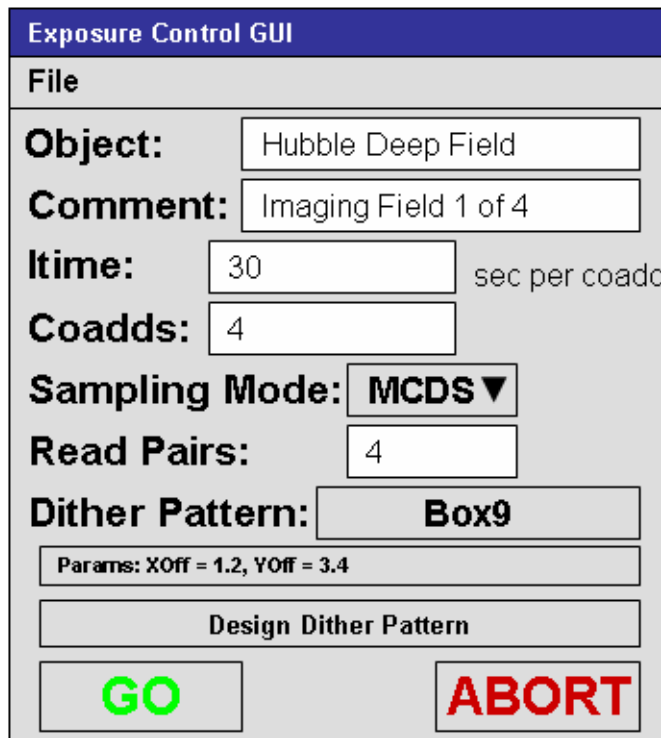
Figure 69: *MOSFIRE Exposure Control GUI*

5.4.2.2.11 Mechanism Control GUI

This GUI (Figure 70) will provide to the user the means to set the mechanisms as required for each observation. Even though MOSFIRE will have eight software controlled mechanisms, the options presented to the user for instrument setup during observing is reduced to two options: exposure mode (imaging or spectroscopy) and filter. The exposure mode sets the position of the grating-mirror exchange mechanism, and filter sets the positions of the dual filter wheel, pupil size, and detector focus. The flexure compensation is performed without user interaction. The dust cover is only used when storing the instrument, and will be controlled by observatory staff using scripts. The Cryogenic Slit Unit (CSU) will be controlled with its own dedicated GUI (see below).
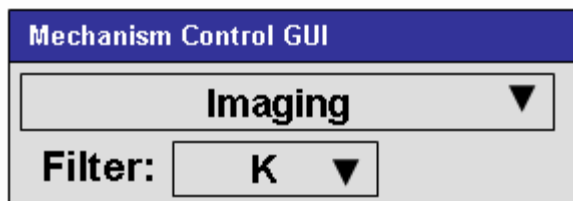
Figure 70: *MOSFIRE Mechanism Control GUI*

5.4.2.2.12 Temperature Control GUI

This GUI is used to set the target temperature of the regulated temperature controller and specify locations of the temperature settings. Other engineering controls may be provided here, but most engineering is done at the command line.

5.4.2.2.13 Power Control GUI

This GUI is used to switch power on and off. This GUI looks very similar to the Power Status GUI, but the buttons are clickable. Clicking on a button switches the power of the outlet represented by the button to the opposite state. It is unlikely an astronomer would use this GUI.

5.4.2.2.14 CSU Control GUI

The MOSFIRE CSU Control GUI (Figure 71) is used to define, adjust, and perform CSU configurations. Configurations define the positions of the slit and their widths in files called MOSFIRE Slit Configuration (MSC) files.

The MSCGUI will have the ability to read and write MSC files. Users will more often use the MOSFIRE Automatic Slit Configuration Generator to create the most efficient mask for a given field. The slit configuration created by MASCGEN will be stored in a MSC file. This file would then be opened by the MSCGUI for any possible tweaking. The user would then submit the mask to the CSU server (normally via the MOSFIRE Desktop and MGS) to configure the CSU. To describe the MSC to the server, a series of keywords defining the position of each slit and the

associated width would be set. Then, a final keyword is set to force the CSU server to enact the configuration.

The MSCGUI will look very similar to the MSSGUI, but it would not be read-only. Positions and widths of the slits could be manually entered into the cells in the table. Optionally, in the graphical representation, the slits could be dragged to the desired position. The zoomed view of the selected row would be provided for finer adjustment.
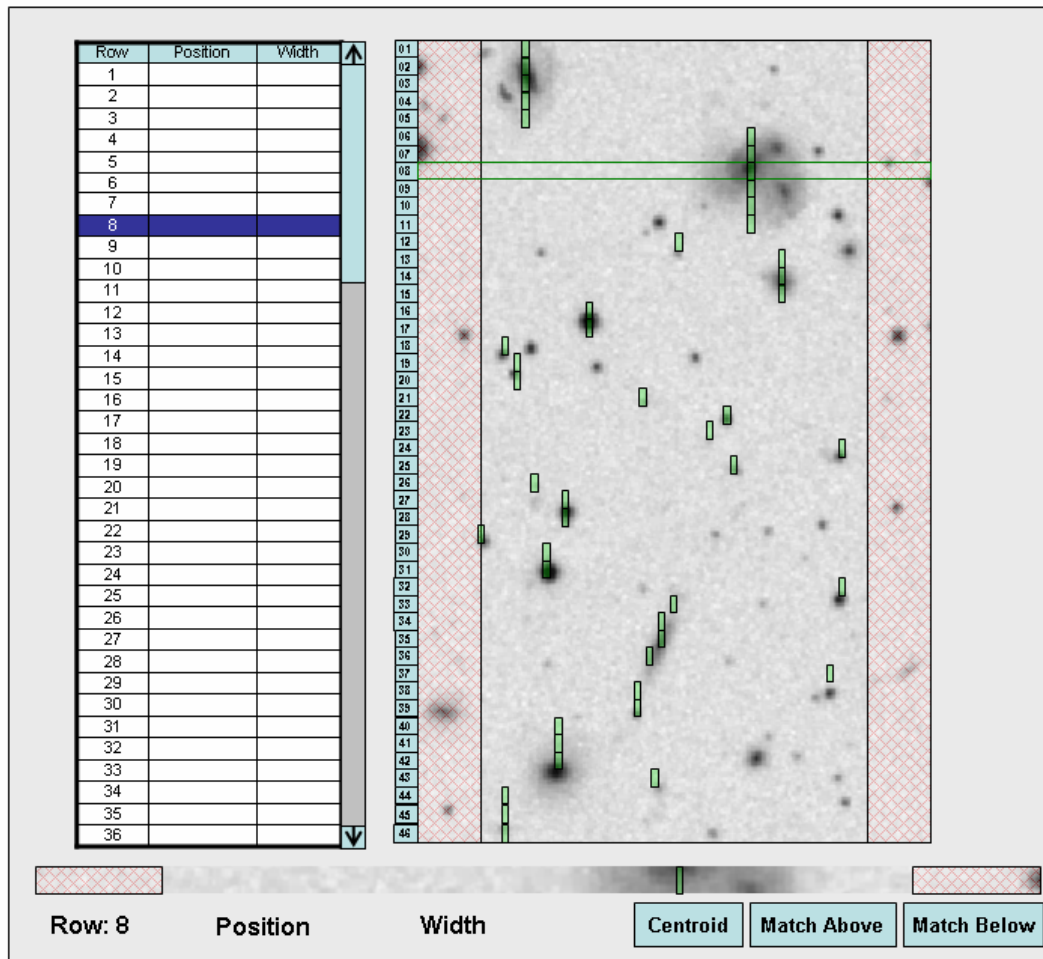
Figure 71: *MOSFIRE CSU Control GUI*

The MSCGUI would have additional functionality for manual creation of a slit configuration. A user would be able to load in an archived image of the field. They would then be able to adjust the position of the MOSFIRE field of view on the field, as well as the rotation. A field acquisition panel would be provided to load in oversized images so that the field of view could be properly placed. Once the desired field of view is obtained, the user could move the positions of the slits by dragging them on to the object they wish to sample. A few tools would be provided to help position the slits on objects, such as centroiding. Also, buttons will be provided to help align adjacent slits.

5.4.2.3 CSU Configuration Software

MASCGEN is the CSU configuration software which is a stand-alone application that allows an observer to generate a configuration file for the MOSFIRE CSU. This software will be based on the process currently used for the LRIS and DEIMOS instruments and will permit the user to design a CSU configuration from a list of object positions. The CSU configuration software will include a mask simulator similar to the DSIMULATOR application used with LRIS and DEIMOS to preview the mask configuration.

5.4.2.4 Image Viewing Software

MOSFIRE will use existing programs for image display. MOSFIRE data will be written to disk in the standard FITS format. Therefore, programs such as DS9 and Quicklook v2 (written as part of the OSIRIS project) can be used with little or no modification.

5.4.2.5 Data reduction

MOSFIRE spectra will differ from long-slit NIR spectra insofar as the data reduction must handle more book-keeping because of the multiple apertures, but otherwise, the same steps of flat-fielding, background subtraction, wavelength calibration and flux calibration are required. Several NIR long-slit reduction packages are already in use at Keck. These include the REDSPEC IDL[2] package developed at UCLA that is the Keck-supported NIRSPEC reduction tool, plus a suite of faint object NIR reduction scripts written by Steidel's group for NIRSPEC data. In addition, there are several existing data-reduction packages/pipelines used for multi-object spectroscopy at Keck, most notably the automated IDL-based package written by the DEEP team for DEIMOS data[3]. Most of the algorithms for accurate background subtraction and automated wavelength calibration are already coded in these packages and need only be adapted for MOSFIRE. Some aspects of MOSFIRE reductions should be simpler because the slits are located at fixed y-coordinate positions so slit boundaries will be known *a priori*. We intend to integrate the mask design software with the data reduction pipeline in much the same way DEIMOS does, where mask design parameters are stored in the image FITS headers for reference by the on-sky alignment software, the reduction software, and for efficient archiving of spectral data. The mask-design and observation-planning tool, integrated with the reduction pipeline, will be delivered with the completed instrument.

An important element of the reduction pipeline will also be an accurate optical model of both the f/15 Cassegrain focal plane of Keck I and the resulting spatial and spectral mapping to the MOSFIRE focal plane. Given the position of a slit in the focal plane, and which order sorting filter is installed in the beam, it will be possible to accurately predict the wavelength versus detector X-position, and the Y-positions of both the slit edges and the location of the targeted object within each slit. This information provides the observer with a good knowledge of the spectral coverage provided by each slit (for planning purposes) and the reduction pipeline with first guesses that allow quick convergence on the full 2-D wavelength solution of each slitlet.

---

[2] http://www2.keck.hawaii.edu/inst/nirspec/redspec/index.html
[3] http://alamoana.keck.hawaii.edu/inst/deimos/pipeline.html

5.4.3   Interfaces

5.4.3.1   Hardware-Server Interfaces

5.4.3.1.1   ASIC

The hardware interface to the ASIC is an off-the-shelf USB 2.0 compliant interface, provided by a Rockwell engineered interface board called the Jade2 card. To manage the USB port, Rockwell has created a Hardware Abstraction Layer (HAL), built upon the Microsoft .NET framework. The detector server is built upon the WMKO legacy framework KTL. This server therefore runs only in the Solaris environment. This presents the challenge of interfacing with the COM DLL, running in a Windows environment, with the detector server, running in the Solaris environment. A common technology that can bind with a COM component and a legacy C component, yet provide inter-platform communication, is needed. The best technology for this is Java. There exist a few Java-to-COM bridges that allow a Java object to bind to an object in a COM library.

The selection of the particular implementation of the bridge will be a task of the detailed design phase. Java can bind with legacy C code using the Java Native Interface, or JNI, as is used in KJava, the Java-KTL interface (see below). Java Remote Method Invocation (RMI) would provide the necessary inter-platform operability, allowing Java code to be called across a network, even across operating systems.

To summarize, the interface from detector server to detector is comprised of the following items:

- Detector server running on a Solaris machine, using legacy KTL code.

- Java JNI library, which translates C code to Java code, and invokes a Java Virtual Machine to execute.

- Within the JNI library, an RMI client is created to access the Windows machine.

- On the Windows machine, an RMI server is run to handle requests from RMI client in Solaris. This server is the MOSFIRE ASIC Server.

- MAS uses a Java-to-COM bridge to bind to Rockwell COM DLL.

- COM DLL uses Microsoft .NET services to interface with the Hardware Abstraction Layer server.

- HAL interfaces with the off-the-shelf USB device driver that interfaces with the Jade2 ASIC interface card.

- Jade2 processes commands (and optionally conditions power) from USB to ASIC.

- ASIC controls detector.

5.4.3.1.2 Serial RS-232

Most of the components in the MOSFIRE instrument are accessed through a serial connection, particularly RS-232. These components are the Lake Shore 218 temperature monitor, the Lake Shore 340 temperature controller, the pressure gauges through the Varian Multigauge controller, the mechanism controllers, and the CSU.

There is nothing special about the serial communication required for these components. The housekeeping components are identical to the ones used in OSIRIS, and the communication protocol will be reused. This protocol consists of a set of utility functions that open, configure, read from, and write to a standard serial device. The mechanism controllers and CSU will be able to use these functions as well.

Table 26 details the supported connection configuration for each device. Bold items specify our implementation.

Device	Baud Rate	Data Bits	Parity	Stop Bits
LakeShore 218 Temperature Monitor	300, 1200, **9600**	7	**Odd**	1
LakeShore 340 Temperature Controller	300, 1200, 2400, 4800, **9600**, 19200	7, 8	**Odd**, Even, None	1
Varian Multi-Gauge Controller	1200, 2400, 4800, 9600, **19200**	7, **8**	Odd, Even, **None**	1
Rotary Motor Controller	**19200**	**8**	**Even**	1
Flexure Compensation	9600 - **115200**	**8**	**None**	1
Detector Focus	**19200**	**8**	**Even**	1
CSEM CSU	**115200**	**8**	**None**	1

Table 26: *Configurations for serial devices*

MOSFIRE will use Lantronix ETS8P terminal servers to handle the communication of the serial devices. A terminal server is a device that receives serial commands over Ethernet, converts them back from TCP/IP to serial, multiplexes them, and sends it to the appropriate serial component. The reasons for using a terminal server are:

- Allows for control of multiple devices from one host computer.

- Since protocol is Ethernet, allows for remote control from any computer on the network.

- Ethernet extends cable lengths beyond the typical ~15m maximum cable length recommendation of RS-232.

- Ethernet allows for conversion of signal to fiber optics, providing for electrical isolation of instrument electronics from the telescope support structure.

- Same fiber optic that allows communication to the ASIC control computer will be used, reducing the number of cables in the cable wrap.

Signals sent through the terminal server are in the TCP/IP format, and therefore the serial commands must be converted to packets to be sent over the network. WMKO has developed a small service that does just that, called `tnet`. This service was used very successfully for OSIRIS and will be used again for MOSFIRE.

5.4.3.1.3 Ethernet

In order to power cycle the terminal server, the power controllers were selected as to have an Ethernet interface, for, if they had a serial interface, powering off the terminal server would eliminate the communication path to the power controller. A set of utility functions similar to that used for serial communication is used for Ethernet communication over a socket. The power controller and communication method will be identical to that used for OSIRIS.

5.4.3.2 UI-Server Interfaces

This section describes the methods for User Interfaces, such as GUIs and scripts, to interface with the hardware servers.

5.4.3.2.1 KTL

When the Keck Telescopes were being built, the WMKO software group, led by William Lupton, Al Conrad, and Hilton Lewis developed a set of functions called the Keck Task Library (KTL) to provide standardization for event-driven applications. These functions would become the core of the RPC functions supported by future Keck instrument servers and clients. MOSFIRE is no exception. By use of KTL, we can build our servers upon the same framework that has evolved over the lifetime of the Observatory, and ensure that both servers and clients will be stable and maintainable by the WMKO programming staff.

As mentioned above, MOSFIRE will build its servers upon a KTL framework called `rpcKey_server`. This server allows the relatively quick creation of hardware servers that have a KTL compliant interface built-in. Therefore, any KTL compliant client, such as `show` and `modify` is available for immediate use at the command line or in scripts.

5.4.3.2.2 KJava

KJava is a package written by UCLA Software Engineer Jason Weiss as part of the OSIRIS project that allows programs written in Java to interact with a KTL server. It uses the Java Native Interface (JNI), a specification that allows communication between Java objects and native C code stored in a sharable object library. KJava is comprised of a set of C code that implements the `show`, `modify`, and `cshow` capabilities of the standard KTL clients, with an additional method for gathering all of the keywords and their properties from a server, and corresponding Java code,

supplied in a Java Archive (JAR) file, to be added to the client application. The C side code mirrors the code for standard KTL clients, and handles all RPC communication.

A client that wishes to monitor keyword changes of a server starts a KJava "CShow", and registers a listener to watch for keyword change events. The listener must implement the `KJavaCShowListener` interface, providing an implementation of the `KJavaCShowCallback` method that will handle the event triggered when the value of a keyword changes asynchronously.

5.4.3.3   Server-Server Interfaces

The section describes the necessary communications between a server and another server.

5.4.3.3.1   Hardware Server-Global Server

The hardware server, or more generally subserver, to global server interface is similar to the UI-Server interface: RPC-based, keyword services over Ethernet. The observatory-developed, generic, RPC-based client-server software includes a number of functions and tasks for server-to-server keyword communications based on the functions in the Keck Task Library.

At its lowest level, the communications consists of RPC functions. Above that are the KTL keyword functions `ktl_open, ktl_read, ktl_write, ktl_ioctl, ktl_close`. And, above this level are an application's tasks and libraries

The global server registers itself as a listener of the subservice keywords that it maps as meta-keywords. Its own keyword list is updated much in the same way a `cshow` is performed, via KTL callbacks. The MGS, when it starts up, reads keyword configuration files for all the services it needs to contact for keyword information. It starts keyword monitors for all keywords that are not local to it, using the `ktl_ioctl KTL_CONTINUOUS` option so that it has current values for all specified keywords. Any server can then contact the MGS for a current value for any keyword.

5.4.3.3.2   Detector Server FITS Header Keyword Gathering

The MOSFIRE Detector Server (MDS) is responsible for creating the image FITS file which contains header keyword data as well as image data. The header data not only comes from the instrument servers, but from the telescope ACS and DCS servers as well.

The MDS obtains detector keyword values from itself and all other keyword values needed with "oneshot" calls to the various servers. The interface is the same as described above – standard KTL keyword calls on top of RPC network communications. When a server receives the "oneshot" message from the MDS it replies with a list of keyword-value pairs, predefined for that particular service.

This interface quickly supplies a timely snapshot of the entire system's status, as reflected in keywords, for the MDS's FITS writer to add to the image data for the FITS file.

5.4.3.3.3   Mechanism Server-Telescope

The server-to-telescope interface is also RPC-based, keyword services over Ethernet, the same as described above for the server-to-server interface. In this case, the top-level application's code consists of procedures for coordinating mechanism movements with DCS telescope and/or rotator positions.

A task called `watch_keywords` has been created for NIRC2 that watches specific keywords and takes action according to how their value changes. It uses the KTL interface to connect to servers and act on its list of specified keywords, each one of which can have a callback associated with it. This task will be used to monitor DCS keywords and send commands to MOSFIRE servers to facilitate coordinated operation. It also serves to insulate instrument servers from possible DCS problems. Instances of `watch_keywords` will be used by the MOSFIRE Flexure Compensation and Pupil Rotator servers to coordinate their movements.

5.5   Operational Modes

Four main observing modes are envisioned for MOSFIRE:
- direct imaging mode,
- MOS acquisition imaging mode,
- multi-object spectroscopic mode and
- long-slit spectroscopic mode.

These four modes and their requirements are described in more detail below.

5.5.1   Direct Imaging Mode

This mode is used to perform wide-field infrared imaging. All bars of the CSU are moved to the fully open position and the grating/mirror turret is rotated to the mirror position. In addition to the typical exposure settings (integration time, coadditions, etc.), the user must specify the field position, position angle, and filter. A user will often take a series of exposures in a dither pattern to increase the field of view or improve noise performance, or take a set of exposures with different filters.

5.5.2   Fine Acquisition Mode

This mode is used when acquiring a field for spectroscopy. Imaging with the slit mask in place is required in order to set the MOSFIRE field of view in the correct position on the sky so that the slits are accurately placed on the desired objects. The method requires a direct imaging frame, but with the slit bars deployed to strategic positions so that any small offsets and rotation needed to line up the slits can be calculated.

In this mode, the bars are deployed to their spectroscopic positions, except for 3-5 rows which are used for alignment stars. These bars would be opened up to create "alignment boxes" large enough

(e.g., 4" width x 7.3" height) to ensure that the chosen alignment stars would be visible after coarse pointing. Coarse acquisition will be made by adjusting the instrument rotator to the correct sky PA, and then placing a pre-determined guide star at a specified position on the guider, a method very similar to that used with the DEIMOS instrument on the Keck II telescope. For this coarse acquistion to work effectively, the relationship between the coordinate systems of the guider and MOSFIRE must be known to ~1" precision. Guiding is enabled after the coarse acquisition stage.

A direct image through the mask will then allow the positions of the alignment stars with respect to the alignment box edges to be calculated, and compared with the positions specified in the mask design file. The necessary rotational and translational offsets (usually <0.1 degrees and <1", respectively) are then calculated and sent to the telescope control system, and the offsets are made while guiding. This process can be iterated if necessary. Once the stars are where the observer wants them, the bars used for alignment can be redeployed to their spectroscopic position, which may be narrow slits centered on the alignment stars, or science targets that can be covered with the same mask Y-position. Users may switch back to the fine alignment mode amidst a series of spectroscopic observations to check alignment.

5.5.3   Multi-Object Spectroscopic Mode

After acquisition, the user would then redeploy the slits to perform the type of observations MOSFIRE was designed for: multi-object spectroscopy. In this mode, the grating is deployed, replacing the flat imaging mirror. An order sorting filter (which may already have been deployed for the alignment process) is used to select the desired order of dispersion. Typical integration times expected for the instrument are in the 600 to 1800 second range, dependent on band and detector noise characteristics.

The observer will often want to nod along the slit by a few arcseconds or pixels; the desired nod distance would be accounted for in determining the minimum slit length and relative object position within slitlets during the mask design stage.

5.5.4   Long-Slit Spectroscopic Mode

In this mode, multiplex factor is sacrificed in order to increase coverage of a target in the spatial direction. Some or all of the slits are aligned to the same horizontal (X) position with the same slit width for observations of single targets. Since a full slit configuration would not need to be defined, this mode is useful for quickly acquiring and sampling opportunistic targets, e.g. following up transient phenomena soon after discovery, or observing an extended source. The spectral range can be adjusted by selecting the X-position in the MOSFIRE focal plane. A similar mode will also be useful for calibrations, in which one may wish to sample particular parts of the instrument focal plane (e.g., telluric and flux standard stars).

5.5.5   Selected Use Cases

5.5.5.1   Defining and Taking an Exposure: Imaging Mode

1. The user tells the telescope operator the coordinates of the center of the field and position angle, and the telescope is moved to the corresponding position.

2. The user defines the exposure parameters in the MECGUI. This includes:

    - Exposure Time
    - Coadditions
    - Sampling Mode and number of reads
    - User information, such as object name, frame comment

3. The user sets filter in MMCGUI.

4. The user selects Imaging mode in the MMCGUI.

5. The user presses the "GO" button on the MECGUI.

6. The MECGUI calls a script with arguments that set the above settings.

7. The script performs a number of modify calls to the global server to set above settings.

8. Setting observing mode to Imaging in global server causes it to tell the Rotary Mechanism Server controlling the Grating-Mirror exchange to put the imaging flat mirror into place.

9. Filter is a coordinated keyword of the global server. Setting it causes the two filter wheel servers to put the filter in place by finding the wheel with the corresponding filter, moving it into the beam, and moving the other wheel to the open position. The detector focus is automatically adjusted to the position that corresponds to the filter selection. If the filter is K, the pupil is adjusted to match the Keck primary. Then, the pupil is rotated to match rotation of field as telescope tracks across the sky. The rotation rate and starting position are determined by asking the DCS where the telescope is pointing.

10. Global server sets integration time, coadditions, sampling mode, and reads in MDS.

11. Global server starts exposure by setting "go" keyword in detector server.

12. Detector server handles communication with ASIC. Initiates clocking and taking of frame, and waits for data to come back. Progress is monitored and various status keywords are set to track.

13. When keywords are set, the global server announces this via a KTL event.

14. On startup, the MOSFIRE Desktop registers with the global server using KJava as interested in events. When a keyword changes value, the desktop's KJavaCShowCallback function is called with the keyword name and new value.

15. The new value is visualized in the MESGUI, and the progress bar is updated to reflect current progress in exposure.

16. When data comes back, detector receives each read and processes them into a single data frame. The noise frame and quality array are calculated.

17. The detector server writes data, noise, and quality array to a multi-extension FITS file.

18. Image viewing software automatically opens up new frames written to disk.

5.5.5.2 Acquiring a Field

1. Prior to observing, the user has created both a science slit configuration and a fine-acqusition slit configuration using the MASCGEN or MSCGUI, as described below. The fine-acqusition configuration is identical to the science configuration except for the bars assigned to alignment stars.

2. The pixel position that the guide star would fall on the guider image corresponding to defined slit configuration is noted.

3. MSCGUI is used to determine the desired position relative to the alignment box edges where each alignment star should fall on in imaging mode.

4. At the telescope, user tells telescope operator approximate position of field and position angle. Telescope is moved to that position.

5. Rough alignment is achieved by placing a guide star on the calculated pixel of the guider.

6. Guiding is started.

7. User takes an imaging frame as described above (it may be necessary to obtain a short "sky" frame for determination of the alignment box edge positions). The position of both the box edges and the alignment object are determined automatically, and the offsets required to place the stars at the desired positions are calculated and reported to the user.

8. User allows offset and rotation to be executed using Telescope GUI.

9. Telescope GUI calls scripts that perform offset and rotation calls to DCS.

10. Steps 7 through 9 may be repeated if necessary.

5.5.5.3 Defining and Taking An Exposure: Spectroscopic Mode

1. User creates a MSC file using MASCGEN or the MSCGUI as descibed below.

2. User takes MSC file to observatory.

3. Field is acquired and aligned using method above.

4. User sets observing mode to spectroscopy using MMCGUI. This moves the grating into place.

5. User loads MSC file in MSCGUI, tweaks according to conditions as necessary, and executes.

6. User takes spectroscopic frame similar to imaging frame as described above.

5.5.5.4   Configuring a Slit Mask

The following describes two ways of configuring a slit mask for MOSFIRE.

5.5.5.4.1   Scenario 1: Preplanned observation with optimized slit config files

For each field of interest:

1. Observer creates a list of objects similar to what is now used to create masks with LRIS and DEIMOS. The list contains objects, possible guide stars and alignment stars with their coordinates and priorities.

2. Observer runs MASCGEN.

3. Observer feeds list to MASCGEN.

4. MASCGEN performs a Monte-Carlo style optimization to determine the best configuration of the CSU and rotator PA to obtain spectra from the most objects in priority order. User input will include information on minimum distance of a target from a slit edge, planned nod amplitude in the slit direction, the portion of the MOSFIRE field in the X-direction to be used (depending on the particulars of desired wavelength coverage).

5. MASCGEN allows interactive adjustment of suggested optimization.

6. Observer accepts or repeats with changes.

7. MASGEN writes two MSC files containing the CSU setup, the science configuration and the fine acquisition configuration.

8. Observer repeats for each field of interest.

9. Observer loads the MSC file into the MSCGUI after arrival at the observatory

10. Observer tweaks the configuration in the MSCGUI if desired.

11. Observer submits the MSC file via MSCGUI

12. MSCGUI contacts the CSU server to configure the mechanism via a series of keywords which define the mechanism's bar pair positions then sends the keyword which causes the configuration to begin.

13. Observer waits until slit mask is ready (typically 1-3 minutes).

14. At this point the CSU is ready for any calibration images or for the observer to perform the final on-sky alignment for the observation.

5.5.5.4.2   Scenario 2: On-the-Fly Slit Configuration

Observer creates a slit configuration on the fly.

1. Observer uses MMCGUI to command the CSU to open the mask for imaging.

2. Observer takes an image, stored as FITS file.

3. Observer loads the FITS file into the MSCGUI.

4. FITS file is resized and rotated as necessary to display in MSCGUI display window with CSU overlay.

5. Observer manually selects objects on the image with the pointer and enters slit width.

6. MSCGUI draws a slit of the appropriate width at the selected position.

7. Observer optionally presses the "centroid" button and the slit is fine adjusted to the object centroid.

8. Observer fine tunes positioning of slit using zoomed row image in MSCGUI.

9. Observer creates the MSC file with the MSCGUI.

10. MSCGUI configures the CSU as in step 12 above.

11. Observer waits until slit mask is ready (a few to several minutes).

A similar procedure is followed if the observer wishes to manually create a slit mask based on an archived image. The MSCGUI would support the opening and reformatting of any FITS file, as well as a few other common image file types.

5.6 Interface with the Keck I Telescope and WMKO Facilities

The mechanical configuration of MOSFIRE is based on the Keck I telescope Cassegrain focus envelope as used for the LRIS instrument. The following constraints are being used in the mechanical design of MOSFIRE:

1. Envelope size compatible with the LRIS envelope
2. Weight not more than LRIS (without including the weight of the Cassegrain ADC)
3. Rotator design similar to LRIS
4. Instrument dewar center of gravity located on the rotator bearing axis
5. Handler design similar to LRIS
6. Same defining points as LRIS

MOSFIRE creates a storage problem on Keck I; there are no more Nasmyth deck positions available unless an instrument is retired. Given the time frame for MOSFIRE delivery (mid-2009) it seems likely that either the Forward Cassegrain Module will be retired by that time, or a Keck I re-allocation of instruments will take place. If the Forward Cassegrain Module is still in use we propose moving it to a "campaign" mode of operation and storing it on the Keck I dome floor. With these considerations in mind we have identified the space currently used to store the Forward Cassegrain Module on the Keck I Nasmyth deck as the storage position for MOSFIRE.

The instrument will use three (two large and one small) CCR heads. These will be supplied from a single compressor. This will require the installation of helium lines on Keck I, and the installation of a compressor in the Keck I mechanical room. The instrument requires a glycol cooling supply for the instrument electronics and an air supply for the defining point drive motors.

The current plan proposes that WMKO will design and build the rotator based on the LRIS design, with improvements based on our experience with the LRIS rotator. WMKO will also be responsible for the instrument handler, and the usual interfaces (glycol, helium, etc.). New interface panels will be installed at the Keck I Cassegrain and RT1 positions to provide the additional connections required for MOSFIRE.

5.7 Integration and Testing

Optics assembly will occur in the clean room of Robinson Laboratory at CIT. Once assembled, the collimator and camera will be independently tested at room temperature either at CIT or at UCLA. These tests will confirm predicted optical performance and gravity stability (flexure). CIT, UCLA and UCSC personnel will participate in the optical test design and analysis.

System integration and testing for MOSFIRE will occur at CIT. Assembly will begin in the fall of 2007, with the first cool down cycle planned for February or March of 2008. We have reserved the High Bay Facility of the Downs-Lauritsen Laboratory on the CIT campus for the final phase of the project. This facility has an overhead crane that can easily handle the large structures. The team will design and fabricate laboratory assembly stands for all of the major sub-assemblies. An

existing flexure test stand, originally assembled for ESI in the UCO shops in Santa Cruz, will be used for mounting the entire Cassegrain module containing the fully assembled instrument (Figure 72). This stand allows for placing the instrument in all of the gravity orientations that will be encountered at the Keck I Cassegrain focal station.

As was our experience with NIRSPEC, NIRC2 and OSIRIS, these large cryogenic instruments require a 3-week typical cycle time for cool down, experiment and warm up. In general, we allow only one cool down per month. Time is allotted for up to 12 cryogenic cycles. The first pump out of the dewar and first cool down occur during the Fabrication and Procurement Phase. We expect to install the CSU in time for the 3rd cool down. The science grade detector will be used on the 7th cool down.

An Acceptance Test Plan (ATP) will be drafted during the detailed design phase and this plan will drive final testing of the instrument. The plan will be modeled on experience with OSIRIS.

5.8   Preliminary Instrument Assembly and Servicing Procedures

MOSFIRE is a large and heavy cryogenic instrument. Careful consideration has been given to assembly and potential servicing operations during the instrument preliminary design. The instrument and its contents have been arranged to provide reasonable access to the majority of the moving parts without a major dismantling of the instrument's structure. This section describes the procedures and equipment required for initial integration of the instrument. It also includes descriptions and procedures for gaining access to the various components which might require access for service during the life of the instrument.

5.8.1   Instrument Assembly

The procedures described here will be used during the instrument integration when the structure is assembled for the first time. Some of the procedures and equipment utilized will be unique to this process, whereas other equipment and procedures will also be used for servicing access, if necessary. Table 27 describes the basic steps required to assemble MOSFIRE in the high-bay facilities at Caltech. Some of the assembly will be done with the instrument sitting on its handler in order to gain experience with the fixtures and procedures that will allow MOSFIRE's internal mechanisms to be serviced at the telescope if necessary. In order to be able to lift the heavier components and assemblies and install them in a horizontal fashion, counter-balanced lifting structures will have to be designed and built. Rough order of magnitude time estimates for completing each step are included. Estimated weights of the components and assemblies which must be lifted during each procedure are also listed.

MOSFIRE Assembly Procedures:

Procedure #	Description	Estimated Time (minutes)	Estimated Component Weight (lbs.)
1	Using the overhead crane, lift the rotator module and position it in the ESI Test Stand. Rotate the test stand so that the rotator bearing faces upwards.	20	2000
2	Using the overhead crane, lift the Vacuum Chamber Main Barrel and Instrument Mount Ring sub-assembly onto place on the bearing's inner race and bolt in place.	45	840
3	Using the overhead crane, lift and lower the Internal Structure Support Tube (G-10) and its attached floating shield into place and secure.	25	190
4	Using overhead crane, position Bulkhead B on Instrument Assembly Stand (IAS) with the forward-facing side of Bulkhead B pointing upwards	15	215
5	Using overhead crane, attach Filter Wheel Assembly (w/ mount brackets) to Bulkhead B	15	85
6	Using overhead crane, position Bulkhead B Spacer Tube onto Bulkhead B and bolt in place	15	135
7	Lift and position the Internal Structure Stiffening Tube onto Bulkhead B and bolt in place	15	30
8	Using overhead crane, remove Bulkhead B sub-assembly from the IAS and place it on a Temporary Support Ring (TSR)	15	465
9	Using overhead crane, position Bulkhead A on IAS with the front-facing surface of Bulkhead A facing upwards. Rotate the IAS so that the rear-facing surface of Bulkhead A faces upwards.	15	245
10	Using overhead crane, attach Camera Barrel Assembly(w/ mount bracket) to Bulkhead A	15	130
11	Attach the Pupil Wheel mechanism Mount Platform to Bulkhead A.	10	2
12	Use the IAS to flip Bulkhead A over. Using the overhead crane, remove Bulkhead A sub-assembly and place it on a the Bulkhead B sub-assembly. Bolt the sub-assemblies together.	20	380
13	Using the overhead crane, lift the assembled bulkheads off of the TSR and lower the assembly into the center of the structur'e cylidrical floating shield. Attach the floating shield.	20	845
14	Once the Internal Structure's cylindracl shield is attached, lift the structure into the vacuum chamber with the overhead crane. Bolt Bulkhead A to the Internal Structure Support Tube.	30	935
15	Using the ESI Test Stand, rotate the instrument so its axis is horizontal. Release the Rotator Module from the test stand and back it onto the Installation Supports (temporary rail sections). Using the overhead crane, remove MOSFIRE and the Rotator Module from the ESI Test Stand and place it on MOSFIRE's Handler.	45	4000
16	Install Pupil Rotator mechanism (w/ mount bracket) onto Mount Platform Vacuum Chamber's front opening.	20	15
17	Install Grating/Imaging Mirror Turret's Mount Bracket onto Bulkhead A	15	38
18	Install three cold head assemblies onto vacuum chamber. Make thermal connections to internal structure through openings in Bulkhead A	90	65 each
19	Utilizing a custom lifting fixture and the overhead crane to assist, install the Grating/Imaging Mirror Turret onto its mount bracket and secure.	30	110
20	Utilizing a custom lifting fixture and the overhead crane to assist, install the CSU (w/ mount brackets) into place on Bulkhead A.	45	80
21	Install the Field Lens Assembly onto Bulkhead B through the rear opening in the Vacuum Chamber and secure.	15	35
22	Utilizing a custom lifting fixture and the overhead crane to assist, install the Collimator Barrel Assembly (w/ mount bracket) onto Bulkhead B and secure.	20	65
23	Utilizing a custom lifting fixture and the overhead crane to assist, install the Bulkhead C Standoff Tube onto Bulkhead B and secure.	15	85
24	Utilizing a custom lifting fixture and the overhead crane to assist, install the Flexure Compensation System (FCS) (& Bulkhead C) onto the Bulhead C Standoff Tube.	15	75
25	Install the Detector Head Assembly onto the Camera Barrel	15	25
26	Install the Getter Assembly onto Bulkhead B and attach the detector head thermal straps to the detector cold head.	30	10
27	Using a custom lifting fixture and the overhead crane, install the rear cover shields.	45	120
28	Using a custom lifting fixture and the overhead crane, install the Rear Vacuum Chamber Cover.	45	200
29	Using a custom lifting fixture and the overhead crane, install the front cover shields & baffles.	45	120
30	Using a custom lifting fixture and the overhead crane, install the Front Vacuum Chamber Cover. The Guider Assembly, Window Assembly, and Dust Cover Assembly have been pre-assembled onto the front cover.	45	425
31	Using a custom lifting fixture and the overhead crane, install the Cable Wrap Assembly.	60	325
32	Using a custom lifting fixture and the overhead crane, install the Electronics Rack Assembly.	90	470
	Total Time (Minutes)	960	
	Total Time (Hours)	16.0	

Table 27: *MOSFIRE initial assembly procedures.*
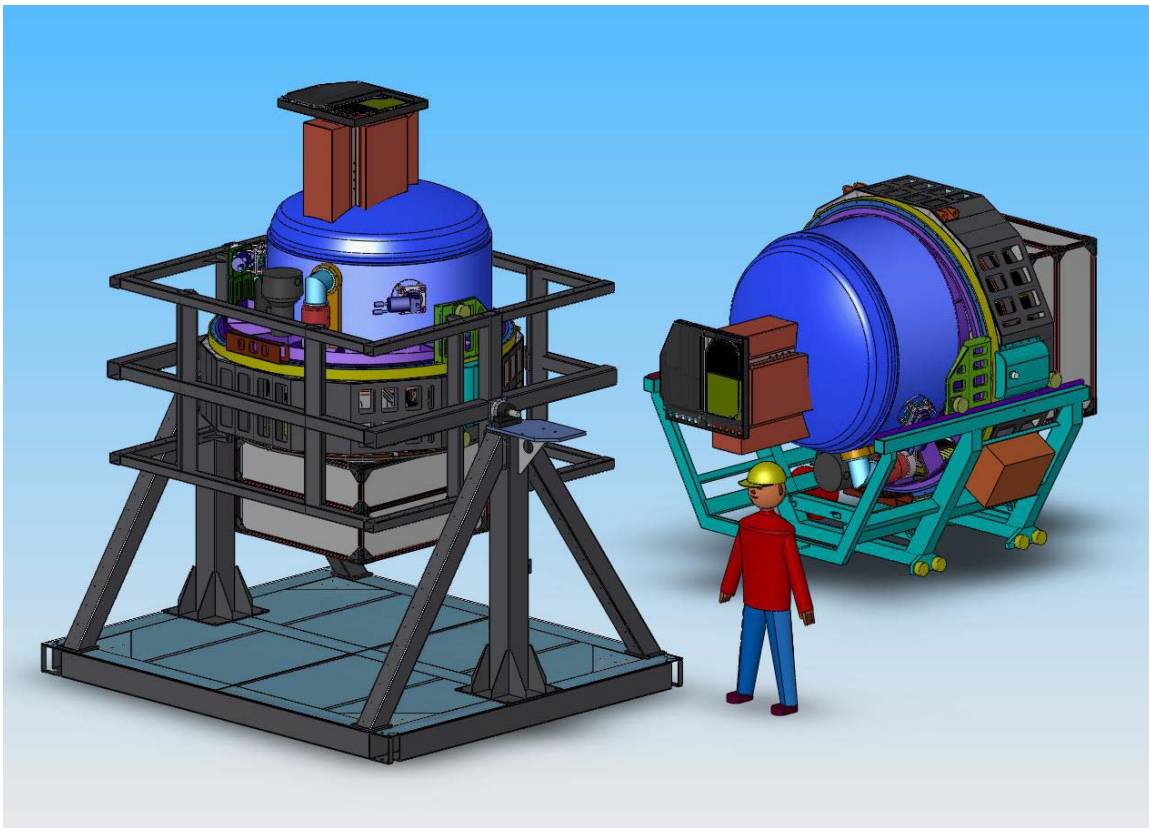
Figure 72: *This image depicts MOSFIRE installed in the ESI test stand (left) and sitting on its handler (right).*

5.8.2 Instrument Servicing

External instrument mechanisms have been located to provide adequate access should maintenance be required. Internal mechanisms have been designed with a goal of 10 years minimum service prior to maintenance. But, the layout of the instrument's internal structure has been designed to provide adequate access to internal mechanisms in the event that servicing is required. All of the moving parts within MOSFIRE can be accessed without removing the internal structure or the shielding which surrounds the cylindrical portion of it. Access is provided from both the front and the rear of the instrument via the front and rear covers. Access to the rear is a bit more cumbersome due to the positions of the electronics rack and the cable wrap. But, since instrument warm-up will likely take about a week, there is time to remove these assemblies should rear access be required.

Since access to all of the internal mechanisms can be obtained through the vacuum chamber end caps, MOSFIRE can be serviced on the Nasmyth deck (Figure 73 and Figure 74) with the appropriately designed lifting harnesses and fixtures. Appropriate measures, such as portable "clean-room" enclosures, will need to be employed whenever the dewar is opened.
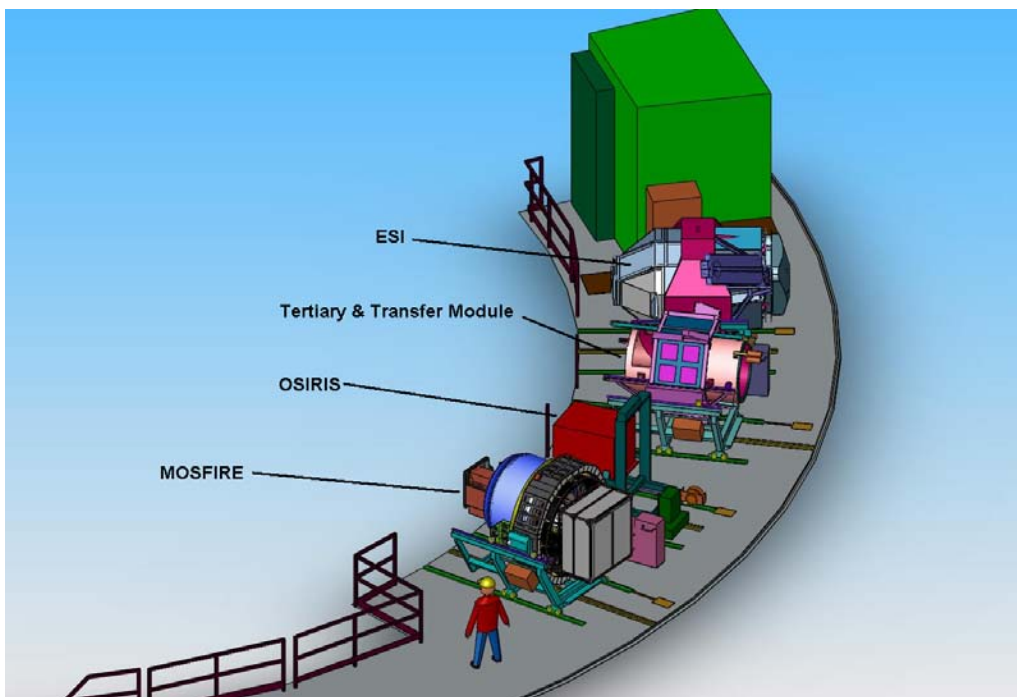
Figure 73: *Image depicting MOSFIRE and some other instruments which reside on the Nasmyth Deck, for comparison. Note that the Keck II Nasmyth Deck is represented in the image, but that MOSFIRE will reside at Keck I.*
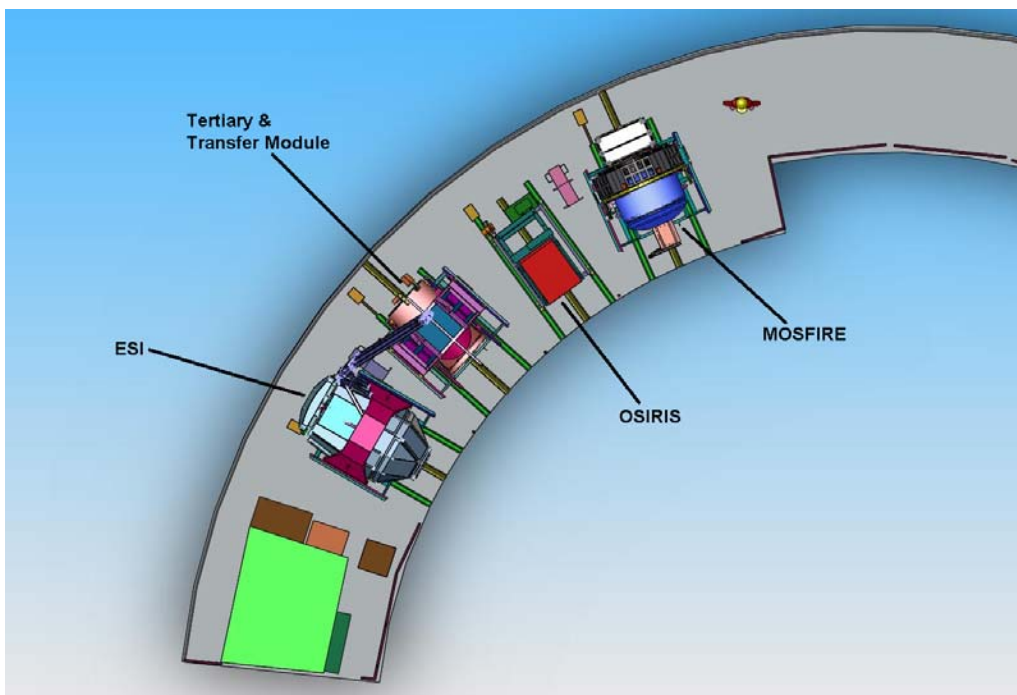
Figure 74: *Plan view Comparing MOSFIRE footprint on Nasmyth Deck to the footprint of previous instruments which reside on the Nasmyth Deck.*

5.8.2.1 Front Cover Access

Removal of the front cover and shield provides immediate internal access to three sub-assemblies. The CSU, grating/mirror exchange assembly, and window heater assembly can be accessed directly with the front cover removed (Figure 75). Two other assemblies, the left and right instrument refrigerator heads can be accessed for connecting and disconnecting their thermal straps once the CSU is removed. There are cut-outs in Bulkhead A behind the CSU bars to provide access to the refrigerator head straps. A sixth assembly, the pupil mechanism, can be accessed and removed once the grating/mirror exchange assembly has been removed.
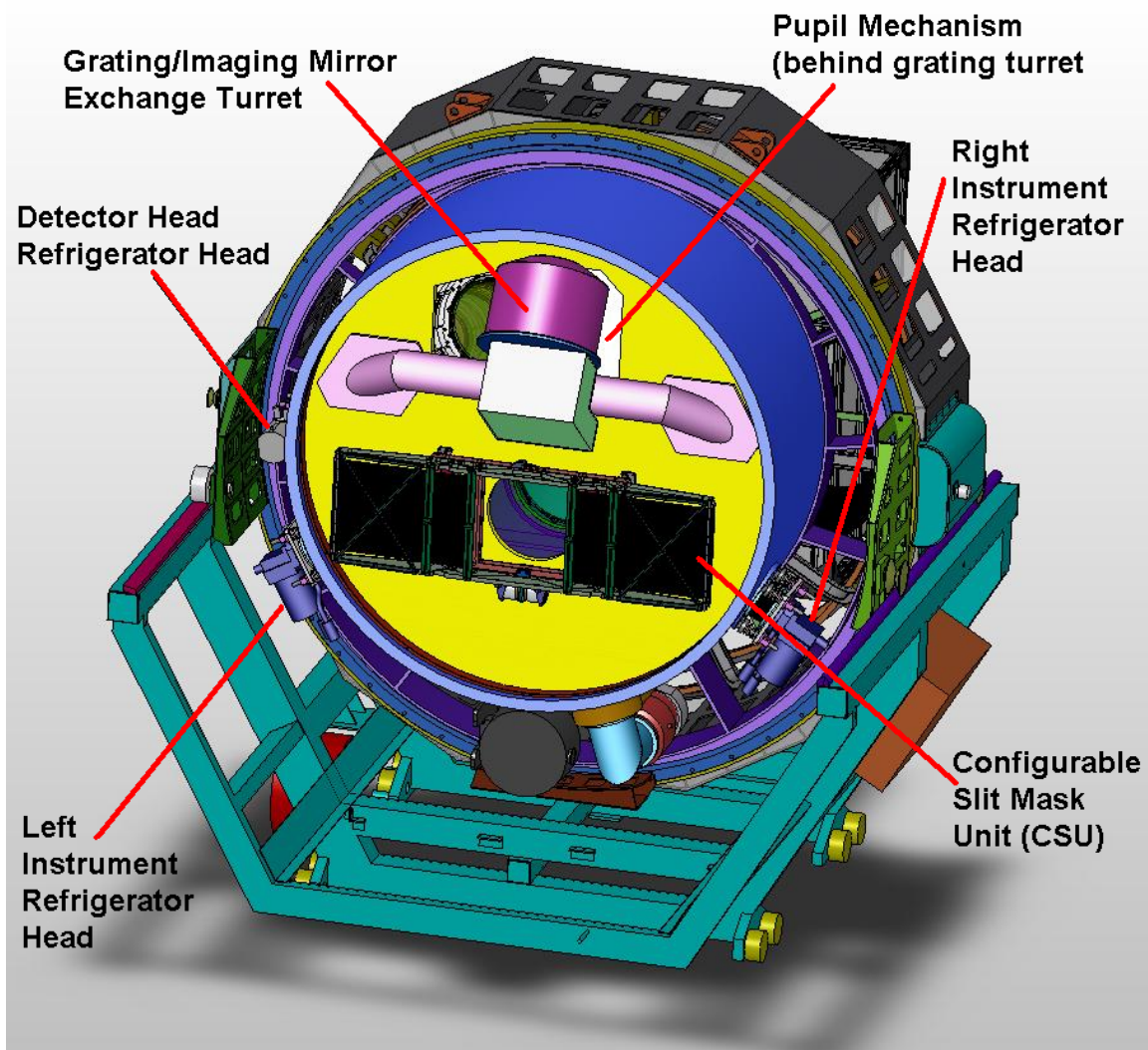
Figure 75: *MOSFIRE with the front cover and shields removed. Accessible sub-assemblies are indicated.*

5.8.2.2   Rear Cover Access

Removal of the rear cover and shield provides immediate internal access to six sub-assemblies, as well (Figure 76). The flexure compensation system (FCS), detector head, collimator barrel, detector refrigerator head, getter assembly, and filter wheel assembly can be accessed directly with the rear cover removed. A seventh sub-assembly, the field lens assembly, can be accessed after the collimator barrel and the FCS supports are removed. Only the filter wheel assembly's drive and positioning hardware can be accessed with the unit installed in the instrument. The hub bearings cannot be accessed unless a portion of the rear main bulkhead (Bulkhead B) is removed. In order to remove this section of the rear main bulkhead, the field lens must be removed.
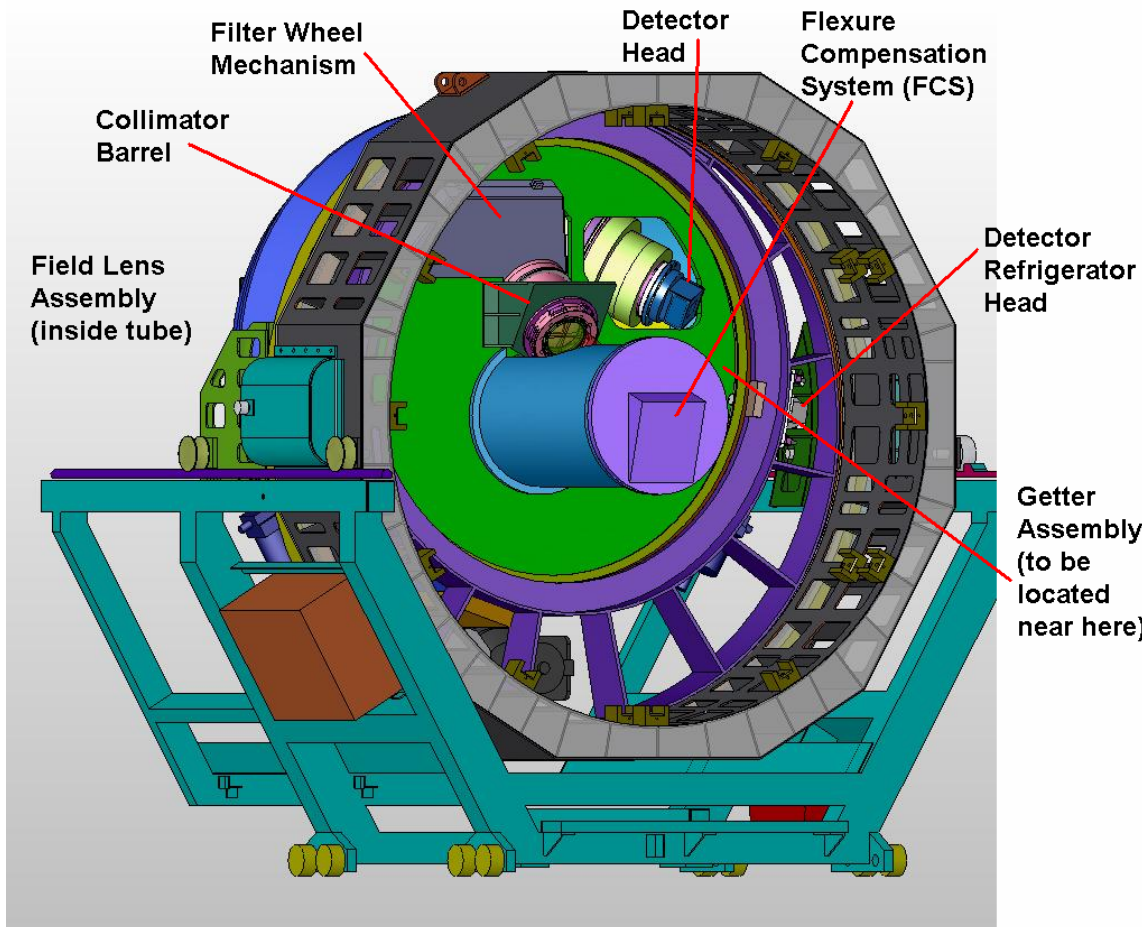
**Figure 76**: *MOSFIRE with Electronics Rack, Cable Wrap, and rear cover and shields removed. Accessible sub-assemblies are indicated.*

6 MANAGEMENT PLAN

6.1 Project Structure and Organization

The MOSFIRE project structure is a team effort involving UCLA, CIT, UCSC and WMKO. Professors Ian McLean (UCLA) and Charles Steidel (CIT) are the co-principal investigators. In addition, the co-PIs also hold specific roles within the team. McLean acts as overall Project Manager and Steidel is the Project Scientist. Professor McLean was PI and Project Manager for the NIRSPEC instrument for WMKO from 1994-1999 (McLean et al. 1998). He has 15 years of experience as Director of the Infrared Lab at UCLA and 10 years prior to that at the Royal Observatory Edinburgh Astronomy Technology Center. McLean has provided many instruments for observatories over this period of time, including the very first infrared cameras for astronomy (IRCAM: UKIRT 1986), a twin-channel camera for Lick Observatory, and a wide-field infrared camera for NASA's SOFIA. All of these instruments also had spectroscopic capability. Steidel was PI for LRIS-B, the UV/blue-optimized channel for the LRIS (WMKO) and is very experienced in multi-object and near-IR faint object spectroscopy.

To provide experienced leadership in the three critical areas of instrumentation, optics and software, Keith Matthews (CIT), Prof. Harland Epps (UCSC) and Prof. James Larkin (UCLA) will oversee these areas as co-Investigators. Matthews will be the overall Instrument Scientist for the entire project and will be responsible for the final system integration. Matthews was the PI for NIRC and NIRC2 at Keck and he has been involved in the development of infrared instruments since the inception of the field. Professor Harland Epps is one of the country's leading authorities on the optical design of astronomical spectrographs. He has provided the design of most of the Keck's existing complement of instruments, including HIRES, LRIS, ESI and DEIMOS. Professor James Larkin is currently PI of OSIRIS, a state-of-the-art diffraction-limited integral field spectrometer for the WMKO adaptive optics system (J.E. Larkin et al. 2002). As the Observatory's most recent instrument, this complex and sophisticated infrared instrument, with its fully automated data reduction pipeline, will provide the most significant source of heritage.

The organization chart (Figure 77) shows the structure of the project team. A senior engineer or faculty member at each of the partner institutions is responsible for budget and schedule in each of the major work areas, mechanics, optics, electronics, software and observatory interfaces. Overall program management resides with the WMKO Instrument Program Manager Sean Adkins and the WMKO new instrument development process will be followed.

6.2 Project Management

Overall management of the MOSFIRE project is the responsibility of the WMKO instrument program manager Sean Adkins. For the team, McLean at UCLA will act as the executive project manager. Technical and administrative staff at UCLA, CIT and UCSC will assist him to prepare the reports required by WMKO and TSIP. As the Organization chart shows, senior and experienced people will lead each major sub-discipline and provide regular and detailed report in each area.
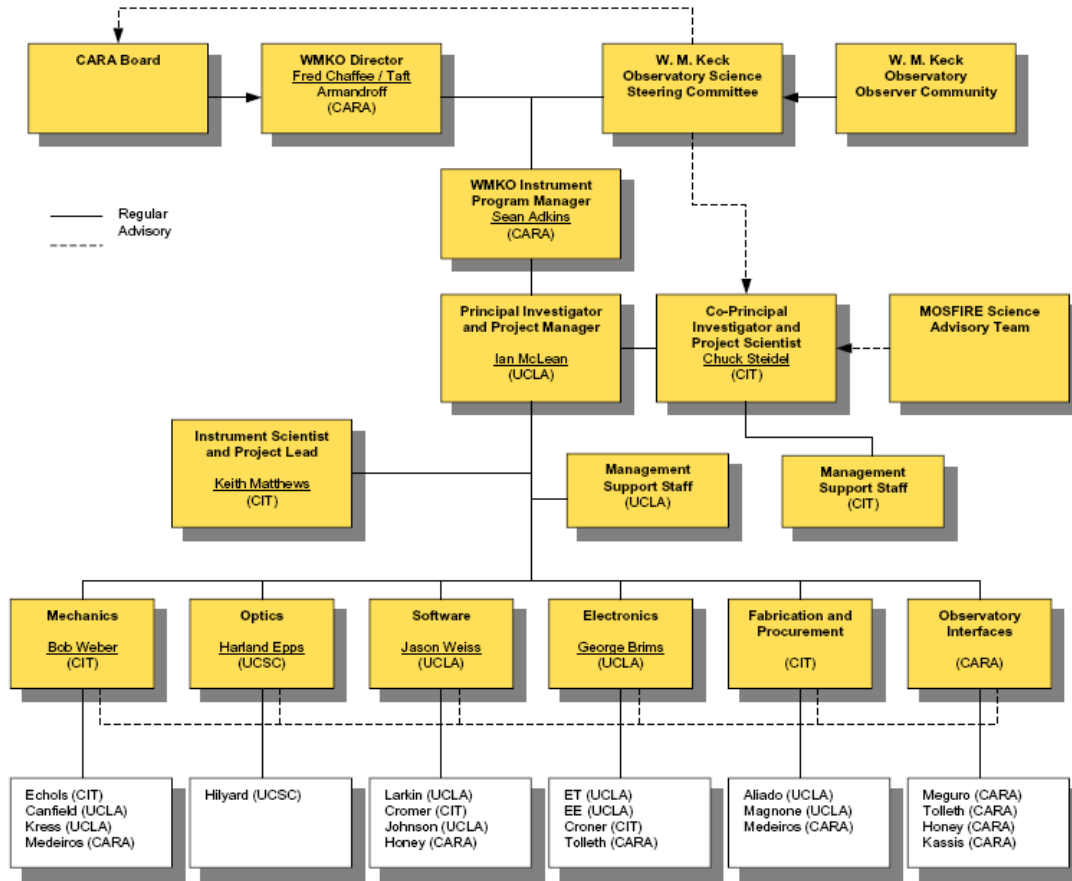
Figure 77: *MOSFIRE Organizational Chart*

6.3   Risk Assessment and Management

From the beginning of the MOSFIRE project several important choices were made that considerably reduce the risks associated with this instrument and the potential for cost growth. Among these decisions are the following:

1. Smaller field of view – more affordable optics
2. Single infrared detector – one quarter the cost of a 4-detector mosaic; eliminates issues associated with the gaps between detectors that would be present in a mosaic.
3. Grating dispersion using multiple orders – a single fixed grating is much more stable and considerably less expensive than multiple dispersion elements; cost-effective and highly practical solution.
4. Configurable Slit mask Unit (CSU) – completely eliminates slit mask manufacture and cryogenic handling to exchange slit masks. We discuss below how we have handled the remaining risks in producing the CSU.

5. Re-use of software from OSIRIS and other recent CARA projects – yields significant reduction in manpower effort for software and provides a product familiar to CARA staff and users alike.
6. Installation at the Keck I Cassegrain focal station – eliminates handling/scheduling problems on the over-crowded Keck II telescope; heritage with LRIS is enabled and an extra reflection (the tertiary mirror) is eliminated.

The greatest risk area is the CSU. We are actively managing this risk through a development program with the Swiss company CSEM. We first placed CSEM under contract to study our requirements in detail and they are now under contract to produce a prototype of the MOSFIRE CSU that will be tested cryogenically before the MOSFIRE detailed design is completed. CSEM will then manufacture and test the complete MOSFIRE CSU and its associated control electronics and software. A parallel development by the EMIR team is under way with a Dutch company and we are in contact with the EMIR group to monitor progress.

The second area of perceived risk lies in the large optical components. To reduce risk in this area we have worked to get the design finished to the pre-construction level before PDR. This goal has been achieved and long-lead glass blanks have been ordered. In addition, lens-mounting options have been analyzed for displacements and stresses.

Schedule slip is a risk in any engineering project involving significant development effort. For MOSFIRE we intend to carefully manage costs to remain within our funding profile. We view this as a design to cost project, and we are prepared to implement descope options if the schedule begins to slip. Areas of potential de-scope are: a simpler CSU with fewer slit bars and perhaps slower operation, a more restricted field of view, elimination of a second filter wheel mechanism, elimination of the pupil tracking mechanism, elimination of the flexure compensation mechanism, and simplification of software.

6.4 Work Breakdown Structure

A WBS diagram for MOSFIRE is shown in Figure 78. Key WBS elements are also included in the top-level MOSFIRE schedule shown in
 Figure 79. More detailed schedules are available. WBS element 1.3 "Instrument Design and Fabrication" contains all of the deliverables required to produce the finished instrument. These deliverables are organized in a manner consistent with the product structure defined for the instrument (see Figure 4). For each deliverable, the work is broken down into the actual tasks required to produce the finished and qualified components of the system.

Using our combined experience building OSIRIS, NIRSPEC, NIRC2, LRIS and ESI we identify all the major components of the system, group them and execute the design, development and fabrication in the best order for sub-assembly testing and readiness for system integration. Although each partner will have well-defined work packages, it is through the seamless merging of the engineering efforts at all four places that we expect to get the greatest benefit. For example, while CIT will take the lead on all aspects of the cryo-mechanical engineering, UCLA staff will provide drawing and fabrication support.
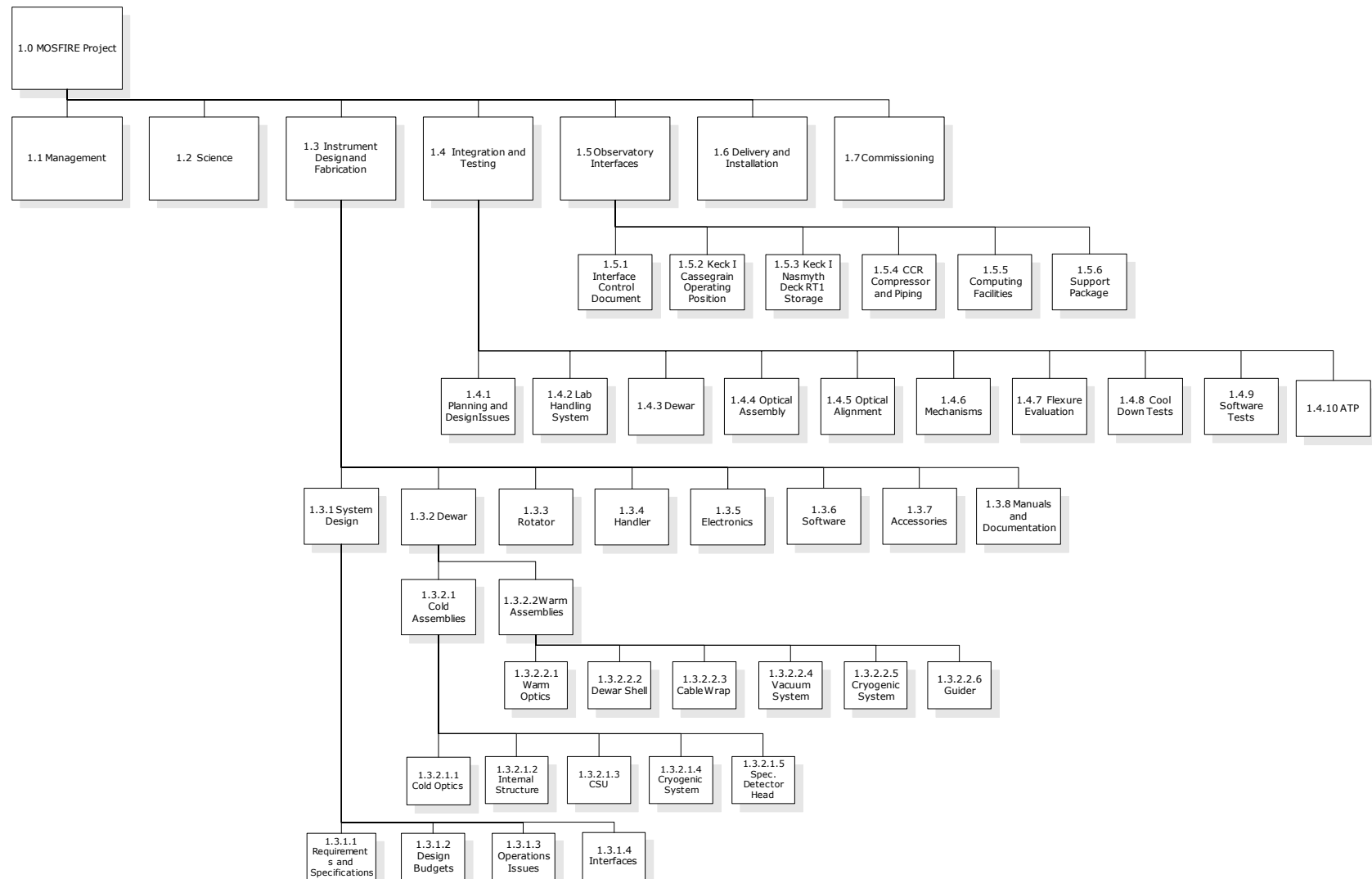
Figure 78: *MOSFIRE Work Breakdown Structure*

The division of the major work packages is as follows:

- Mechanical – CIT
- Optics – UCSC
- Electronics – UCLA

- Software – UCLA
- Interfaces – CARA
- Integration and Testing – CIT

As indicated by the final bullet above, system integration and testing for MOSFIRE will occur at CIT, but the entire team will participate in delivery and installation.

6.5   Schedule

A top-level schedule for the MOSFIRE project is shown in
 Figure 79. The overall duration of this project is estimated at 4 years plus a 6 month installation and commissioning period. The effective start date was July 15, 2005 and the end date is projected to be December 31, 2009. MOSFIRE will complete its PDR in April 2006. This will be followed by a detailed design phase lasting approximately 8 months. The detailed design phase will then be followed by a full scale development phase of 18 months and a final integration and testing phase requiring 1 year.

During the detailed design phase we will develop prototype lens cells and test lens mounting techniques. Fabrication of the vacuum shell, internal optical bench, mechanisms and Handler will begin early in 2007. Optics procurement is already under way in terms of glass acquisition. Immediately after PDR, the crystal optics will be ordered. Our goal is to receive the vacuum shell from PCI by December 2007 and perform the first pump down shortly afterwards.

The Fabrication and Procurement phase will begin January 2007. Parts will be installed into the dewar throughout the year. The first cool down cycle with substantial thermal mass will be in February 2008. Ten cold cycles are planned at a rate of about 1 per month, with a contingency of 2 additional cycles. The CSU is expected to arrive by May 2008 in time for the 3rd cool down cycle. Optics and detector delivery are both targeted for June 2008, which should also signify the end of the fabrication and sub-assembly testing phase and the beginning of I & T.

Warm alignment of the optics and imaging tests using a mux will be carried out in July 2008. During the 4th cool down cycle in August 2008 we will obtain First Light with the mux. The 5th and 6th cool downs will occur in September and October 2008. By the 7th cool down (January 2009) we expect to be ready for First Light with the science detector. Cool down cycles during February and March 2009 will take us to system evaluation level. A Readiness Review will be held in April 2009 coincident with cool down #10. May and June 2009 are held in reserve and Pre-Ship Review will be in June 2009 followed by shipment to Hawaii.

First light on Keck I is planned for mid-August 2009. Handover of the instrument will occur in December 2009 with shared risk operations beginning in Semester 2010A.
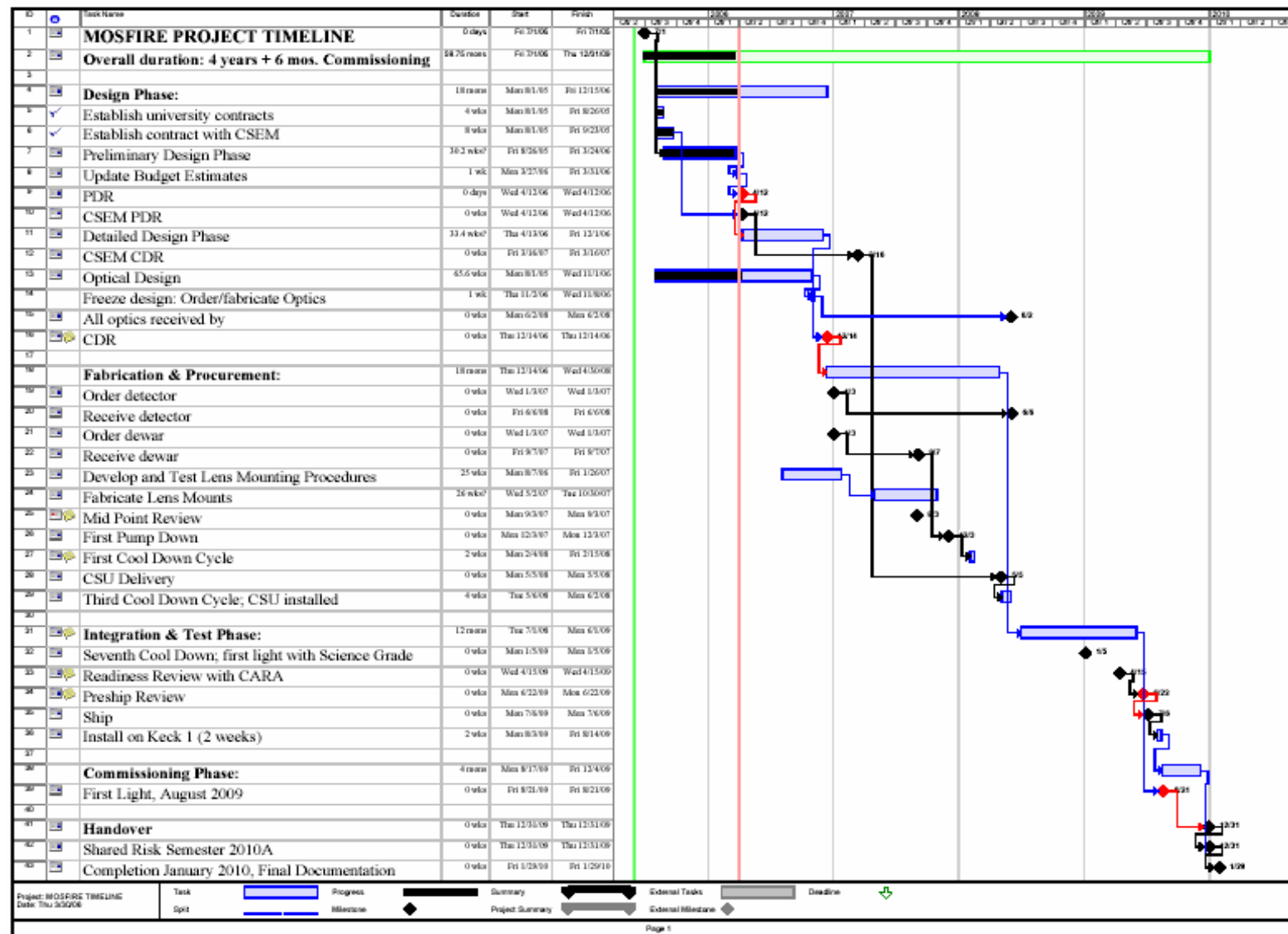
Figure 79: *Top level MOSFIRE Schedule*

6.6 Deliverables

CARA and the MOSFIRE team will agree to a list of deliverables, including the following items:

- Reports and budget information as requested
- The completed MOSFIRE instrument, with all electronics, computers, cables and attachments needed to operate the instrument
- Operational software and source code
- Handling Equipment
- Documentation, including all engineering drawings, schematics, etc.
- Acceptance Test Report
- User's Manual
- Shipping containers
- A reasonable set of spares parts as agreed with CARA

6.7 Milestones and Reviews

CARA's instrument program provides for specific reviews involving the participation of independent external reviewers. Reviews are organized and conducted by the CARA instrument program manager and the report of the review panel is formally made to the WMKO director. The review reports are also sent to the SSC, the instrument program manager and the MOSFIRE project team. We have identified 8 reviews that will be conducted for the work in this project. The major milestones and reviews for this project are shown in Table 28.

Year	Month	Milestone
2005	July	Project start
2006	April	Preliminary Design Review
2006	December	Detailed Design Review
2007	November	Full Scale Development mid-point Review
2008	December	Pre-ship Readiness Review
2009	June	Pre-ship Review
2009	August	First Light
2009	September	Acceptance Review
2009	November	Operational Readiness Review
2009	November	Science Verification Review
2009	December	Project Complete

Table 28: *Milestones and Reviews*

6.8 Budget

The overall budget for the MOSFIRE project is shown in Figure 80. The total cost for the project is estimated at $12,266,168 including an allowance for inflation and a contingency on labor and materials. The budget shown in Figure 80 includes the first year of the project, currently in

progress. The project duration is 54 months starting on July 1, 2005 and ending in December 2009. The project budget has been divided into 5 project years, with the last 6 months of the project included in the final year.

The first year of the project was fully funded by the Telescope System Instrumentation Program (TSIP) in the amount of $2,452,629 in exchange for 24 nights of observing time. To fund the balance of the proposal we have requested funding from the TSIP program for approximately one half of the remaining project costs, or $4,913,664 in exchange for an additional 48 nights of observing time over years 2 through 5 of the project. The balance of the project is being funded through a gift of $4.9M from Gordon and Betty Moore. This gift has been offered in annual amounts to complement the anticipated funding from the TSIP for years 2 through 5 of the project.

In year 1 the project has completed the preliminary design phase, and based on a successful PDR the project will continue through the remaining phases consisting of detailed design, full scale development, installation and commissioning of the instrument. Design and construction of the instrument will be subcontracted by WMKO to UCLA, CIT and UCSC. WMKO will implement the observatory interfaces and support facilities required by the instrument as well as provide program management, reporting and reviews.

To develop the budget estimate for MOSFIRE the instrument was broken down into discrete components using a product structure approach and this breakdown was used to establish labor and materials estimates. This budget has been reviewed as part of the preliminary design phase and represents the current best estimate of the cost to design and build MOSFIRE.

The total project budget includes all of the costs to add the required infrastructure on the Keck I telescope and includes an allowance of 4% inflation for labor costs in project years 2 through 5. A contingency of 15% is allowed for labor and 10% on equipment and materials. 5% contingency is also included for the CSEM contact.

The development of the CSU by CSEM represents a major cost component at $2.5M. Foreign travel is included in this budget to allow for at least 2 people to make a total of four visits to CSEM over the course of the contract.

Details of the materials costs and the observatory infrastructure costs are provided in Figure 81 and Figure 82

It should be noted that none of the collaborating organizations are applying their normal indirect cost rates to the project.

Expenses	Notes	Year 1 (6/1/05 to 5/31/06)	Year 2 (6/1/06 to 5/31/07)	Year 3 (6/1/07 to 5/31/08)	Year 4 (6/1/08 to 5/31/09)	Year 5 (6/1/09 to 11/30/09)	Total for Project
Senior Personnel							
Ian S. McLean, PI		$ 15,481	$ 30,963	$ 30,963	$ 30,963	$ 30,963	$ 139,333
James E. Larkin, Co-I		$ 10,267	$ 10,267	$ 10,267	$ 10,267	$ 10,267	$ 51,335
Charles C. Steidel, Project Scientist		$ -	$ -	$ -	$ -	$ -	$ -
Keith Matthews, Instrument Scientist	1	$ 101,263	$ 105,314	$ 109,526	$ 113,907	$ 118,464	$ 548,474
Harland Epps, Co-I		$ 15,582	$ 14,258	$ 14,258	$ 14,258	$ -	$ 58,356
Total Senior Personnel		$ 142,593	$ 160,802	$ 165,014	$ 169,395	$ 159,694	$ 797,498
Other Personnel							
Post Doctoral Associates							$ -
Other Professionals (Technician, Programmer, Etc.)	1	$ 371,622	$ 508,914	$ 702,939	$ 802,504	$ 395,181	$ 2,781,160
Graduate Students		$ -	$ -	$ -	$ -	$ -	$ -
Undergraduate Students		$ -	$ -	$ -	$ -	$ -	$ -
Secretarial - Clerical (If Charged Directly)	1	$ 58	$ 4,896	$ 2,596	$ 2,700	$ 2,808	$ 13,058
Other		$ -	$ -	$ -	$ -	$ -	$ -
Total Salaries and Wages		$ 514,273	$ 674,612	$ 870,549	$ 974,599	$ 557,683	$ 3,591,716
Fringe Benefits	2	$ 135,978	$ 179,778	$ 233,455	$ 261,447	$ 149,515	$ 960,173
Total Salaries, Wages and Fringe Benefits		$ 650,251	$ 854,390	$ 1,104,004	$ 1,236,046	$ 707,198	$ 4,551,889
Equipment		$ 723,000	$ 921,000	$ 620,143	$ 321,453	$ 10,000	$ 2,595,596
Travel							
Domestic		$ 10,500	$ 7,750	$ 10,500	$ 9,750	$ 40,000	$ 78,500
Foreign		$ 3,000	$ 8,000	$ 8,000	$ 8,000	$ 3,000	$ 30,000
Other Direct Costs							
Materials and Supplies		$ 8,331	$ 14,500	$ 30,000	$ 36,951	$ 20,000	$ 109,782
Publication Costs/Documentation/Dissemination		$ 4,500	$ 6,750	$ 4,000	$ 6,750	$ 4,000	$ 26,000
Consultant Services	3	$ 30,000	$ -	$ -	$ -	$ -	$ 30,000
Computer Services		$ 5,000	$ 5,000	$ 5,000	$ 5,000	$ -	$ 20,000
Subawards (Subcontracts)	4	$ 28,000	$ -	$ -	$ -	$ -	$ 28,000
Other		$ -	$ -	$ -	$ -	$ -	$ -
Total Other Direct Costs		$ 75,831	$ 26,250	$ 39,000	$ 48,701	$ 24,000	$ 213,782
Total Direct Costs		$ 1,462,582	$ 1,817,390	$ 1,781,647	$ 1,623,950	$ 784,198	$ 7,469,767
Indirect Costs		$ -	$ -	$ -	$ -	$ -	$ -
Total Indirect Costs		$ -	$ -	$ -	$ -	$ -	$ -
Total Direct and Indirect Costs		$ 1,462,582	$ 1,817,390	$ 1,781,647	$ 1,623,950	$ 784,198	$ 7,469,767
Contingency							
Materials (Equipment, Materials and Supplies)	5	$ 73,133	$ 93,550	$ 65,015	$ 35,841	$ 3,000	$ 270,539
Labor (Total Salaries, Wages and Fringe Benefits)	6	$ 97,538	$ 128,159	$ 165,601	$ 185,407	$ 106,080	$ 682,785
Total Contingency		$ 170,671	$ 221,709	$ 230,616	$ 221,248	$ 109,080	$ 953,324
Total Cost including contingency		$ 1,633,253	$ 2,039,099	$ 2,012,263	$ 1,845,198	$ 893,278	$ 8,423,091
Contract to CSEM for CSU	7	$ 750,000	$ 1,068,600	$ 562,900		$ -	$ 2,381,500
5% Contingency on CSEM Contract		$ 37,500	$ 53,430	$ 28,145	$ -	$ -	$ 119,075
Total Cost including contingency for CSEM Contract		$ 787,500	$ 1,122,030	$ 591,045	$ -	$ -	$ 2,500,575
Observatory Interfaces							
Labor (Total Salaries, Wages and Fringe Benefits)	8	$ 25,110	$ 46,495	$ 189,735	$ 550,786	$ 5,235	$ 817,361
Materials (Equipment, Materials and Supplies)		$ -	$ -	$ 76,750	$ 240,100	$ -	$ 316,850
Travel		$ 3,000	$ 17,000	$ 17,000	$ 17,000	$ -	$ 54,000
Contingency	9	$ 3,767	$ 6,975	$ 36,136	$ 106,628	$ 786	$ 154,292
Total Interface Costs		$ 31,877	$ 70,470	$ 319,621	$ 914,514	$ 6,021	$ 1,342,503
Total Project Costs		$ 2,452,629	$ 3,231,599	$ 2,922,929	$ 2,759,712	$ 899,299	$ 12,266,168
Funding Profile							
Actual (Year 1) + Projected TSIP funding	10	$ 2,452,629	$ 1,228,416	$ 1,228,416	$ 1,228,416	$ 1,228,416	$ 7,366,293
Private funding	11	$ -	$ 1,662,764	$ 1,581,290	$ 1,374,363	$ 281,458	$ 4,899,875
Total Funding		$ 2,452,629	$ 2,891,180	$ 2,809,706	$ 2,602,779	$ 1,509,874	$ 12,266,168

Notes:
1. Inflation allowed for labor costs at 4% per year for years 2 through 5
2. Benefits are 28% for UCLA and UCSC, and 26% for CIT
3. Possible contract to Breault
4. Purchase effort for measurement of cryo indices
5. Materials contingency is 10%
6. Labor contingency is 15%
7. Contract is for design and manufacture of CSU
8. WMKO benefits are 29%
9. Contingency is 10% for materials and 15% for labor
10. TSIP funding based on 12 nights per year for years 2 through 4,
and 6 nights in year 5, value per night $102,368.
11. Private funding commitment made for years 2 through 5,

Figure 80: *Detailed MOSFIRE budget*

6.8.1   Materials Cost

The materials cost for MOSFIRE, not including the contract to CSEM is estimated at $2.7M as shown in Figure 81. This amount corresponds to the total expenditures for the equipment line item and the materials and supplies line item in the detailed budget shown in Figure 80. Most of the materials costs such as the optics, grating, dewar fabrication and the science detector are based on quotations from suppliers.

Materials Cost Summary

Cabinets	$ 7,000
Cable Wrap	$ 20,000
Cables	$ 17,500
CCD Guider Electronics and Detector	$ 40,000
Connectors (100)	$ 10,000
Coolers	$ 10,451
CCR Heads	$ 88,000
Detector Electronics ASIC driver boards	$ 15,000
Development Platforms	$ 15,000
Dewar Shell (vendor)	$ 165,425
Electronics Enclosures, Wireways and Panels	$ 15,000
Other Sub-assemblies (CIT shops)	$ 75,000
Filters (Y, J, H, K and Ks)	$ 100,000
Flexure Compensation System (Physik Instrument)	$ 142,000
Grating (new)	$ 80,000
Grating/Mirror Exchange stage, complete	$ 50,000
Guider optics	$ 86,600
Guider Structures	$ 10,000
H2-RG detector + tax (Rockwell quote)	$ 655,000
High Bay Clean Room Facilities	$ 60,000
Instrument Control & Data Handling Computers	$ 46,028
Internal optics + spare blanks	$ 821,400
Internal Structures (parts only)	$ 34,943
Lakeshore 218 and Sensors	$ 6,000
Lakeshore 340, Sensors and Heater	$ 5,000
Motor Controllers (10)	$ 20,000
Power Supplies, terminal servers, black boxes	$ 5,000
Raw materials (metal)	$ 25,000
Shipping Costs	$ 10,000
Shipping crates (3)	$ 15,000
Software licenses	$ 20,000
Supplies	$ 9,831
Vacuum System	$ 25,200
Total for Materials	**$ 2,705,378**

Figure 81: Materials Cost Summary

6.8.2 Observatory Interface Costs

The observatory interface costs are detailed in Figure 82. These costs include a 4% inflation rate for labor costs in project years 2 through 5. In the overall project budget we have allowed a 15% contingency on labor and a 10% contingency on equipment and materials for the observatory interface costs.

Item	Labor $	Material $	Total Cost
Rotator	$ 110,192	$ 138,000	$ 248,192
Handler	$ 29,478	$ 33,500	$ 62,978
Support Package	$ 20,431	$ -	$ 20,431
Instrument Program Management	$ 130,420	$ -	$ 130,420
Keck I Cassegrain Focal Station	$ 36,464	$ 29,800	$ 66,264
CCR Helium Connections	$ 101,137	$ 61,750	$ 162,887
Keck I Nasmyth Deck RT1 Position	$ 72,575	$ 47,800	$ 120,375
Computing Facilities	$ 32,863	$ 6,000	$ 38,863
Software Reconfiguration	$ 56,873	$ -	$ 56,873
Reviews	$ 92,449	$ -	$ 92,449
Installation and Commissioning	$ 134,479	$ -	$ 134,479
Totals	**$ 817,361**	**$ 316,850**	**$ 1,134,211**

Figure 82: *Observatory Interface Cost Details*

7   REFERENCES

1. Alcock, Charles et al. 2004, "Building the System from the Ground Up, Second Community Workshop on the Ground-based O/IR System", National Optical Astronomy Observatory.

2. Erb, D.K., Steidel, C.C., Shapley, A.E., Pettini, M., and Reddy, N.A. 2006, ApJ, submitted. "The Stellar, Gas, and Dynamical Masses of Star-Forming Galaxies at z~2".

3. Martini, P., and DePoy, D.L., SPIE, 4008, 695 "Optimal Resolutions for IR Spectroscopy Through the OH Airglow".

4. R. Kibrick et al. 2000, "Active Flexure Compensation Software for the Echellette Spectrograph
    and Imager on Keck-II", Proc. SPIE 4009, p. 262-273.

5. R. Kibrick et al. 2003, "A comparison of open versus closed loop flexure compensations for two
    Keck optical imaging spectrographs: ESI and DEIMOS", Proc. SPIE 4841, p. 1385-1398.

6. S. B. Larson 1996, "NIRSPEC Optics Design Note 2.02: Guider Camera".

7. S. M. Faber et al. 2002, Proc. SPIE 4841.

8. S.M Faber et al. 2003, SPIE, 4841,1657

9. S. Henein et al. 2003, "Mechanical Slit Mask Mechanism for the James Webb Space Telescope Spectrometer", in Proc. 10th European Space Mechanisms and Tribology (ESMAT) Symposium, San Sebastian, Spain, ESA SP-524, pp.201-208.

10. P. Spanoudakis et al. 2004, in Opticon: Workshop on Reconfigurable Slit Masks.

11. I. S. McLean et al. 1998, Proc. SPIE Vol. 3354, 566.

12. J.E. Larkin et al. 2002, Proc. SPIE 4841.

8   MOSFIRE ACRONYMS

- API: Application Programming Interface

- ASIC: Application Specific Integrated Circuit

- BCS: Balanced Composite Substrate

- CARA: California Association for Research in Astronomy

- Cass: Cassegrain

- CDS: Correlated Double Sampling

- COM: Component Object Model

- COO: Caltech Optical Observatories

- CSU: Cryogenic Slit Unit

- DEIMOS: Deep Imaging Multi-Object Spectrograph

- DLL: Dynamically Linked Library

- DRP: Data Reduction Pipeline

- ESI: Echellette Spectrograph and Imager

- FCS: Flexure Compenstation System

- FITS: Flexible Image Transport System

- GUI: Graphical User Interface

- HAL: Hardware Abstraction Layer

- HgCdTe: Mercury-Cadmium-Teluride

- IDL: Interactive Data Language

- IR: InfraRed

- JAR: Java Archive

- JNI: Java Native Interface

- KTL: Keck Task Library

- LRIS: Low Resolution Imaging Spectrograph

- LVDT: Linear Voltage Differential Transformer

- MAS: MOSFIRE ASIC Server

- MASCGEN: MOSFIRE Automatic Slit Configuration Generator

- MCDS: Multiple Correlated Double Sampling (Fowler Sampling)

- MCSS: MOSFIRE CSU Server

- MDFS: MOSFIRE Detector Focus Server

- MDS: MOSFIRE Detector Server

- MECGUI: MOSFIRE Exposure Control GUI

- MESGUI: MOSFIRE Expsoure Status GUI

- MFCS: MOSFIRE Flexure Compensation Server

- MGS: MOSFIRE Global Server

- MMCGUI: MOSFIRE Mechanism Control GUI

- MMSGUI: MOSFIRE Mechanism Status GUI

- MOSFIRE: Multi-Object Spectrograph for InfraRed Exploration

- MPCGUI: MOSFIRE Power Control GUI

- MPRGUI: MOSFIRE Pressure Status GUI

- MPRS: MOSFIRE Pressure Server

- MPSGUI: MOSFIRE Power Status GUI

- MPWS: MOSFIRE Power Server

- MRMS: MOSFIRE Rotary Mechanism Server

- MSC: MOSFIRE Slit Configuration File

- MSCGUI: MOSFIRE CSU Control GUI

- MSSGUI: MOSFIRE CSU Status GUI

- MTCGUI: MOSFIRE Temperature Control GUI

- MTCS: MOSFIRE Temperature Control Server

- MTGUI: MOSFIRE Telescope GUI

- MTMS: MOSFIRE Temperature Monitor Server

- MTSGUI: MOSFIRE Temperature Status GUI

- MVC: Model-View-Controller Architecture

- NIRC2: Near InfraRed Camera 2

- NIRES: Near InfraRed Echelle Spectrometer

- NIRSPEC: Near InfraRed Spectrograph

- OIR: Optical/Infrared

- OSIRIS: OH-Suppressing InfraRed Imaging Spectrograph

- PI: Physik Instrumente

- RMI: Remote Method Invocation

- RPC: Remote Procedure Call

- SCA: Sensor Chip Assembly

- TCP/IP: Transmission Control Protocol/Internet Protocol

- UCLA: University of California, Los Angeles

- UCO: University of California Observatories

- UCSC: University of California, Santa Cruz

- UI: User Interface

- USB: Universal Serial Bus

- WMKO: W. M. Keck Observatory

9   APPENDICES

Separate documents (pdf) for each of the items listed below are posted on the MOSFIRE web site.

9.1   Requirements Document

Draft Requirements for MOSFIRE: Multi-Object Spectrometer for Infra-Red Exploration, Version 1.0, March 30, 2006

9.2   Preliminary Interface Control Document

Draft Interface Control Document for MOSFIRE, Version 1.0, March 31, 2006, W.M. Keck Observatory

9.3   Compliance Matrix

Draft Requirements Compliance Matrix for MOSFIRE, Version 1.0, March 30, 2006

9.4   CSEM Documents

RP01 CSU Design and Analysis
RSM_CSE_TN_13_Iss2_State_machine_description
RSM_CSE_TN_07_User function list
RP02 CSU Control Rack User Manual
PL01 EUX Test Plan